



National Library
of Canada

Bibliothèque nationale
du Canada

Canadian Theses Service

Service des thèses canadiennes

Ottawa, Canada
K1A 0N4

NOTICE

The quality of this microform is heavily dependent upon the quality of the original thesis submitted for microfilming. Every effort has been made to ensure the highest quality of reproduction possible.

If pages are missing, contact the university which granted the degree.

Some pages may have indistinct print especially if the original pages were typed with a poor typewriter ribbon or if the university sent us an inferior photocopy.

Reproduction in full or in part of this microform is governed by the Canadian Copyright Act, R.S.C. 1970, c. C-30, and subsequent amendments.

AVIS

La qualité de cette microforme dépend grandement de la qualité de la thèse soumise au microfilmage. Nous avons tout fait pour assurer une qualité supérieure de reproduction.

S'il manque des pages, veuillez communiquer avec l'université qui a conféré le grade.

La qualité d'impression de certaines pages peut laisser à désirer, surtout si les pages originales ont été dactylographiées à l'aide d'un ruban usé ou si l'université nous a fait parvenir une photocopie de qualité inférieure.

La reproduction, même partielle, de cette microforme est soumise à la Loi canadienne sur le droit d'auteur, SRC 1970, c. C-30, et ses amendements subséquents.

THE UNIVERSITY OF ALBERTA

BOREHOLE AND TUNNEL STABILITY IN ROCK
WITH ANISOTROPIC STRENGTH AND IMPERFECTIONS

by

ALAN KWOK LUN KWONG

A THESIS

SUBMITTED TO THE FACULTY OF GRADUATE STUDIES AND RESEARCH
IN PARTIAL FULFILMENT OF THE REQUIREMENTS FOR THE DEGREE OF
DOCTOR OF PHILOSOPHY

DEPARTMENT OF CIVIL ENGINEERING

EDMONTON, ALBERTA

SPRING 1990



National Library
of Canada

Bibliothèque nationale
du Canada

Canadian Theses Service

Service des thèses canadiennes

Ottawa, Canada
K1A 0N4

NOTICE

AVIS

The quality of this microform is heavily dependent upon the quality of the original thesis submitted for microfilming. Every effort has been made to ensure the highest quality of reproduction possible.

If pages are missing, contact the university which granted the degree.

Some pages may have indistinct print especially if the original pages were typed with a poor typewriter ribbon or if the university sent us an inferior photocopy.

Reproduction in full or in part of this microform is governed by the Canadian Copyright Act, R.S.C. 1970, c. C-30, and subsequent amendments.

La qualité de cette microforme dépend grandement de la qualité de la thèse soumise au microfilmage. Nous avons tout fait pour assurer une qualité supérieure de reproduction.

S'il manque des pages, veuillez communiquer avec l'université qui a conféré le grade.

La qualité d'impression de certaines pages peut laisser à désirer, surtout si les pages originales ont été dactylographiées à l'aide d'un ruban usé ou si l'université nous a fait parvenir une photocopie de qualité inférieure.

La reproduction, même partielle, de cette microforme est soumise à la Loi canadienne sur le droit d'auteur, SRC 1970, c. C-30, et ses amendements subséquents.

ISBN 0-315-60219-8

THE UNIVERSITY OF ALBERTA

RELEASE FORM

NAME OF AUTHOR ALAN KWOK LUN KWONG

TITLE OF THESIS BOREHOLE AND TUNNEL STABILITY IN
ROCK WITH ANISOTROPIC STRENGTH
AND IMPERFECTIONS

DEGREE FOR WHICH THESIS
WAS PRESENTED DOCTOR OF PHILOSOPHY

YEAR THIS DEGREE GRANTED SPRING 1990

Permission is hereby granted to THE UNIVERSITY OF ALBERTA LIBRARY to reproduce single copies of this thesis and to lend or sell such copies for private, scholarly or scientific research purposes only.

The author reserves other publication rights, and neither the thesis nor extensive extracts from it may be printed or otherwise reproduced without the author's written permission.

(SIGNED) Alan Kwong.....

PERMANENT ADDRESS:

2111 Raintree Village
6651 Ranchview Drive, N.W.
Calgary, Alberta
Canada T3G 1P3

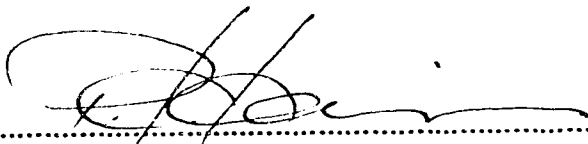
DATED April 26, 1990

THE UNIVERSITY OF ALBERTA

FACULTY OF GRADUATE STUDIES AND RESEARCH

The undersigned certify that they have read, and recommend to the Faculty of Graduate Studies and Research, for acceptance, a thesis entitled BOREHOLE AND TUNNEL STABILITY IN ROCK WITH ANISOTROPIC STRENGTH AND IMPERFECTIONS submitted by ALAN KWOK LUN KWONG in partial fulfilment of the requirements for the degree of DOCTOR OF PHILOSOPHY.

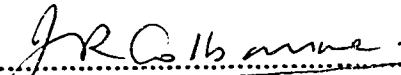
Dr. P. K. Kaiser


.....
Supervisor

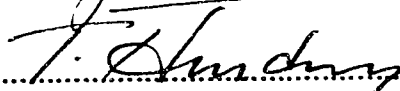
Dr. D. Chan


.....
Co-Supervisor

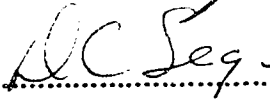
Dr. J. R. Colbourne


.....

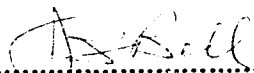
Dr. T. Hrudey


.....

Dr. D. Sego


.....

Dr. S. Bell


.....
External Examiner

Date 26 April 1990.....

ABSTRACT

The analysis of underground opening stability requires the understanding of different possible failure mechanisms. An eigenvalue analysis was conducted to investigate various modes of deformation around a borehole.

The development of yield zones around boreholes with the presence of local weaknesses such as joints and fissures were also investigated. Local weaknesses are represented in the finite element studies by elements with a material strength lower than that of the surrounding elements. The process of yield initiation and propagation around a borehole was captured and studied in detail for several cases.

These results point out the importance of local weaknesses or imperfections on the borehole failure mechanism. A rock mass can often be treated as a transversely isotropic material with the variation of strength being a function of the orientation of the weakness plane relative to the principal stress. Hence, by adopting a generalized failure criterion for rock that exhibits transversely isotropic strength, the effect of distributed weakness on the yield initiation, propagation and failure mechanism of a borehole may be studied.

The model implemented into the finite element program is assumed to be linearly elastic, brittle perfectly plastic. A number of cases with different parameter combinations were studied and the results summarized in a chart which permits an identification of different modes of borehole failure mechanisms. It was found that

elastic block-type failure mechanisms, similar to those generated by local weaknesses, are also possible. Practical implications of the different modes of failure and the characteristics of the ground convergence curves for the design and monitoring of underground openings such as tunnels are discussed.

A special finite element analysis was conducted to reproduce the block-type failure mechanism which was observed during laboratory tests of a circular opening in jointed coal.

Finite element analyses were also conducted to simulate the block-type failure mechanism which was observed during the construction of the Frejus Tunnel linking France and Italy.

Finally, a simplified approach was adopted to study the extent and shape of the yield initiation zone near a circular opening by comparing the elastic stress distribution with the Mohr-Coulomb yield criterion and the transversely isotropic yield criterion. The extent of the yield initiation zone estimated by the simplified approach was compared with that generated by the finite element analysis.

Results from this research also provide a basic understanding for the failure mechanisms observed in other underground openings such as caverns.

ACKNOWLEDGEMENT

The author wishes to express his deepest gratitude to his supervisor Dr. P. K. Kaiser for his interest and intense enthusiasm in the subject, and his guidance and support for this research. His ideas and valuable discussions throughout the development of this research are very much appreciated.

The author also wishes to thank Dr. D. Chan for his assistance on the numerical aspects of this research and Dr. S. Thomson for his review of my thesis. The financial support provided by the NSERC Strategic Grant No. G1336 is gratefully acknowledged. The computer facilities at the University of Alberta and also the supercomputer facility provided by the University of Calgary which made this numerical work possible are acknowledged.

TABLE OF CONTENTS

CHAPTER	PAGE
1. INTRODUCTION.....	1
1.1 Problems encountered during drilling deep boreholes...	2
1.2 Scope of thesis and research approach.....	3
2. REVIEW OF STUDIES RELATED TO BOREHOLE BREAKOUTS.....	7
2.1 Introduction.....	7
2.2 Factors affecting borehole stability.....	9
2.2.1 Stresses at the borehole wall.....	10
2.2.2 In-situ horizontal far-field stress ratio N	11
2.2.3 Horizontal to vertical far-field stress ratio K_0 and drilling fluid density.....	12
2.2.4 Temperature.....	13
2.2.5 Weakness planes.....	14
3. INVESTIGATION OF BOREHOLE INSTABILITY BY EIGENVALUE ANALYSES.....	16
3.1 Introduction.....	16
3.2 Physical meaning of eigenvalues and eigenvectors.....	19
3.3 Deformation mode assessment by eigenvalues and eigenvectors.....	23
3.4 Shear band formation in confined compression test.....	25
3.5 Modes of deformation of a circular opening (borehole).	26
3.6 Summary and Conclusions.....	31

4. EFFECTS OF WEAKNESSES ON BOREHOLE FAILURE	
MECHANISMS.....	4 1
4.1 Introduction.....	4 1
4.2 Simulation of borehole drilling by finite element method.....	4 2
4.3 Selection of location for weaknesses.....	4 4
4.4 Borehole failure mechanism in the presence of weaknesses.....	4 7
4.5 Practical implications of findings for design and monitoring of underground opening.....	5 1
4.6 Summary and conclusions.....	5 3
5. EFFECTS OF ORIENTED WEAKNESSES ON BOREHOLE FAILURE	
MECHANISMS.....	6 6
5.1 Introduction.....	6 6
5.2 Properties of transversely isotropic model.....	6 7
5.2.1 Reduction of transversely isotropic yield criterion to isotropic yield criterion.....	6 9
5.2.2 Transversely isotropic yield criterion for cohesive material ($\phi=0$).....	6 9
5.2.3 Transversely isotropic yield criterion for purely frictional material ($c=0$).....	7 1
5.3 Strength parameters for transversely isotropic yield criterion.....	7 2
5.4 Implementation of transversely isotropic yield criterion into finite element code SAGE.....	7 3

5.4.1 Testing of implemented model.....	7 4
5.5 Borehole failure mechanisms in transversely isotropic rocks.....	7 6
5.6 Practical implications of findings for design and monitoring of underground openings.....	8 1
5.7 Summary and conclusions.....	8 3
 6. INVESTIGATION OF UNDERGROUND OPENING FAILURE MECHANISMS IN TRANSVERSELY ISOTROPIC ROCKS.....	 9 9
6.1 Failure mechanisms of small circular openings in coal...	9 9
6.1.1 Description of results from Test MC-4.2.....	1 0 0
6.1.2 Generation of failure mechanisms by finite element analysis.....	1 0 1
6.1.3 Summary and conclusions.....	1 0 4
6.2 Failure mechanisms of a tunnel in rock with parallel weakness planes.....	1 0 5
6.2.1 Description of failure mechanisms at Frejus Tunnel.....	1 0 6
6.2.2 Summary and conclusions.....	1 1 0
 7. SIMPLIFIED APPROACH TO PREDICT YIELD INITIATION ZONES AROUND BOREHOLES IN ROCKS.....	 1 2 2
7.1 Introduction.....	1 2 2
7.2 Stress distribution around circular openings.....	1 2 3
7.3 Extent of yield initiation zones around a borehole.....	1 2 4
7.3.1 Von Mises yield criterion.....	1 2 5
7.3.2 Mohr-Coulomb yield criterion	1 2 6

7.3.3 Yield Criterion for transversely isotropic rock (Nova and Sacchi, 1979).....	1 2 9
7.4 Limitations of applicability and conclusions.....	1 3 0
8. SUMMARY, CONCLUSIONS AND PRACTICAL IMPLICATIONS.....	1 4 4
8.1 Summary.....	1 4 4
8.2 Practical implication to oil drilling.....	1 4 8
8.3 Practical implication for design and monitoring of underground openings.....	1 5 0
9. REFERENCES.....	1 5 3
APPENDIX A Subroutine program for eigenvalue computation.	1 6 4
APPENDIX B Elastic deformation properties of transversely isotropic rock.....	1 7 1
B.1 Elastic constitutive matrix for transversely isotropic rocks.....	1 7 1
B.2 Determination of elastic constants for transversely isotropic rocks.....	1 7 7
APPENDIX C Properties of transversely isotropic model.....	1 8 1
C.1 Summary of transversely isotropic models.....	1 8 1
C.2 Reduction of transversely isotropic yield criterion to isotropic yield criterion.....	1 8 2
C.3 Determination of strength parameters for transversely isotropic yield criterion.....	1 8 4

APPENDIX D	Elasto-plastic finite element formulation.....	189
D.1	Elasto-plastic constitutive matrix formulation.....	189
D.2	Evaluation of $\langle \frac{\partial F}{\partial \sigma} \rangle$ for transversely isotropic yield criterion.....	193
APPENDIX E	Implementation of model and input data instructions for SAGE (Cyber 205 version) (Last update - June 01, 1987).....	197
E.1	General features of SAGE.....	197
E.2	Implementation of transversely isotropic model into SAGE.....	199
E.3	Input data instructions.....	208
APPENDIX F	Input file example.....	252

LIST OF TABLES

TABLE	PAGE
C.1 List of references for transversely isotropic models.....	181
C.2 Determination of α and β for the transversely isotropic yield criterion.....	188
E.1 Material properties input in SAGE.....	250

LIST OF FIGURES

FIGURES		PAGE
2.1	Modes of rupture initiation near borehole (Modified from Maury, 1987).....	1 5
3.1	Deformation and failure modes of deep boreholes from bifurcation analysis.....	3 2
3.2	Modes of deformation from eigenvalue analysis of elasto-plastic matrix.....	3 3
3.3	Finite element idealization for the study of shear band formation in confined compression test.....	3 4
3.4	Yield zone development in confined compression test.....	3 5
3.5	Finite element meshes for eigenvalue analysis of borehole deformation modes.....	3 6
3.6	Ground convergence curves for Mesh A and B at $N=1.0$	3 7
3.7	Eigenvalues of the global stiffness matrix at $P_i=16.4\%$ for Meshes A and B.....	3 8
3.8	Displacement vector plots for an unstable borehole at $P_i = 16.4\%$ ($u/ue = 3.89$).....	3 9
3.9	Modes of deformation for an unstable borehole at $P_i = 16.4\%$ ($u/ue = 3.89$).....	4 0
4.1	Finite element mesh for the study of borehole failure mechanisms in rock with local weaknesses.....	5 5
4.2	Sequences for finite element simulation of borehole drilling.....	5 6

4.3	Location for yield initiation around the periphery of a borehole in homogeneous ground.....	5 7
4.4A	Development of failure mechanisms around boreholes without local weaknesses (N=0.5).....	5 8
4.4B	Development of block-type failure mechanisms around boreholes with two local weaknesses (N=0.5).....	5 9
4.4C	Development of block-type failure mechanisms around boreholes with one local weakness and a weakness plane (N=0.5).....	6 0
4.5	Development of continuous yield zones around boreholes with local weaknesses (N=0.5 and 1.0).....	6 1
4.6	Stress distribution along line in x-direction (Case B: Two symmetric weaknesses).....	6 2
4.7	Stress distribution along line in y-direction (Case B: Two symmetric weaknesses).....	6 3
4.8	Ground convergence curves for borehole with local weaknesses (Cases A to D).....	6 4
4.9	Ground strain curves for four locations in Case D.....	6 5
5.1	Transversely isotropic yield criterion for cohesive material ($\phi=0$).....	8 5
5.2	Transversely isotropic yield criterion for purely frictional material ($c=0$).....	8 6
5.3	Deviatoric stress at failure versus orientation of weakness planes-Experimental results on Martinsburg slate (data after Donath, 1963).....	8 7
5.4	Confined compression test by finite element simulation.....	8 8

5.5	Eigenvalue analysis of elasto-plastic constitutive matrix for transversely isotropic material.....	89
5.6A	Development of borehole failure mechanisms in transversely isotropic rocks (Cases E and F).....	90
5.6B	Development of borehole failure mechanisms in transversely isotropic rocks (Cases G and H).....	91
5.7A	Direction of failure planes for Case E.....	92
5.7B	Direction of failure planes for Case F.....	93
5.7C	Direction of failure planes for Case G.....	94
5.8	Stress distribution along x-direction for Case G: weakness planes at $N=0.5$ and $\eta=90^\circ$	95
5.9	Stress distribution along y-direction for Case G: weakness planes at $N=0.5$ and $\eta=90^\circ$	96
5.10	Ground convergence curves for circular opening in transversely isotropic rocks.....	97
5.11	Ground strain curves at three locations along the x-direction for Case G: weakness planes at $\eta=90^\circ$	98
6.1	Sketch of sample for Test MC-4.2 (first rupture of the opening wall and extent of rupture zone at the end of the test).....	111
6.2	Finite element mesh for the study of failure mechanisms around circular openings in jointed coal.....	112
6.3	Comparisons of the extent of simulated yield zones with the observed rupture zones.....	113

6.4	Closures of opening wall at four locations for Test MC-4.2 (Comparisons of simulated closures with the measured).....	114
6.5	Ground strain curves measured from fifteen extensometers for Test MC-4.2.....	115
6.6	Ground strain curves at fifteen locations for Test MC-4.2 (Comparisons of simulated strain with the measured).....	116
6.7	The effects of major discontinuities on the modes of failure in Frejus Tunnel.....	117
6.8	Finite element mesh for the study of Frejus Tunnel.....	118
6.9	Development of yield zones and ground convergence curves for the Frejus Tunnel.....	119
6.10	Convergence between two opposite points on the tunnel wall for Directions A to F.....	120
6.11	Extent of yield zones around the Frejus Tunnel from other studies.....	121
7.1	Definition of symbols for stress calculation around a circular opening.....	133
7.2	Stress distribution for a circular opening in an elastic, homogeneous, isotropic material.....	134
7.3	Extent and shape of yield initiation zones for Von Mises yield criterion.....	135
7.4	Conditions of yielding for weaknesses.....	136
7.5	Orientation of weakness planes and major principal stresses around a borehole.....	137
7.6	Conditions of yielding for rock mass and weaknesses.....	138

7.7	Location and extent of yield initiation zones for $N=1.0$ (Mohr-Coulomb yield criterion).....	139
7.8	Location and extent of yield initiation zones for $N=0.5$ (Mohr-Coulomb yield criterion).....	140
7.9	Comparisons of the spatial extent of yield initiation zones (Simplified approach and finite element analysis by Kaiser et al., 1985).....	141
7.10	Location and extent of yield initiation zones for $N=1.0$ (Transversely isotropic yield criterion).....	142
7.11	Location and extent of yield initiation zones for $N=0.5$ (Transversely isotropic yield criterion).....	143
8.1	Summary of modes of failure.....	152
B.1	Definitions for the coordinate system.....	179
B.2	Uniaxial compression tests for the determination of elastic constants for transversely isotropic rocks.....	180
C.1	Determination of strength parameters for Martinsburg slate.....	187
D.1	Definitions for planes of transverse isotropy in the finite element coordinate system.....	196
E.1	Types of elements available in SAGE.....	251
F.1	Finite element idealization for demonstration of input file.....	257
F.2	Confined compression test for demonstration of input file.....	258

LIST OF SYMBOLS

a	Radius of circular opening
c	Cohesion intercept of linear rock mass strength envelope
c_w	Cohesion intercept of linear joint strength envelope
c_{\max}	Maximum cohesion intercept for transversely isotropic material
c_{\min}	Minimum cohesion intercept for transversely isotropic material
c_{res}	Residual cohesion intercept for transversely isotropic model
E	Modulus of elasticity for isotropic material
E_1	Modulus of elasticity in the plane of transverse isotropy
E_2	Modulus of elasticity normal to the plane of transverse isotropy
G	Shear modulus for isotropic material
G_2	Shear modulus in plane normal to the plane of transverse isotropy
K_0	Horizontal to vertical far-field stress ratio, $\frac{\sigma_H}{\sigma_V}$
N	Horizontal far-field stress ratio, $\frac{\sigma_h}{\sigma_H}$
p_s	Pressure inside opening

$P_i = \frac{P_s}{\sigma_H}$	Pressure inside opening normalized to the maximum far-field stress σ_H (given as a percentage)
R	Radius of maximum extent of yield zone in a specific orientation
r	Distance from the center of a circular opening
u_a	Radial displacement at the wall of an opening
u_c	Convergence of an unsupported opening in elastic material
u_r	Radial displacement at r
u_x, u_y, u_z	Displacement in the direction of local coordinates x, y, z
Y	Yield function
α	Ratio of $\frac{\tan\phi_{\max}}{\tan\phi_{\min}}$
β	Ratio of $\frac{c_{\max}}{c_{\min}}$
ξ	Angle between direction of minor principal stress and the plane of transverse isotropy
ε	Strain
μ	Angle between the direction of weakness plane and the direction of major principle stress
η	Angle between the direction of major principal stress and the plane of transverse isotropy ($\eta + \xi = 90^\circ$)
ν	Poisson's ratio for isotropic material

ν_1	Poisson's ratio characterizing the extensional strain response in the plane of transverse isotropy due to a compressive stress acting parallel to the plane of transverse isotropy
ν_2	Poisson's ratio characterizing the extensional strain response in the plane of transverse isotropy due to a compressive stress acting normal to the plane of transverse isotropy
ϕ	Angle of friction for rock mass, slope of linear strength envelope
ϕ_w	Angle of friction for joint, slope of linear strength envelope
ϕ_{\max}	Maximum angle of friction for transversely isotropy material
ϕ_{\min}	Minimum angle of friction for transversely isotropy material
ϕ_{res}	Angle of friction at residual strength for transversely isotropy model
σ_c	Uniaxial unconfined compressive strength
σ_H	Maximum horizontal total far-field stress
σ_h	Minimum horizontal total far-field stress
σ_m	Stresses in the plane of transverse isotropy
σ_n	Stresses normal to the plane of transverse isotropy
σ_r	Radial stress
σ_v	Vertical stress

σ_θ	Tangential stress
$\sigma_1, \sigma_2, \sigma_3$	Major, intermediate and minor principal stresses
τ	Shear stress
ψ	Angle from the direction of minor principal stress to the plane of failure
θ	Angle from the direction of minor principal stress to a point of interest
χ	Angle of rotation between two coordinate systems x, y, z and x', y', z'
$[\]$	Denotes a matrix, not necessary square
$[\]^T$	Denotes the transpose of a matrix
$\{ \}$	Denotes a vector with elements placed vertically
$\langle \rangle$	Denotes the transpose of a vector, i.e. $\langle \rangle^T = \{ \}$
$[\] \{ \}$	Matrices and vectors placed side by side represent matrix multiplication

1 INTRODUCTION

Rocks differ significantly from many other engineering materials because of the presence of discontinuities in the form of fissures, joints, bedding planes, etc. The engineering properties and the behaviour of a rock mass depend on the strength of the intact rock and the number, orientation, spacing and strength of the discontinuities. In this thesis, discontinuities are termed weaknesses.

An underground opening, whether it is a borehole or a tunnel, drilled in rock, is likely to encounter such weaknesses. Even with a regular pattern of weaknesses in a rock mass, there are many possible configurations and locations for weaknesses to intersect an opening. The behaviour of an opening will depend on its size and location relative to the weaknesses. It is sometimes difficult to analyze underground opening stability because the strength of the rock mass will depend on the size of the opening. For example, if an opening is small relative to the weaknesses, then the behaviour will be governed by the properties of the rock mass. In this case, weaknesses are referred to as fissures. If the size of the opening increases, then there are more chances for the opening to intersect the weaknesses. The behaviour of the opening will then be dominated by them. Weaknesses in this case, are referred to as joints because the properties of the joints and their effects (extent and orientation) on the failure modes of the opening have to be considered.

In the analysis of underground opening stability, most of the research work assumes the rock mass to be homogeneous. This

occurs when the size of the opening is relatively small compared to that of the fissures, or an opening is in a highly fractured rock mass. In this research, the effect of weaknesses (size and relative location) on the failure mechanism of underground openings is presented.

While this study is directed at borehole failure mechanisms, the results and findings are directly applicable to the design and monitoring of underground openings such as tunnels.

1.1 Problems Encountered During Drilling Deep Boreholes

Borehole breakouts and excessive wall movements are widely observed in exploration holes for oil, gas and oil sands. Borehole wall movements and breakouts may occur during drilling, before the casing can be cemented into place or during production in the producing formation. In recent years, the high costs of drilling deep boreholes in frontier areas combined with the decrease in revenue due to low oil prices have put pressures on the oil drilling industry to intensify research on borehole failure mechanisms. A better understanding of the factors that dominate the failure process is needed before guidelines can be established for the control or prevention of borehole instability. Improvements in borehole stability control techniques would not only lead to a marked reduction in drilling costs but also to an increase in the quality of geophysical logs.

The physical processes that control the deformation and failure of a borehole are not fully understood because of an incomplete understanding of the relevance of the following factors:

1. Magnitude and directions of the in situ far-field stresses;
2. Stress concentrations created by the borehole;
3. Extent, orientation and distribution of weaknesses near a borehole;
4. Strength and deformation properties of the rock mass and imbedded weaknesses;
5. Stress redistribution process as initiated by the weaknesses;
6. Pore and fracture pressure as well as radial flow;
7. Dynamic pressure fluctuations during the drilling operation;
8. Thermal stresses induced by the temperature difference between the drilling fluid and the rock mass;
9. Permeability change in the rock mass due to the migration of fine particles from the drilling fluid into the pores and fractures of the rock mass; and
10. Chemical interaction of the drilling fluid and the rock mass.

Any combination of these factors may cause excessive deformation or instability of the borehole wall which in turn may lead to increased drilling times due to stuck pipe, and sometimes, abandonment of the hole. The cost of borehole instability related to delays and redrilling costs continues to cause major expenditures, in the order of millions of dollars per year, for the Canadian petroleum industry.

1.2 Scope of Thesis and Research Approach

The purpose of this research is to investigate several of the factors which control the formation of different modes of failure of

deep boreholes. It is hoped that the results presented in this thesis will assist the oil drilling industry in developing guidelines for the control or prevention of borehole failures. Although this study is focused on borehole failure mechanisms, the results provide a better understanding for the failure modes observed in underground construction, tunnelling or mining.

The two most important mechanisms leading to borehole failure are ductile yielding (plastic flow) and brittle rupture of the borehole wall. Ductile yielding typically occurs in materials such as clay shales which are often encountered in production areas. The oil industry generally handles problems in clay shale by changing the chemical composition of the drilling mud. This aspect and ductile yielding will not be considered in this study. Instead it will concentrate on the problem of breakouts in brittle rocks which are frequently observed in Alberta and other parts of Canada.

Of the ten factors listed earlier, the first five were investigated by the author because of their relevance in controlling of the brittle rupture process.

Although borehole breakouts are frequently observed, it is seldom possible to obtain sufficiently detailed or quantitative measurements in the field to allow a comprehensive evaluation of the actual failure mechanisms. Hence, it is necessary to simulate the most relevant processes numerically and to compare the results with laboratory tests. In order to understand the failure mechanisms of a borehole, the process of yield initiation, propagation and eventually rupture of the wall must be known. In this thesis, these processes are investigated by the finite element method because it can take

into account complex boundary conditions as well as variations in material properties and is able to provide displacement fields during the yielding processes at each step of the analysis. The following approaches were adopted and documented:

1. In chapter 2, a review of the approaches adopted by others to study borehole instability problems is presented. The capabilities of these approaches are addressed.
2. In chapter 3, possible modes of deformation at the borehole wall are investigated by studying the eigenvalues and their corresponding eigenvectors of the global stiffness matrix in the finite element analysis. The physical meaning of eigenvalues and eigenvectors are discussed.
3. The effects of local weaknesses on the mode of failure around a borehole are investigated in Chapter 4. Local weaknesses are represented in the finite element analysis by elements with a reduced strength. The development of yield zones and the resulting stress redistribution caused by the local weaknesses is highlighted.
4. The influence of weakness orientation on the modes of failure is described in Chapter 5. A generalized failure criterion for transversely isotropic material was adopted and implemented into a finite element program. Parameters necessary for the model were identified from published test results. The failure mechanisms obtained in this chapter are compared with those determined in Chapter 4.

5. The transversely isotropic model presented in Chapter 5 is used to simulate the failure mechanisms observed in laboratory tests (Guenot, 1979) and in the field (Lunardi, 1980). The extent and shape of the observed rupture zones are compared with the yield zones from the finite element analysis.
6. A simplified approach to approximate the extent and shape of yield initiation zones around circular openings is described in Chapter 7. The results generated from the simplified approach are compared with those from the finite element analysis.
7. In chapter 8, a summary chart is provided to assist in identifying various modes of failure based on the information contained in the previous chapters. Conclusions and practical implications to borehole drilling and for the design and monitoring of underground openings are discussed.

2 REVIEW OF STUDIES RELATED TO BOREHOLE BREAKOUTS

2.1 Introduction

In the following, some recent findings from analytical, numerical and laboratory studies of deep borehole failure mechanisms are reviewed. The intention is to provide an overview of the various approaches that have been used to investigate this problem and to gain insights into the mechanisms that may cause borehole instability during drilling.

Although many different approaches have been used to study the problem of borehole stability, they can be basically divided into five groups:

1. Elastic stresses from analytical closed-form solutions have been applied to failure criteria of rock in order to determine the approximate location and extent of the yield initiation zones (e.g., Daemen (1983) and Detournay and St. John (1988)). This simplified method is ideally suited for parametric studies. However, the extent of the yield initiation zones give only an indication where and how failure starts but not how it propagates because stress redistribution process is neglected. It is important to distinguish between yield initiation and propagation because different mechanisms may be involved.

2. Analytical solutions for the determination of plastic strains and the extent of yield zones have been derived from plasticity theory (e.g., Daemen and Fairhurst (1972)). These methods are suitable for comparing the extent of yield zones for different constitutive relationships and different yield criteria. However, they are only applicable to continuum behaviour and are based on homogeneous material assumptions with relatively simple boundary conditions (e.g., far-field stress ratio N equal to unity). Solutions for boreholes in non homogeneous material are not readily available.
3. The finite element method has been used to study the extent of yield zones (e.g., Desai and Reese (1970), Morita and Gray (1980)). This method can take into account more complicated boundary conditions and the presence of local weaknesses such as joints. However, displacement fields are normally assumed to be continuous within the body and therefore, it cannot adequately model separation of sheared surfaces or multiple instability modes. Nevertheless, this method was adopted because local weaknesses can be represented by elements with a reduced strength. The influence of local weaknesses on borehole stability under various far-field stress ratios can then be studied.
4. A new approach, recently developed by Vardoulakis (1988), treats borehole stability as a bifurcation phenomenon. This approach appears promising because it can distinguish between the two dominant modes of failure: the formation of shear bands and the buckling of slabs at the borehole wall under uniform far-field

stresses. The bifurcation analysis is mathematically complex and much more research is needed to verify it. However, some of the concepts of this method will be adopted in conjunction with the finite element analyses.

5. A numerical simulation procedure based upon the boundary element method and a micromechanics model are used to model the progressive spalling of the borehole wall (Ewy et al., 1987). The borehole boundary is discretized into many small elements and the cross section of the borehole is changed by removing elements where the tangential stresses exceed the strength of the rock and by placing new elements at the stable boundary. The stresses are recalculated and the process repeated until a stable borehole shape is reached. More research is needed to investigate the effects of stress concentration at the tip of the breakout and the stress redistribution process before this model can properly simulate failure.

2.2 Factors Affecting Borehole Stability

The initiation and propagation process of yielding around boreholes is influenced by many factors as pointed out in Chapter 1. It is necessary to understand each individual factor better before an elaborate analysis can be carried out. The following serves to highlight some aspects which are currently being studied by different researchers.

2.2.1 Stresses at the Borehole Wall

A solution for the distribution of stresses around a circular opening in an elastic material was first proposed by Kirsch (1898). It shows that the deviatoric stress (difference between tangential stress σ_θ and radial stress σ_r) is greatest at the wall. For materials which satisfy the Mohr-Coulomb yield criterion, yielding is expected to initiate at the opening wall. Once the rock has yielded, stresses must be redistributed and the yield zone propagates into the rock. Santarelli et al. (1986) have shown that non-linear or confining pressure-dependent elasticity can lead to a decrease in tangential stress at the opening wall and to a maximum deviatoric stress at some distance from the wall. The resulting stress distribution is very similar to that near an opening in elastic, perfectly plastic rock (e.g., Obert and Duvall, 1967). Therefore, Santarelli et al. suggested that yield initiation can occur inside the rock and propagate toward the opening wall. This theory provides a possible explanation for the failure mechanism which was observed by Hoek and Brown (1980) where rupture was first noticed inside the rock. This may also help to explain the observation made by many researchers (including Maury, 1987) that yielding is often not experienced at the underground opening wall when the stresses predicted for elastic rock reach the strength. Stress levels exceeding the strength by a factor of two to three are often needed to induce failure.

2.2.2 In Situ Horizontal Far-Field Stress Ratio N

Gough and Bell (1982) suggest that borehole breakouts are caused primarily by shearing in zones of concentrated compressive stresses resulting from non-equal horizontal far-field stresses ($N \neq 1.0$). Zoback et al. (1985) and Haimson and Herrick (1986) suggest that, for homogeneous materials, the angle and extent of the breakout is a function of the strength of the material and the in-situ horizontal far-field stress ratio. The direction of the maximum extent of the breakouts should correspond to the direction of the minor principal stress. Therefore, knowledge of the breakout angle and extent, together with the rock strength properties should permit determination of the in-situ far-field stresses.

Contrary to the findings from the aforementioned authors, Kaiser and Maloney (1987) and Ewy et al. (1987) indicated that knowledge of the borehole breakout angle or extent cannot be used to back-calculate the in-situ far-field stresses with sufficient accuracy. Kaiser and Maloney have shown that the borehole breakout angle is sensitive to the strength of the rock (i.e., the cohesion intercept), and that the direction of the breakout does not necessarily correspond to the direction of the minor principal stress. This is supported by Ewy et al. who found that there is no unique relationship between the in situ stresses and the breakout shape and size. The same breakout angle can be obtained from different combinations of strength and stresses.

2.2.3 Horizontal to Vertical Far-Field Stress Ratio K_0 and Drilling Fluid Density

Drilling fluid is used to remove the cuttings and to apply a support pressure to the borehole wall. The magnitude of the support pressure can be adjusted by varying the density of the drilling fluid (0.0 Mg/m^3 for air, 1.0 Mg/m^3 for water to 2.1 Mg/m^3 for heavy mud). By varying the drilling fluid density, borehole breakouts or excessive deformation may be prevented. Guenot (1987) suggested that four different modes of failure can occur near a borehole depending on the relative magnitude of the support pressure and the horizontal to vertical far-field stress ratio. The principal stresses (tangential σ_θ , radial σ_r , and vertical σ_v) at the borehole wall can be adjusted by changing the support pressure. The four failure modes at the wall are shown in Figure 2.1, and are described as:

- 1) Mode A- Shear surface resembling an onion peel-like shape if $\sigma_\theta > \sigma_v > \sigma_r$
- 2) Mode B- Shear surface resembling a torodial shape if $\sigma_v > \sigma_\theta > \sigma_r$
- 3) Mode C- Shear surface resembling a spiral shape if $\sigma_v > \sigma_r > \sigma_\theta$
- 4) Mode D- Extension mode

Modes A to C are shear failure modes. If the support pressure is much higher than σ_v or σ_θ at the wall, hydraulic fracturing may occur (Mode D). Mode A corresponds to very low support pressure, a condition which is encountered in mining and tunnel construction. It is perceived to be the most common and relevant mode of borehole

instability. Failure Mode A can be seen in the testing of a) an artificial sandstone (Kaiser and Maloney, 1987) and b) a coal under a combination of shear and buckling, etc. (Kaiser et al., 1985). Modes B and C are seldom observed and remain to be confirmed by laboratory and field testing. A diagram was proposed by Guenot (1988) to indicate which mode of failure is expected as a function of drilling fluid density and in situ stress ratio K_0 . This approach may be suitable for parametric study and remains to be verified experimentally.

2.2.4 Temperature

Because temperature increases with depth, the circulating drilling fluid tends to cool the rock in the lower part of a borehole and warm it up in the upper part. The temperature change caused by the drilling fluid induces thermal stresses in the immediate vicinity of the borehole. These thermal stresses may be beneficial or detrimental to borehole stability. Guenot and Santarelli (1988) and Kaiser and Maloney (1987) have shown that cooling may increase or decrease borehole stability or change the failure mode. Heating of the rock tends to decrease borehole stability and it may be necessary to increase the drilling fluid density in order to keep the borehole in a stable condition. Kaiser and Maloney (1987) have also indicated that increasing mud weight and simultaneous cooling may promote breakouts when $N \neq 1.0$.

The effects of drilling fluid density and temperature can drastically modify the state of stress near a borehole. Hence, proper

control of drilling fluid density and temperature may be an effective means of preventing or controlling brittle borehole failures.

2.2.5 Weakness planes

Babcock (1978) suggested that borehole breakouts were the result of drilling through steeply dipping fractures. His hypothesis is based on the assumption that, depending upon the orientation and location of a weakness plane, shear stresses vary and may exceed the strength of these weaknesses. Analytical solutions for determining the extent of the yield zones are given by Daemen (1983) who compared the shear stresses in elastic rock on a given plane with its shear strength. These solutions may be applicable to estimation of the yield initiation zone. Parametric studies based on a similar approach can be found in Kaiser and Maloney (1987), who studied the combined effects of drilling fluid temperature and weakness planes on the extent of potential yield initiation zones.

This brief summary introduces only some of the important factors contributing to the stability of a borehole. Much more research is needed to enhance our understanding of the borehole failure mechanisms.

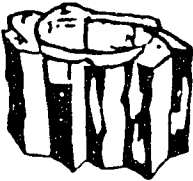
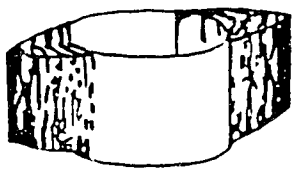
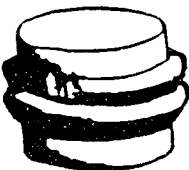
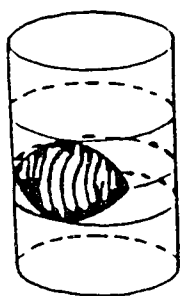
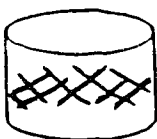
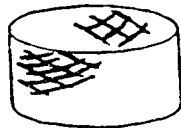
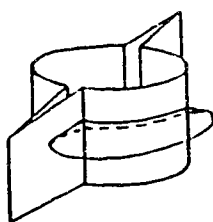
Failure Mode	Horizontal In Situ Stresses	
	Uniform $N=1$	Non-uniform $N \neq 1$
MODE A ($\sigma_{\theta} > \sigma_v > \sigma_r$) SHEAR		
MODE B ($\sigma_v > \sigma_{\theta} > \sigma_r$) SHEAR		
MODE C ($\sigma_v > \sigma_r > \sigma_{\theta}$) SHEAR		
MODE D EXTENSION		

Figure 2.1

Modes of Rupture Initiation near Borehole
(Modified from Maury, 1987).

3 INVESTIGATION OF BOREHOLE INSTABILITY BY EIGENVALUE ANALYSES

3.1 Introduction

Most of the research work on borehole stability is aimed at predicting the extent of the yield zones, the convergence and the internal support pressure at failure. Less attention is given to distinguishing the factors which contribute to the formation of various observed failure modes. Vardoulakis et al. (1988) have recently attempted, by application of the bifurcation theory, to distinguish, analytically, two of the many commonly observed failure modes (formation of shear bands and slabbing). Bifurcation of a deformation process means that at some critical state, the continuing deformation process may branch into two (or more) entirely different modes. Typical examples are: bulging, buckling, shear band or kink band formation commonly observed in unconfined compression tests. Mathematically, bifurcation means that the equations describing the equilibrium condition do not provide a unique solution.

There are basically two approaches to study deformation process at bifurcation. The first approach is based on several simplifying assumptions with respect to material behaviour, loading history and boundary conditions. It is necessary to derive complete solutions for the stress and strain field of a problem in order to predict the modes of deformation at bifurcation. Detail formulation of problem and solution process involved in bifurcation analyses can

be found in Vardoulakis et al. (1978) and Vardoulakis (1984). Analytical solutions for bifurcation analyses are mathematically complex even under simple boundary conditions. The analytical solution depends strongly on the assumed constitutive relationships and therefore parametric studies for different material behaviour under more complicated boundary conditions become extremely difficult.

An alternative approach, to study the deformation process at bifurcation, is to simulate the loading process by finite element analyses. The advantage of the finite element method over closed-form solutions is that it is general enough to be applied to most boundary value problems. More than one incremental displacement solution is possible at the point of bifurcation but each will satisfy the equilibrium equations. This loss of uniqueness can take place when the incremental global stiffness matrix becomes singular (i.e., when the determinant of the incremental global stiffness matrix becomes equal to zero). This condition can be detected by checking whether the lowest eigenvalue of an incremental global stiffness matrix approaches zero (Hill, 1959). The eigenvectors belonging to the eigenvalues which are equal to zero represent different possible modes of deformation at bifurcation. The procedure in the finite element analysis involves an evaluation of the incremental global stiffness matrix and performing an eigenvalue analysis at each loading step.

The finite element method was adopted to study bifurcation problems by de Borst (1986) who studied the development of shear bands in the biaxial testing of sands. De Borst showed that the

formation of shear bands at bifurcation can be clearly represented by the eigenvectors belonging to the lowest eigenvalue. The inclination angle of the shear bands agree very well with those predicted analytically and measured in experiments. The finite element method was also applied to the problem of rock bursting by Bardet (1988). Rock bursting is a violent failure process encountered in deep underground excavations in brittle rock. It involves a rapid convergence and oscillation of the excavation walls, followed by slabbing and failure of the rock. Vardoulakis (1984) analysed this instability mode as a surface instability phenomenon. Bardet (1988) showed: 1) that the stresses from the finite element method at the onset of surface instability agree with those analytically calculated following Biot (1965), and 2) that surface instability may be induced by several modes of deformation with closely spaced eigenvalues which are not considered in the bifurcation analysis by Vardoulakis (1984). This example shows that the finite element method has advantage over the analytical method in the evaluation of modes of deformation.

Borehole instabilities was studied by Vardoulakis et al. (1988) as bifurcation phenomena. For a deep borehole situated in a homogeneous isotropic medium subjected to a uniform stress at infinity, the basic mode of deformation is the uniform closure of the borehole wall. Vardoulakis et al. (1988) found, analytically, that another possible bifurcation mode, which also satisfies the homogeneous boundary condition, is the warping of the borehole wall. Vardoulakis et al. (1988) suggested that this warping may lead to the two, frequently observed failure modes: 1) the formation of

shear bands at the borehole wall, and 2) the buckling of slabs due to activation and subsequent unstable propagation of pre-existing latent cracks parallel to the surface (Figure 3.1). Whether shear bands will form or slabbing occur depends on the material parameters (angle of friction) and on the assumption that the material is rigid-plastic with strain hardening and dilatant behaviour.

The objective of this study is to assess whether it is possible to use the finite element method to detect the bifurcation point of a borehole when the internal pressure is gradually reduced. It is not intended to compare the modes of deformation with that found in Vardoulakis et al. (1988) because the constitutive relationship used in this study is different from their assumptions. Rather, it is hoped that this study will provide an understanding on the eigenvalue approach on the problem of bifurcation of boreholes using the finite element method.

3.2 Physical Meaning of Eigenvalues and Eigenvectors

In order to understand the significance of eigenvalue analysis, it is necessary to first consider the quantity termed the perturbation energy. Perturbation energy is a measure of the stability of a structure subjected to a slight external disturbance. It is defined as:

$$w = \int_V \langle \Delta \sigma_{ij} \rangle \{ \Delta \epsilon_{ij} \} dv \quad (3.1)$$

where,

$\Delta\sigma_{ij}, \Delta\epsilon_{ij}$ = Incremental stress and incremental strain tensors respectively;

dv = Differential volume element for integration.

For elastic and strain hardening materials, the perturbation energy is always positive. For perfectly plastic material, it is zero and for strain softening material it is negative. Therefore a zero or negative perturbation energy indicates unstable behaviour. The perturbation energy is different from plastic work since work is still required to deform a perfectly plastic or strain-softening material, and plastic work is always positive.

Expressing the incremental stress strain relationship of a material as:

$$\Delta\sigma_{ij} = C_{ijmn} \Delta\epsilon_{mn} \quad (3.2)$$

where,

C_{ijmn} = Incremental stress strain relationship;

and substitute Equation 3.2 into Equation 3.1. Equation 3.1 then becomes:

$$w = \int_V \Delta\epsilon_{ij} C_{ijmn} \Delta\epsilon_{mn} dv, \quad (3.3)$$

Let us now study the relationship between Equation 3.3 and eigenvalue. In the formulation of a finite element analysis, the following general type of nonlinear equilibrium equation is arrived:

$$[K] \{\Delta\delta\} = \{\Delta R\} \quad (3.4)$$

where,

$[K] = \int_V [B]^T [C] [B] dv$ (Global stiffness matrix);

$[B] =$ Strain displacement matrix;

$[C] =$ Constitutive matrix;

$\{\Delta\delta\} =$ Incremental displacement vector;

$\{\Delta R\} =$ Incremental external load vector.

Given an externally applied load increment, $\{\Delta R\}$, the displacement increment, $\{\Delta\delta\}$, defined in this manner is solved. Because the equations of equilibrium will not be satisfied exactly in a numerical analysis, an iterative procedure is required to ensure that the error is small and will not be accumulated in subsequent load steps. Discussions on the numerical iterative procedure and convergence scheme used in SAGE (code used for this analysis) are presented by Chan (1986). For a stable structure, unique solutions for the displacement increment, $\{\Delta\delta\}$, can be found and there is only one set of displacement increments that satisfy equilibrium under a given set of boundary conditions. When the structure becomes unstable, however, the deformation process may bifurcate or branch into entirely different modes. Mathematically, bifurcation means

that there are more than one set of displacement increment solution. This loss of uniqueness can take place when the global stiffness matrix, $[K]$, becomes singular (i.e., the determinant of $[K]$ becomes equal to zero).

The eigenvalues, λ , for a global stiffness matrix, $[K]$, by mathematical definition, is given as:

$$[K] \{\Delta\delta\} = \lambda \{\Delta\delta\} \quad (3.5)$$

Multiplying both sides by $\langle\Delta\delta\rangle$, Equation 3.5 becomes:

$$\langle\Delta\delta\rangle [K] \{\Delta\delta\} = \langle\Delta\delta\rangle \lambda \{\Delta\delta\}$$

or,

$$\langle\Delta\delta\rangle [K] \{\Delta\delta\} = \lambda = \text{constant} \quad (3.6)$$

After substituting $[K] = \int_V [B]^T [C] [B] dv$ into Equation 3.6, it becomes:

$$\int_V \langle\Delta\delta\rangle [B]^T [C] [B] \{\Delta\delta\} dv = \lambda \quad (3.7)$$

Since $\langle\Delta\delta\rangle [B]^T = \langle\Delta\epsilon\rangle$, where $\langle\Delta\epsilon\rangle$ is the incremental strain vector, therefore Equation 3.7 becomes:

$$\int_V \langle\Delta\epsilon\rangle [C] \{\Delta\epsilon\} dv = \lambda \quad (3.8)$$

By comparing the form of Equations 3.3a and 3.8, it can be seen that the eigenvalues of the global stiffness matrix are related to the perturbation energy. Zero perturbation energy and zero eigenvalue

indicate that the structure is unstable. If there is more than one zero eigenvalue, it is possible to have more than one mode of deformation. Therefore the instability point also corresponds to the bifurcation point. It is now clear that bifurcation can be detected by searching for more than one zero eigenvalue of $[K]$ in the finite element analysis. However, in a numerical process, the point at which the lowest eigenvalue becomes exactly zero cannot be detected (de Borst, 1986), therefore we may take approximation and consider small eigenvalue being equal to zero. Since the eigenvectors in Equation 3.6 are the displacement increments, they represent different modes of deformation at bifurcation.

3.3 Deformation Mode Assessment by Eigenvalues and Eigenvectors

Before investigating the possible modes of deformation of an unstable borehole, the eigenvalues and eigenvectors of the constitutive matrix of a single element for a linear elastic and a linear elastic, perfectly plastic material will be considered in order to understand the basic modes of deformation under simple boundary conditions. The results of the eigenvalue analyses are shown in Figure 3.2. For a linear elastic material under plane strain conditions, the minimum energy required to deform an element is by pure shearing as indicated by the lowest eigenvalue. The remaining two modes of deformation are extension/compression, and uniform extension (or uniform compression). It shows that the eigenvalues

for an elastic material are always positive, indicative of a stable deformation process.

For a linear elastic, perfectly plastic material, the confined compression test is considered. In this case, the vertical stress is increased until yielding occurs and then the stress dependent constitutive matrix is evaluated. The Mohr-Coulomb yield criterion is assumed. The same three modes of deformation are found. For a perfectly plastic material, the eigenvalue is zero at the yield point indicating the deformation process is in a state of an unstable equilibrium. The extension/compression deformation mode has the lowest eigenvalue ($\lambda=0$).

At the bottom of Figure 3.2, a Mohr strain circle is constructed from the eigenvector belonging to the zero eigenvalue. In the Mohr strain circle, Point A represents the extension/compression mode of a plane normal to the direction of the minor principal stresses σ_3 . Point B corresponds to the plane, or line, of zero extension of the same mode. Since every point on the strain circle has the same eigenvalue, points A and B represent the same mode of deformation, only they are looking from a different frame of reference. According to the strain circle, the inclination of the failure plane in a material with $\phi=45^\circ$ takes place on a plane inclined at $\psi=67.5^\circ$. This is exactly the inclination of the failure plane expected from limit equilibrium stress considerations (see Mohr stress circle in Figure 3.2). In the laboratory testing of soil samples under confined compression conditions, it is often found that slip planes will form at large strain. Also the inclination angle of the slip planes are sometimes relatively close to that predicted from the Mohr stress circle. The following

section will show that slight inhomogeneities in the material may change the deformation process from one mode to another.

3.4 Shear Band Formation in Confined Compression Test

In this section, a plane strain, confined compression test is simulated numerically using the finite element method. The material is assumed to be transversely isotropic with its strength being a function of the orientation of the weakness planes relative to the principal stresses (model introduced by Nova and Sacchi, 1979). The details of this model and the material parameters adopted will be discussed in Chapter 5. The finite element idealization of the specimen is shown in Figure 3.3. The left vertical and bottom boundary were assumed to be perfectly smooth with free vertical and horizontal movement boundaries, respectively. An element with a reduced strength relative to the surrounding elements was placed on the right edge at mid height to introduce non-homogeneous deformation or imperfection in the specimen. Hence, yielding will have to initiate at this location. The loading of the sample is simulated by controlling the displacement at the top while keeping the confining pressure σ_3 constant.

The results of the analysis are presented in Figure 3.4. Without the weak element, the strain within the specimen is uniform and therefore the shear strength is mobilized everywhere at the same time. The resulting mode of deformation is uniform as expected from the previous eigenvalue analysis of the constitutive matrix.

However, a slight imperfection within the specimen causes a localization and leads to the formation of two shear bands. The development of the yield zone at three stages of the test is shown in Figure 3.4. Yielding is initiated at the single weak element and propagates at 45° to the direction of the minor principal stress (for $\phi=0^\circ$). These yield zones propagate in the form of narrow bands until they reach the specimen boundary. During subsequent deformation, the bands get wider. The angle of the shear band (at 45° to the direction of the principal stresses) is as expected from limit equilibrium considerations ($\psi=45^\circ+\phi/2=45^\circ$ if $\phi=0^\circ$).

This example demonstrates that imperfections in a body can change and often dominate the deformation process. Although the inclination angle of the shearing planes from finite element simulation agree with that from limit equilibrium consideration, the shearing mode results from weak element introduction cannot be treated as true bifurcation. In the following section, the possible modes of deformation of a circular opening will be investigated without imperfections in the material, loading and boundary conditions.

3.5 Modes of Deformation of a Circular Opening (Borehole)

In this study, plane strain conditions are assumed to be representative for a deep section of a borehole. Wall deformations are assumed to take place in a plane normal to the borehole axis (i.e., the problem can be treated as a 2D plane strain case). The borehole is situated in a homogeneous, isotropic rock mass, and subjected to a

uniform, constant stress at infinity. The material behaviour is treated as linear elastic, perfectly plastic satisfying the Mohr-Coulomb yield criterion. Yielding is induced by gradually reducing the internal pressure in the borehole. At each step of pressure reduction, the eigenvalues and the corresponding eigenvectors of the global stiffness matrix are calculated using a standard library subroutine program IMSL (1987). Appendix A provides a brief description of how this subroutine program is implemented into SAGE. The analysis is continued until the error in convergence cannot be reduced below the allowable tolerance (0.0001) within 50 iterations. The error in convergence is defined as:

$$\text{error} = \frac{|\Delta \delta^i|}{|\delta^i|} \leq \text{tolerance} \quad (3.4)$$

where,

- $|\Delta \delta^i|$ = Norm of the change in incremental nodal displacements of the whole structure at iteration i ;
- $|\delta^i|$ = Norm of the total nodal displacements of the whole structure at iteration i .

Two different mesh densities (Mesh A with 56 elements and Mesh B with 128 elements) were employed to study the effects of mesh refinement on the eigenvalues (Figure 3.5).

The normalized ground convergence curve (u/u_c , where u_c = convergence of the unsupported opening in an elastic material) for

both meshes A and B is shown in Figure 3.6. The convergence is the same everywhere because the horizontal far-field stress ratio N is equal to unity. The two convergence curves are identical and demonstrates that the amount of displacement at the borehole wall is not affected by the mesh refinement. The analysis was temporarily stopped at $P_i=16.4\%$ because further pressure reduction will cause the error in convergence greater than the allowable tolerance. P_i is the pressure inside the borehole normalized to the maximum far-field stress ($P_i = \frac{P_s}{\sigma_H} N$, p_s is the actual support pressure). The analysis was then continued by prescribing uniform displacements at the borehole wall using Mesh B only. Very small displacement of 0.005 mm was prescribed and the eigenvalues and eigenvectors of the global stiffness matrix were again evaluated. The analysis was finally stopped at $u/u_c = 6.23$ because it was found that further prescribing displacements did not render any changes in the eigenvalues and eigenvectors. Minimum λ/E at this last step was found to be 0.0010.

The first seven lowest eigenvalues for Mesh A are plotted as a function of P_i in Figure 3.7a. The lowest λ/E value starts to decrease at $P_i=30\%$, and the curve is relatively steep at $P_i=16.4\%$. The lowest λ/E for Mesh A at $P_i=16.4\%$ is 0.0047. This value of λ/E (0.0047) is relatively close to zero. The internal pressure corresponds to zero eigenvalue can be extrapolated from the last point of the curve. If the same extrapolation is done for the rest of the eigenvalues, it is found that they do not converge to the same pressure although they are close. This indicates that the lowest eigenvalue will reach a value

of zero first and there is no other zero eigenvalue. Therefore there is instability but no bifurcation.

Figure 3.7b shows the effect of mesh refinement on the first seven lowest eigenvalues at $P_i=16.4\%$. At $P_i=16.4\%$ (and $u/u_c = 3.89$), the minimum eigenvalue, $\lambda/E=0.0047$, for Mesh A is reduced by 50 % to 0.0024 for the refined mesh. This figure also shows that the difference between the lowest and the seventh lowest λ/E value for the refined Mesh B is lower than that in Mesh A. This may explain the reason that the lowest eigenvalue is not exactly zero or cannot be decreased any more is probably due to numerical accuracy, both mesh refinement and calculation precision.

The eigenvectors at $P_i=16.4\%$ ($u/u_c = 3.89$) for the first seven lowest eigenvalues from Mesh B are presented in Figure 3.8 to scale and are simplified in the schematic diagrams of Figure 3.9. The deformation modes for the first seven lowest eigenvalues are not affected by mesh refinement. Mode 1 corresponds to the uniform closure of the borehole wall. Three other deformation modes are: Mode 2 corresponding to a translation, where the displacements at the borehole wall are of same magnitude and direction, Mode 3, elliptical deformation, where the magnitudes of the displacements are increased on one side and decreased on the adjacent side, and Mode 4 called 'warping mode', where the displacements of the borehole wall create a wave-like shape as described by Vardoulakis (1988).

The uniform closure of the borehole wall (Mode 1) from Mesh B has λ/E equal to 0.0024. We have mentioned earlier that in numerical process, the point at which the eigenvalue is exactly equal

to zero cannot be detected. Therefore, we may consider very small eigenvalue being equal to zero. In this analysis, we may consider the lowest $\lambda/E = 0.0024$ to be zero for the following reasons:

1. The lowest eigenvalue corresponds to an uniform closure of the borehole wall which is expected for a borehole situated in a homogeneous isotropic rock mass subjected to uniform far-field stresses;
2. The structure has reached an unstable point at $P_i=16.4\%$. This means that there should be at least one zero energy mode. Figure 3.7a and 3.7b show that the lowest eigenvalue tends toward zero below $P_i=16.4\%$. The magnitude of λ/E is affected by mesh refinement.

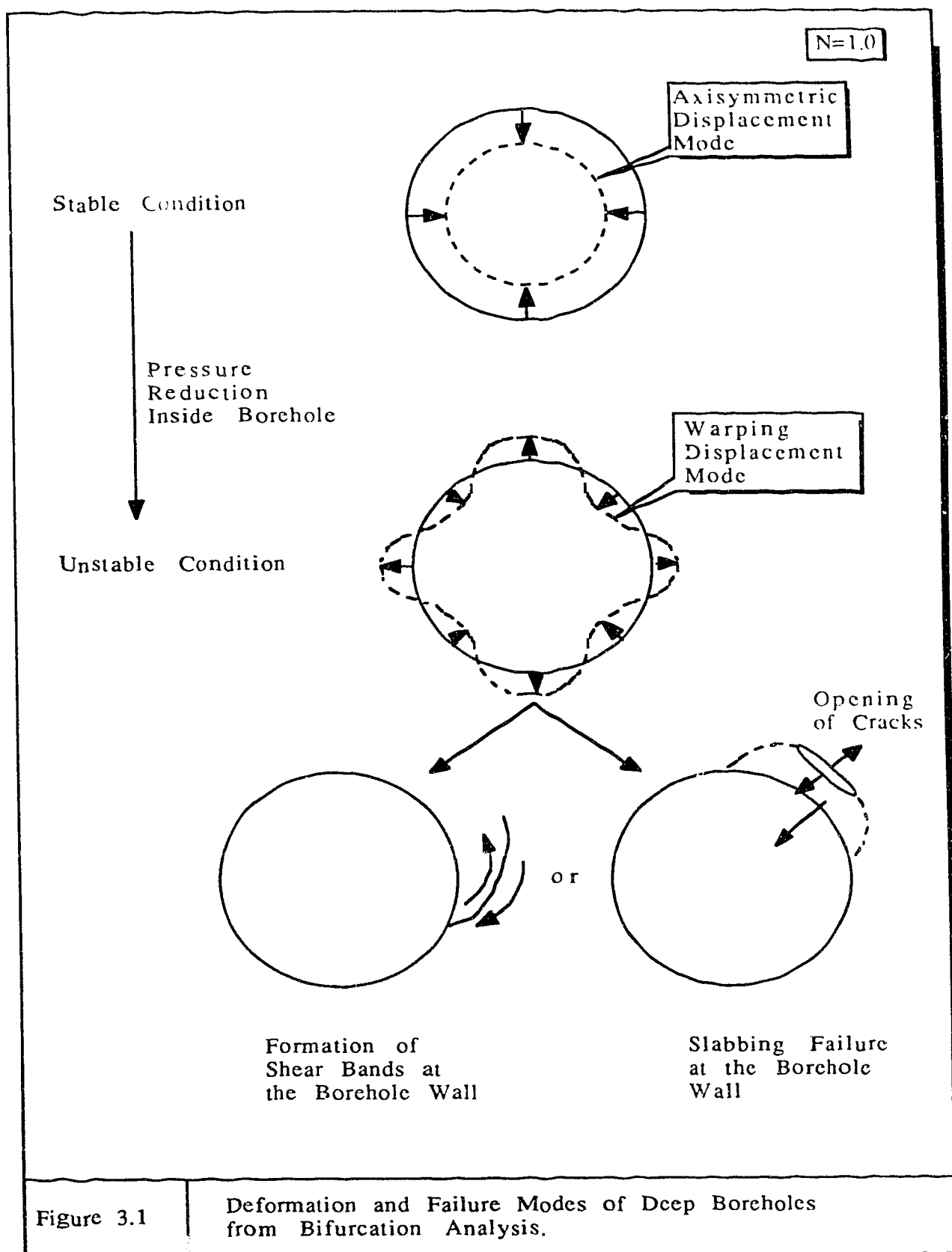
The other six eigenvectors cannot be considered as zero energy mode at this time because their eigenvalues do not converge to zero at pressure below $P_i=16.4\%$. Recall from Section 3.4 that slight imperfections in the material can often change the deformation mode. The eigenvalues for Mode 2 to 4 are higher than for Mode 1 but they are relatively close together. This may suggest that each of the three modes may govern the deformation process if slight disturbances favour their formation. Such disturbances near the borehole may be induced by local variations (e.g., due to rock stiffness variations) or by weaknesses (discussed in later chapter).

3.6 Summay and Conclusions

The lowest eigenvalue obtained in this study is not exactly zero, but it is small enough to be considered as zero. The approach described in this chapter deserves further study because it is general enough to be applied to most boundary value problems. It is recommended in the future study that more refined mesh to be used to gain an understanding of the trend of the eigenvalues.

For a borehole situated in a homogeneous isotropic rock mass subjected to uniform far-field stresses, the basic mode of deformation for a stable borehole is the uniform closure of the borehole wall. Other modes of deformation (translation, elliptical deformation, or warping) may become dominant depending upon the influence of imperfections near the borehole. The warping mode of deformation proposed in the analytical bifurcation analysis by Vardoulakis (1988) happens to be one of the deformation mode found in this study with eigenvalue relatively close to zero. The translation and elliptical modes of deformation found in this study deserve further study by analytical bifurcation analysis and laboratory verification.

From the finite element simulation of a confined compression test, it is found that slight imperfections in the specimen can change the failure mechanism from the basic homogeneous deformation to the formation of shear bands or zones. This aspect of change of failure mechanisms has initiated the investigation of the effects of imperfections on deep borehole failure mechanisms which will be discussed in the following chapters.



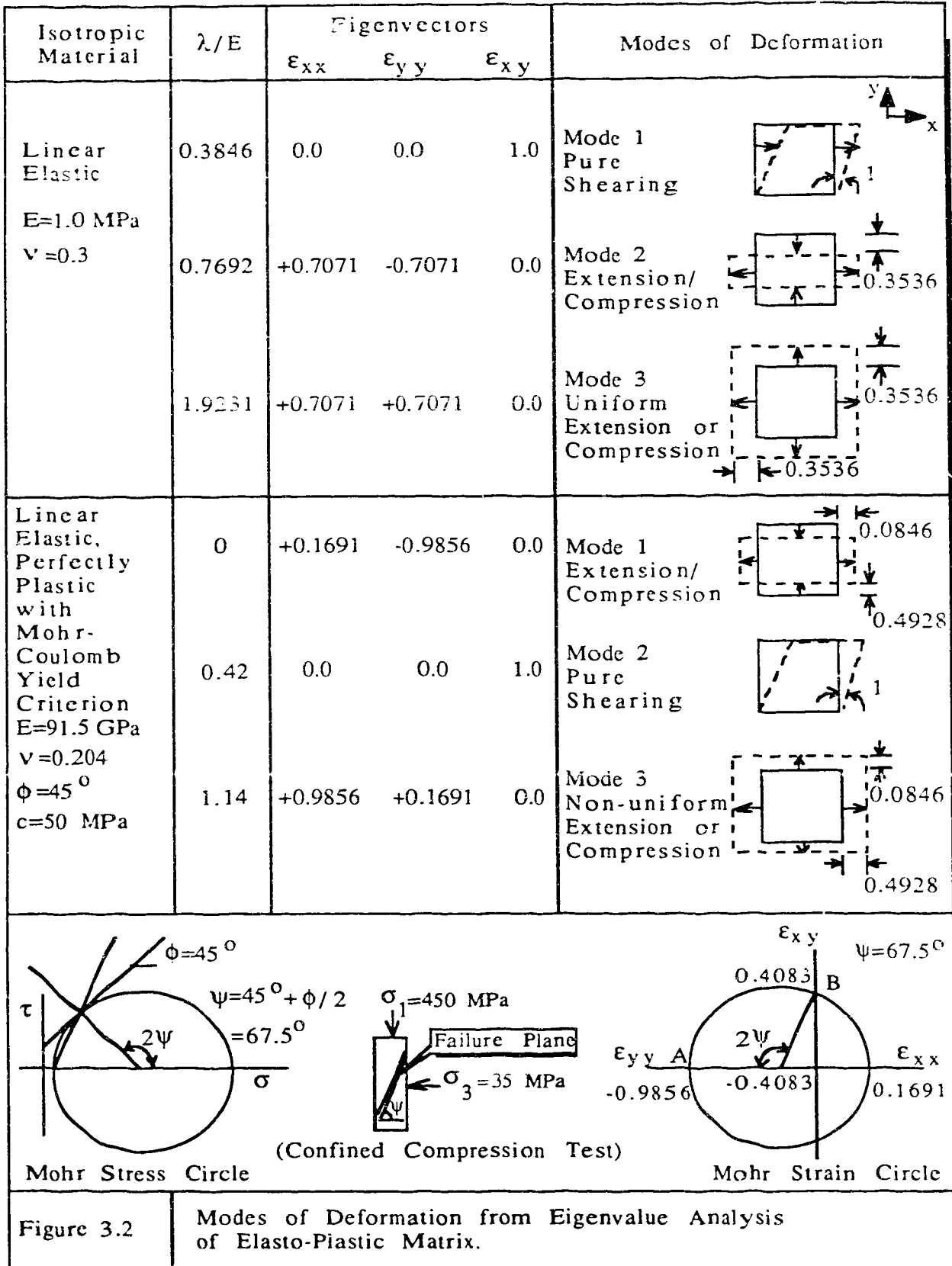


Figure 3.2

Modes of Deformation from Eigenvalue Analysis of Elasto-Plastic Matrix.

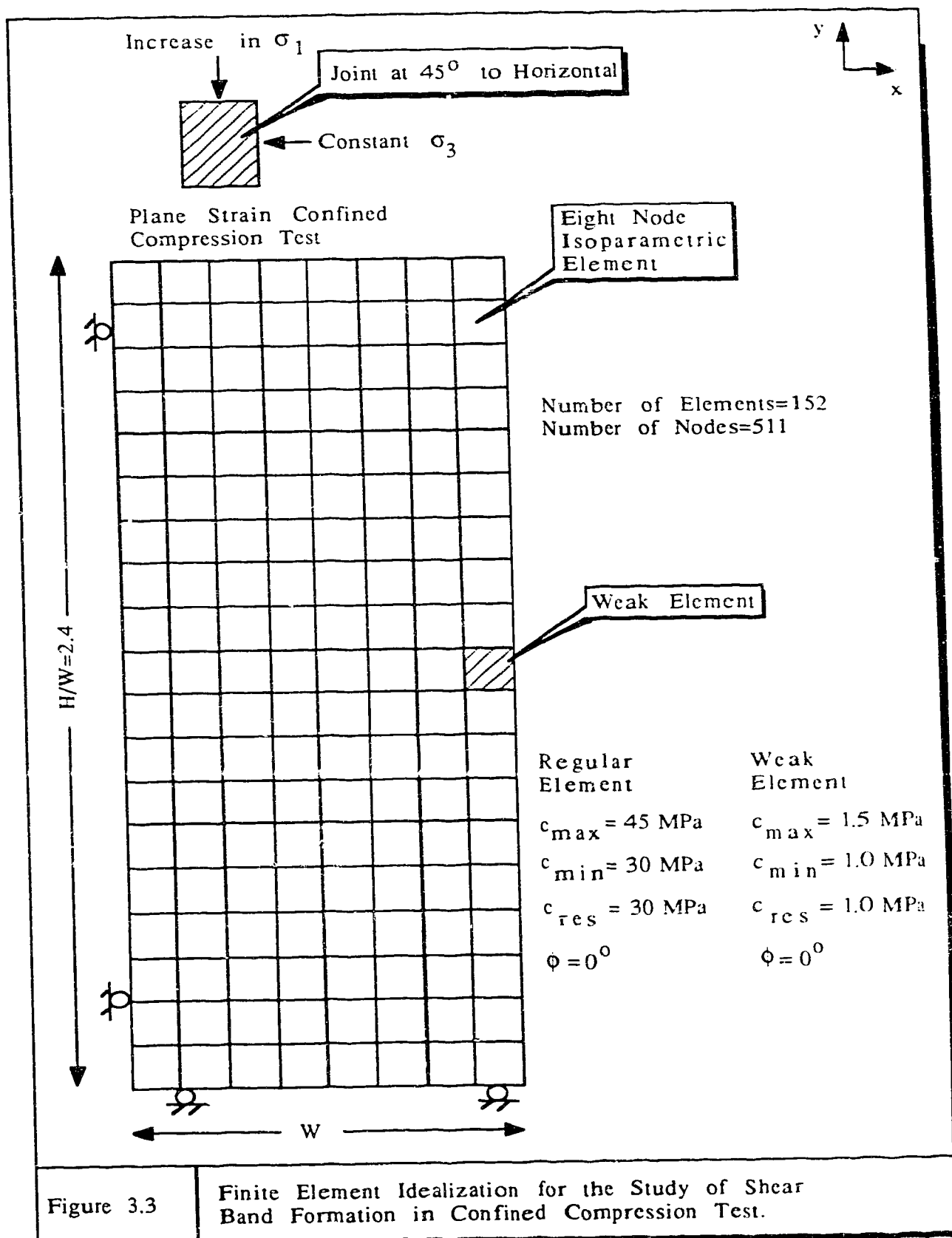
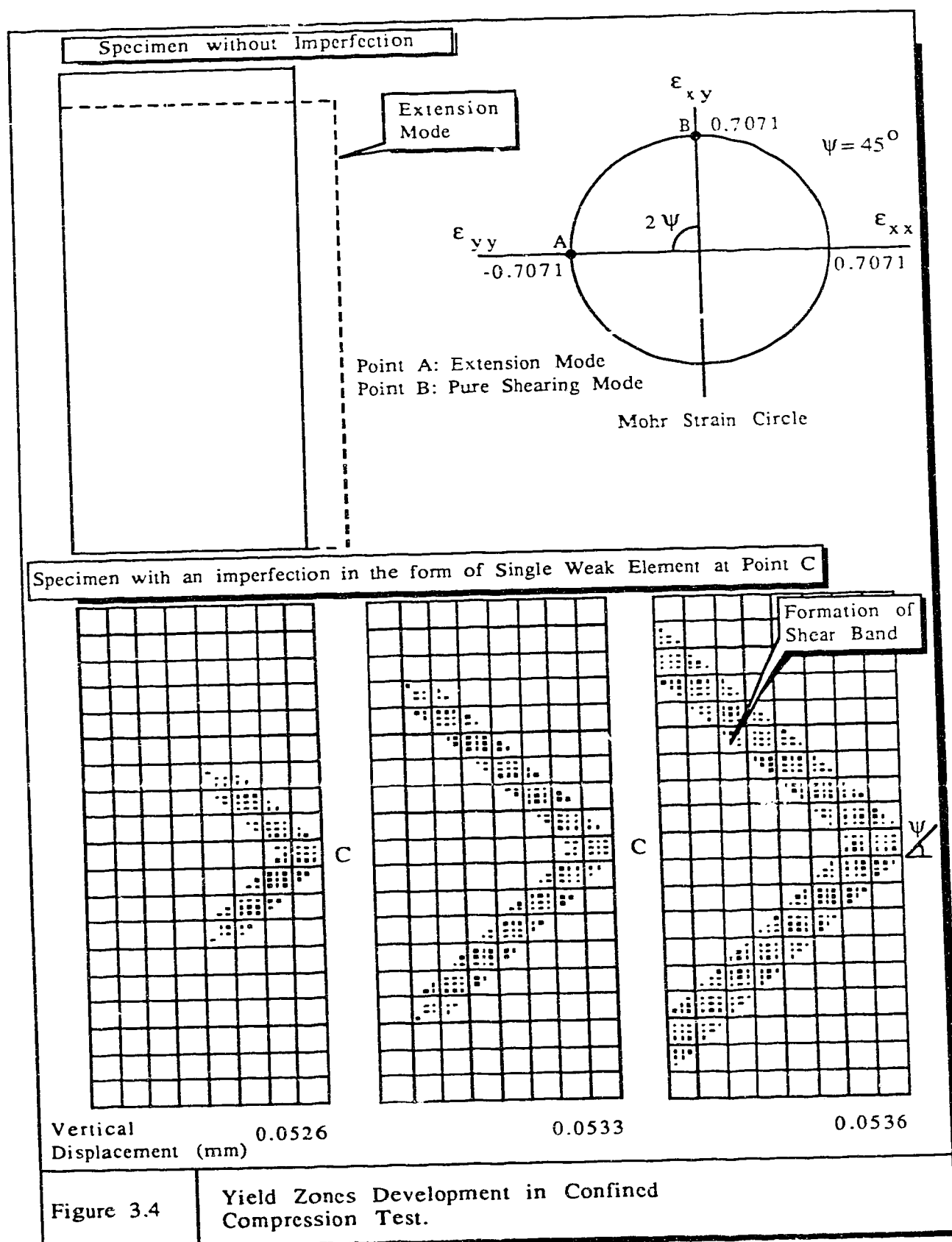
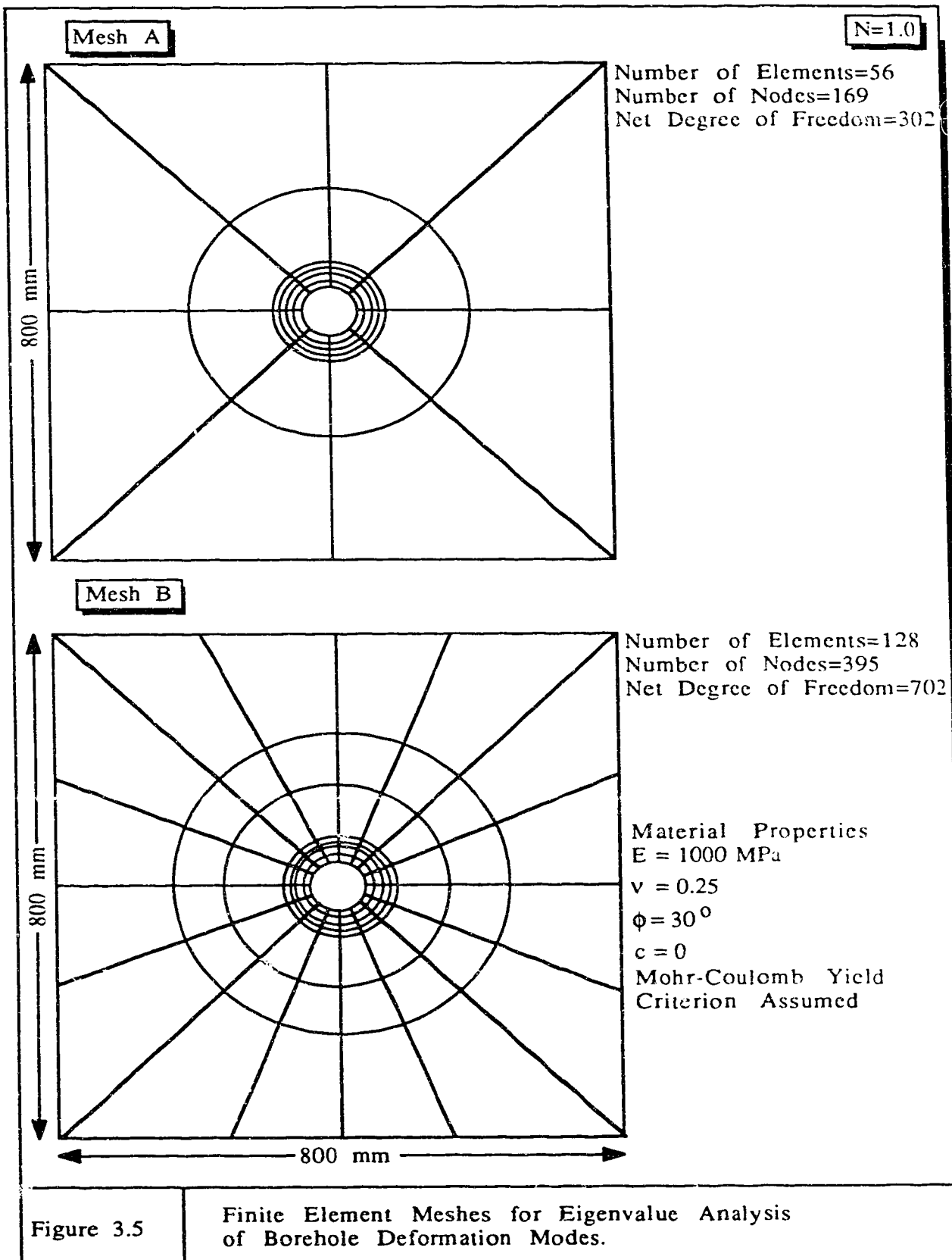
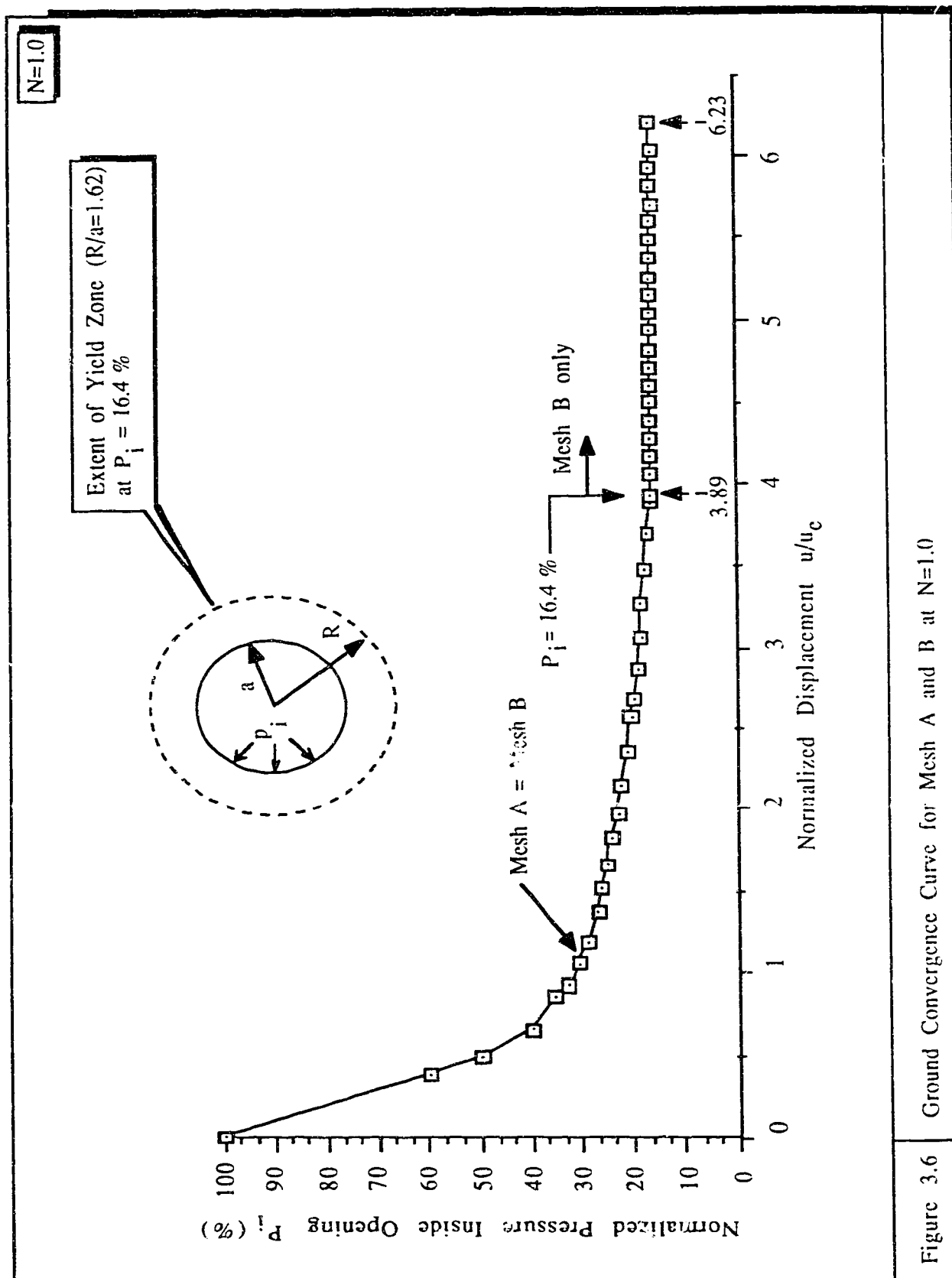


Figure 3.3

Finite Element Idealization for the Study of Shear Band Formation in Confined Compression Test.





Figure 3.6 Ground Convergence Curve for Mesh A and B at $N=1.0$

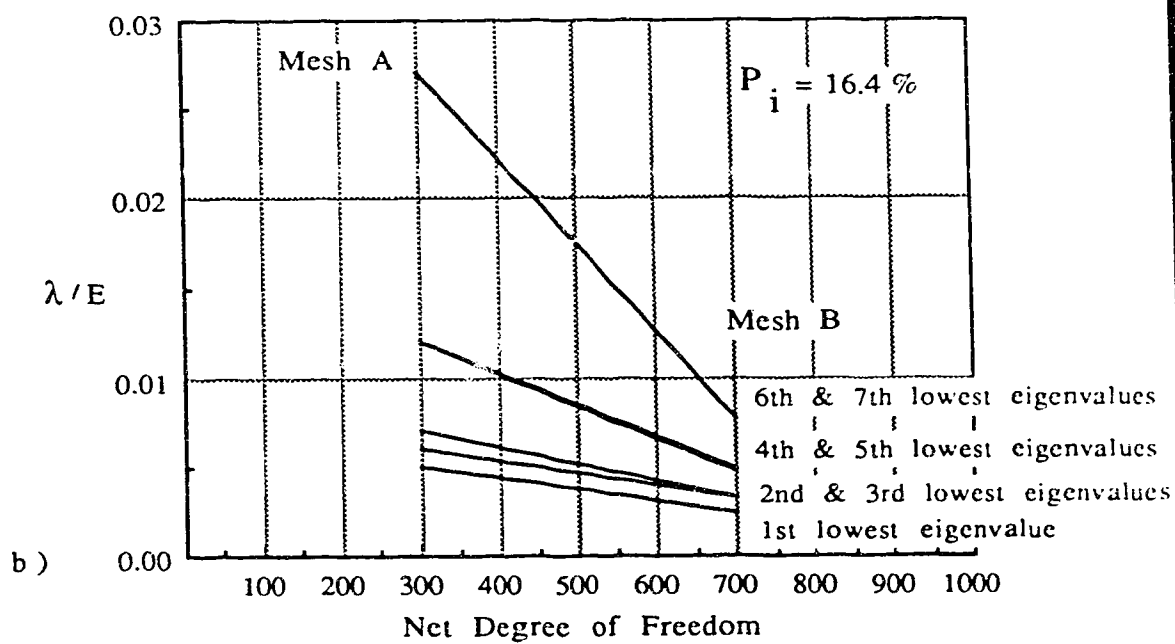
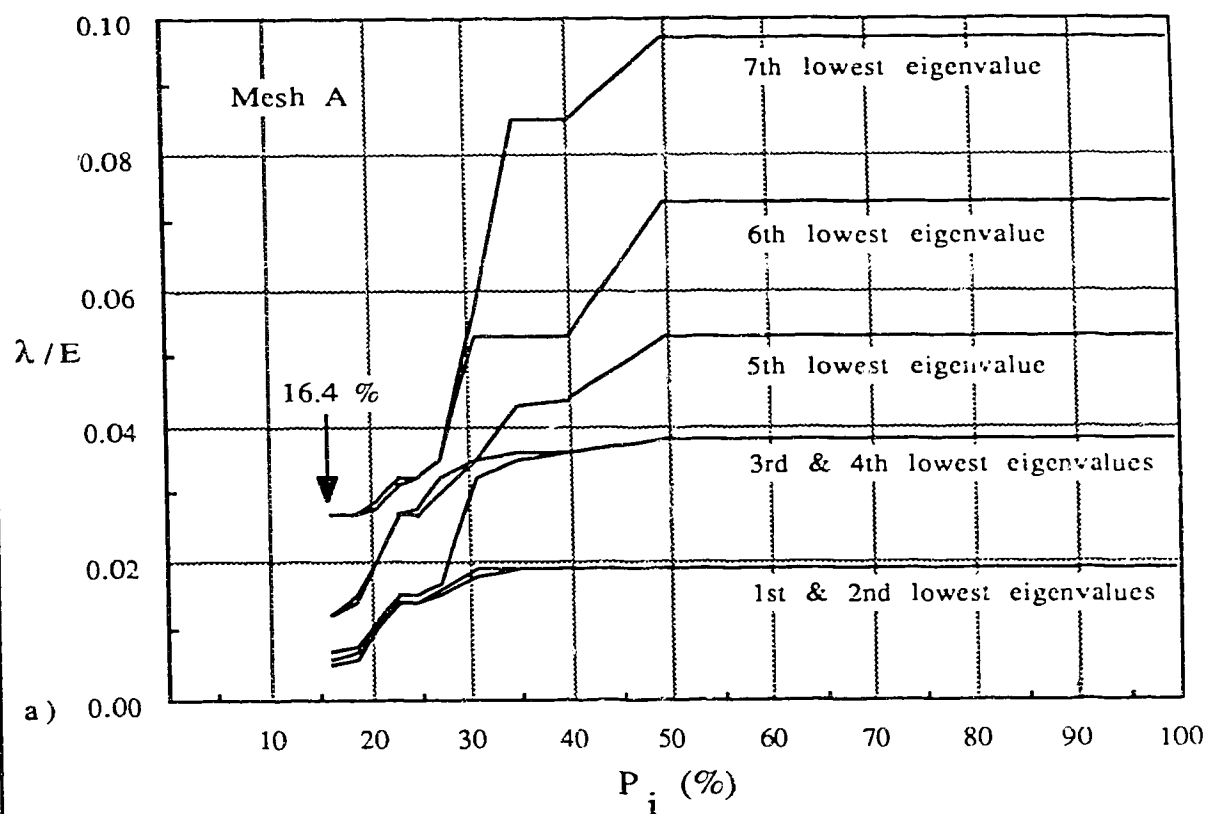
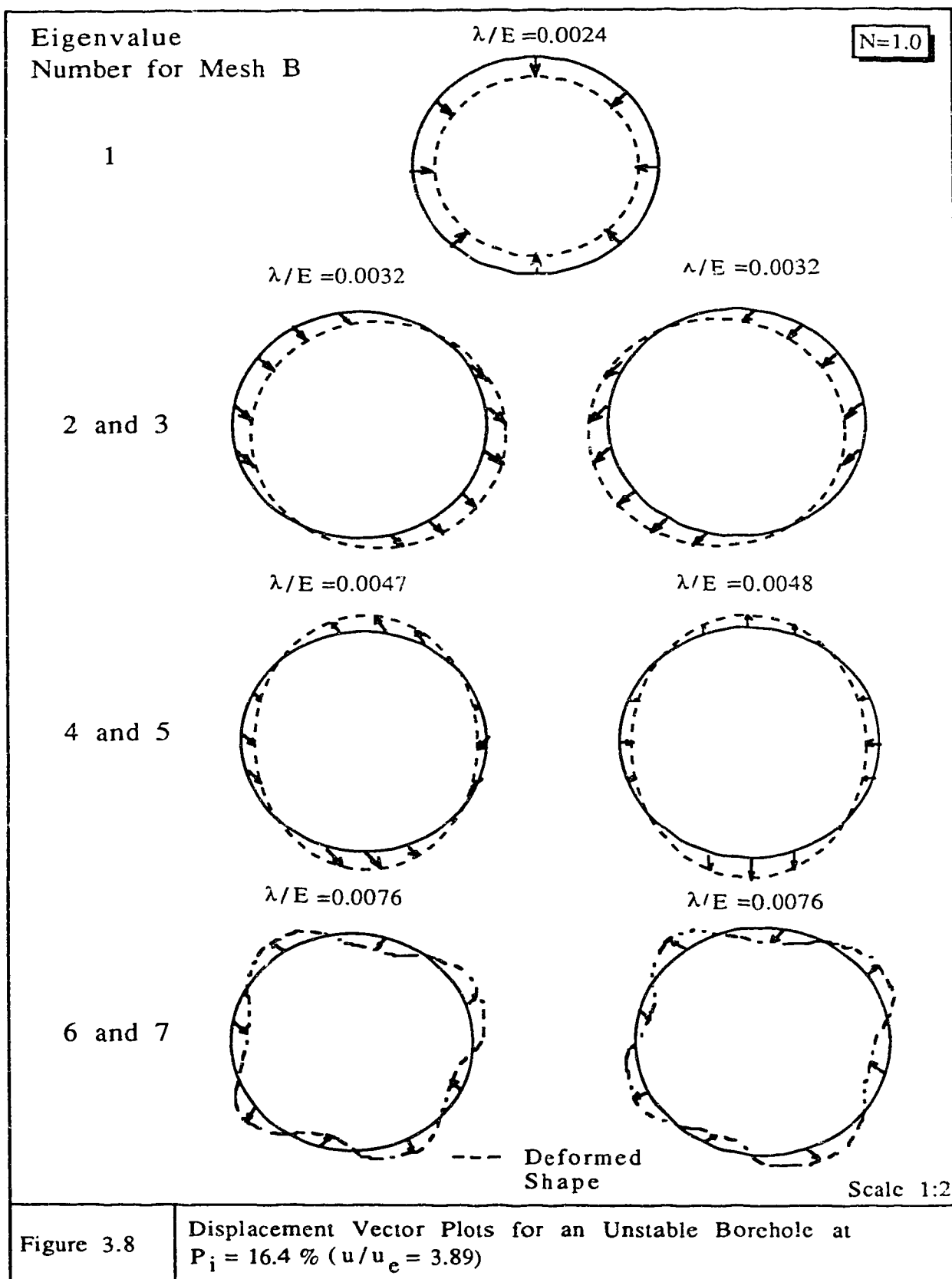


Figure 3.7

Eigenvalues versus Pressure for Mesh A



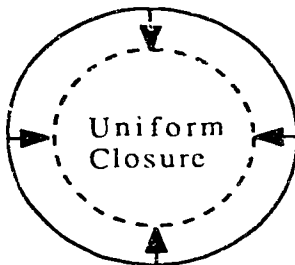
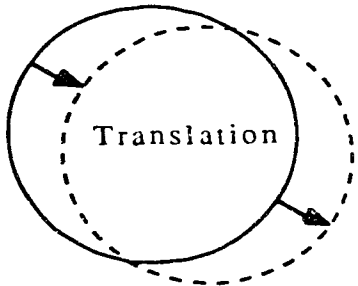
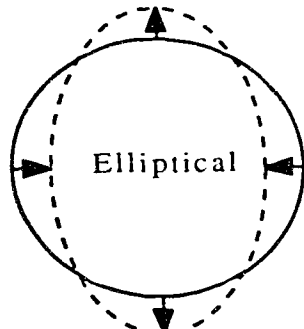
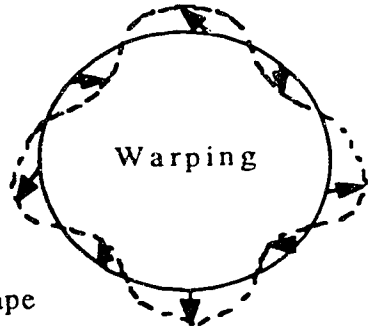
Mode	Eigenvalue Number	Eigenvalue λ/E		Mode of Deformation	
		Mesh A	Mesh B		
①	1	0.0047	0.0024	 <p>Uniform Closure</p>	
②	2	0.0062	0.0032	 <p>Translation</p>	
	3	0.0065	0.0032		
③	4	0.0123	0.0047	 <p>Elliptical</p>	
	5	0.0123	0.0048		
④	6	0.0269	0.0076	 <p>Warping</p>	
	7	0.0271	0.0076		
<p>----- Deformed Shape</p>					

Figure 3.9

Modes of Deformation for an Unstable Borehole at $P_i = 16.4\%$ ($u/u_e = 3.89$)

4 EFFECTS OF WEAKNESSES ON BOREHOLE FAILURE MECHANISMS

4.1 Introduction

Chapter 3 has also shown that slight imperfections in a homogeneous specimen can change the failure mechanism from homogeneous yielding to the formation of localized yield zones. The objective of this component of the research was to investigate, by finite element simulations, various failure mechanisms of a borehole in the presence of imperfections such as fissures and joints. Depending upon the size of borehole relative to the weaknesses, and also their orientation and distribution in a rock mass, there are many possible configurations and locations for local weaknesses to intersect a borehole wall. It is not intended that all possible cases be studied, but rather, to investigate whether the presence of local weaknesses change the failure mechanisms of a borehole, and to capture the development of such a failure mechanism by finite element simulations.

In this finite element study, weaknesses are represented by elements of reduced strength.

4.2 Simulation of Borehole Drilling by Finite Element Method

The analyses were conducted with the finite element code SAGE, developed by Chan (1986). Figure 4.1 shows the finite element mesh which is composed of 8-node quadrilateral, isoparametric elements outside the borehole and 6-node triangular isoparametric elements inside the borehole. Displacements are prevented in the x-direction along the center line of the borehole and in the y-direction along the bottom boundary.

The simulation sequence is illustrated in Figure 4.2. The analysis of the different cases introduced later followed the steps listed below:

- Step 1. Apply initial stresses to all elements by loading the right boundary with the minimum horizontal far-field stresses (σ_h) in the horizontal x-direction and the upper boundary with the maximum horizontal far-field stresses (σ_H) in the horizontal y-direction. The horizontal far-field stress ratio N is given as the ratio of σ_h to σ_H . (The borehole is drilled in the vertical z-direction and plane strain conditions are assumed).
- Step 2. Remove elements inside the borehole. Determine the unbalanced nodal forces at the borehole boundary.
- Step 3. Reinstate the initial stresses by applying nodal forces at the borehole boundary equal but opposite in direction to those determined in Step 2.
- Step 4. Change the properties of all elements to linear elastic, perfectly brittle plastic. Select the location of weaknesses and

change the properties of corresponding elements to weak element properties.

Step 5. Simulate drilling by proportionally and incrementally reducing the nodal forces around the periphery of the borehole.

Step 6. Repeat Step 5 until the error in convergence cannot be reduced below the allowable tolerance (0.001) within 50 iterations. Tolerance is defined as the ratio of the norm of the change in incremental nodal displacements of the whole structure at iteration i to the norm of the total nodal displacements of the whole structure at iteration i (see Equation 3.4).

The Von Mises yield criterion was used for all the elements. The elements represent weak rocks such as chalk (Hoek and Bray, 1977) and their properties are summarized below:

	Rock Mass Local Weaknesses	
Peak Uniaxial Yield Strength (MPa)	5	1
Residual Uniaxial Yield Strength (MPa)	1	0.2
Young's Modulus E , (MPa)	1000	1000
Poisson's Ratio, ν	0.25	0.25

4.3 Selection of Location for Weaknesses

Because the weak elements have a reduced strength, yielding is expected to occur first at them. Once yielding is initiated, a further reduction of support pressure inside the borehole will cause the elements which are near to the weak elements to yield due to stress redistribution. The yielding process propagates in a stable manner until a failure mechanism is formed. In this section, a simplified analysis is presented to provide some basis for selecting the best location for weaknesses so that different failure mechanisms can be observed.

For a borehole situated in an elastic, homogeneous, isotropic rock mass, the stress components at the borehole wall are:

$$\sigma_r = P_i \sigma_H \quad (4.1a)$$

$$\sigma_\theta = \sigma_H (N+1) - 2 \sigma_H (N-1) \cos 2\theta - P_i \sigma_H \quad (4.1b)$$

$$\sigma_v = \nu (\sigma_r + \sigma_\theta) \text{ for plane strain condition} \quad (4.1c)$$

where,

$\sigma_r, \sigma_\theta, \sigma_v$ = Radial, tangential and vertical stresses;

P_i = Support pressure at the borehole wall normalized to σ_H (given as a percentage);

σ_H = Maximum horizontal far-field stress;

σ_h = Minimum horizontal far-field stress;

$$N = \frac{\sigma_h}{\sigma_H},$$

ν = Poisson's ratio;

θ = Angle from direction of σ_h to point of interest.

Yielding is initiated at the borehole wall if the stress components (σ_r , σ_θ , σ_v) satisfy the Von Mises yield criterion, i.e., the material has yielded if:

$$F((\sigma_r - \sigma_\theta)^2 + (\sigma_\theta - \sigma_v)^2 + (\sigma_v - \sigma_r)^2 - 2Y^2) = 0 \quad (4.2a)$$

or, is elastic if:

$$F((\sigma_r - \sigma_\theta)^2 + (\sigma_\theta - \sigma_v)^2 + (\sigma_v - \sigma_r)^2 - 2Y^2) < 0 \quad (4.2b)$$

where, Y = Unconfined compressive strength

In this example, σ_H is assumed to be 5 MPa and ν to be 0.25. For $N=1.0$, σ_θ in Equation 4.1b is reduced to $10 - 5P_i$. The Von Mises yield criterion of Equation 4.2a becomes only a function of P_i (i.e., independent of θ). This suggests that yielding is initiated at every point around the periphery of borehole and that there are no preferred locations for introducing weak elements. However, if $N=0.5$, the Von Mises yield criterion is a function of P_i as well as θ . Figure 4.3 assists in determining the location for potential yield initiation of weak elements around the periphery of a borehole. In this figure, the minimum unconfined compressive strength, Y_{min} , required to prevent yield initiation is plotted against θ for $P_i = 0\%$ and 80% . Y_{min} is obtained by substituting Y_{min} for Y and setting

$2Y_{\min}^2 = (\sigma_r - \sigma_\theta)^2 + (\sigma_\theta - \sigma_v)^2 + (\sigma_v - \sigma_r)^2$ in Equation 4.2a. The normal and weak elements are assumed to have an unconfined compressive strength of 5 and 1.9 MPa, respectively. If a single weak element is placed at location A ($\theta = 45^\circ$), then yielding could just be initiated at this location when $P_i = 80\%$ (this is assuming the borehole after excavation is immediately supported by an internal pressure of 4 MPa). Once yielding is initiated at A, the surrounding elements could become unstable because of 1) yield propagation from the weak element, and 2) stress redistribution due to the presence of weak element. The normal elements, which are located between $0^\circ < \theta < 57.5^\circ$, also yielded when the internal pressure finally dropped to zero ($P_i = 0\%$). On the other hand, placing weak elements in the range of $57.5^\circ < \theta < 90^\circ$ (arrow labeled B) will not promote yield propagation because the surrounding elements are stable even at no support pressure. This analysis shows that, in choosing the critical locations for weak elements to initiate and propagate to the surrounding elements, it is also necessary to consider those elements which will become unstable when the internal pressure is dropped. It will be shown later in this chapter that, by placing weak elements at $\theta = 45^\circ$, the failure mechanisms of a borehole can in fact be changed. It will also be shown that they are not affected if $\theta > 60^\circ$. Although the analysis presented above can only predict yield initiation, it serves to provide a basis for selecting critical locations for weak elements and for choosing the stress ratio for the following analysis.

4.4 Borehole Failure Mechanisms in the Presence of Weaknesses

Case A in Figure 4.4A shows the development of a continuous yield zone as the support pressure is reduced, if no weaknesses are introduced for $N=0.5$. The dots in the figure denote the Gaussian integration points which have reached yielding. The shape of this yield zone is similar to those simulated by Wong and Kaiser (1986) for a shallow tunnel in soft ground. Cases B to D (Figure 4.4B and 4.4C) show the process of yield initiation and propagation around a borehole in the presence of weaknesses for $N=0.5$. They showed that local weaknesses can change the shape of the yield zones and the type of failure mechanisms from those without weaknesses. With $N=0.5$ and two weaknesses introduced near the borehole, a yield zone is initiated at the weak elements, and propagates in the form of narrow bands which eventually merge. An elastic block of rock, enclosed within the bands of the yielded rock, tends to be pushed into the opening if further deformations are permitted to occur as the internal support pressure is further reduced. This elastic block acts similarly to a key block and, if kept in place, prevents the surrounding yielded material from moving or collapsing into the opening. This kind of failure mechanism is analogous to the one introduced by the key block theory (Goodman and Shi, 1985) for blocky, non-yielding rock. In cases B to D, however, a 'key block' is surrounded by yielded rock. Progressive failure and ultimate rupture of the borehole is only possible once the confinement provided by the block to the surrounding yielded rock is released, i.e., when the block is allowed to move excessively.

The development of this failure mechanism is termed block-type failure. It is not only dependent on the presence of weaknesses, but on the stress ratio N , the number of weaknesses and their locations or proximity to the borehole.

Figure 4.5 illustrates several situations that were studied but where block-type failure mechanisms did not develop. This figure demonstrates that:

- 1) Single weakness may induce yield initiation but normally does not influence the ultimate shape or extent of the yield initiation zone because the weak element is quickly incorporated into a general yield zone. Block-type failure mechanism cannot develop because no converging yield zones exist. Hence, the end product is independent of the location of a single weakness (see Figure 4.5, left side).
- 2) Two (or more) weaknesses in regions of low stress concentration do not promote the development of block-type failure (Figure 4.5, top and middle for $N=0.5$). The top case confirms the analysis in Section 4.3 that placing weak elements at $\theta > 60^\circ$ do not promote yield propagation.
- 3) If N is equal to unity, the presence of weaknesses does not greatly change the development of a continuous uniform yield zone (as predicted by analytical or numerical solutions for a homogeneous continuum).
- 4) For $N=0.5$, the same was observed if two weaknesses are far apart or arranged so that yield zones degenerate into a single zone (see Figure 4.5, bottom).

This study supports the earlier findings presented in Chapter 3 that the presence of weaknesses may change the failure mechanism under certain conditions. In boreholes under sufficiently non-uniform far-field stresses, the presence of weaknesses, if critically located at or near the borehole wall, will change the failure mechanism from a fully yielded zone to a mode with an elastic block enclosed by narrow bands of yielded rock. Whereas it is difficult to describe mathematically the process of yield propagation at this stage of this study, much evidence in support of this failure mechanism can be found in underground construction. Chapter 6 will describe such a failure mechanism observed during laboratory testing of coal and in actual tunnel construction. The observed failure mechanism will be compared with the results from a finite element simulation following the procedure outlined in this chapter.

In the presence of weaknesses, the stress distribution near a borehole will not be uniform and will not correspond to that near an opening in an elastic, homogeneous, isotropic material. The stress distribution along the x-direction for an elastic, homogeneous, isotropic material and the case with two symmetric weaknesses are compared in Figure 4.6. Figure 4.6(a) shows that at $P_i=100\%$, weaknesses lead to a distribution of σ_r and σ_θ differs slightly from those in a homogeneous, isotropic material. The borehole becomes unstable when the two bands of yielded rock merge together at $P_i=50.5\%$. The distribution of σ_r and σ_θ at this state differ significantly from that of the homogeneous case between $r/a=1$ to 2.5. At a distance of r/a greater than 2.5, the distribution of σ_r and

σ_θ approaches that of the homogeneous case indicating that the stresses are not affected by the presence of weaknesses. The presence of weaknesses lead to a large decrease in radial stress away from the borehole. This decrease in radial stress is in agreement with the failure mechanism with an elastic block enclosed in yielded rock. The stress distribution along the y-direction is presented in Figure 4.7. For $P_i=100\%$, Figure 4.7(a) indicates that the stress distribution of σ_r and σ_θ with weaknesses do not differ significantly from that of the homogeneous case. When the two bands of yielded rock merge together at $P_i=50.5\%$, the distribution of σ_θ follows the same pattern observed in the x-direction (i.e., great difference at $r/a=1$ to 2.5 and no difference at $r/a > 2.5$). However, the distribution of σ_r with weaknesses at $P_i=50.5\%$ differs only slightly from that of the homogeneous case.

The stress distribution in Figure 4.6(a) are redrawn in Figure 4.6(b) showing the deviatoric stress ($\sigma_\theta - \sigma_r$). For an elastic, homogeneous, isotropic material, the deviatoric stress is maximum at the borehole wall indicating that yielding should initiate there and propagate into the rock. However, weaknesses lead to a different distribution of stresses such that the maximum deviatoric stress is away from the borehole wall, at a distance of r/a equal to 2.06 for this case. This corresponds to the location where the two bands of yielded rock merge. This analysis suggests that weaknesses will lead to a critical stress condition inside the rock such that the propagation and merging of the two bands of yielded rock becomes possible. The deviatoric stress distribution along the y-direction in Figure 4.7(a) are also redrawn in Figure 4.7(b). In this direction, the deviatoric

stress from the case with weaknesses is very low at the borehole wall and that their distribution is slightly lower than that from the homogeneous case at $r/a > 2.06$. This may explain the reasons why yield propagation did not go towards the y-direction.

Santarelli et al. (1986) addressed the question of whether yielding initiates at the borehole wall or inside the rock. They have shown that a material with non-linear or confining pressure-dependent elasticity can lead to critical stress conditions inside the rock rather than at the borehole wall. Hence, yielding could be initiated inside the rock and propagate toward the borehole wall. The present study provides an alternative reason for critical stress conditions inside the rock, i.e., weaknesses at or near the borehole wall. It seems likely that such conditions are frequently encountered in reality.

4.5 Practical Implications of Findings for Design and Monitoring of Underground Openings

While this study is directed to borehole failure mechanisms, the results and findings are directly applicable to the design and monitoring of underground openings such as tunnels.

The ground convergence curves for the x and y-directions of Cases A to D are shown in Figure 4.8. It should be noted that Case A with no weakness is stable until P_i is reduced to 30 %. At this pressure, u/u_c in the x and y-directions are equal to 46.3 and 2.6, respectively. The curve in the x-direction is shown only up to $u/u_c =$

13 in order to compare the trend of the four different cases more clearly. It is interesting to observe that all convergence curves in the y-direction tend towards the same point (about $1.5 u_c$ at 50 % support pressure) indicating that the convergence at this stage does not permit differentiation between the various modes of failure. In the x-direction where the deformations are much larger, the same observation can be made (at about $10 u_c$). Case D, with a weak joint, needs much higher support pressures (at more than $6.5 u_c$) than Cases A to C to prevent collapse and to maintain small displacements or good ground control. In general, it can be concluded that convergence measurements are good indicators of instability but poor indicators for the identification of the type and location of the failure mechanisms (Kaiser, 1987).

Localized measurements are needed to establish the actual mode of behaviour and to detect the location of instabilities. This is illustrated in Figure 4.9 where the simulated ground strain data that would be detected by Extensometers I to IV (Case D) is presented. Extensometers I (in the y-direction), II and IV (at the x-direction) are in non-yielded rock and therefore give no indication that a major instability is approaching. Even at collapse ($P_i < 50 \%$), only 0 to 0.24 % average strain is recorded at these locations. However, the strategically well placed Extensometer III provides early evidence of instability ($> 2 \%$ strain at $P_i = 75 \%$). It follows that measurements of relative displacements at appropriate locations are needed to properly locate and identify failure modes. Pattern monitoring will likely miss critical conditions and only strategically well placed

instruments, based on a clear vision of the potential failure mode, can be useful (Kaiser, 1987).

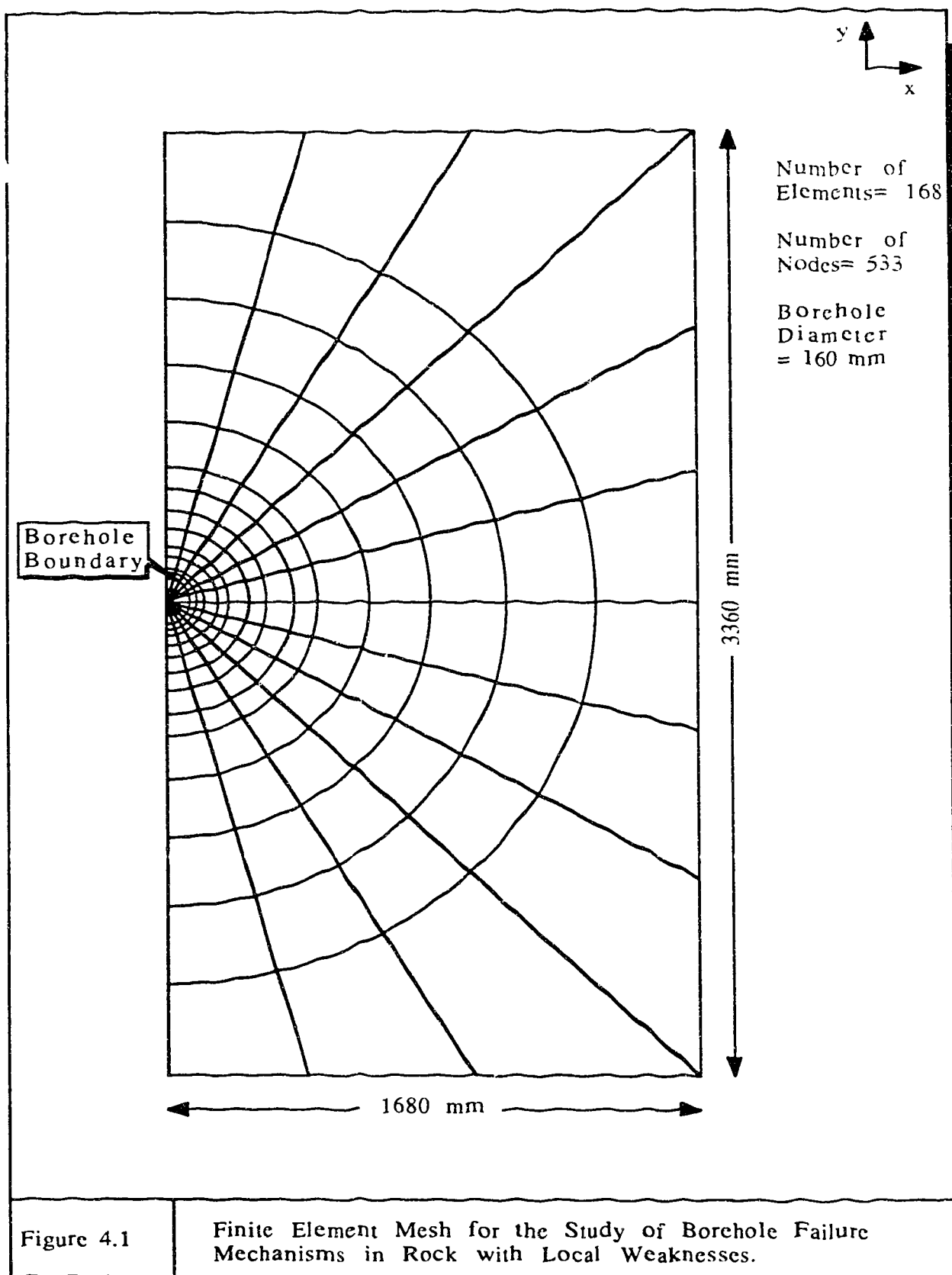
4.6 Summary and Conclusions

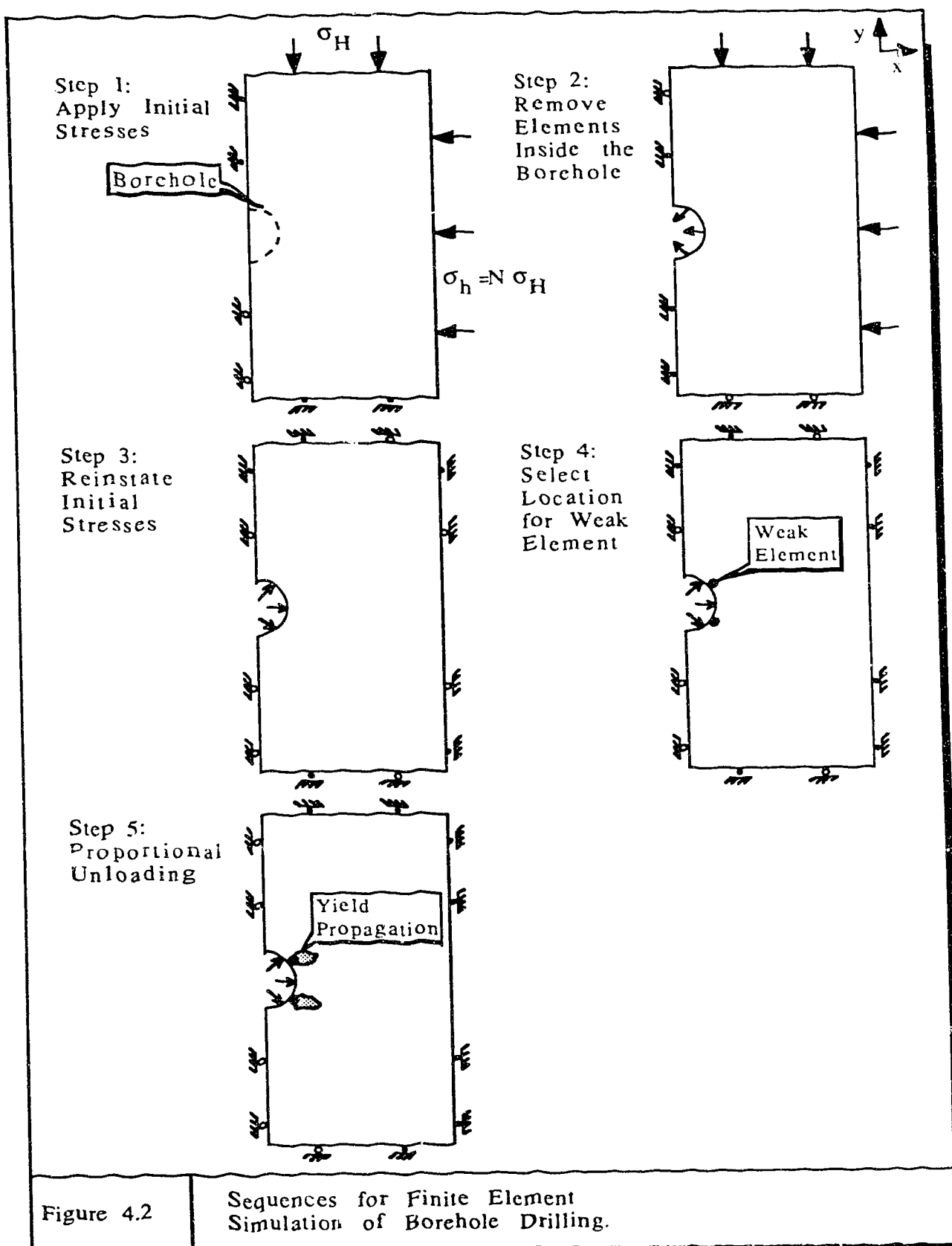
Since rock masses are seldom homogeneous, weaknesses cannot be ignored for the assessment of stability for boreholes and underground construction. A kinematically acceptable block-type failure mechanism can develop if there are multiple weaknesses under non-uniform far-field stresses, provided that sufficient yielding is allowed. The presence of weaknesses may lead to higher deviatoric stresses inside the rock and cause yield initiation at some distance behind the wall.

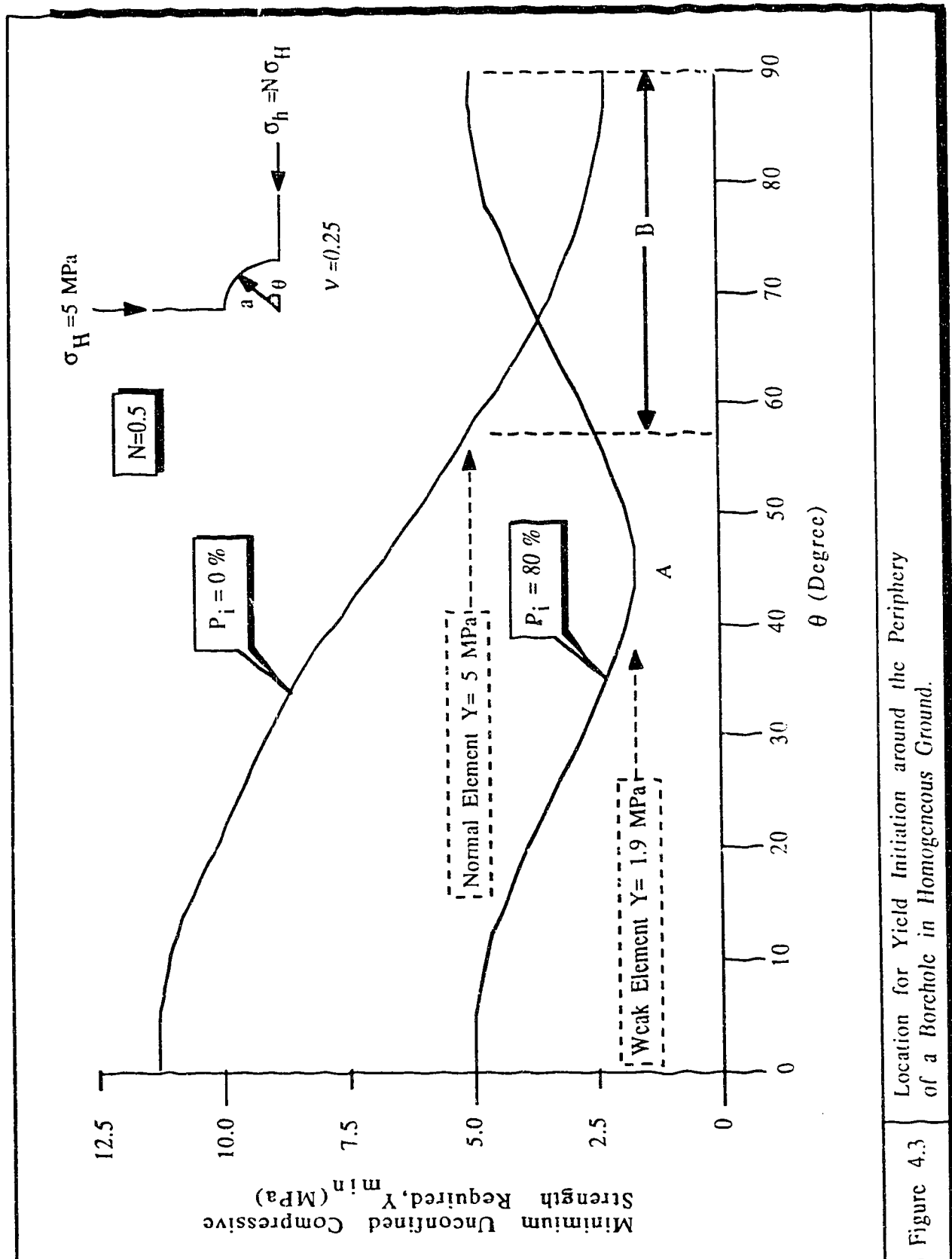
Convergence measurements at the wall of an opening are insufficient to differentiate amongst the various modes of failure. Instruments for monitoring purposes must be located at strategic positions which are based on a hypothesis of several likely behaviour and failure modes. Measurements taken from these carefully selected locations are to be compared with predictions from numerical or analytical models in order to confirm the assumed modes of failure.

The results presented above illustrate that knowledge of the locations, extent and number of weaknesses are essential for the design of a stable borehole or other underground openings. However, the locations, orientation and distribution of joints, fissures and other discontinuities in a rock mass are extremely variable and

difficult to quantify or predict. Fortunately, many sedimentary and metamorphic rocks show preferred orientations or regular patterns of weaknesses. The rock mass can therefore often be treated as a transversely isotropic material with the variation of strength being a function of the orientation of the weakness planes. In the next chapter, this aspect and the effect of weakness orientation and stress ratio on the yield initiation and propagation around a borehole will be studied, and the resulting failure mechanisms compared with those described in this chapter.







Case A:
No Weaknesses

$N=0.5$

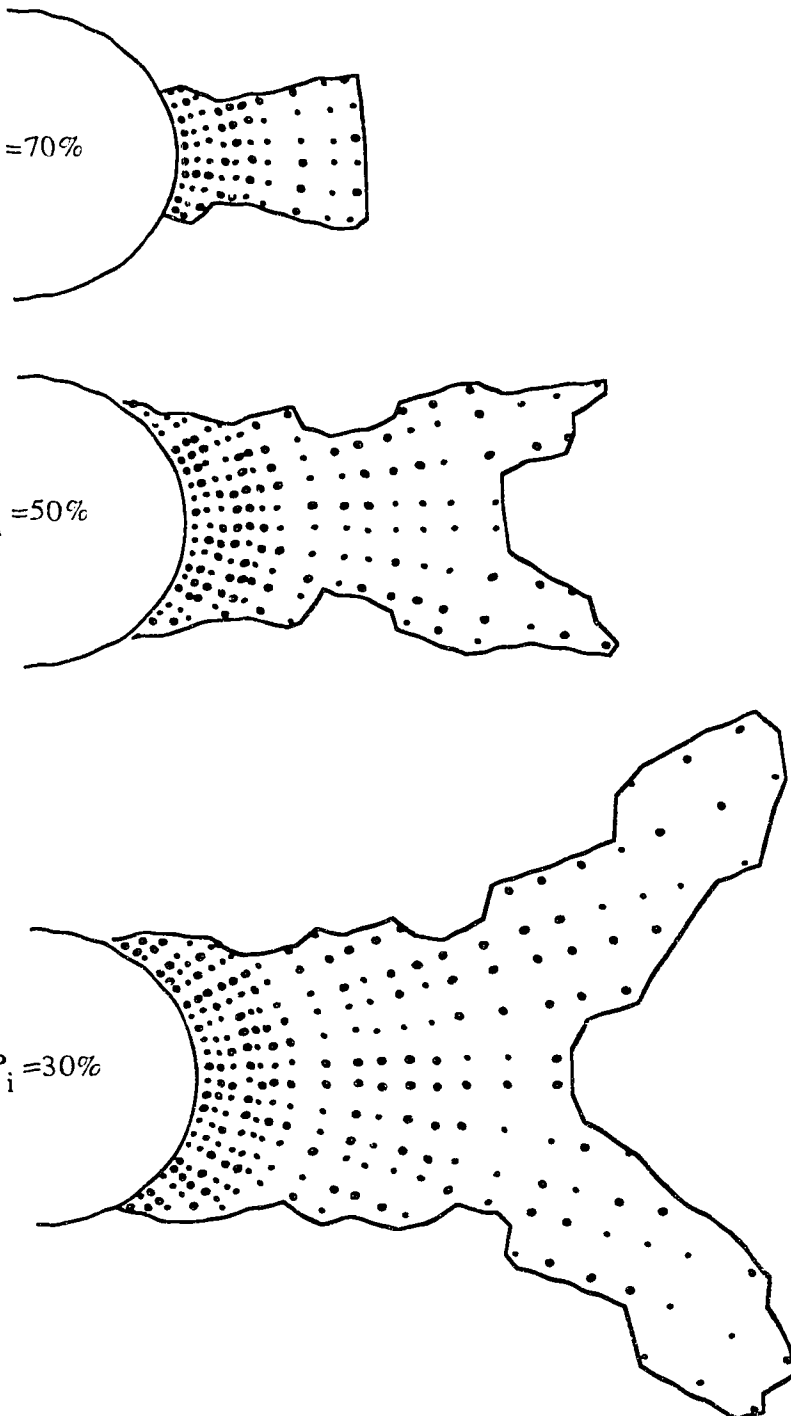
$P_i = 70\%$

$P_i = 50\%$

$P_i = 30\%$

Figure 4.4A

Development of Failure Mechanisms around
Boreholes without Local Weaknesses ($N=0.5$).



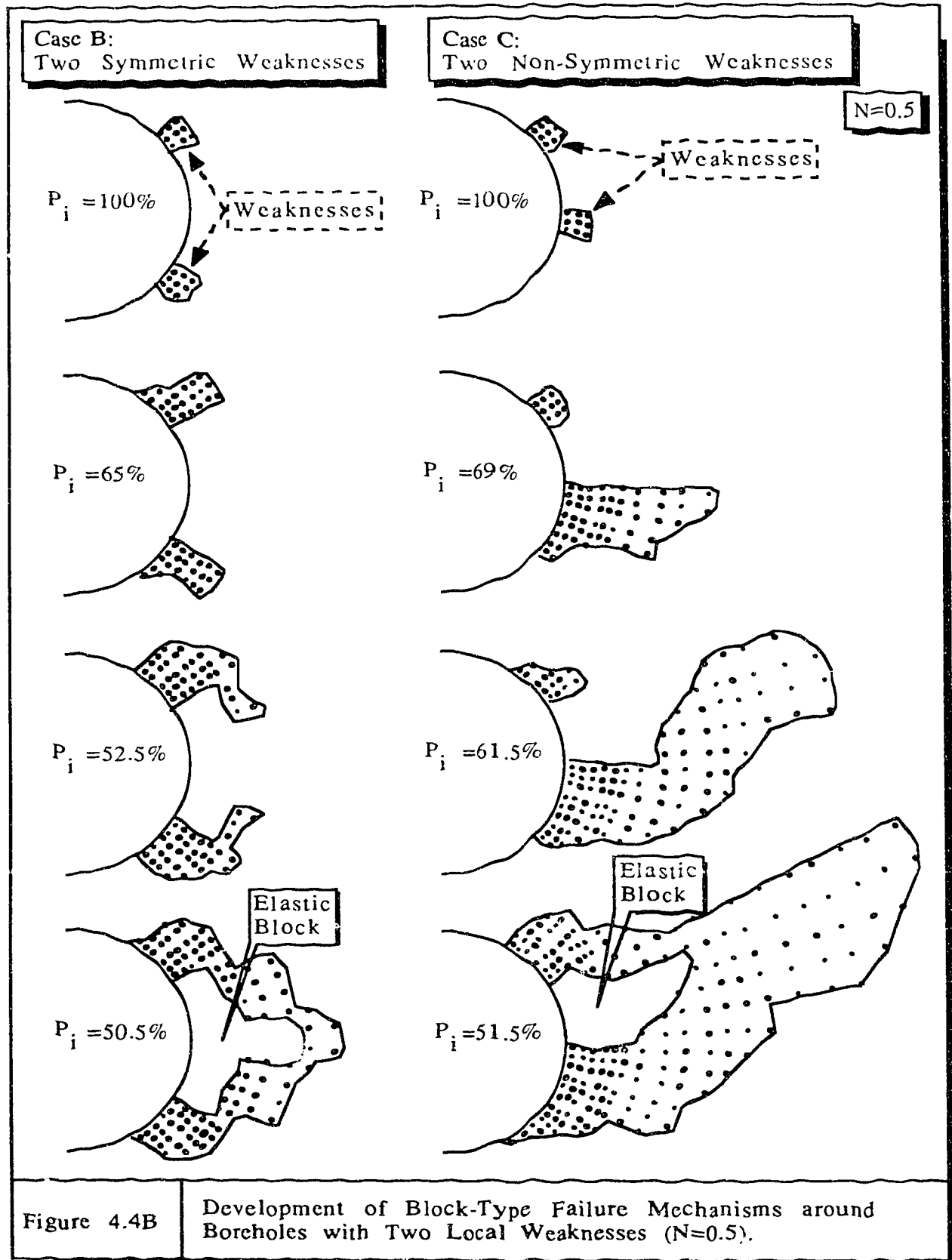


Figure 4.4B

Development of Block-Type Failure Mechanisms around Boreholes with Two Local Weaknesses ($N=0.5$).

Case D: One Weakness and
One Weak Plane

$N=0.5$

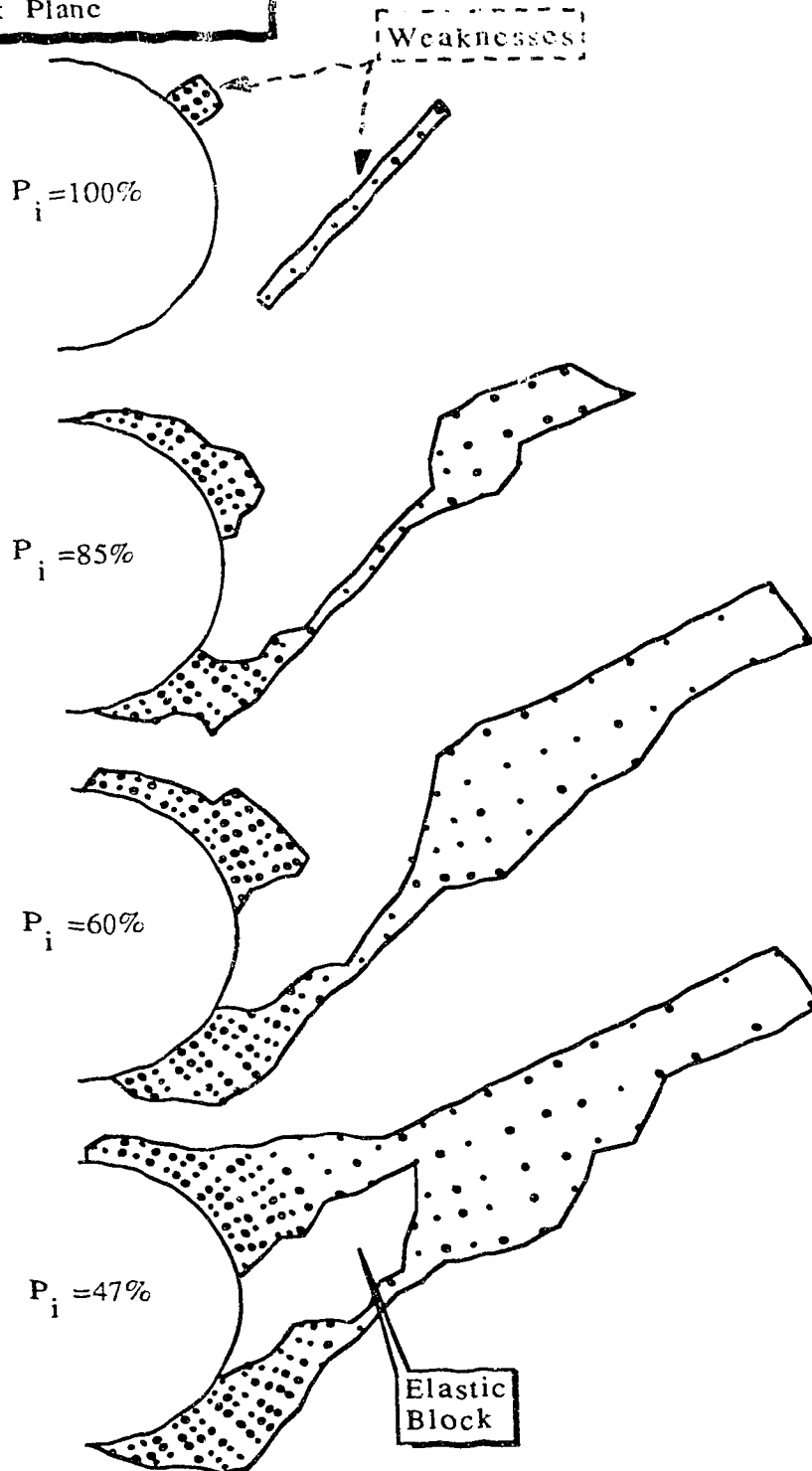


Figure 4.4C

Development of Block Type Failure Mechanisms around
Boreholes with One Local Weakness and A Weakness
Plane ($N=0.5$).

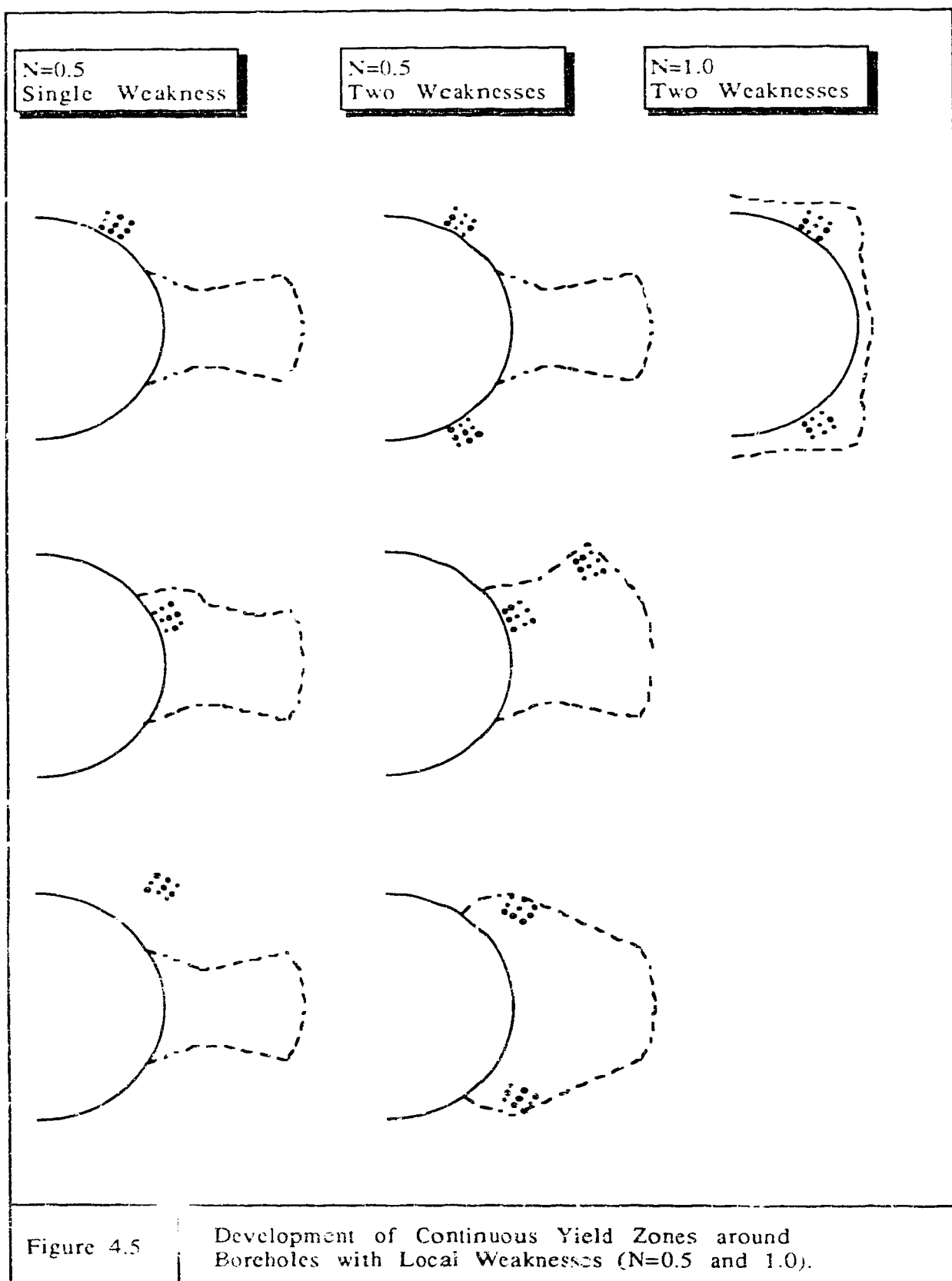
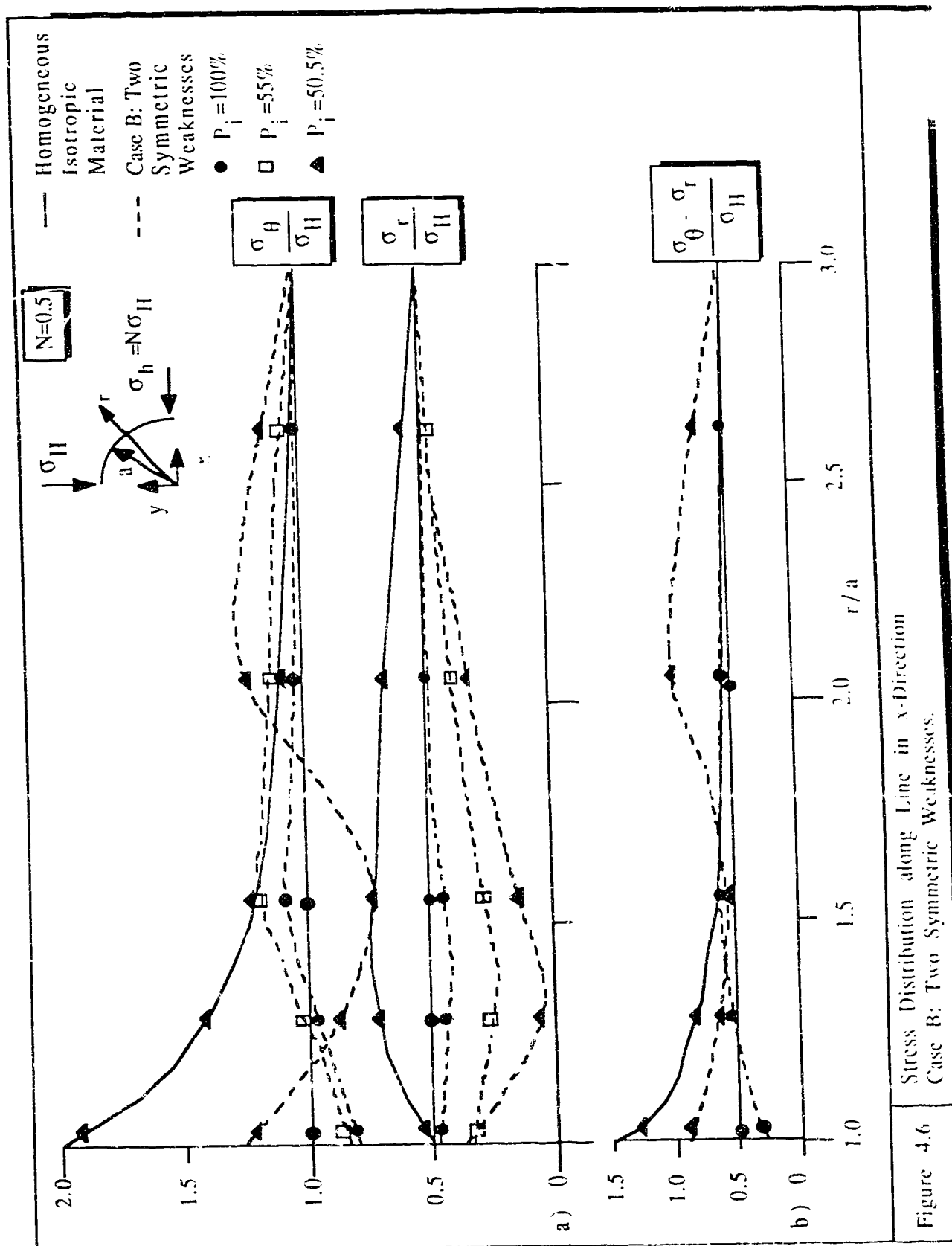
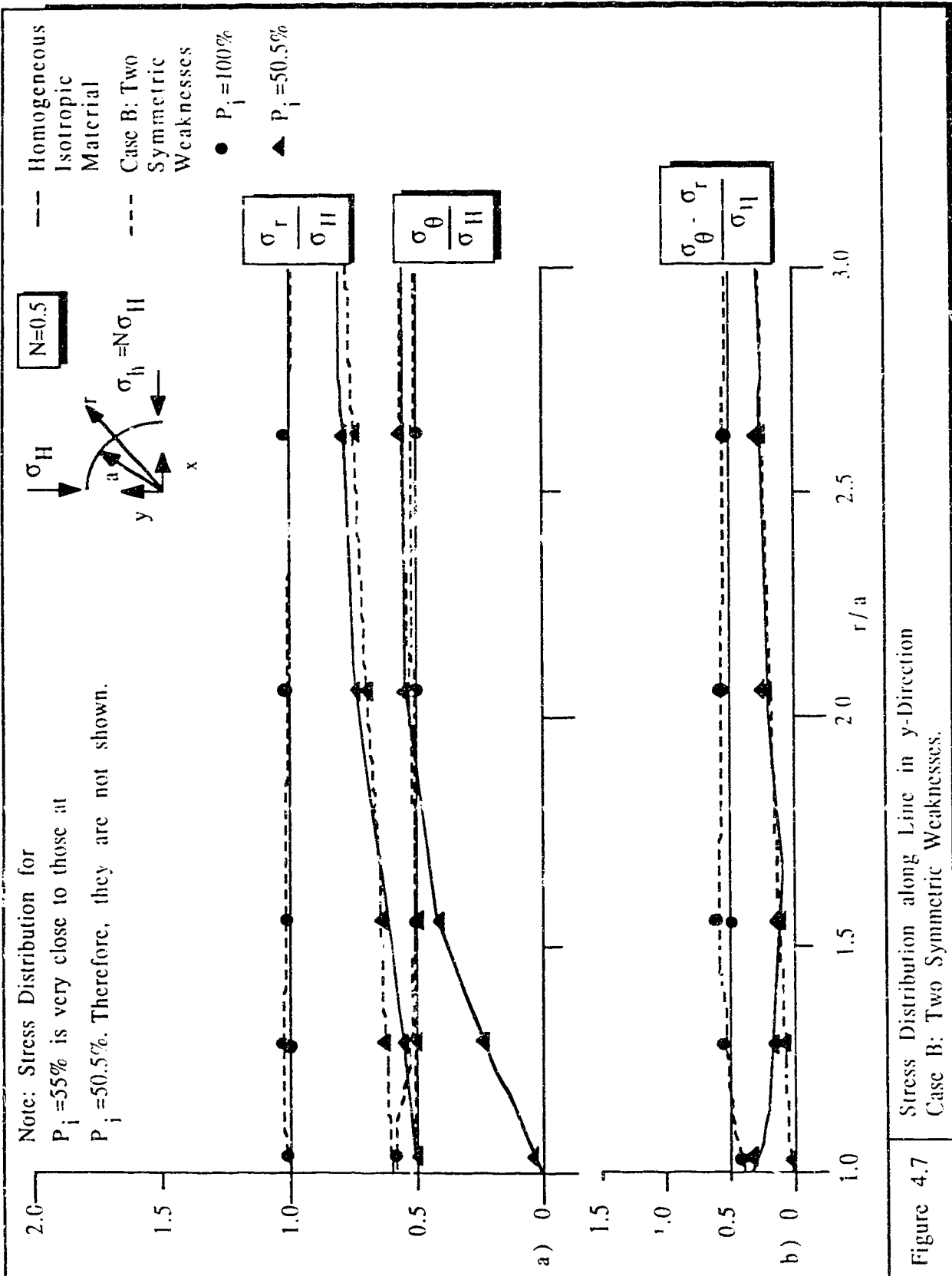


Figure 4.5

Development of Continuous Yield Zones around Boreholes with Local Weaknesses ($N=0.5$ and 1.0).





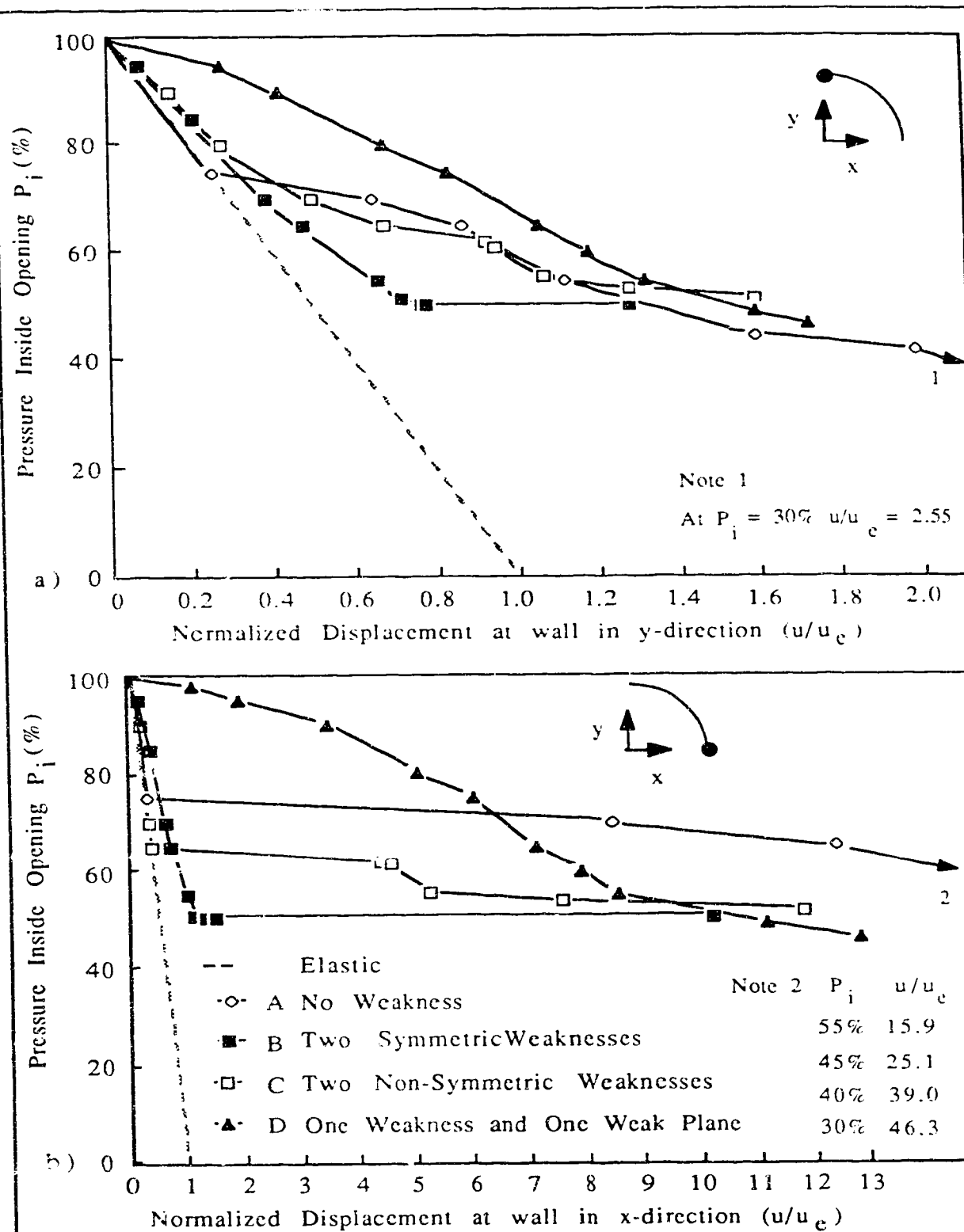


Figure 4.8

Ground Convergence Curves for Borehole
with Local Weaknesses (Cases A to E).

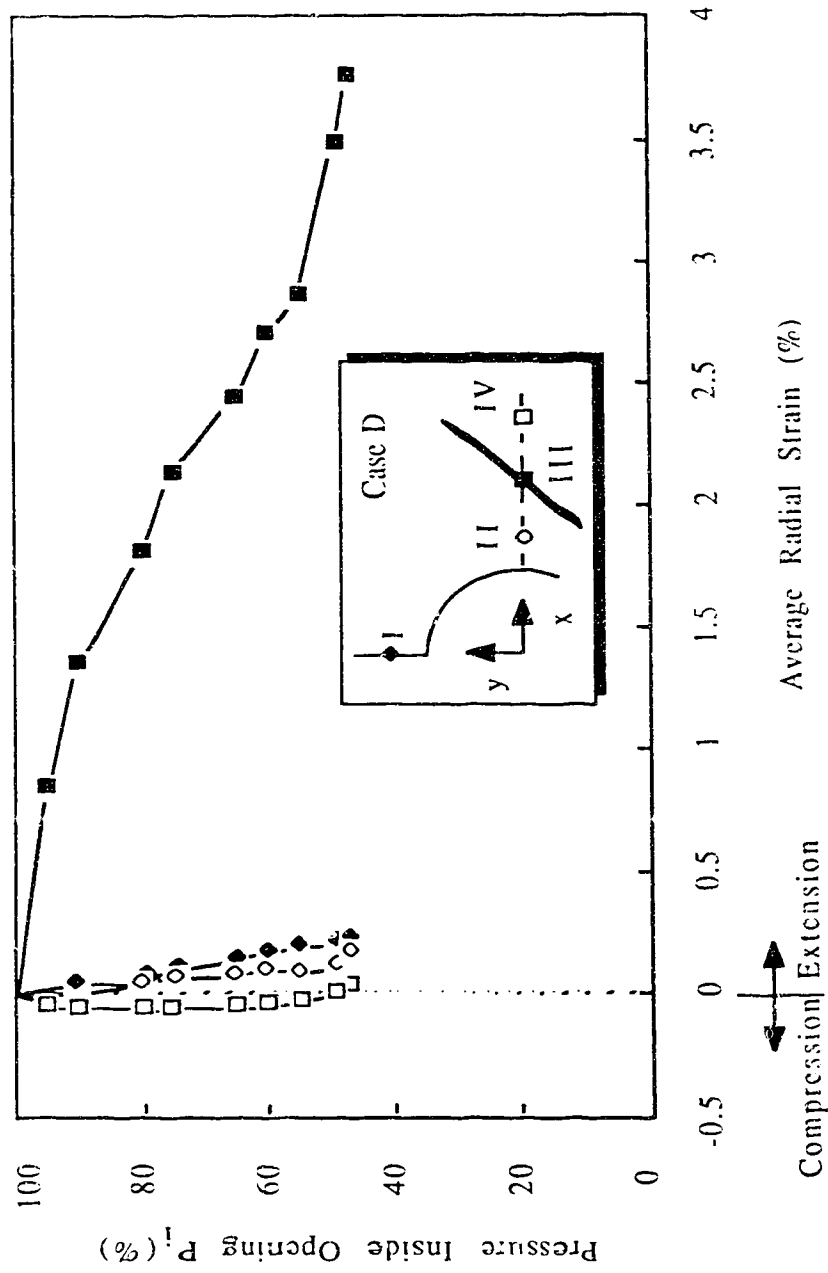


Figure 4.9 Ground Strain Curves for Four Locations in Case D.

5 EFFECTS OF ORIENTED WEAKNESSES ON BOREHOLE FAILURE MECHANISMS

5.1 Introduction

The development of yield zones around boreholes in the presence of imperfections in the form of local weaknesses such as single joints or fissures have been investigated by the finite element simulations described in Chapter 4. It was found that the number of weaknesses and their locations or proximity to the borehole are important factors which influence the development of different types of failure mechanisms. Many sedimentary and metamorphic rocks show preferred orientations or regular patterns of weaknesses and a rock mass can often be treated as a transversely isotropic material with the variation of strength being a function of the orientation of the weakness planes. In this chapter, the objective is to study the effect of the weakness orientation and the horizontal far-field stress ratio, N , on the yield initiation and propagation modes around a borehole and to compare the resulting failure mechanisms with those described in Chapter 4.

A generalized yield criterion developed by Nova and Sacchi (1979) for rock which exhibits transversely isotropic strength was adopted, and implemented into the finite element code SAGE (Chan, 1986).

5.2 Properties of Transversely Isotropic Model

The model is assumed to describe a linear elastic, brittle perfectly plastic rock. Appendix B.1 illustrates that five constants (E_1 , E_2 , ν_1 , ν_2 , G_2) are needed to characterize the elastic deformation properties of this transversely isotropic material. The five elastic constants can be determined by performing three uniaxial compression tests as indicated in Figure B.2 in Appendix B.2.

Several yield criteria have been proposed for transversely isotropic material. Table C.1 in Appendix C.1 provides a list of references on the study of transversely isotropic materials. Different assumptions have been made to describe the variation of strength with the orientation of the weakness planes, and all of these require a considerable amount of curve fitting of test data in order to obtain the parameters for the model.

The theory proposed by Nova and Sacchi (1979) was adopted for this study because 1) the yield criterion is applicable to a three dimensional state of stress, 2) only four strength parameters are needed to describe the variation of strength as a function of the orientation, 3) the four strength parameters can be identified from available or published test data, and 4) the yield criterion can be reduced to the Mohr-Coulomb and the Tresca yield criteria for isotropic material.

For a state of stress in the standard triaxial test, the yield criterion developed by Nova and Sacchi (1979) takes the following general form:

$$\begin{aligned}
F = & \frac{(\sigma_1 - \sigma_3)}{2} - \left\{ \left\{ [(\alpha \cos^2 \eta + \sin^2 \eta) c_{\min} \right. \right. \\
& + (\sigma_m \beta \cos^2 \eta + \sigma_n \sin^2 \eta + \tau_{mn} \sin 2\eta) \tan \phi_{\min}] \\
& * [(\cos^2 \eta + \alpha \sin^2 \eta) c_{\min} + (\sigma_m \beta \sin^2 \eta + \sigma_n \cos^2 \eta \\
& - \tau_{mn} \sin 2\eta) \tan \phi_{\min}] \left. \right\}^{1/2} \\
& - \sin 2\eta \left[\tan \phi_{\min} \sigma_m \frac{(\beta - 1)}{2} + c_{\min} \frac{(\alpha - 1)}{2} \right] \quad (5.1)
\end{aligned}$$

where.

$$\sigma_m = \sigma_1 \cos^2 \eta + \sigma_3 \sin^2 \eta;$$

$$\sigma_n = \sigma_1 \sin^2 \eta + \sigma_3 \cos^2 \eta;$$

$$\tau_{mn} = \frac{(\sigma_1 - \sigma_3)}{2} \sin 2\eta;$$

$$\alpha = \frac{c_{\max}}{c_{\min}};$$

$$\beta = \frac{\tan \phi_{\max}}{\tan \phi_{\min}};$$

$$\eta = \text{Angle between the direction of } \sigma_1 \text{ and the plane of transverse isotropy (see Figure 5.1);}$$

$$\sigma_m = \text{Stresses in the plane of transverse isotropy;}$$

$$\sigma_n = \text{Stresses normal to the plane of transverse isotropy;}$$

$$\sigma_1 = \text{Major principal stress;}$$

$$\sigma_3 = \text{Minor principal stress;}$$

$$c_{\max} = \text{Maximum cohesion intercept;}$$

$$c_{\min} = \text{Minimum cohesion intercept;}$$

$$\phi_{\max} = \text{Maximum angle of friction;}$$

$$\phi_{\min} = \text{Minimum angle of friction;}$$

$$F = \text{Yield function} = 0 \text{ (if material is yielded);}$$

$$< 1 \text{ (if material is elastic).}$$

Only four parameters needed to describe the variation of strength as a function of the orientation of the weakness planes relative to the major principal stresses (c_{\max} , c_{\min} , ϕ_{\max} and ϕ_{\min}).

5.2.1 Reduction of Transversely Isotropic Yield Criterion to Isotropic Yield Criterion

The transversely isotropic yield criterion of Equation 5.1 can be reduced to an isotropic yield criterion by putting $\alpha=\beta=1$. Appendix C.2 shows that the resulting yield criterion takes the following form:

$$\frac{(\sigma_1 - \sigma_3)}{2} = [(c + \sigma_1 \tan \phi) (c + \sigma_3 \tan \phi)]^{1/2} \quad (5.2)$$

Equation 5.2 predicts the stresses at yielding being the same as those predict by the well known Mohr-Coulomb yield criterion although expressed in a different form. Equation 5.2 can be further reduced to the Tresca yield criterion if $\phi=0$, i.e.:

$$\frac{(\sigma_1 - \sigma_3)}{2} = c \quad (5.3)$$

5.2.2 Transversely Isotropic Yield Criterion for cohesive material ($\phi=0$)

For $\phi=0$, the transversely isotropic yield criterion of Equation 5.1 reduces to:

$$F = \frac{(\sigma_1 - \sigma_3)}{2} - \left\{ [(\alpha \cos^2 \eta + \sin^2 \eta) c_{\min} * (\cos^2 \eta + \alpha \sin^2 \eta) c_{\min}]^{1/2} - \sin 2\eta \left[c_{\min} \frac{(\alpha - 1)}{2} \right] \right\} \quad (5.4)$$

For vertical and horizontal planes of transverse isotropy ($\eta=0^\circ$ and 90°), Equation 5.4 becomes:

$$F = \frac{(\sigma_1 - \sigma_3)}{2} - \sqrt{\alpha} c_{\min} \quad (5.5a)$$

Also, for plane of transverse isotropy at 45° to σ_1 ($\eta=45^\circ$), Equation 5.4 becomes:

$$F = \frac{(\sigma_1 - \sigma_3)}{2} - c_{\min} \quad (5.5b)$$

Equations 5.5a to 5.5b indicate that regardless of the orientation of the weakness planes, the failure planes (Figure 5.1) in a frictionless material are always orientated at 45° from the direction of σ_1 . Figure 5.1 also shows that minimum resistance to yielding is reached when the weakness planes are orientated at 45° to the direction of σ_1 for all values of α (Point A). Maximum resistance to yielding is $\sqrt{\alpha} c_{\min}$ and is reached when the weakness planes are orientated at $\eta=0^\circ$ or 90° (Points B and B').

5.2.3 Transversely Isotropic Yield Criterion for Purely Frictional Material ($c=0$)

For a purely frictional material, the transversely isotropic yield criterion in Equation 5.1 reduces to:

$$F = \frac{(\sigma_1 - \sigma_3)}{2} - [(\sigma_m \beta \cos^2 \eta + \sigma_n \sin^2 \eta + \tau_{mn} \sin 2\eta) \tan \phi_{\min} * (\sigma_m \beta \sin^2 \eta + \sigma_n \cos^2 \eta - \tau_{mn} \sin 2\eta) \tan \phi_{\min}]^{1/2} - \sin 2\eta \left[\tan \phi_{\min} \sigma_m \frac{(\beta - 1)}{2} \right] \quad (5.6)$$

For vertical and horizontal planes of transverse isotropy ($\eta=0^\circ$ and 90°) respectively, Equation 5.6 becomes:

$$F = \frac{(\sigma_1 - \sigma_3)}{2} - \sqrt{\sigma_1 \sigma_3} \beta \tan \phi_{\min} \quad (5.7)$$

For any other orientation (η), Equation 5.6 cannot be reduced any further and a parametric study was carried out to produce Figure 5.2. It is interesting to note that for the two cases ($\phi_{\min}=15^\circ$ and 40°), minimum resistance to yielding (Points C and D in Figure 5.2) is reached on planes orientated at $45^\circ - \phi_{\min}/2$ from the direction of σ_1 for all values of β (1 to 3). This result is expected from the Mohr stress circle in Figure 5.2. Failure will first occur on planes orientated at $45^\circ - \phi_{\min}/2$ from the direction of σ_1 . Figure 5.2 also shows that if $\beta=1$, resistance to yielding is independent of weakness orientation (i.e., in isotropic material).

5.3 Strength Parameters for Transversely Isotropic Yield Criterion

In order to measure the strength parameters (c_{\max} , c_{\min} , ϕ_{\max} and ϕ_{\min}) for the transversely isotropic yield criterion, a number of triaxial tests have to be carried out to measure the variation of axial stress at failure as a function of the confining pressure and of the weak plane inclination angle η . The testing procedure is described in Appendix C.3. A typical set of experimental results on slate obtained from Donath (1963) is shown in Figure 5.3. The deviatoric stress at failure predicted from the transversely isotropic yield criterion are plotted for comparison with the experimental results. It can be seen that better predictions are made if the weakness planes are orientated close to the potential failure planes.

The following table summarizes the strength parameters for different materials. They were determined from published data using the procedure described in Appendix C.3.

Experimental Results	Material	c_{\min} (MPa)	ϕ_{\min}	α	β
Donath (1963)	Martinsburg Slate	7.1	20°	13.5	6.5
Attawell and Sandford (1974)	Penrhyn Slate	14.4	30°	5.4	2.0
McLamore and Gray (1967a)	Austin Slate	37.5	17°	2.6	4.0
McLamore and Gray (1967b)	Green River Shale	27.7	18°	1.7	2.1

5.4. Implementation of Transversely Isotropic Yield Criterion into Finite Element Code SAGE

Five constants (E_1 , E_2 , ν_1 , ν_2 and α) to characterize the elastic deformation properties of a transversely isotropic material and four constants (c_{\max} , c_{\min} , ϕ_{\max} and ϕ_{\min}) to describe the transversely isotropic yield criterion are needed. The transversely isotropic yield criterion was implemented into the finite element code SAGE (Chan, 1986). In this model, the material is assumed to behave linearly elastic up to peak with a sudden decrease in strength from peak to residual. The peak strength is governed by the four strength parameters (c_{\max} , c_{\min} , ϕ_{\max} and ϕ_{\min}) and the residual strength by the two parameters (c_{res} and ϕ_{res}). The transition from peak to residual strength is reflected in an abrupt reduction of c_{\max} to c_{res} and ϕ_{\max} to ϕ_{res} . The material is assumed to deform in a perfectly plastic manner after the residual strength is reached. The sudden contraction of the yield surface after the peak strength has been mobilized, will leave the state of stress outside the yield surface when the strength has decreased to residual. In plasticity analyses, if the stress state is outside the yield surface, which is inadmissible, it is often assumed that the stress state can be found by projecting the current stress state onto the yield surface. Therefore, it is assumed that the stress state after the peak strength will be the projection of the peak stress on to the yield surface (Chan, 1986). The method of stress calculation during the transition from peak to residual strength is discussed in detail by Chan (1986).

The elasto-plastic constitutive matrix for this model is presented in Appendix D. The plastic strain increment is assumed to be perpendicular to the yield surface (i.e., associated flow rule is assumed), and for a frictional material, volume is increased due to shearing. Appendix E describes the implementation of the model into the computer code, and also provides instructions on how to set up an input file. In Appendix F, the input and output files of a simulated confined compression test, on a material with weakness planes at $\eta = 35^\circ$, are attached for reference.

5.4.1 Testing of Implemented Model

A simple confined compression test under plane strain conditions was simulated in order to test whether the program provides the predicted stresses at yielding. Four elements with 21 nodes were used for the finite element mesh and it was loaded by prescribing vertical displacements in small increments under a constant confining pressure of 35 MPa. The material selected for this example is Martinsburg slate (Donath, 1963). The peak and residual strength parameters are given as follows:

Peak Strength Parameters	Residual Strength Parameters
$\phi_{\max} = 67^\circ$	$\phi_{\text{res}} = 20^\circ$
$\phi_{\min} = 20^\circ$	$c_{\text{res}} = 7.1 \text{ MPa}$
$c_{\max} = 95.9 \text{ MPa}$	
$c_{\min} = 7.1 \text{ MPa}$	

Three analyses were carried out with weakness planes orientated at $\eta=0^\circ$, 35° and 90° . The results are shown in Figure 5.4, and they indicate that the material behaves as a linear elastic, brittle, perfectly plastic material with yielding reached at the predicted stress level. In this example, the lowest strength is reached when the weakness planes are orientated at $\eta=35^\circ$ which is also the direction of the failure plane ($\eta=45^\circ-\phi_{\min}/2$, if $\phi_{\min}=\phi_{\text{res}}=20^\circ$ (for peak and residual)). It should be noted that in this example, ϕ_{\min} is assumed to be equal to ϕ_{res} , and this is the reason why there is no abrupt drop in strength when the weakness planes are orientated to the direction of the failure plane. If ϕ_{res} was assumed less than ϕ_{\min} , then there would also be a drop in strength for weakness planes orientated at $\eta=35^\circ$.

An eigenvalue analysis of the elasto-plastic constitutive matrix was carried out for the above case with the weakness planes orientated at $\eta=35^\circ$. The physical meaning of the eigenvalues and their corresponding eigenvectors were discussed in Section 3.2. The results of the eigenvalue analysis are summarized in Figure 5.5. It can be seen from this figure that the modes of deformation for transversely isotropic material are the same as those for an isotropic material. The Mohr strain circle at the bottom of Figure 5.5 indicates that the potential failure planes are orientated at $\psi=55^\circ$ which is expected from limit equilibrium considerations. The two analyses presented above demonstrate that the transversely isotropic yield criterion is correctly implemented into the finite element program.

5.5 Borehole Failure Mechanism in Transversely Isotropic Rocks

Four cases (E to H) with different combinations of far-field stress ratio and weakness plane orientation were studied. The material properties were assumed to correspond with those reported by Donath (1963) for Martinsburg slate. The peak and residual strength parameters were already described in Section 5.4.1. The elastic deformation properties are summarized below:

Elastic Deformation Properties

$$E_1 = 91.5 \text{ GPa}$$

$$E_2 = 59.1 \text{ GPa}$$

$$\nu_1 = 0.204$$

$$\nu_2 = 0.331$$

$$G_2 = 24 \text{ GPa}$$

The development of the failure mechanisms are summarized in Figures 5.6A and 5.6B. It can be seen that block-type failure mechanisms (Cases E and G), similar to those generated with local weaknesses in homogeneous, isotropic rock (Figures 4.4B and 4.4C) also develop if the weakness orientation is either horizontal ($\eta=90^\circ$) or vertical ($\eta=0^\circ$) and the far-field stress ratio differs from unity. This is because yield initiation and early yield zone expansion occurs at positions similar to those that were introduced selectively by local weaknesses. In other words, if the far-field stress ratio differs from unity, block-type failure mechanism can develop in an isotropic material with local weaknesses present at critical locations or in rock

with transversely isotropic strength. However, under a uniform stress field ($N=1$, Case H), yielding may propagate from two locations but a block-type failure mechanism does not form. It will be shown in Chapter 7 by a simplified approach that if N is unity, yielding will always initiate at the same two locations relative to the direction of the weakness plane. This supports the earlier findings presented in Chapter 4 that the location of yield initiation and the far-field stress ratio are important factors that govern the development of different types of failure mechanisms.

The extent of yield zone for $\eta=0^\circ$ (Case E) is about 2.5 times less than those for $\eta=45^\circ$ (Case F), as shown in Figure 5.6A. However, instability occurs earlier for $\eta=0^\circ$ ($P_i=54\%$ for $\eta=0^\circ$ and $P_i=45\%$ for $\eta=45^\circ$). This is very important to the design of monitoring program because if the extensometers are not closely spaced, then it is possible that this block-type failure mechanisms will not be detected. Once the elastic block is allowed to move into the opening, then controlling the borehole stability may become difficult. These two cases illustrate that measuring the extent of yield zone alone is insufficient to differentiate between various failure mechanisms, and also it cannot be used on its own to decide whether instability is approaching.

The direction of the failure planes at each yielded element for Cases E to G are plotted in Figures 5.7A to 5.7C, respectively. They were calculated on the basis of limit equilibrium prediction that the direction of the failure planes are rotated at $45^\circ - \phi_{\min}/2$ from the direction of the major principal stresses. The direction of the major principal stresses were obtained from the computer output. Since

there are nine integration points at each element, the direction of the failure planes shown in these figures represent the average of the nine integration points, and they were plotted at the center of the element. The failure planes are drawn across the elements for the purpose of illustrating the direction only. The following observations are made:

1. Case E with vertical weakness planes ($\eta=0^\circ$, Figure 5.7A).

At $P_i=70\%$, yielding was first initiated at location A. The failure planes at this location indicated that shearing occurred across the weakness planes, and the direction is orientated towards location B which is inside the rock mass. When the borehole became unstable at $P_i=54\%$, the failure planes near location B clearly indicated the merging of the two yielded zones. The direction of the failure planes at locations A and B support this study that the formation of block-type failure mechanism is kinematically admissible.

2. Case F with weakness planes orientated at 45° to σ_h ($\eta=45^\circ$, Figure 5.7B).

In this case, yielding was first initiated at location C when $P_i=85\%$. The failure planes at this location indicated that shearing occurred across the weakness planes and the direction is orientated towards location D. When instability was reached at $P_i=45\%$, the direction of the failure planes generally ranged between 20° to 60° from the x-axis. This suggests that some of the elements were sheared along the weakness planes and some were across the weakness planes. The yielded zone can be divided into three regions

(I, II and III) as shown in the figure. Regions I, II and III are the areas within which the direction of the failure planes are greater than 45° , equal to 45° and less than 45° , respectively. It is interesting to note that Region II has a very narrow range, an indication that most of the yielded element has failure planes across the weakness planes. This suggests that the yielded rock mass may be highly fractured, and that the method of controlling stability may be different from those with an elastic block formed.

3. Case G with horizontal weakness planes ($\eta=90^\circ$, Figure 5.7C).

Yielding is first initiated at location E when $P_i=50\%$. The direction of the failure planes is horizontal, indicating that shearing has occurred along the weakness planes. This is different from Case E where yielding at the borehole wall is initiated by shearing across the weakness planes. After yielding is initiated by shearing along the weakness planes, the failure planes propagate across the weakness planes, and toward location F which is inside the rock mass. At $P_i=31\%$, the borehole became unstable when the failure planes merged at location F. Similarly to Case E, the direction of the failure planes show that the block-type failure mechanism is kinematically admissible.

The stress distributions along a line parallel to the x-direction for Case G with horizontal weakness planes ($\eta=90^\circ$) and $N=0.5$ are presented in Figure 5.8. At $P_i=100\%$, the stress distribution for Case G with horizontal weakness planes are identical to those of an opening in an elastic, homogeneous, isotropic material because none

of weakness planes yield near the borehole. When the two bands of yielded rock merge at $P_i=31\%$, the distribution of σ_r and σ_θ are significantly different from those of homogeneous isotropic material within a distance of about 2 radii. It is interesting to note that the variation of σ_r , σ_θ and $(\sigma_r - \sigma_\theta)$ along the x-axis are very similar to those with local weaknesses presented in Figure 4.6. Both figures indicate that a maximum in deviatoric stress occurs away from the borehole wall (at $r/a = 1.25$ for Case G). This differs significantly from the stress distribution for an elastic, homogeneous, isotropic material where the maximum in deviatoric stress is found at the borehole wall. The location of the maximum deviatoric stress corresponds to the point where the two bands of yielded rock merge. This study supports the earlier findings that localized yield zones, created by local weaknesses or rock with transversely isotropic strength, will lead to a critical stress condition inside the rock such that the propagation of the yield zone is forced to merge.

The stress distributions along a line parallel to the y-direction for Case G are presented in Figure 5.9. At $P_i=100\%$, the stress distribution for Case G with horizontal weakness planes are identical to those of an opening in an elastic, homogeneous, isotropic material. When the borehole became unstable at $P_i=31\%$, the stress distribution for σ_θ is significantly different from those of homogeneous isotropic material within a distance of about 1.5 radii. However, the stress distribution for σ_r is only slightly less than in a homogeneous isotropic material. These results are very similar to those with local weaknesses presented in Figure 4.7. The deviatoric

stress distribution with horizontal weakness planes is higher than for a homogeneous isotropic material when r/a is less than 1.2.

At the point of merger of the yield zone (Figure 5.8, $P_i=31\%$), the tangential stress at $r/a = 1.2$ is reduced to about 40 % of the tangential stress expected near an opening in elastic rock. This can be of great importance for the design of frictional bolts because the frictional resistance developed between the rock mass and the bolts is a function of the tangential stress. If the tangential stress at this point is reduced, then the frictional resistance will also be reduced. Longer bolts penetrating to $r/a > 1.25$ would be needed in order to reach the area with higher tangential stress, and hence mobilize more frictional resistance.

5.6 Practical Implications of Findings to Design and Monitoring of Underground Openings

The ground convergence curves at two points (R) and (S) for the three cases E to G, ($\eta=0^\circ$, 45° and 90°) with $N=0.5$ are shown in Figure 5.10. The convergence curves at (R) are similar for all three cases because no yielding occurs at this side of the opening and it is difficult to differentiate among the various modes of failure that occur near (S). At point (S), the amount of convergence for the Case F ($\eta=45^\circ$) is much greater than for the two cases $\eta=0^\circ$ and 90° because yielding is initiated at (S) and propagates into a continuous yield zone to relatively larger extent compared to the other two cases. The convergences for the two cases $\eta=0^\circ$ and 90° are similar up to $P_i=55$

% because two independent yield zones on either side of (S) develop for these two cases. The merging of the two bands of yielded rock occur at $P_i=54\%$ for $\eta=0^\circ$ and at $P_i=31\%$ for $\eta=90^\circ$, hence, a borehole with weakness planes parallel to the major principal stress approaches an unstable condition earlier than those with weakness planes parallel to the minor principal stress. This is because yield initiation at the borehole wall is closer to point (S) for the former than for the latter case. Less propagation is needed for the two bands of yielded rock to merge if the initiation zones are closer together.

The simulated ground strain curves at three locations near (S) for Case G ($\eta=90^\circ$) where an elastic block is created is presented in Figure 5.11. When the material is elastic at the point of measurement and at $P_i > 50\%$, the average radial strain at Location V, closest to the borehole wall, is greater than those at Locations VI and VII which are further away from the borehole wall. However, when the borehole becomes unstable at $P_i=31\%$, the highest average radial strain is recorded at Location VI which corresponds to the point where the two bands of yielded rock merge. The average radial strain at Location V tends to decrease rapidly when the two bands of yielded rock merge. This is an indication that the elastic block enclosed within the bands of the yielded rock tends to be unloaded and pushed into the opening. It is also of interest to note that extensometers at all these locations would respond linearly (as if the opening were in elastic rock) until the yield zones merge at $P_i < 50\%$. This is of great practical importance since linear convergence or strain curves are normally associated with stable conditions.

This study supports the earlier findings that convergence measurements are poor indicators for identifying the type and location of failure mechanisms. It follows that localized measurements of relative displacements at appropriate locations are needed to properly locate and identify failure modes.

5.7 Summary and Conclusions

A transversely isotropic yield criterion was implemented in a finite element program in order to study the effects of oriented weaknesses and the far-field stress ratio on the yield initiation and propagation around a borehole, and to compare the failure mechanisms with those generated by local weaknesses. The model describes a linear elastic, brittle, perfectly plastic rock. Four cases with different combinations of weakness orientation and far-field stress ratio were studied. It was found that block-type failure mechanisms similar to those generated by local weaknesses are also possible if the weakness orientation is parallel to the direction of the principal stresses and the far-field stress ratio differs significantly from unity. This is because yielding is initiated at positions similar to those that were introduced selectively by local weaknesses.

Localized yield zones created by local weaknesses or transversely isotropic strength will lead to critical stress conditions inside the rock such that the propagation and merging of the two bands of yielded rock becomes possible.

Convergence measurements at an opening wall are insufficient to differentiate among the various modes of failure. Instruments for

monitoring purposes must be located at strategic positions chosen on the basis of several hypotheses of likely behaviour and failure.

The block-type failure mechanisms identified in this thesis by numerical simulations will in the next chapter be investigated further by comparing numerical predictions with laboratory and field observations.

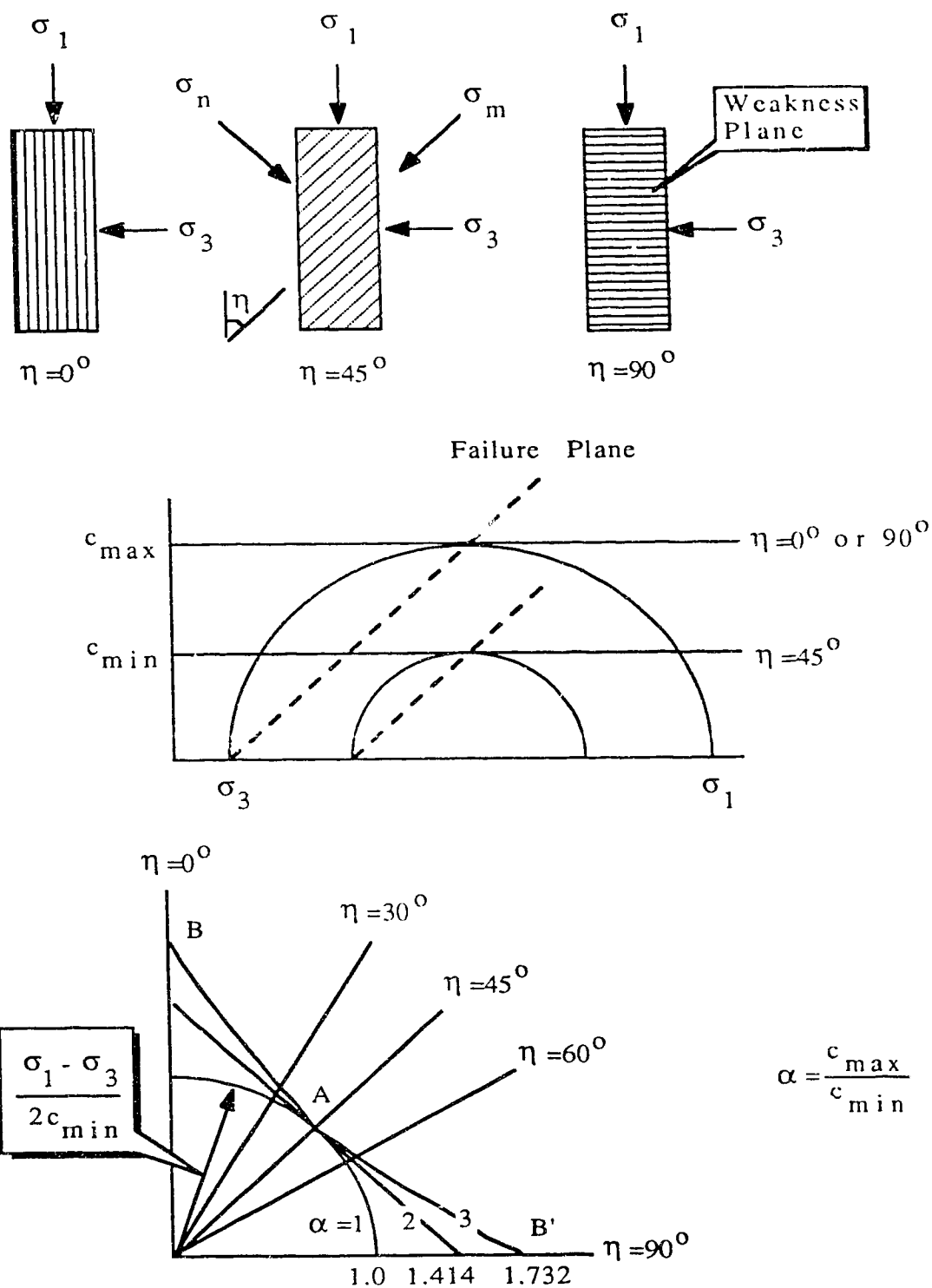


Figure 5.1

Transversely Isotropic Yield Criterion for Cohesive Material ($\phi=0$).

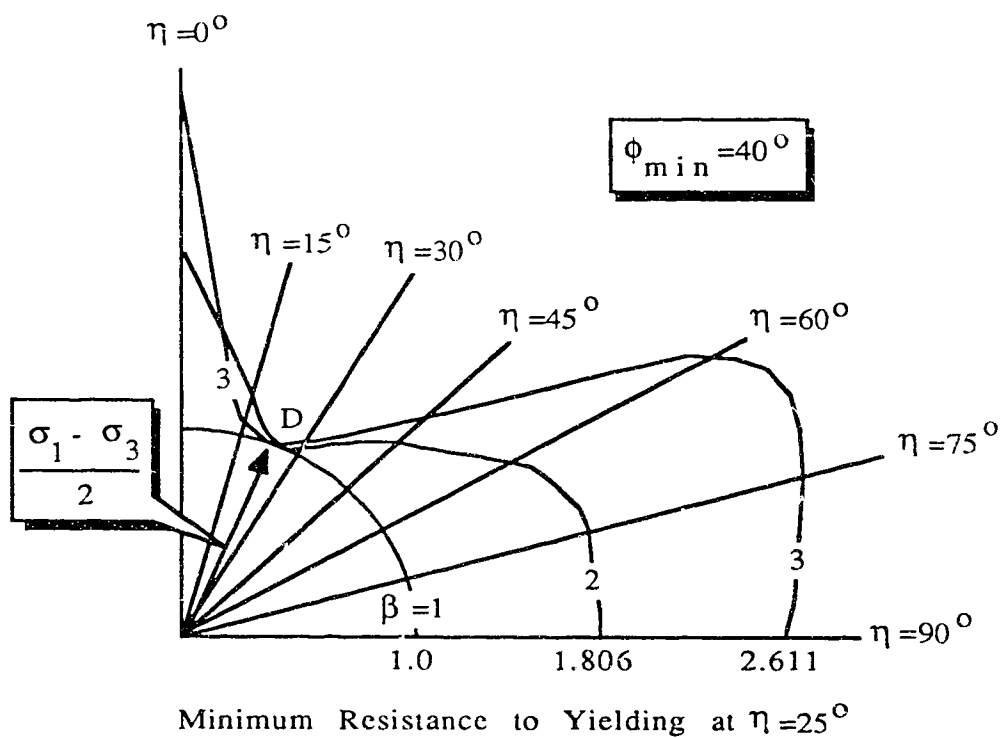
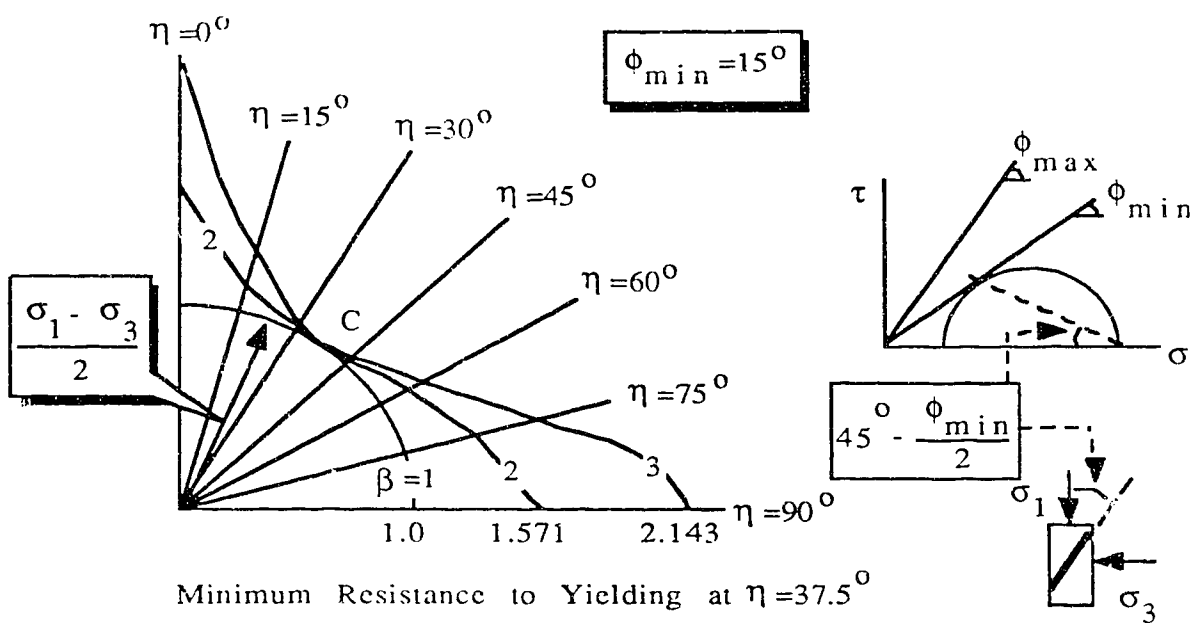


Figure 5.2

Transversely Isotropic Yield Criterion for
Purely Frictional Material ($c=0$).

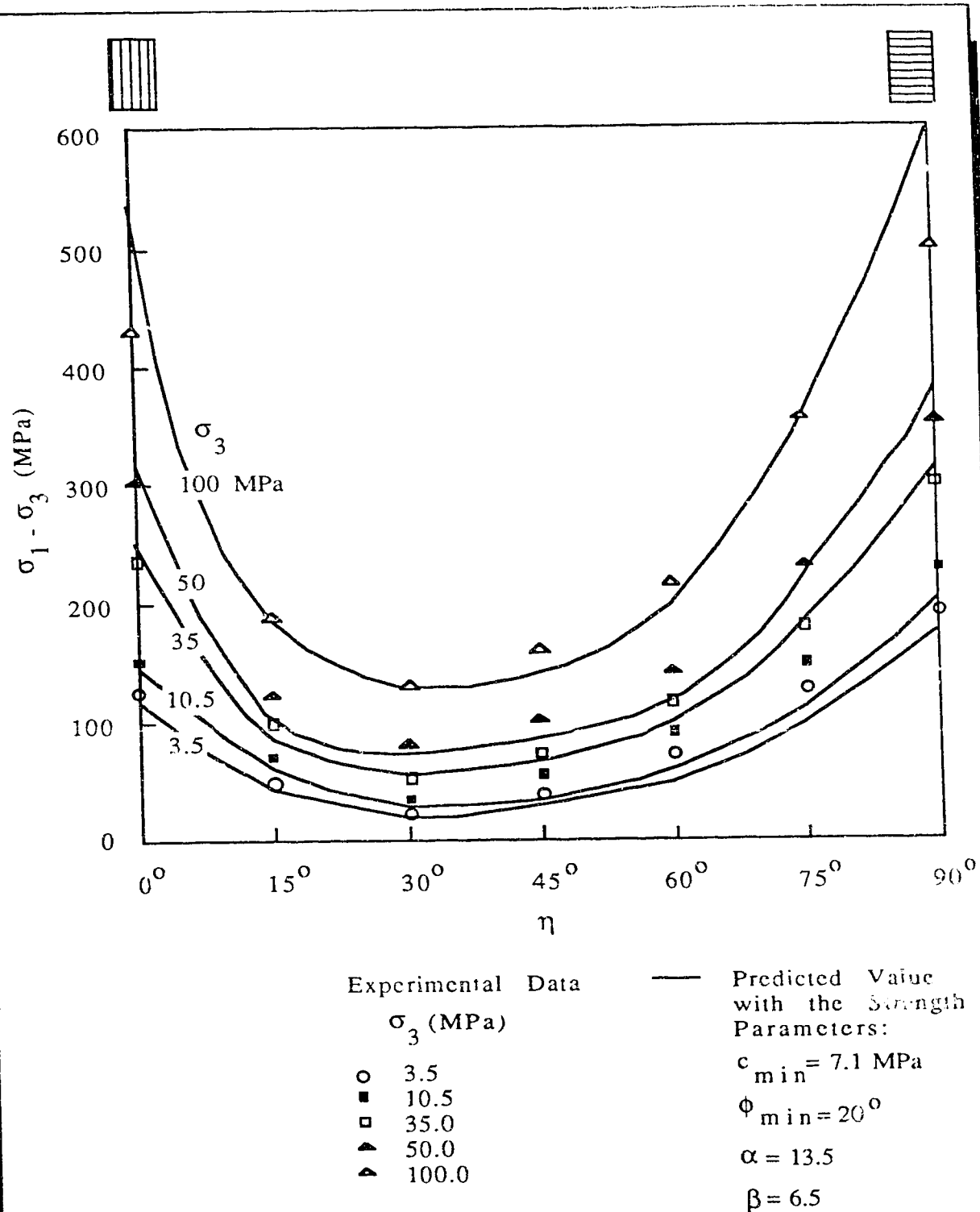
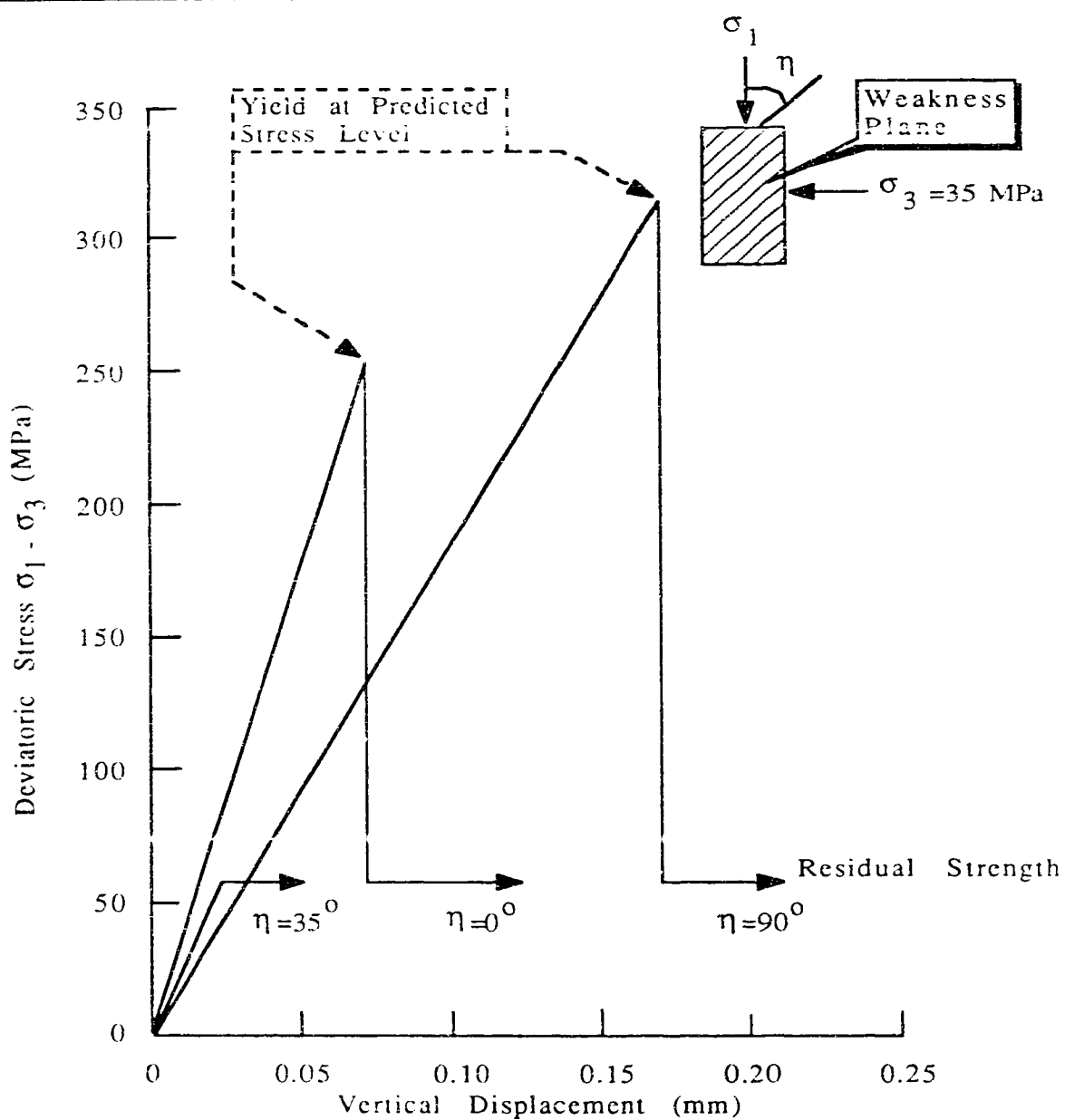


Figure 5.3

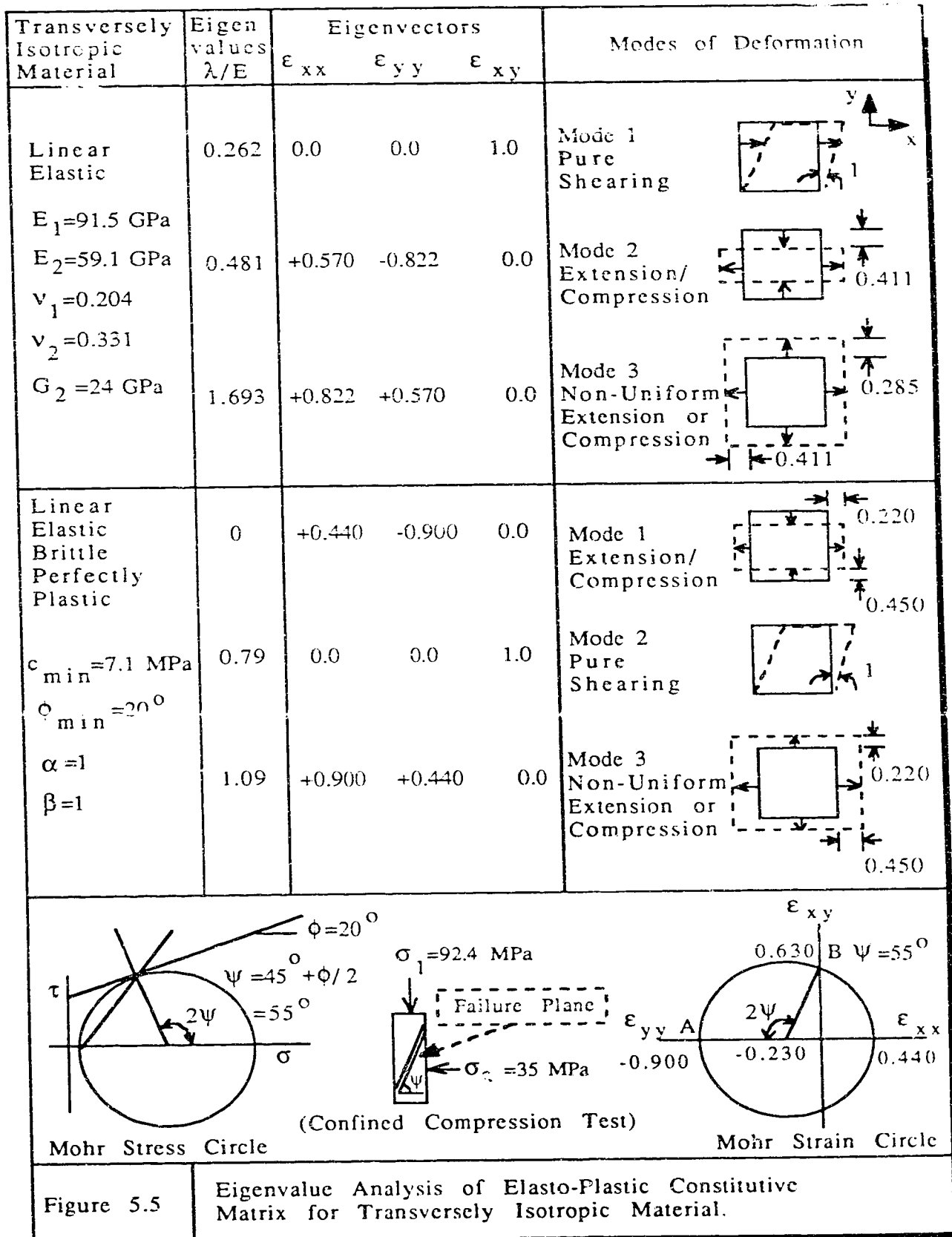
Deviatoric Stress at Failure Versus Orientation of Weakness Plane -Experimental Results on Martinsburg Slate (Data after Donath, 1963).

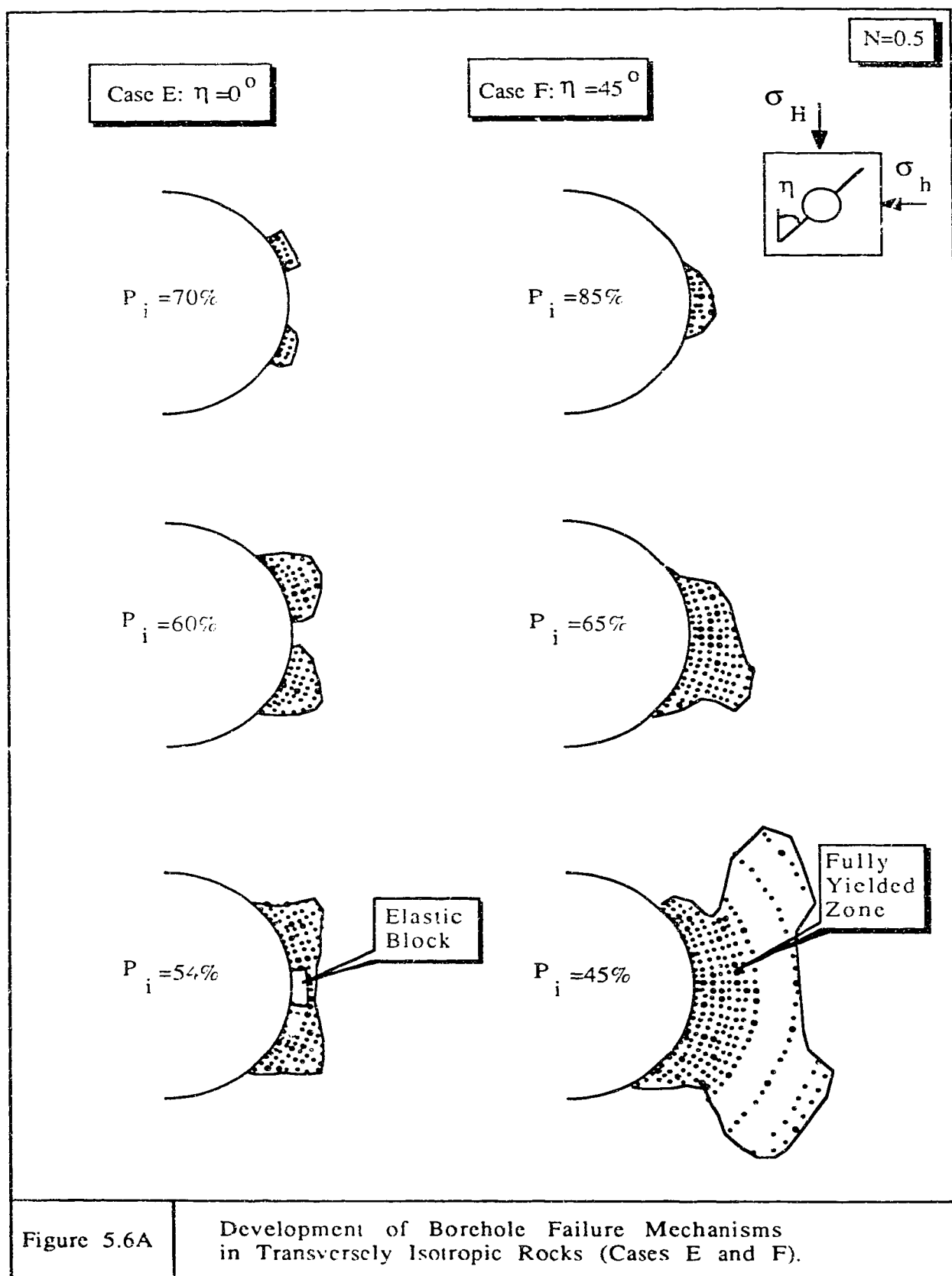


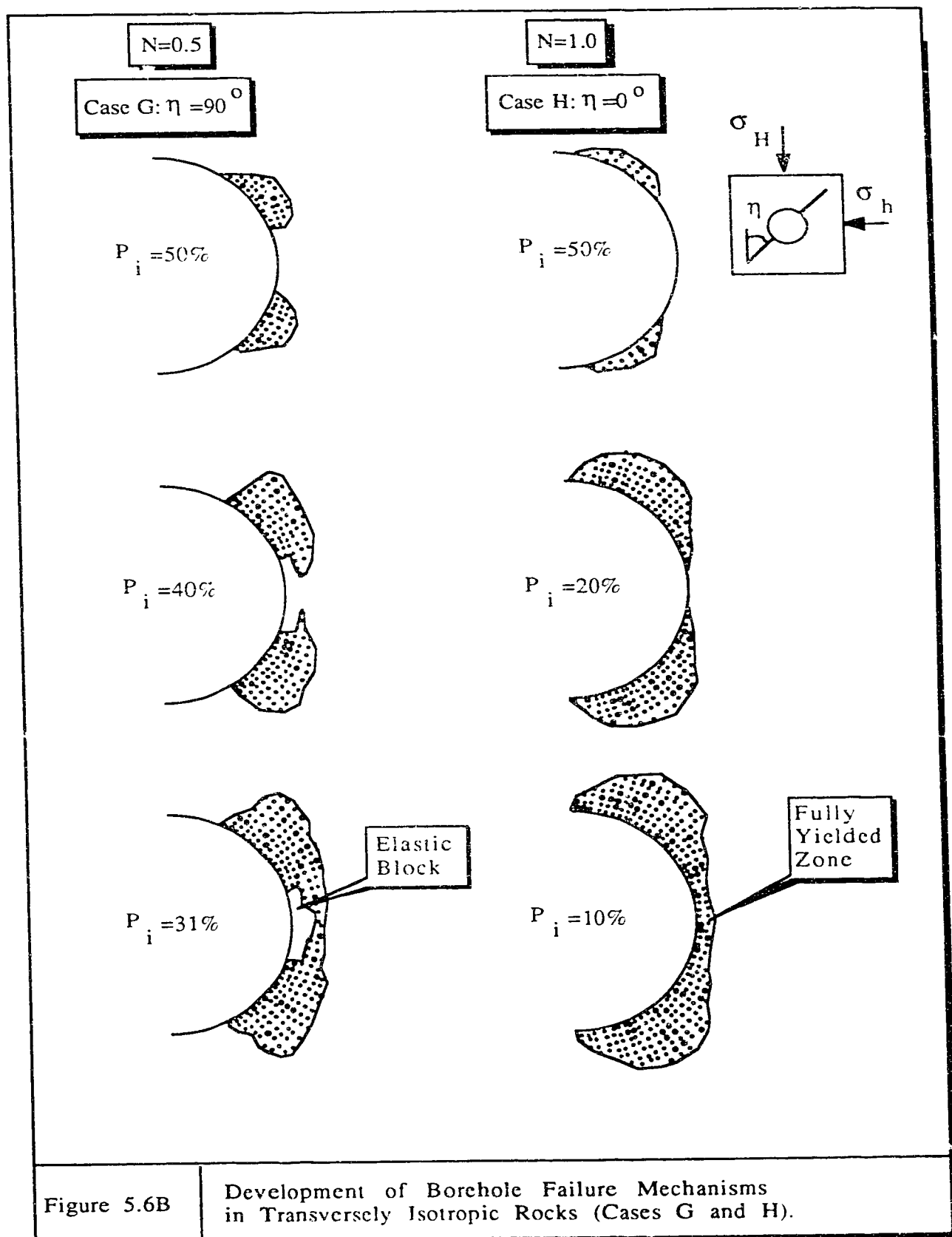
	Peak		Residual
c_{\min} (MPa)	7.1	c_{res} (MPa)	7.1
ϕ_{\min}	20°	ϕ_{res}	20°
α	13.5		
β	6.5		

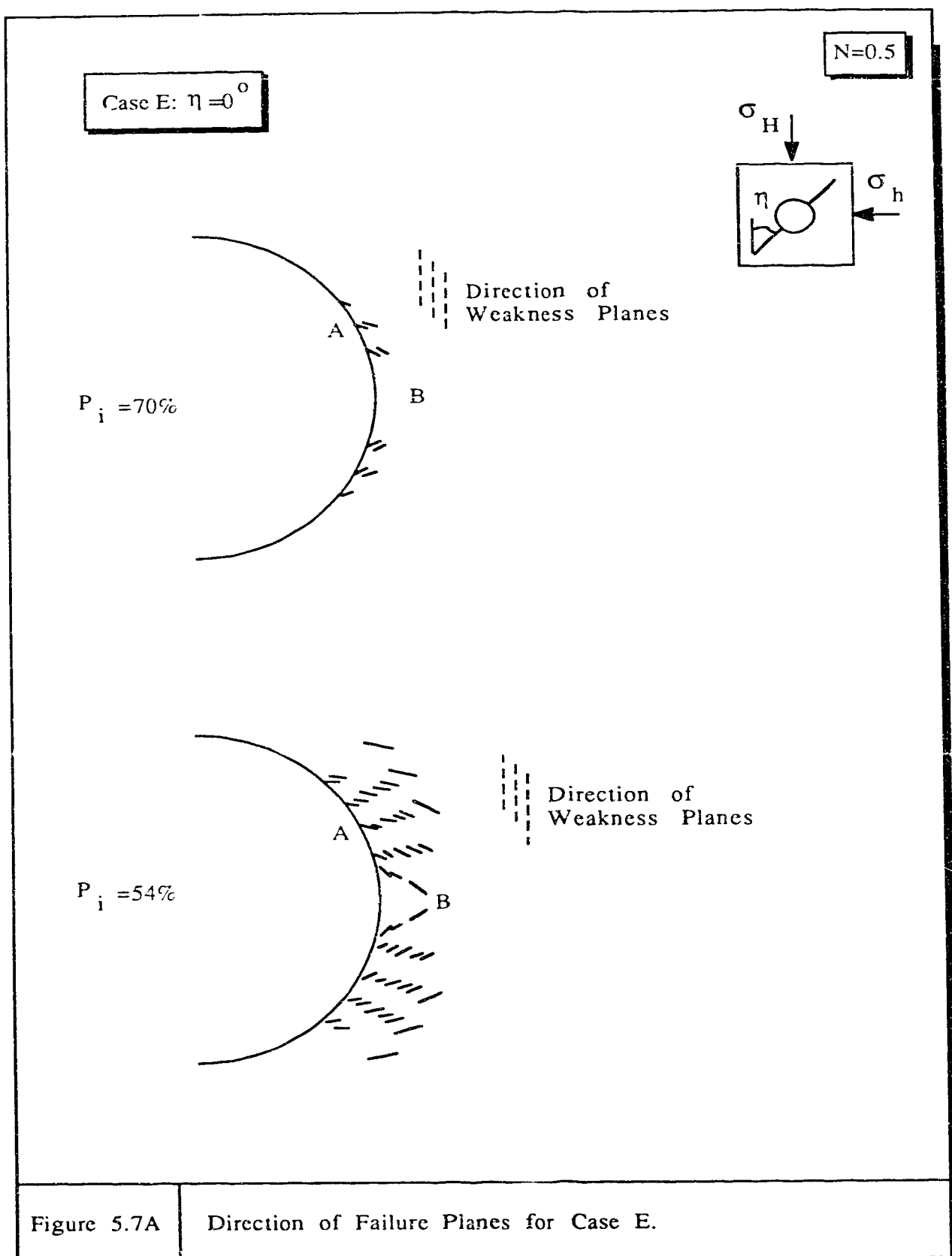
Figure 5.4

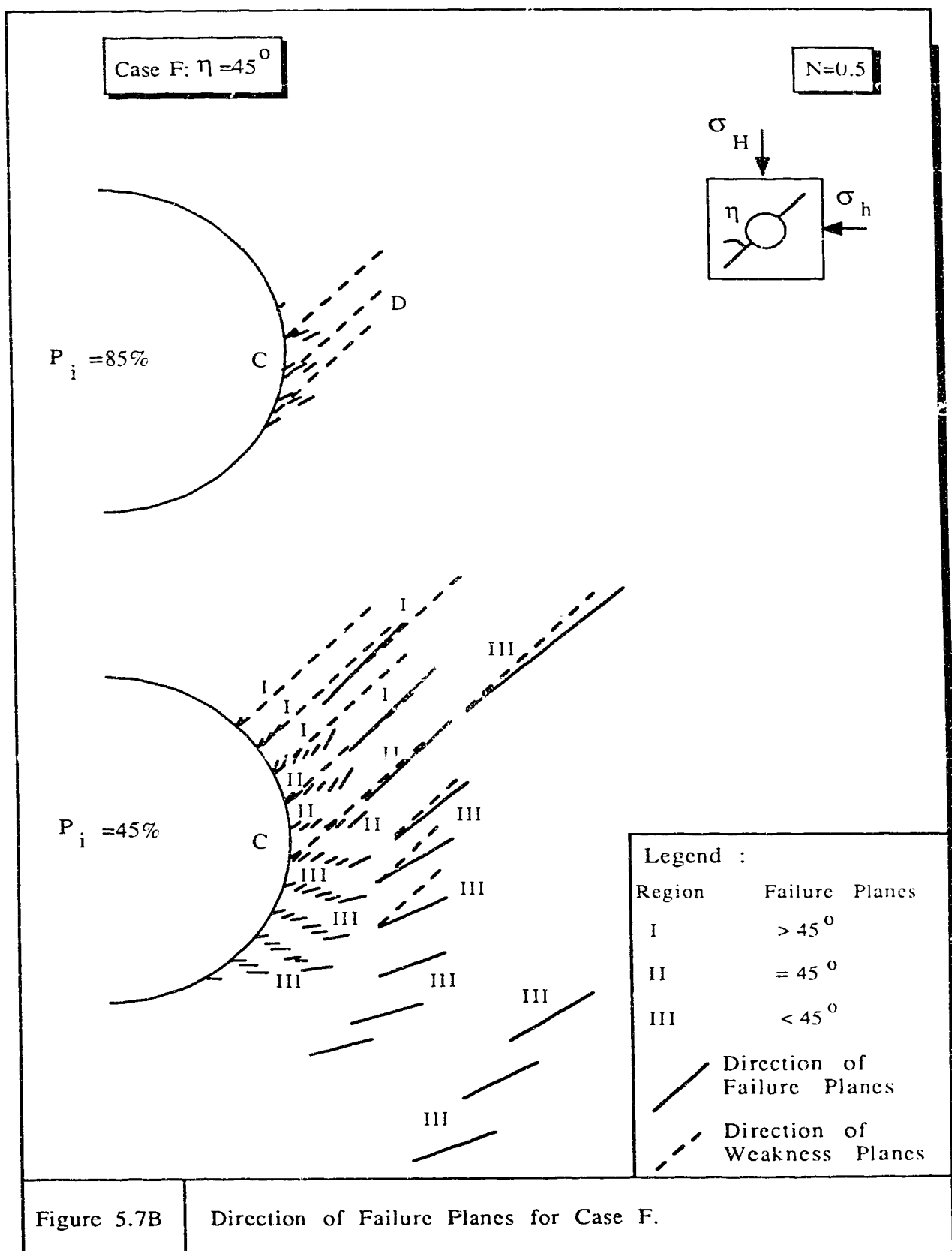
Confined Compression Test by Finite Element Simulation.

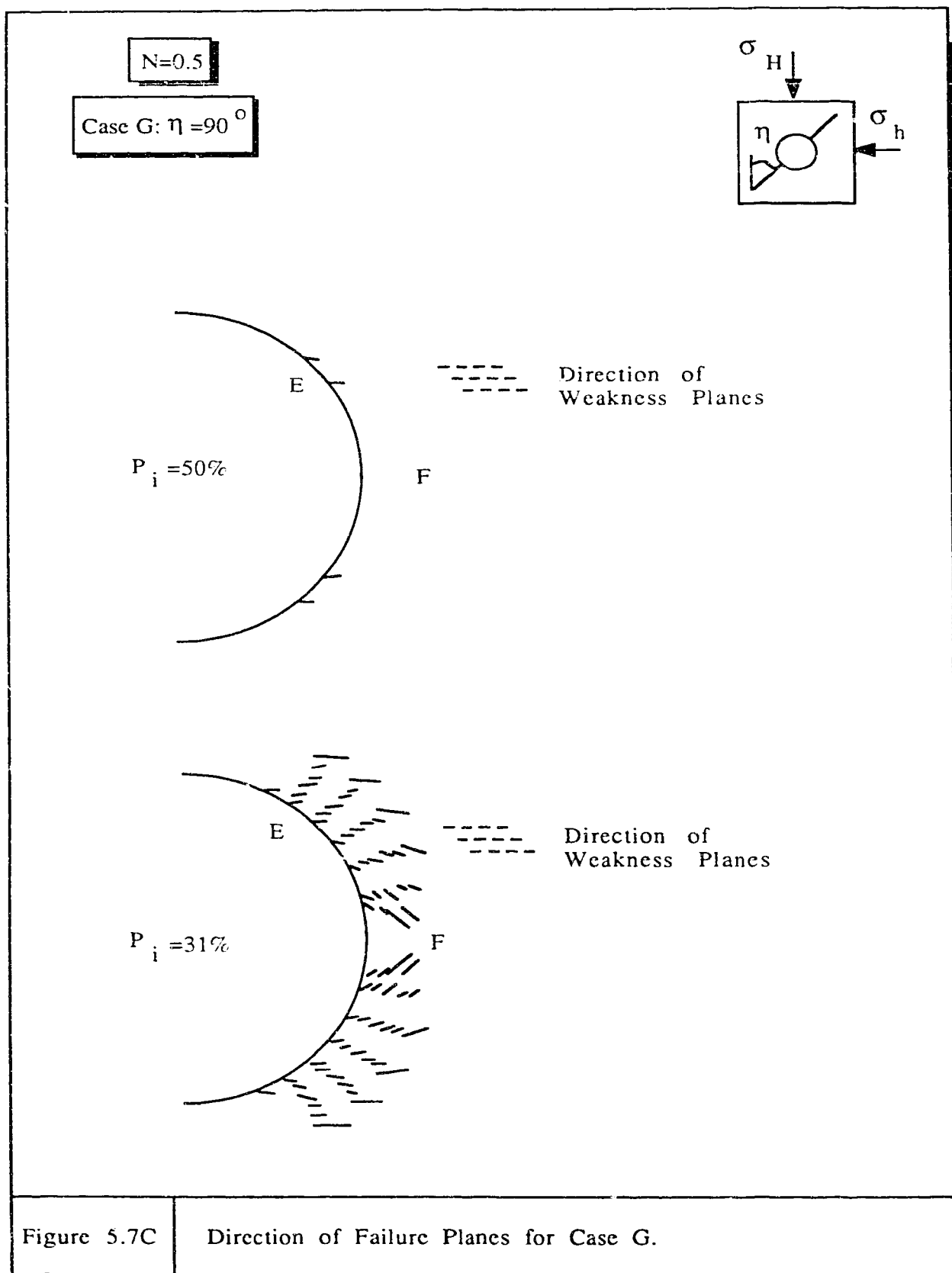












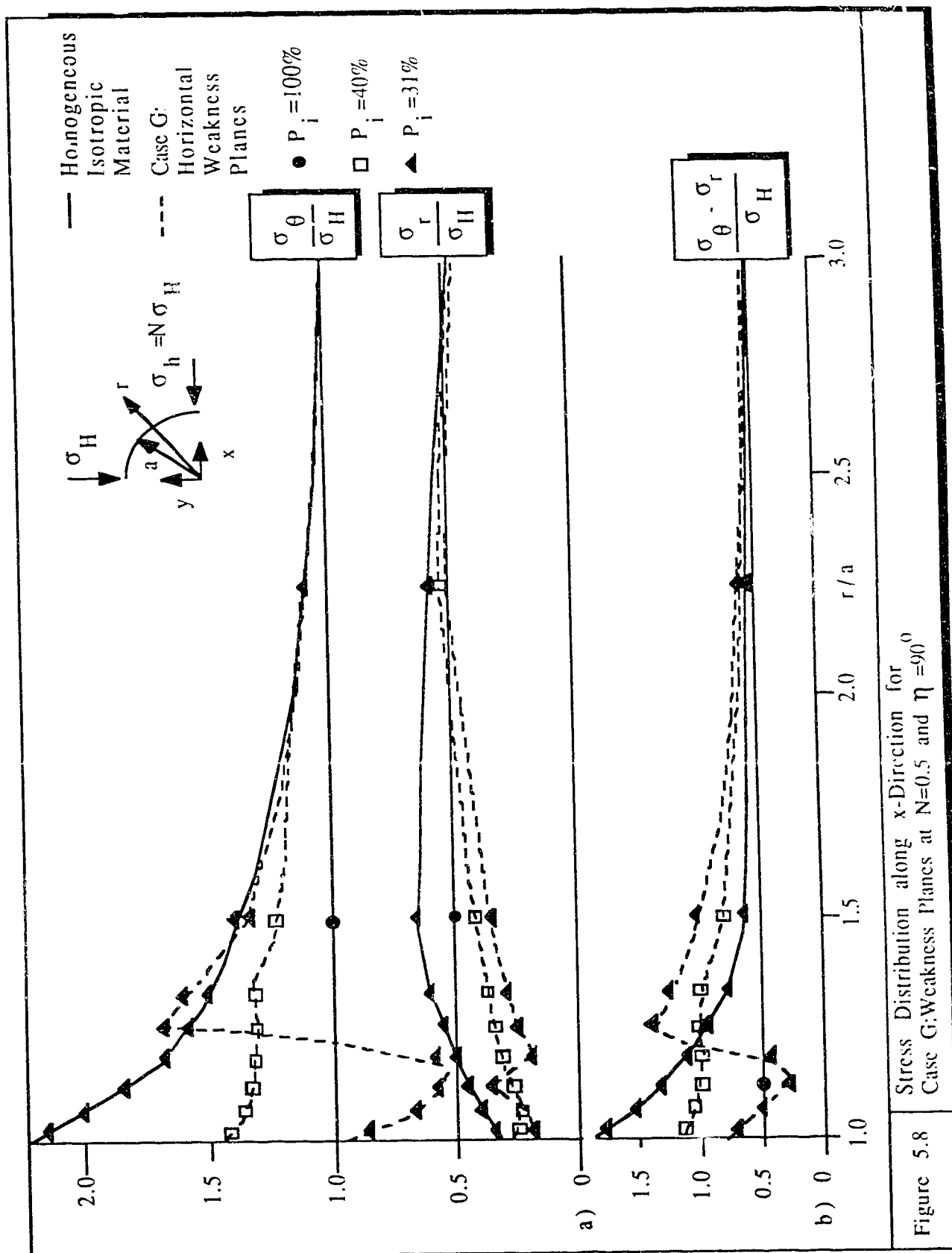


Figure 5.8 Stress Distribution along x-Direction for Case G: Weakness Planes at $N=0.5$ and $\eta=90^\circ$

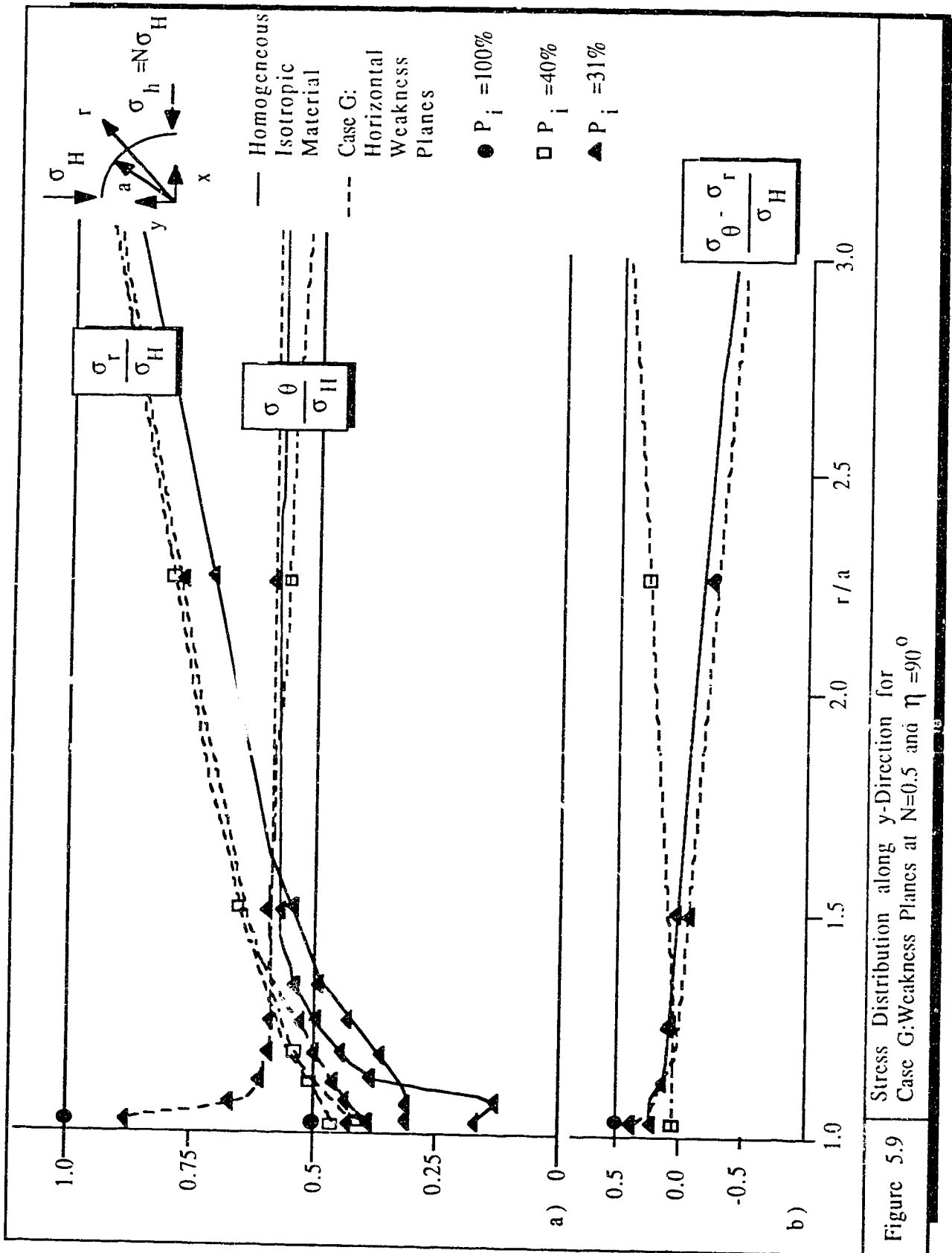


Figure 5.9 Stress Distribution along y-Direction for Case G: Weakness Planes at $N=0.5$ and $\eta=90^\circ$

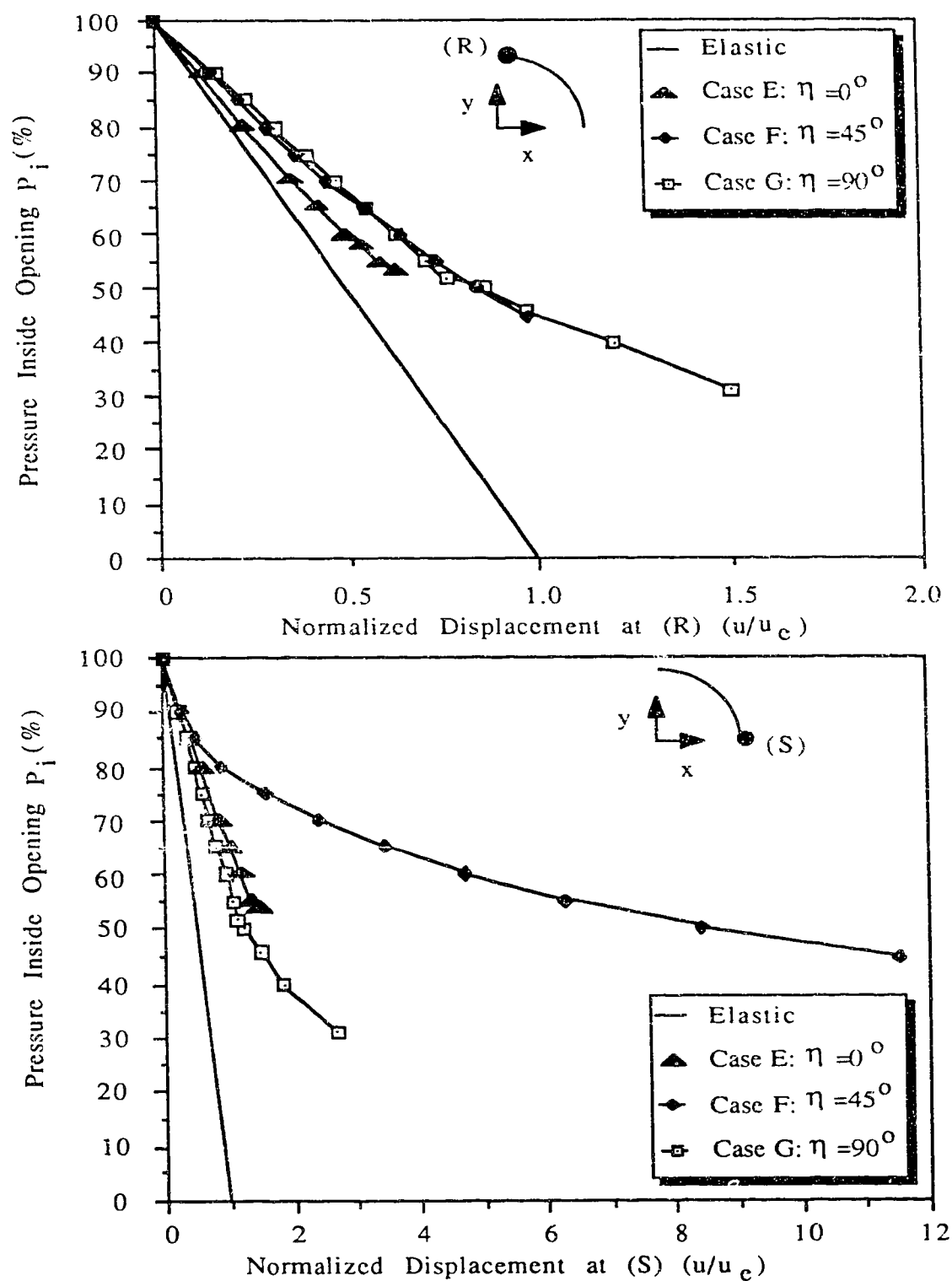


Figure 5.10

Ground Convergence Curves for Circular Opening
in Transversely Isotropic Rocks.

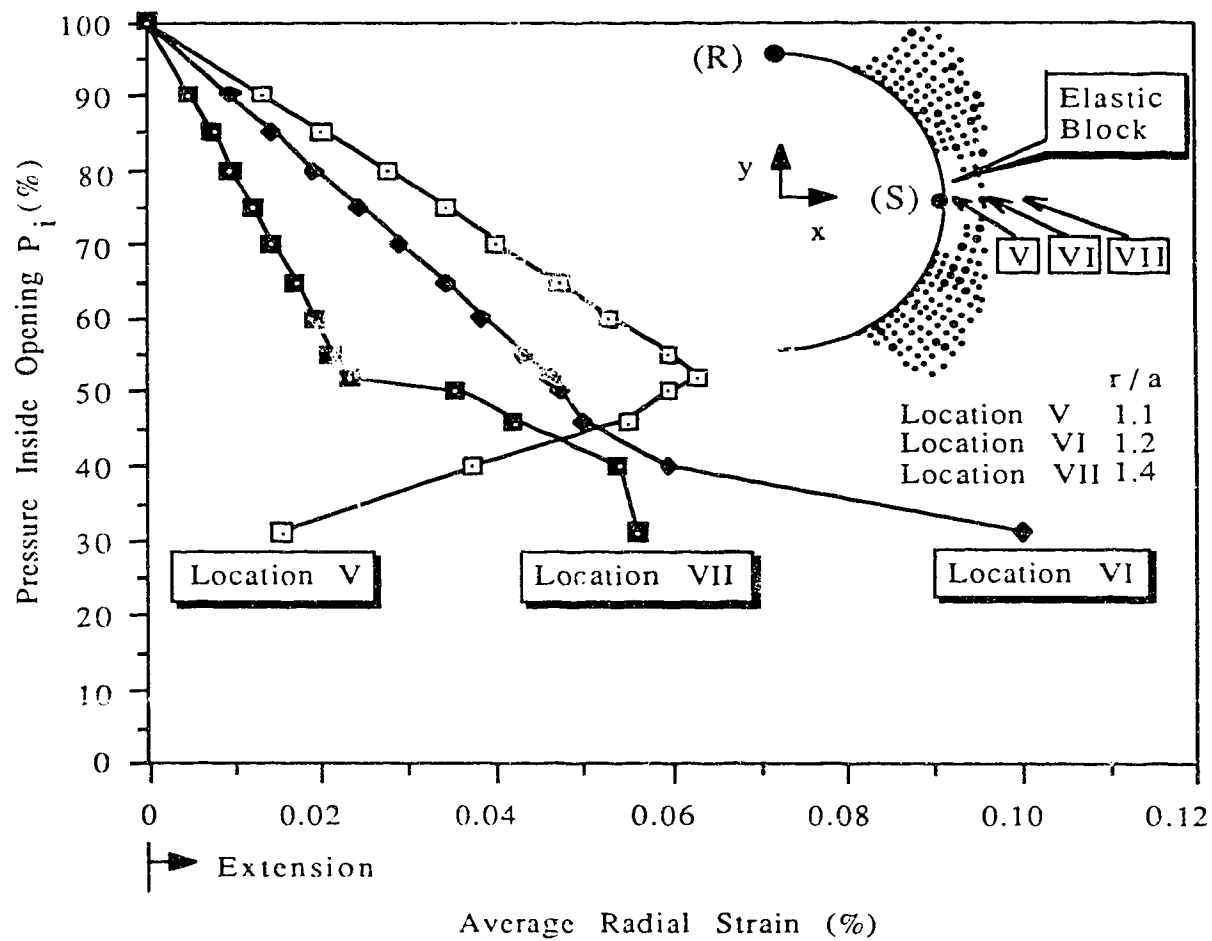


Figure 5.11

Ground Strain Curves at Three Locations
along the x-direction for Case G: Weakness Planes at $\eta = 90^\circ$

6 INVESTIGATION OF UNDERGROUND OPENING FAILURE MECHANISMS IN TRANSVERSELY ISOTROPIC ROCKS

Block-type failure mechanisms similar to those described in Chapters 4 and 5 have been observed in laboratory tests of small circular openings in samples of jointed coal, and during the construction of tunnels in rock with parallel weakness planes. In the following, it is attempted to compare these observed failure mechanisms with those simulated by finite element analyses.

6.1 Failure Mechanisms of Small Circular Openings in Coal

Although problems of borehole instability are widely encountered in hydrocarbon exploration, the mechanisms and processes controlling the occurrence of instabilities and the transition from stable to yielding and later to rupture are not well understood because it is seldom possible to make sufficient measurements in the field to permit a comprehensive evaluation of the actual failure mechanisms. Hence, it is necessary to conduct laboratory tests to simulate the relevant failure processes in a manner that permits collection of sufficient data for conclusive interpretation.

Testing of small circular openings in samples of jointed coal have been conducted by Guenot (1979) to investigate the initiation and propagation of yield zones up to rupture of the wall of the opening. The experimental facilities, the sample preparation techniques and the instrumentation have been described in detail by

Kaiser and Morgenstern (1981). A sample of regularly jointed coal (Test No. MC-4) with time-dependent strength and deformation properties described in Kaiser and Maloney (1982) was tested over a period of two months. The sample was first subjected to a uniform stress ratio ($N=1.0$) in order to assess the deformation properties of the sample (Test MC-4.1). The sample was unloaded and a circular opening of 152 mm in diameter was excavated in the center of the sample. The sample was then subjected to two multi-stage creep tests MC-4.2 and MC-4.3 with six creep stages each. The duration of each creep test was about one day and the stress ratio was kept close to unity ($N=1.08$ and 0.98). Plane strain conditions were maintained by gradual application of longitudinal stresses to ensure zero strain parallel to the opening axis. The sample was instrumented with 15 extensometers located on two concentric rings, at r/a equal 1.46 and 1.98 (r is the radial distance from the center of the opening to the center of the extensometer and a is the radius of the opening).

6.1.1 Description of Results from Test MC-4.2

For Test MC-4.2, the sample was loaded in stages until rupture of the opening wall was visually detected during creep at $\sigma_H = 13.3$ MPa. A v-shaped piece of intact rock, about 20 mm by 20 mm in area, broke from the wall of the opening at this stress level. The propagation of this rupture zone slowed down after 28 hours of creep but the rupture process proceeded immediately after the sample was further loaded to the final stress level at $\sigma_H = 15.9$ MPa. The sample was then unloaded and the loose broken material was

removed from the wall. Figure 6.1 illustrates the shape of the sample at $\sigma_H=13.3$ MPa and the extent of the rupture zone after unloading the sample and removing the loose broken material from the opening. The sample was then reloaded to the final stress level of $\sigma_H=16.6$ MPa (Test MC-4.3) to observe when and to what extent rupture would propagate if the rock mass were no longer confined by the broken rock. A complete description of the failure process for Tests MC-4.2 and MC-4.3 was given by Guenot (1979) and Kaiser et al. (1985).

6.1.2 Generation of Failure Mechanisms by Finite Element Analysis

For the following reasons, it is expected that the yield initiation and propagation process simulated by the finite element analyses will not completely match the observed rupture behaviour:

1. The yield initiation and propagation process simulated in the finite element analysis is limited to small displacements and continuous displacement fields.
2. The time-dependent properties of the coal are not modelled by the finite element analysis code adopted.
3. The material parameters for describing the transversely isotropic strength of coal was not accurately defined.
4. Local weaknesses are present even though the coal sample is, in general, regularly jointed with a predominant joint set.

Nevertheless, an attempt was made to simulate the observed failure mechanism with the following assumptions:

1. The elastic deformation properties of the coal were chosen based on the triaxial test results described in Kaiser (1979).
2. Weak elements were placed in the model because it was found from Figures 5.6A and 5.6B that block-type failure mechanisms are not possible for N equal to unity if no weakness exist.
3. The location of the weak elements and the strength parameters for coal were selected so that a block-type failure mechanisms will develop at a stress level in the vicinity of $\sigma_H=13.3$ MPa.

The simplified approach presented in the following chapter provide guidelines for selecting the strength parameters so that the extent of the yield zones in the finite element simulation will be close to the extent of the observed rupture zone.

Figure 6.2 shows the finite element mesh and the location of the weak elements for this analysis. The material parameters for the analysis are summarized in the table presented in Figure 6.2. Both the rock mass and the local weak element were assumed to be transversely isotropic.

The extent of the yield zones simulated by the finite element analysis, and also the extent of the observed rupture zones are presented in Figure 6.3. Yielding is initiated at four locations on the wall at about $\sigma_H=10$ MPa, and propagates on opposite sides but more rapidly toward the weak elements. An elastic block enclosed by two bands of yielded rock and the weak elements is formed at $\sigma_H=14$

MPa. This block tends to be pushed into the opening if σ_H is further increased. The maximum extent of the simulated yield zone is at r/a equal to 1.4 which is slightly less than the extent of the measured rupture zone of r/a equal to 1.6. Figure 6.3 also shows that block-type failure mechanisms cannot be formed if local weaknesses are not present (see opposite side of weak element).

The closures of the opening wall at four locations (A, B, C and D) are shown in Figure 6.4. It can be seen that the closures predicted by the finite element analysis compare reasonably well with those measured in the tests. Both finite element and measured closures do not give any indication of yield initiation at the wall.

The strains measured from the extensometers at 15 locations around the circular opening are presented in Figure 6.5. Most strain measurements show a sudden increase in compressive strain when the sample is first loaded to $\sigma_H=1.5$ MPa. This was interpreted by Guenot (1979) to be due to the closure of cracks and the compaction of the coal sample. The strain attributed to this effect was subtracted from the measured strain, and the revised curves are presented in Figure 6.6 together with the strains obtained from the finite element analysis. The following comparisons are made:

- 1) It can be seen that at various locations, the strain predicted from the finite element analysis compare extremely well with those measured in the test.
- 2) For the closest row of extensometers (9 to 16), the strain predicted from finite element analysis (except extensometers 16) follow the trend measured in the test. The deviation of extensometer 16

may be due to local variation of strength in the sample. The strain predicted at extensometers 10, 11, 13 and 15 match very well with those measured. Less accurate prediction is made at extensometers 9 and 12.

- 3) Initiation of yielding, which is indicated by the change in curvature, is clearly detected at extensometers 9 to 15.
- 4) For extensometers (17 to 21) away from the opening, all the predicted strain show compression and follow the general trend of those measured. The poorer agreement is because compressive strains due to coal compaction was not included in the predictive model.

6.1.3 Summary and Conclusions

The block-type failure mechanism observed in the laboratory test of an opening in coal could be reproduced by the finite element simulation with a transversely isotropic material model and an assumed local weakness. Despite the uncertainty of the material parameters, it is concluded that the location and the process of yielding simulated in the finite element model compare very well with those measured in the test. The predicted closure of the opening wall and the predicted strains at various locations away from the opening agree well with the measured strains. Local weaknesses are needed for block-type failure mechanisms to develop in transversely isotropic rocks if the stress field is nearly uniform. Finite element analysis is limited to continuous displacement fields, and therefore cannot be used to model the

rupture process after the elastic block is allowed to move into the opening.

6.2 Failure Mechanisms of a Tunnel in Rock with Parallel Weakness Planes

Block-type failure mechanisms similar to those described in coal have been observed during the construction of the Frejus Tunnel which links France and Italy. The tunnel is approximately 13 Km long. The depth of the overburden varies from 600 to 1200 m along most of the length of the tunnel. The tunnel was excavated in part through schist with weakness planes being more or less tangential to the wall of the tunnel as shown in Figure 6.7. The influence of major discontinuities on the modes of failure as described by Lunardi (1980) are illustrated by the three examples in Figure 6.7. More detailed descriptions of the geological condition at the Frejus Tunnel can be found in Lunardi (1980).

It is much more difficult to model the rupture process and the ground response during the construction of a tunnel than the excavation of a circular opening under controlled laboratory condition as described in Section 6.1 for the following reasons:

1. The ground convergence characteristics and the stress distribution around the tunnel is affected by the construction method and sequence, as well as the support system.

2. The wall displacements and ground pressure on the lining of a tunnel may increase with time for several weeks or months depending on the time-dependent behaviour of the rock mass, the rate of advance of the tunnel face and the response of the support system.
3. The rock mass parameters cannot accurately or only with great difficulty be determined for numerical modelling.
4. The presence of local weaknesses may not be known or only be detected during supplemental geological and geotechnical investigations.

Because all of the above uncertainties may affect the analysis of the Frejus Tunnel, the following finite element analysis only attempts to investigate the location of yield initiation, the extent of yield propagation and to provide support for the earlier finding that block-type failure mechanisms may develop in transversely isotropic rocks under uniform far-field stresses provided that local weaknesses are present. No attempt is made to match the simulated with the observed convergences.

6.2.1 Description of Failure Mechanism at Frejus Tunnel

For the following studies, it is assumed that local weaknesses are present and that their locations are as shown in the finite element mesh in Figure 6.8. The excavation process is simulated by reducing the support pressure of the tunnel while the far-field stress $\sigma_H=25$ MPa is kept constant ($N=1.0$). The material parameters shown

in Figure 6.9 are selected on the basis of published test results on schists (Lunardi, 1980).

The extent of the yield zones simulated by the finite element analysis, and the ground convergence curves at 4 points are presented in Figure 6.9. It can be seen that yielding is initiated at $P_i=50\%$ at Locations 3 and 4 first which are opposite to each other at the tunnel wall. When the support pressure is further reduced to 35 %, yielding is also initiated at Location 2 and it propagates toward the weak elements. An elastic block enclosed by the two bands of yielded rock and the weak elements, is formed at $P_i=25\%$ and tends to be pushed into the tunnel as the support pressure is further reduced. This kind of block-type failure mechanism is similar to that observed earlier in coal, and the location agrees well with that observed during the construction of the Frejus Tunnel as shown in Figure 6.7.

The convergence between two opposite points on the tunnel wall for six directions (A to F) are presented in Figure 6.10. This figure also compares the observed convergences obtained from Berst et al. (1980) at four different stations (4.835 Km, 4.994 Km, 5.172 Km, and 6.066 Km) along the Frejus Tunnel. At all four stations along the tunnel, the maximum convergence occurred in Direction D. This supports the findings from the finite element analysis that an elastic block is being pushed into the tunnel in the Direction D before other yielded zones move in. The observed convergence in Direction A is less than that predicted by the finite element analysis. This may be due to the associated flow rule being used in the model. The associated flow rule assumes that the plastic strain increment is

perpendicular to the yield surface (Equation D.4, $Q=F$) which sometimes may tend to over predicting the volume change. It should be emphasized that this case study made no attempt to match the simulated and the observed wall displacements, but rather to investigate the location of yield initiation and the development of yield zone.

The observed convergence in other directions, vary from station to station along the tunnel. This indicates that variation in local conditions (material properties, construction sequence etc.) at different stations along the tunnel can create difficulties for finite element simulation to match with the observed convergence.

The observed convergence in Direction A vary from 100 mm to 480 mm for different stations along the tunnel. Sulem et al. (1987) based on a curve fitting technique suggests that the time-independent convergence is about 20 % of the total observed convergence. The convergence from the finite element analysis (at $P_1=25$ %) is only about 9 mm which is much less than the time-independent convergence (20 mm to 96 mm) as suggested by Sulem et al. (1987). This is because the finite element formulation in the model is based on small strain and small deformation. Large displacements (11 mm to 87 mm) must have occurred when the elastic block of rock moved into the tunnel or when failure propagated.

Finally, the extent of yield zones around the tunnel from the studies by Guenot (1980) and Frank et al. (1980) are schematically illustrated in Figure 6.11. These two studies use the finite element code, ROSALIE, developed at the Laboratoire Central des Ponts et

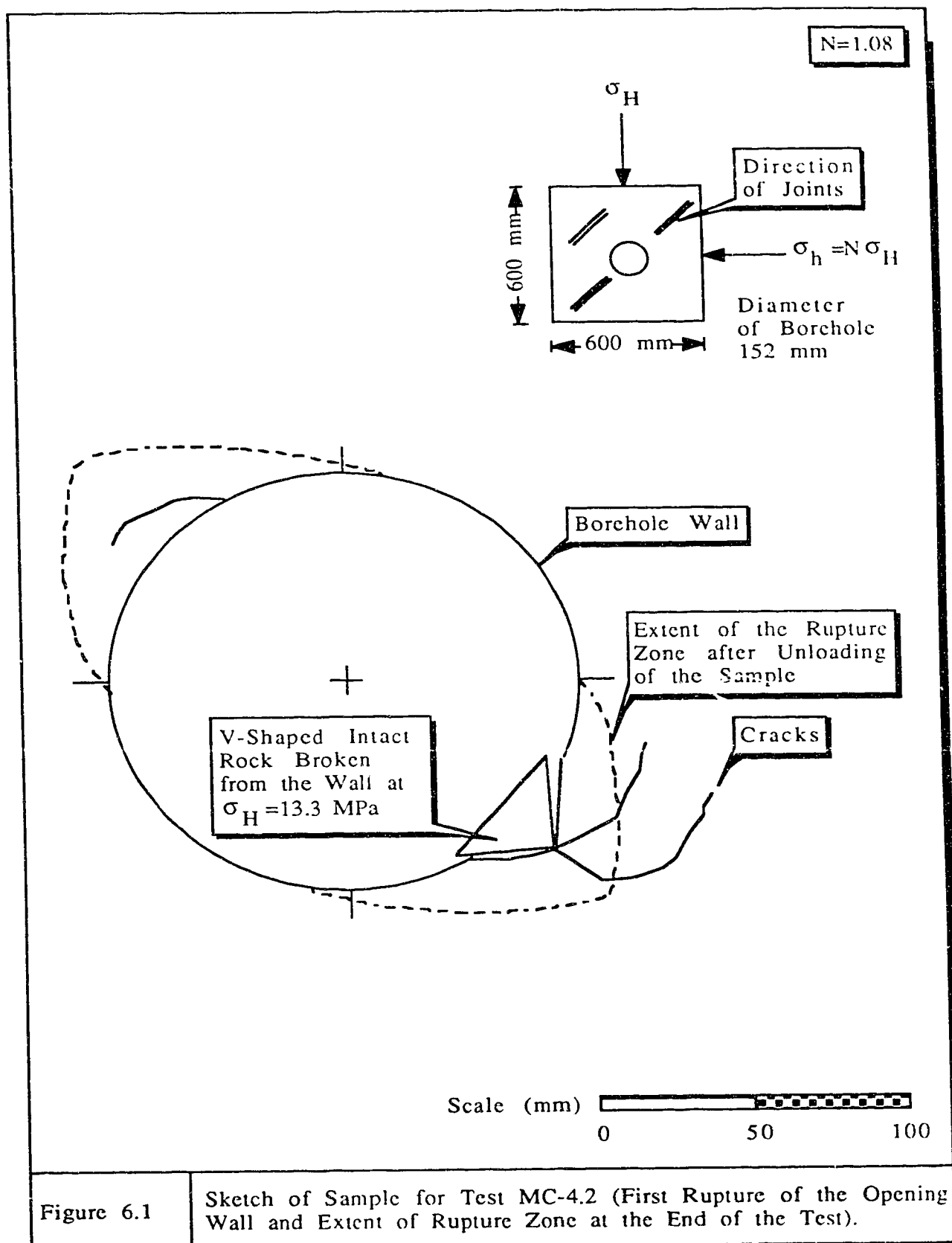
Chaussées in Paris, France. The rock mass is assumed to behave as linearly elastic, perfectly plastic satisfying the Mohr-Coulomb yield criterion. The joint behaviour is similar to the rock mass except that it is brittle and perfectly plastic after reaching the peak strength. The Mohr-Coulomb yield criterion for the joint is expressed in terms of normal and shear stresses at the joint. It is assumed that there is no plastic volume change in the joint. The cohesion and angle of friction for the rock mass and the joint can be found in Figure 6.11. Stress calculation in the finite element code is based on the Modified Newton-Raphson method. Non-associated flow rule can be used. Details of this finite element code is described in Guenot (1980). Guenot (1980) and Frank et al. (1980) studied the cases where the joints are orientated at 50° and 30° to the x-axis, respectively (Figure 6.11). The joints are assumed to be equally distributed around the tunnel. The stresses from the finite element calculation are first substituted into the Mohr-Coulomb yield criterion of the rock mass. If the rock mass has not reached yielding, the stresses are rotated into the normal and shear stresses component at the joint. They are substituted into the Mohr-Coulomb yield criterion to determine whether yielding has occurred in the joint. Both studies show that a block-type failure mechanism does not develop without the presence of a local weakness. Although yielding propagates from Location 2 and 3 similar to those in Figure 6.9, block-type failure mechanism does not develop unless local weaknesses are present when N is equal to unity.

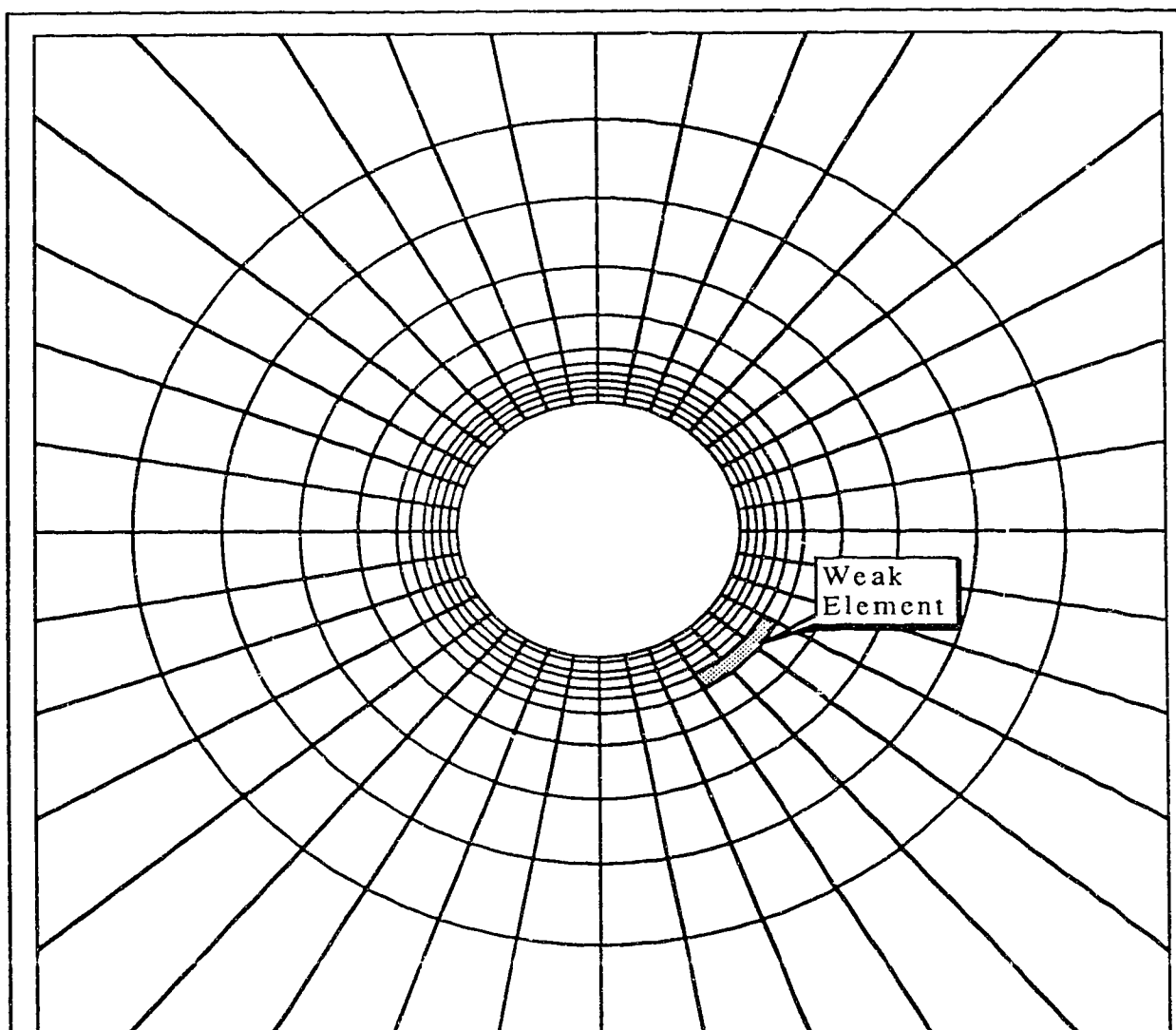
6.2.2 Summary and Conclusions

When a tunnel is excavated through rock with parallel weakness planes under a uniform far-field stress, block-type failure mechanism can only develop if local weaknesses exist and trigger an instability mode. The locations of yield initiation from the finite element simulation agree reasonably well with the field observation.

There are difficulties in modelling the ground convergence behaviour of a tunnel because it is not only a function of the material properties, but also a function of the construction method and sequence, and their interaction with the support system. Convergence measurements between two opposite points on the tunnel wall are good indicators of instability but they cannot identify the modes of failure.

Site investigation and visual monitoring during construction must concentrate on detecting major or dominant weaknesses at critical locations.

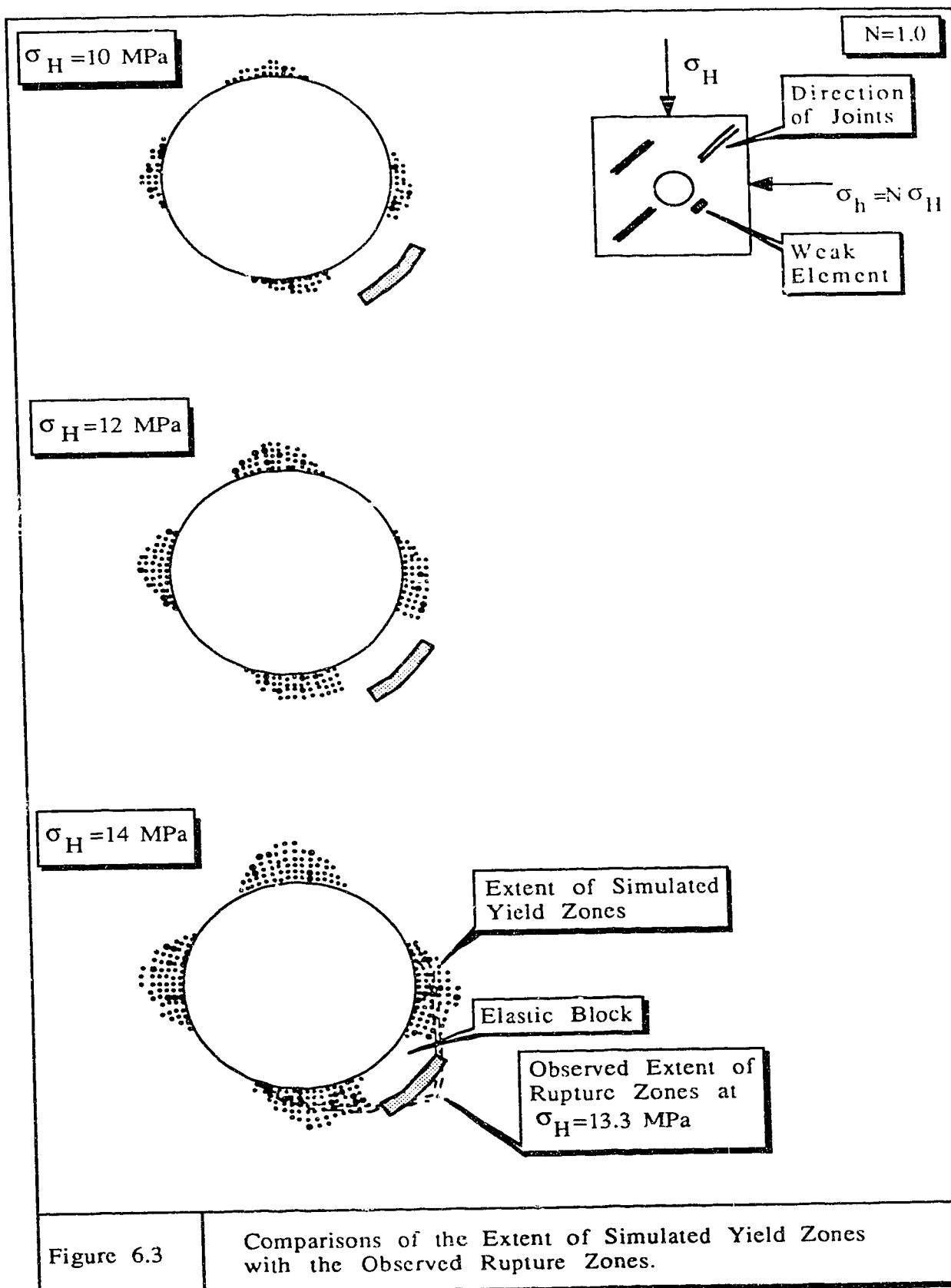




	Elastic Deformation Properties					Strength Parameters		Number of Elements =436 Number of Nodes =1309	
	E_1 (MPa)	E_2 (MPa)	ν_1	ν_2	G (MPa)	c_{min} c_{res} (MPa)	ϕ_{min} ϕ_{res}	α	β
Normal Element	1500	1000	0.2	0.3	500	7.5	7.5°	6.7	13.1
Weak Element	1500	1000	0.2	0.3	500	0	7.5°	1	1

Figure 6.2

Finite Element Mesh for the Study of Failure Mechanisms around Circular Openings in Jointed Coal.



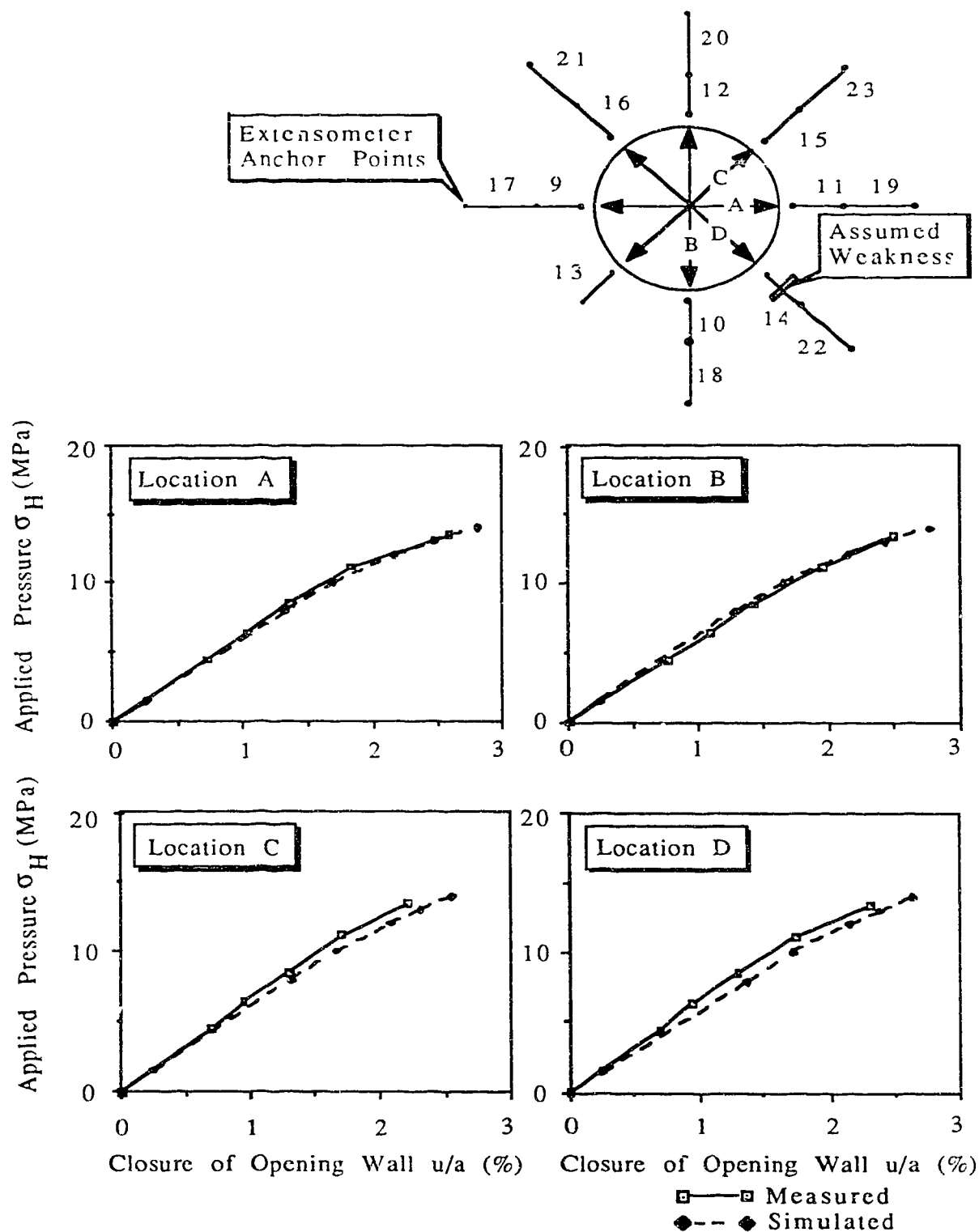


Figure 6.4

Closures of Opening Wall at Four Locations for Test MC-4.2
(Comparisons of Simulated Closures with the Measured).

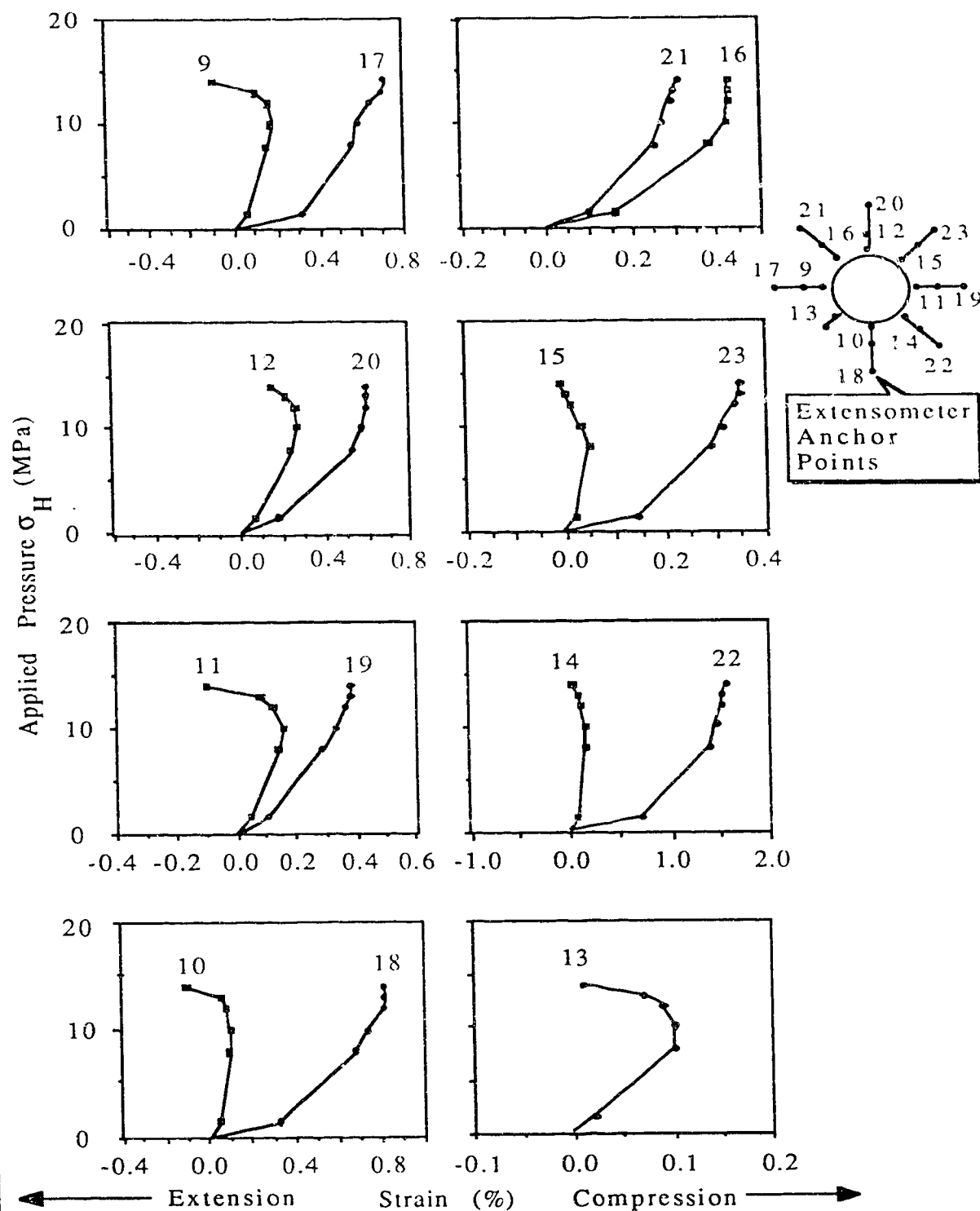


Figure 6.5

Ground Strain Curves Measured from Fifteen Extensometers for Test MC-4.2.

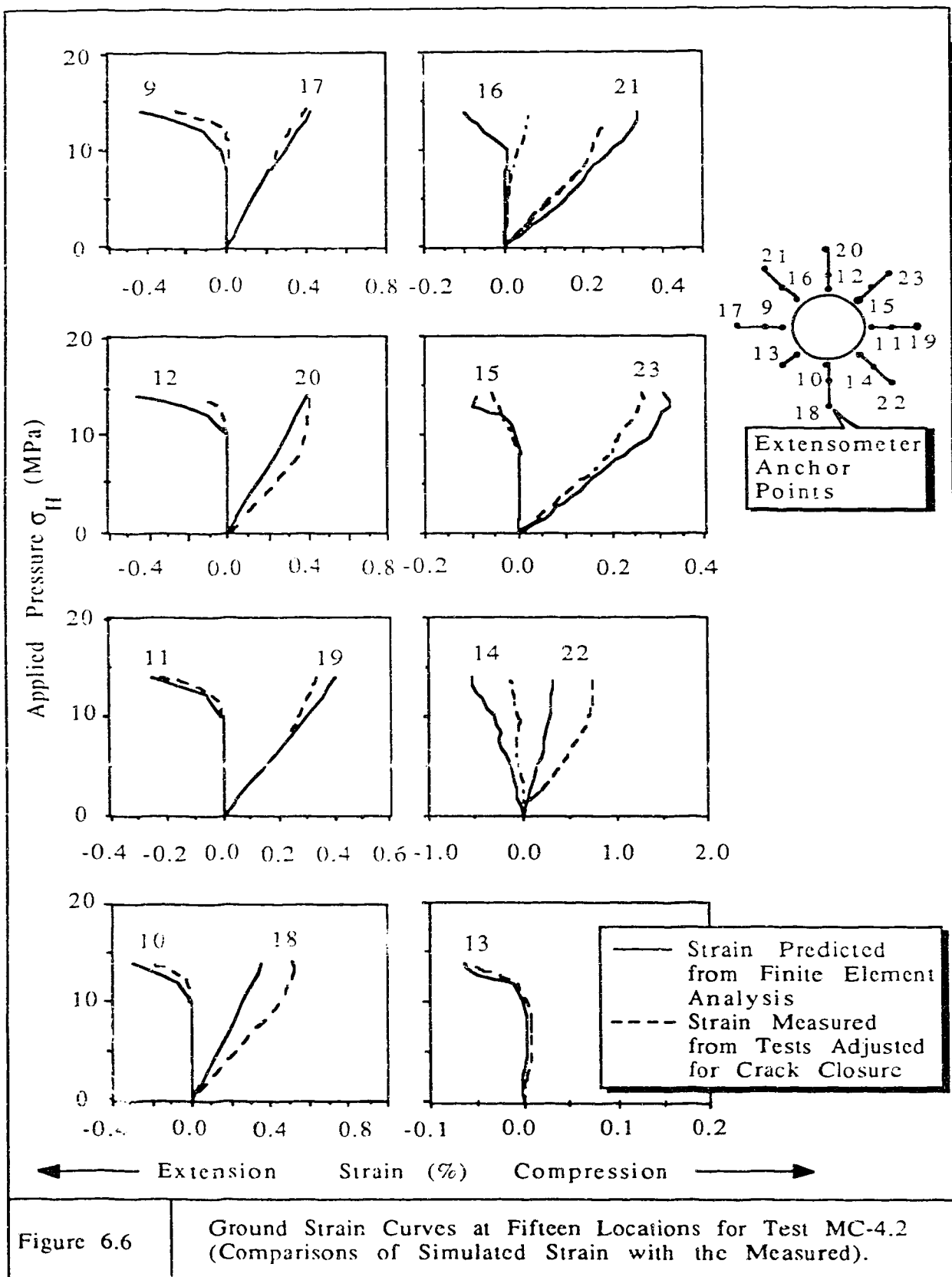
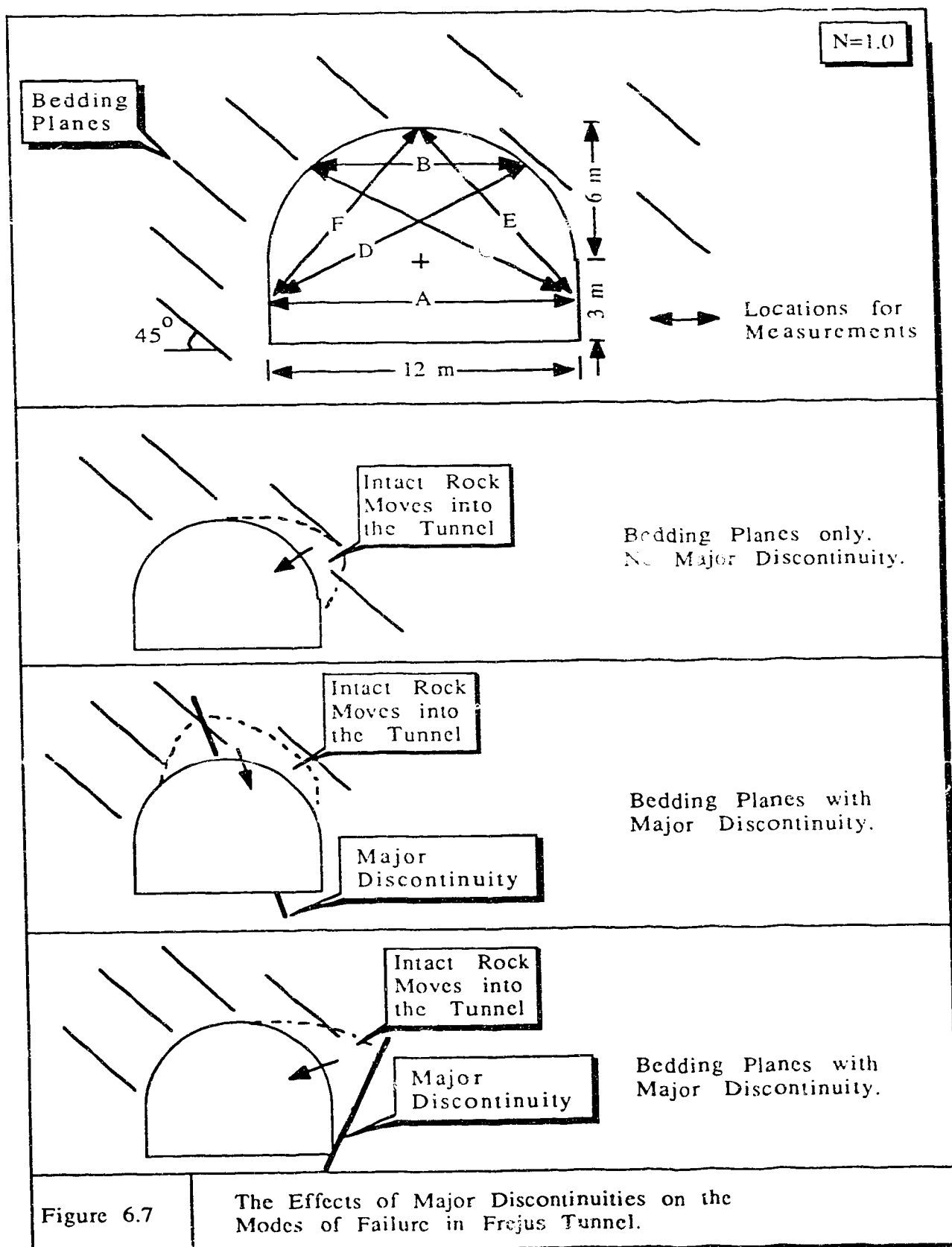
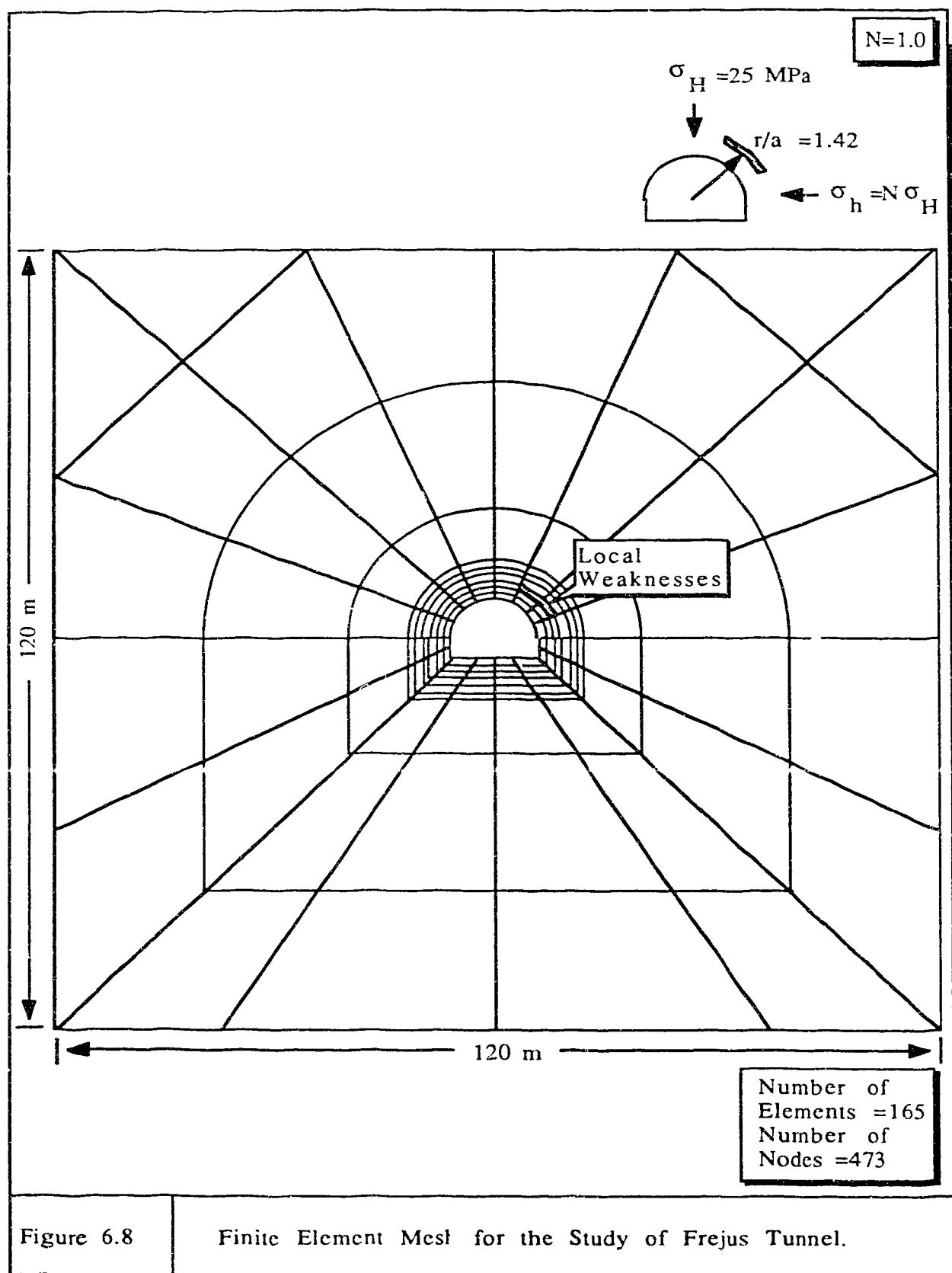
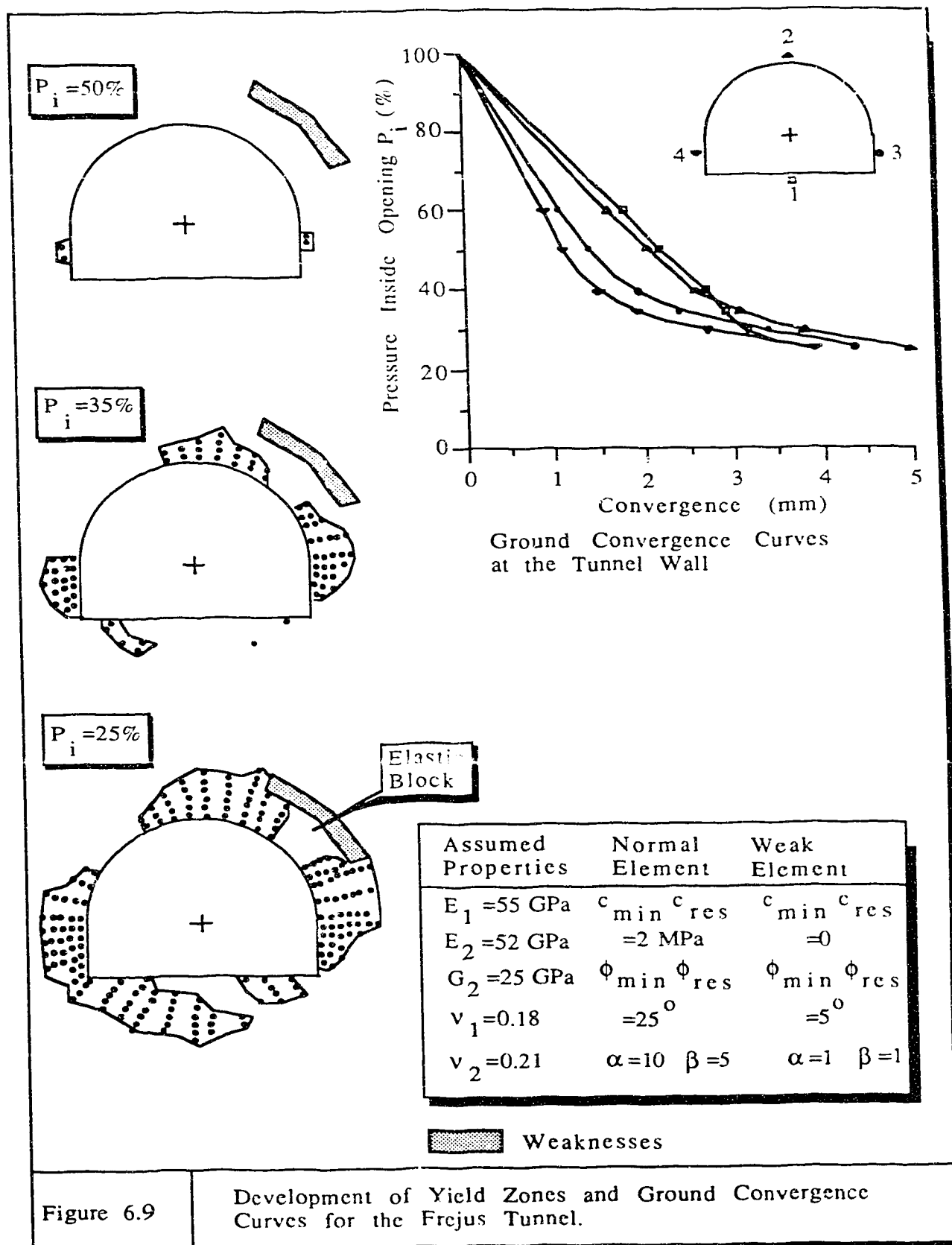


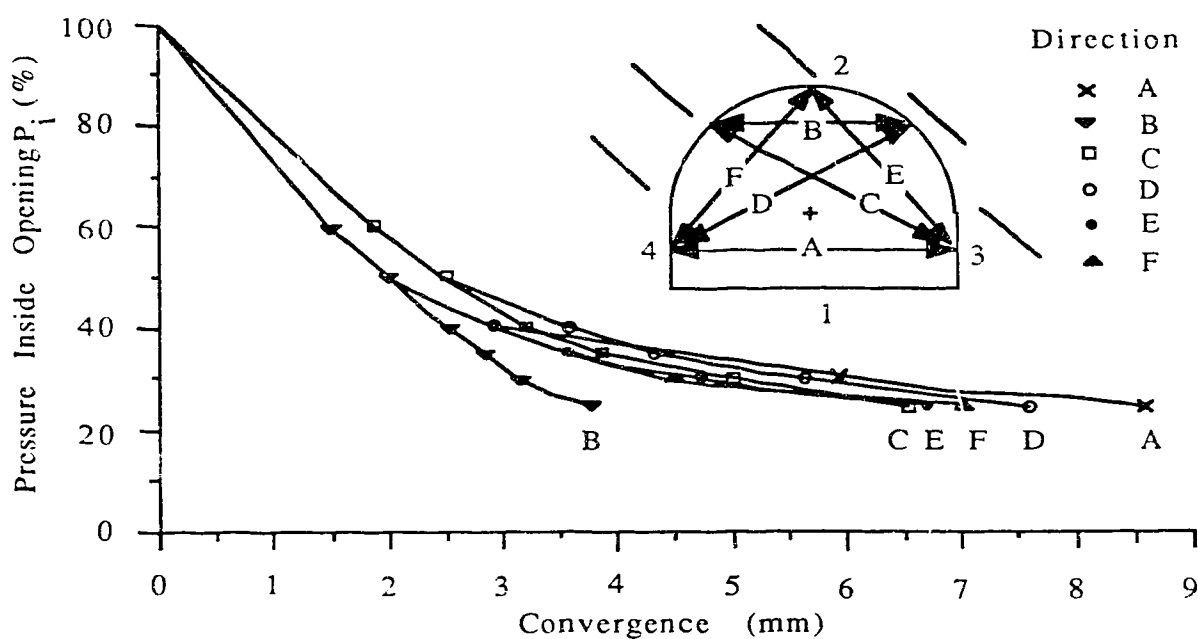
Figure 6.6

Ground Strain Curves at Fifteen Locations for Test MC-4.2
(Comparisons of Simulated Strain with the Measured).









a) Convergence Simulated from Finite Element Analysis (FEA).

		Station at				FEA
		4.835 Km	4.994 Km	5.172 Km	6.066 Km	
Magnitude of Measured Convergence	Large	Direction D	Direction D	Direction D	Direction D	A
		Direction F	Direction B	Direction B	Direction B	D
		Direction E	Direction F	Direction A	Direction C	F
	Small	Direction B	Direction E	Direction C	Direction A	E
		Direction A	Direction C	Direction E		C
		Direction C	Direction A	Direction F		B

b) Convergence Measured in the Field
(Data from Berest et al., 1980).

Figure 6.10

Convergence between Two Opposite Points on the Tunnel Wall for Directions A to F.

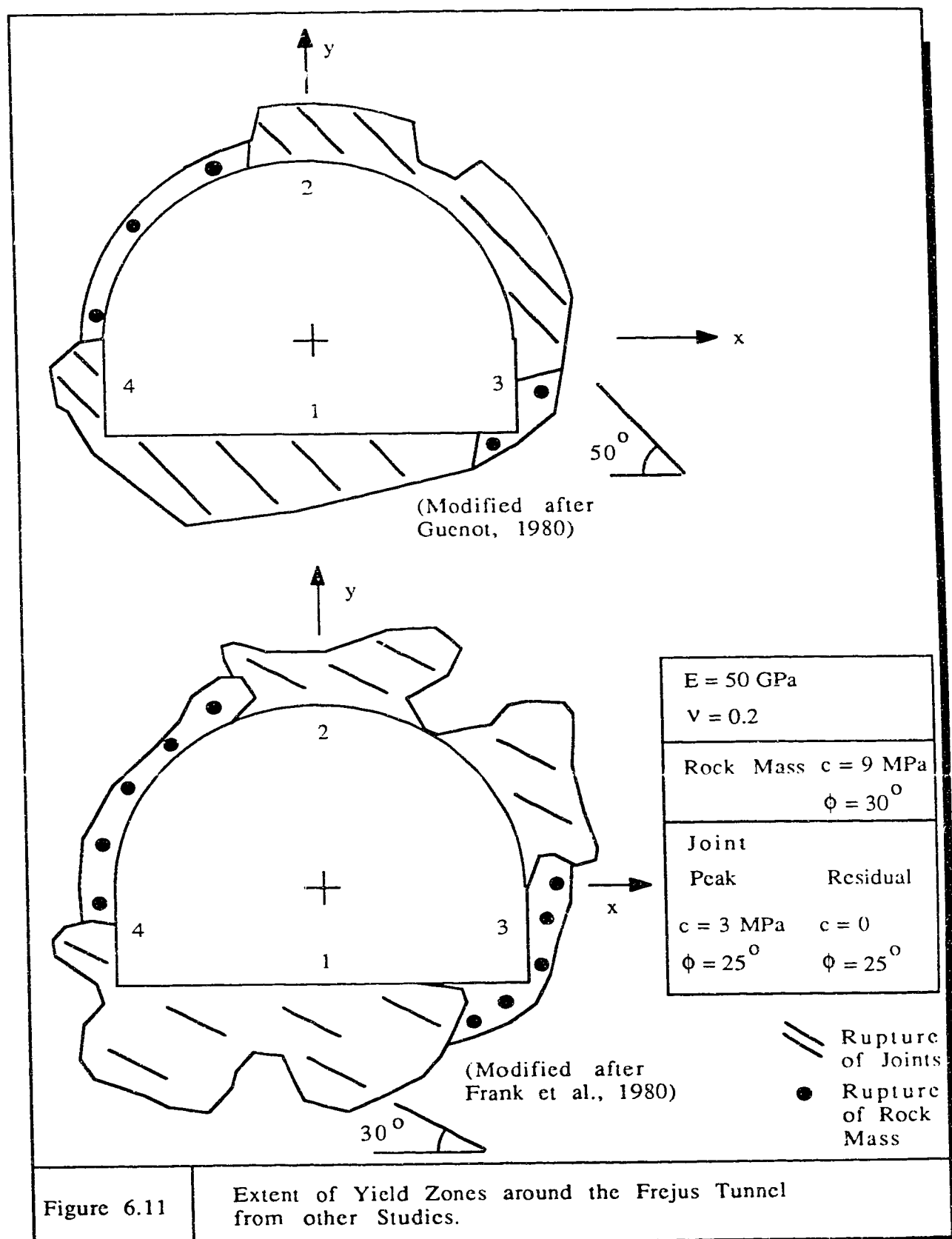


Figure 6.11

Extent of Yield Zones around the Frejus Tunnel
from other Studies.

7 SIMPLIFIED APPROACH TO PREDICT YIELD INITIATION ZONES AROUND BOREHOLES IN ROCK

7.1 Introduction

The finite element method has been used in the previous studies to investigate the various modes of failure around boreholes. The finite element method is no doubt a powerful numerical tool to determine the state of stress and displacement fields around boreholes. However, a considerable amount of time and cost must be expended for each analysis. Hence, a simplified, approximate approach may be useful for the determination of the extent and shape of the yield initiation zones around a borehole.

In this simplified approach, the stresses for a circular opening in an elastic, homogeneous isotropic material are compared to three different yield criteria for rocks. This approach parallels the method developed by Widerhofer (1970), Kastner (1979), and later by Daemen (1983). Experimental justification is given by Kastner (1979) and Jaegar and Cook (1979).

Instabilities around circular openings caused by parallel discontinuities have long been recognized by Szechy (1970) and Hoek and Brown (1980). Recently, Babcock (1978) and Gough and Bell (1982), both based on field observations, presented different views for the cause of breakouts in a borehole. Babcock (1978) suggested that breakouts are the results of the drill encountering steeply dipping fractures while Gough and Bell (1982) suggested that they are exclusively caused by shearing in zones of concentrated

compressive stresses resulting from non-uniform, horizontal far-field stresses. The simplified approach presented in this chapter will demonstrate that both may be contributing factors to the development of yield zones around boreholes.

The extent of the yield initiation zones from this approach is approximate because stress redistribution processes are neglected. Furthermore, the displacement field cannot be determined. Nevertheless, the simplified approach is beneficial for sensitivity studies before a detail finite element simulation is carried out.

7.2 Stress Distribution Around Circular Openings

The stress distribution for a circular opening in an elastic, homogeneous, isotropic material, originally developed by Kirsch (1898), is given in the following (see Figure 7.1 for definition of symbols):

$$\sigma_r = \frac{\sigma_H}{2} \left[(1 + N) \left(1 - \frac{a^2}{r^2}\right) - (1 - N) \left(1 - 4 \frac{a^2}{r^2} + 3 \frac{a^4}{r^4}\right) \cos 2\theta \right] + p_s \frac{a^2}{r^2} \quad (7.1a)$$

$$\sigma_\theta = \frac{\sigma_H}{2} \left[(1 + N) \left(1 + \frac{a^2}{r^2}\right) + (1 - N) \left(1 + 3 \frac{a^4}{r^4}\right) \cos 2\theta \right] - p_s \frac{a^2}{r^2} \quad (7.1b)$$

$$\tau_{r\theta} = \frac{\sigma_H}{2} \left[(1 - N) \left(1 + 2 \frac{a^2}{r^2} - 3 \frac{a^4}{r^4}\right) \sin 2\theta \right] \quad (7.1c)$$

where,

p_s = Support pressure inside the circular opening;

θ = Angle from the direction of σ_h .

In the following studies, plane strain condition is assumed for a deep section of the borehole. Yield initiation zones are defined as the areas where the shear stress equals or exceeds the shear strength of the rock.

The stress distribution in an elastic media is shown in Figure 7.2. It can be seen that, for $N=1.0$, the distribution of σ_r and σ_θ are independent of the orientation θ , and that the maximum deviatoric stress ($\sigma_r - \sigma_\theta$) is found at the borehole wall. Hence, it is expected that yield initiation will occur at the borehole wall and that propagation will be uniform all around. This is an ideal situation where a borehole is situated in a homogeneous material under uniform far-field stresses. For $N=0.5$, yielding is expected at the borehole wall in the direction of σ_h because deviatoric stress is maximum in this area.

7.3 Extent of Yield Initiation Zones around a Borehole

The aim of the following analysis is to predict the extent of the yield initiation zones by substituting the stresses from Equation 7.1 into different yield criteria. Propagation of yield zones due to stress redistribution must be considered separately.

The extent of the yield initiation zones around boreholes are investigated using three different yield criteria as follows:

1. Von Mises yield criterion;
2. Mohr-Coulomb yield criterion; and
3. Transversely isotropic yield criterion developed by Nova and Sacchi (1979).

7.3.1 Von Mises Yield Criterion

The Von Mises yield criterion can be applied to homogeneous isotropic material. It is given as the following:

$$(\sigma_r - \sigma_\theta)^2 + (\sigma_\theta - \sigma_v)^2 + (\sigma_r - \sigma_v)^2 + 6 \tau_{r\theta}^2 = 2 Y^2 \quad (7.2)$$

where,

- Y = Unconfined compressive strength;
 σ_v = Vertical stresses along the borehole axis;
 $= \nu (\sigma_r + \sigma_\theta)$, assuming plane strain condition is maintained.

If the stress components σ_r , σ_θ and $\tau_{r\theta}$ from Equation 7.1 are substituted into Equation 7.2, the extent of the yield initiation zones is determined as follows:

The material is elastic if:

$$(\sigma_r - \sigma_\theta)^2 + (\sigma_\theta - \sigma_v)^2 + (\sigma_r - \sigma_v)^2 + 6 \tau_{r\theta}^2 - 2 Y^2 < 0$$

The material has yielded if:

$$(\sigma_r - \sigma_\theta)^2 + (\sigma_\theta - \sigma_v)^2 + (\sigma_r - \sigma_v)^2 + 6 \tau_{r\theta}^2 - 2 Y^2 \geq 0$$

The extent of the yield initiation zones for $N=1.0$, 0.75 and 0.5 are presented in Figure 7.3. The result shows that for homogeneous isotropic material, the location and shape of the yield initiation zones are a function of the stress ratio. For $N=0.5$, the yield initiation zones extend towards the direction of σ_h . This is in agreement with the hypothesis from Gough and Bell (1982) that systematic oriented borehole breakouts are caused by non-uniform far-field stresses.

7.3.2 Mohr-Coulomb Yield Criterion

According to the Mohr-Coulomb yield criterion, yielding of a rock mass is initiated when:

$$s = c + \sigma_n \tan \phi \quad (7.3)$$

where, s = shear strength of the rock mass;
 c = cohesion intercept;
 ϕ = angle of friction;
 σ_n = normal stress.

However, weak discontinuities with a strength lower than that of a rock mass are often present around boreholes or tunnels. Yielding of a weakness depends on its strength and orientation. This is illustrated schematically in Figure 7.4. μ is the angle from the direction of weakness planes to the direction of major principal stresses. Yielding will occur if the weakness is orientated at $\mu^{**} \leq \mu \leq \mu^*$ (see Figure 7.4). The procedure adopted to check the extent of yield initiation zones can be summarized as follows:

1. Obtain stress components σ_r , σ_θ and $\tau_{r\theta}$ from Equation 7.1;
2. Calculate δ from the Mohr stress circle as shown in Figure 7.5(a);
3. Obtain θ and ξ (angle of weakness planes from the direction of σ_h , Figure 7.5(b);
4. Calculate μ from δ , θ , and ξ . The relationship between μ , δ , θ , and ξ is shown in Figure 7.5(b).
5. Check whether rock mass has yielded as shown in Figure 7.6(b);
6. If rock mass does not yield, check whether the weakness yields as shown in Figure 7.6(c).

Figure 7.7 shows that for $N=1.0$, the yield initiation zone of the rock mass is circular, whereas it is non-uniform if weaknesses are present. Yielding occurs both in the rock mass and in the weaknesses. Figure 7.8 presents the extent of the yield initiation zones for $N=0.5$. For weaknesses orientated at $0^\circ \leq \xi \leq 20^\circ$ and $80^\circ \leq \xi \leq 90^\circ$, the yield initiation zones are extended towards the direction of σ_H , whereas it is at the margin of the yielded rock mass zone if $45^\circ \leq \xi \leq 70^\circ$. Both Figures 7.7 and 7.8 support the

hypothesis of Babcock (1979) that borehole breakouts can be the results of the drill encountering weaknesses. The location of overstressing is very sensitive to orientation of the weaknesses and the stress ratio.

In order to demonstrate the validity of the simplified approach, the extent of the yield initiation zones are compared with those from a finite element analysis (Kaiser et al., 1985). The finite element analysis was carried out assuming that the rock mass would behave like an elasto-plastic material with anisotropic strength characteristics. The assumed, isotropic deformational properties of the elements are, Young's modulus $E=1.5$ GPa and Poisson's ratio $\nu=0.2$. The anisotropic strength behaviour was obtained by simultaneous consideration of the following criteria:

- Linear elastic, perfectly plastic stress-strain relation for intact rock satisfying the Mohr-Coulomb yield criterion ($\phi=30^\circ$ and $c=4$ MPa).
- Directional yield criterion to describe the strain-softening behaviour of the discontinuities (peak cohesion $=1.5$ MPa, ultimate cohesion $=0.3$ MPa and $\phi=30^\circ$).

The finite element method provides the extent of the yield zone after stress redistribution. It is compared with the yield initiation zone predicted by the simplified approach in Figure 7.9. This figure shows the comparisons of the spatial extent of the yield initiation zones around circular openings at different levels of applied stress. When yielding first occurs in the weaknesses at $\sigma_H=5$ MPa, the yield zone predicted by the finite element analysis is larger

than the extent of yield initiation zone towards the direction of σ_H . When the rock mass starts to yield at $\sigma_H=7$ MPa, the spatial extent of yield initiation zones due to weaknesses and in the rock mass are very similar to those predicted by the finite element analysis. When more yielding occurs in the rock mass at $\sigma_H=13$ MPa, the spatial extent of the yield initiation zones due to weaknesses predicted by the simplified approach are very close to those predicted by finite element analysis. At the final stress level of $\sigma_H=15$ MPa, the simplified approach underestimates the radial extent of yield initiation zones for both weaknesses and rock mass but the spatial distribution is still very similar. The above comparisons suggest that although the simplified approach underestimates the radial extent of yield initiation zones due to yielding of weaknesses or the rock mass, the shape of the yield initiation zones predicted by the simplified approach are similar to those predicted by finite element analysis at all level of applied stress and can be used to estimate the expected borehole response. The effects of stress redistribution do not seem to dominate as long as the yield initiation zones are limited to $r/a \leq 1.2$.

7.3.3 Yield Criterion for Transversely Isotropic Rock (Nova and Sacchi, 1979)

In this section, the extent of yield initiation zones are investigated for rock that exhibits transversely isotropic strength. The stresses from Equation 7.1 are substituted into the yield criterion of Equation 5.1 developed by Nova and Sacchi (1979).

Figure 7.10 and 7.11 show the location and extent of yield initiation zones for $N=1.0$ and 0.5 , respectively. Figure 7.10 confirms the earlier findings from the Mohr-Coulomb yield criterion that the presence of weaknesses will create non-uniform yield initiation zones (four zones) even for $N=1.0$. Figure 7.10 also shows that, for $N=1.0$, the location of yield initiation at the borehole wall is only a function of the weakness orientation. Figure 7.11 demonstrates that, for $N=0.5$, four yield initiation zones are created when weaknesses are parallel to the principal stress axes. For almost all other weakness orientations, only two yield initiation zones will be created at the borehole wall. In Section 5.5, it was shown that, for $N=0.5$, the yield initiation zones will act like local weaknesses and promote the formation of the block-type failure mechanisms when the weaknesses are parallel to the principal stress axes. Chapter 6 shows that, for $N=1.0$, block-type failure mechanisms cannot be created if the two yield zones are too far apart unless there are distinct weaknesses located at some critical point around the boreholes.

7.4 Limitations of Applicability and Conclusions

The spatial extent of yield initiation zones determined from the simplified approach presented here is slightly underestimated because stress redistribution is neglected. However, the simplified approach provides a rational tool for the assessment of the location and shape of yield initiation zones around boreholes or underground openings before a detail finite element analysis is carried out.

The following conclusions can be drawn from this chapter:

1. For a homogeneous, isotropic rock mass, the location and shape of yield initiation zones are affected by the far-field stress ratio N .
2. The presence of local weaknesses in the rock mass near a borehole will result in a non-uniform yield initiation zones around a borehole even if N is equal to unity.
3. Four yield initiation zones are created at the borehole wall if a borehole is drilled in a stratified material and under uniform stress. The locations of these four yield initiation zones are only a function of the weakness orientation. The simplified approach can be used to assess the extent and shape of the yield initiation zones because, if $N = 1$, block-type failure mechanisms cannot be developed unless there are distinct weaknesses located at some critical point between the yield initiation zones.
4. For a borehole drilled through a stratified material, and if N deviates from unity, two or four yield initiation zones are created depending on the orientation of the weakness planes relative to the direction of the principal stresses. The simplified approach can be used to assess the extent and shape of the yield initiation zones if only two yield initiation zones are created because block-type failure mechanisms cannot be developed unless there are distinct weaknesses located at some other critical points near the borehole. However, the simplified approach cannot be used to assess the extent and shape of the yield initiation zones if the weakness planes are aligned with either the maximum or minimum far-field stresses, because these four yield initiation zones will act like local

weaknesses and promote the formation of block-type failure mechanisms.

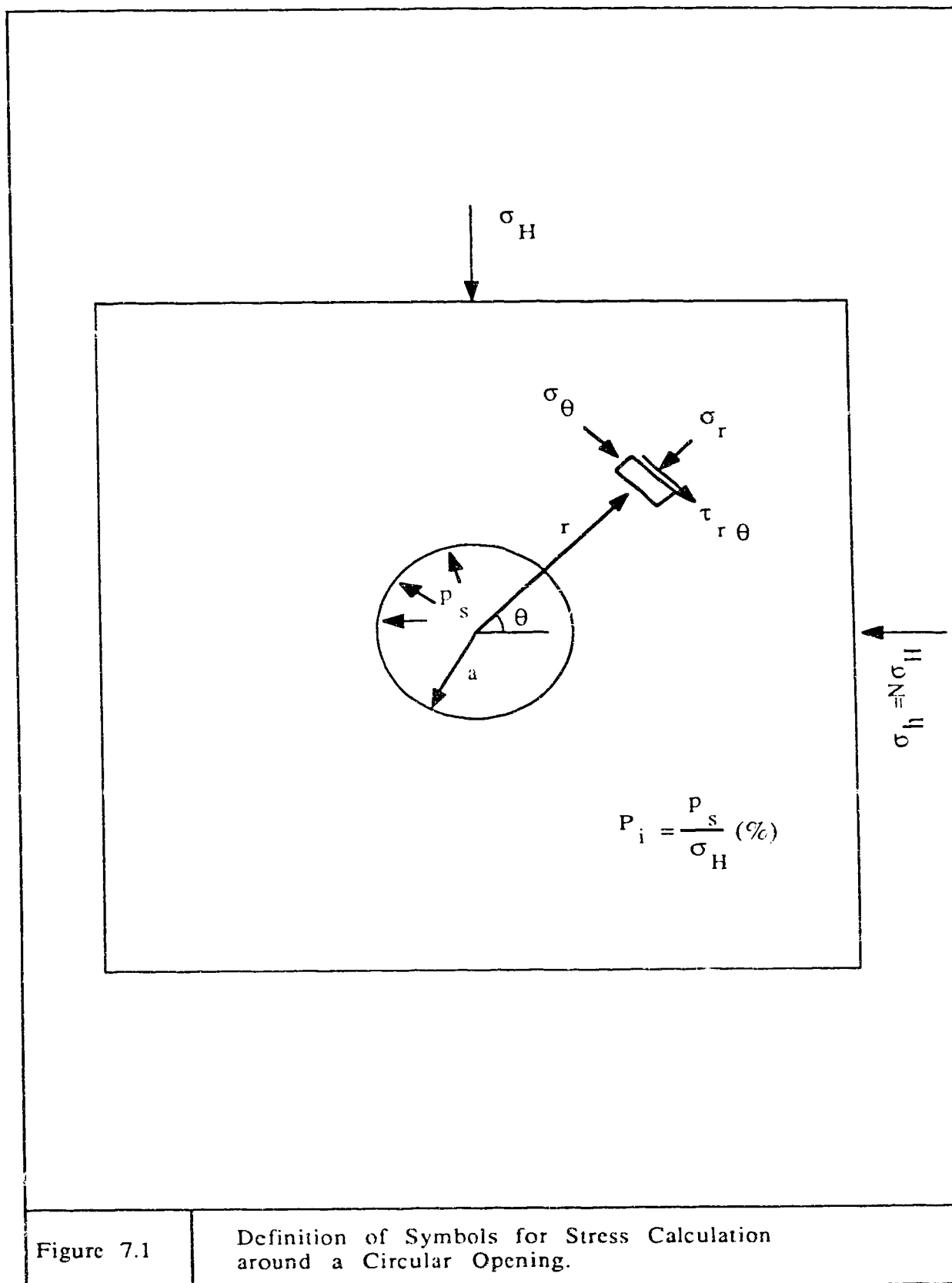
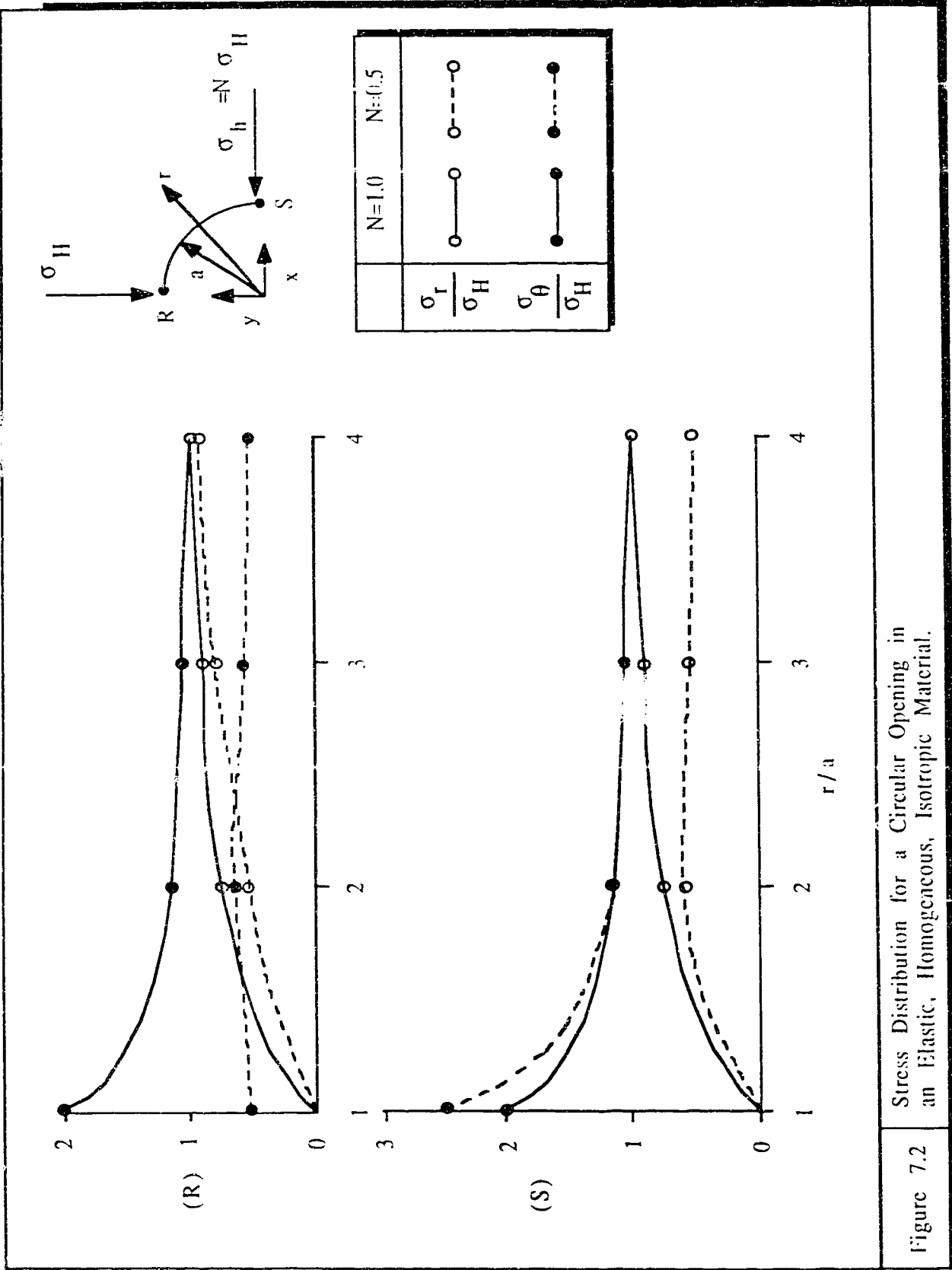
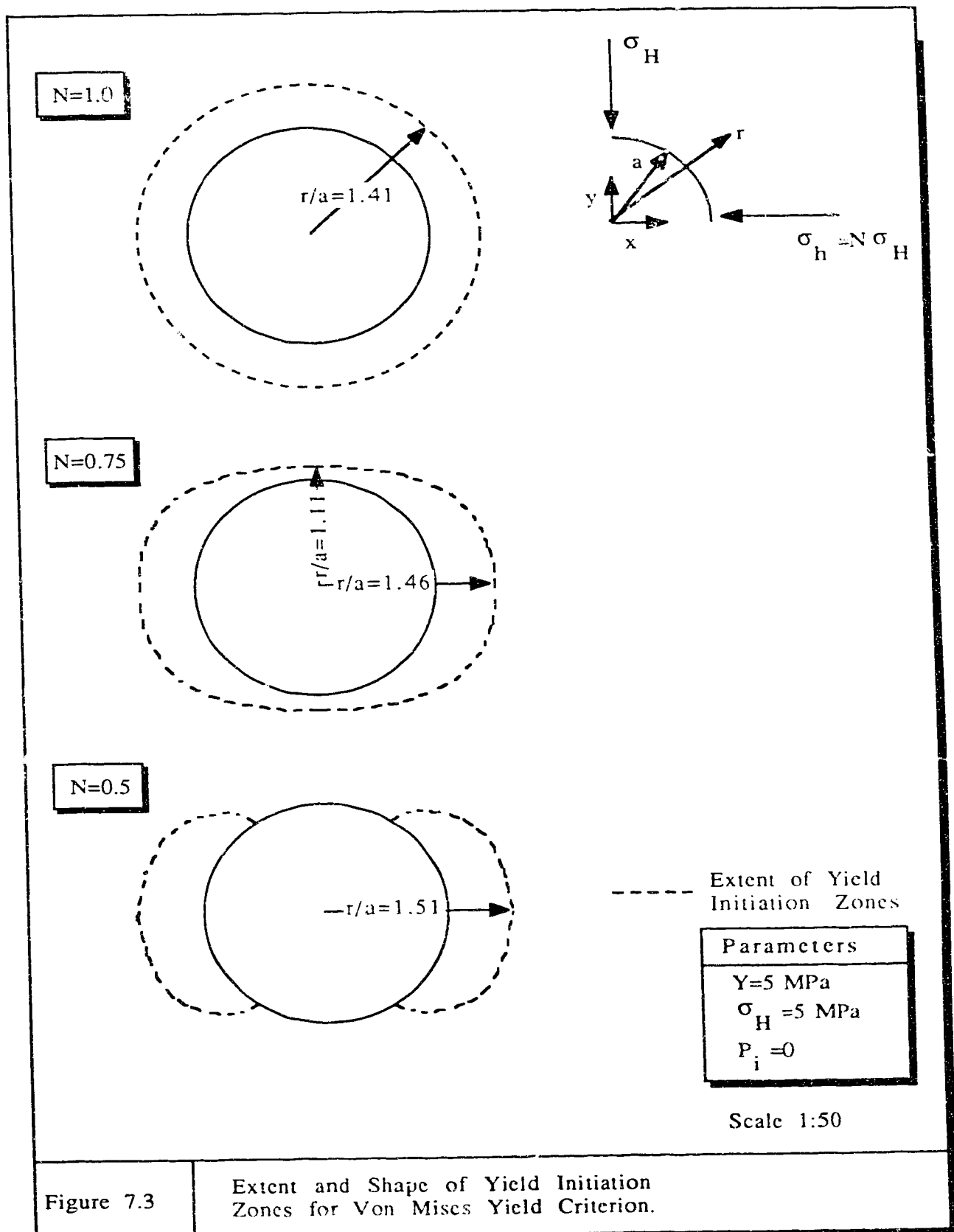
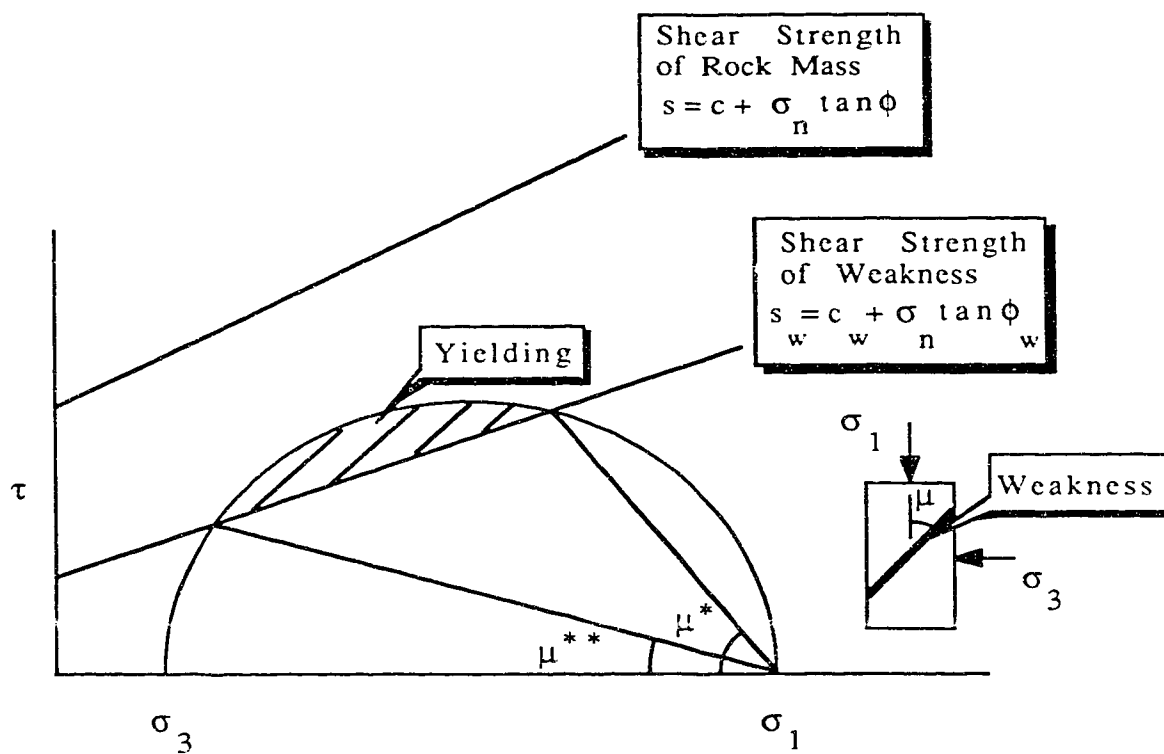


Figure 7.1

Definition of Symbols for Stress Calculation
around a Circular Opening.





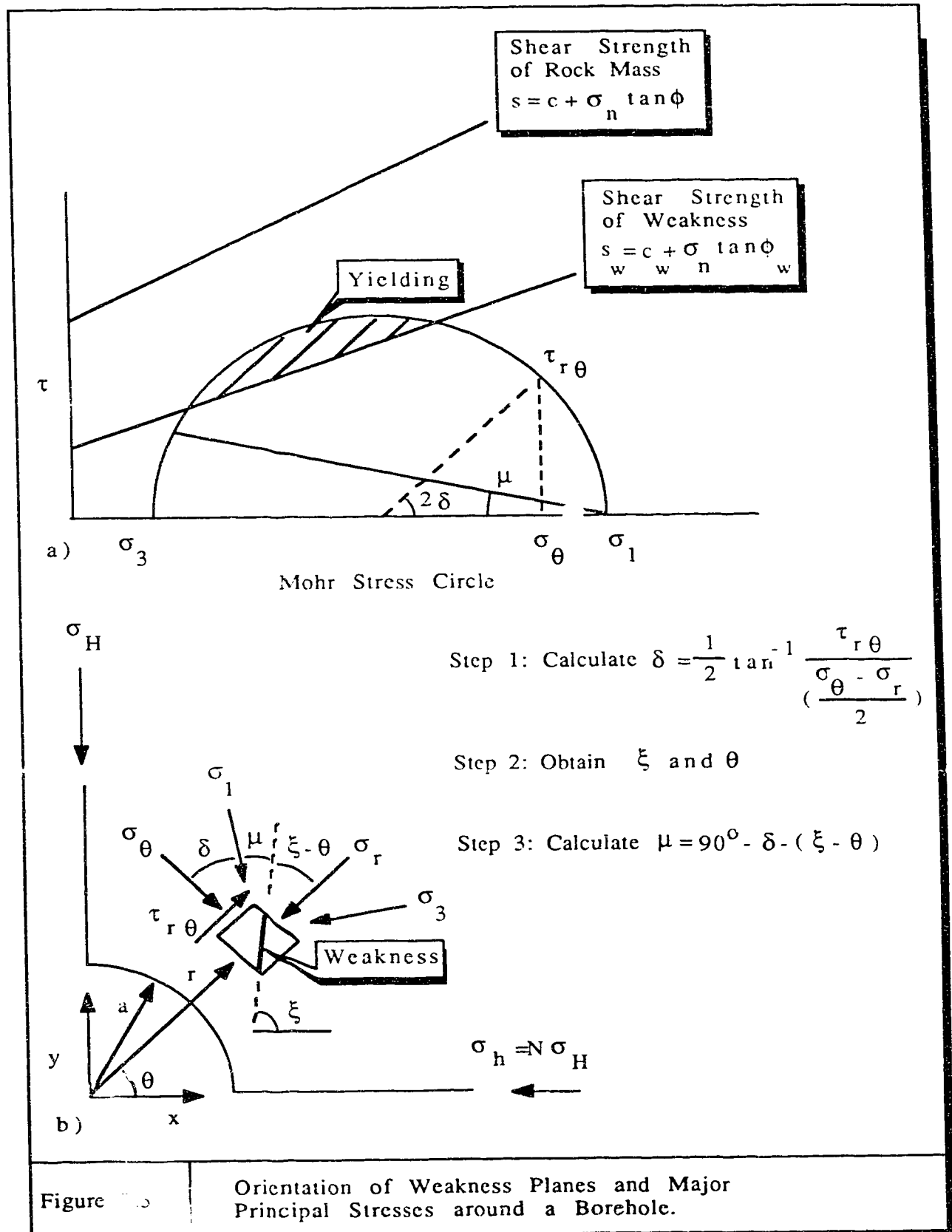


Note: Weakness Yields if

$$\mu^{**} \leq \mu \leq \mu^*$$

Figure 7.4

Conditions of Yielding for Weaknesses.



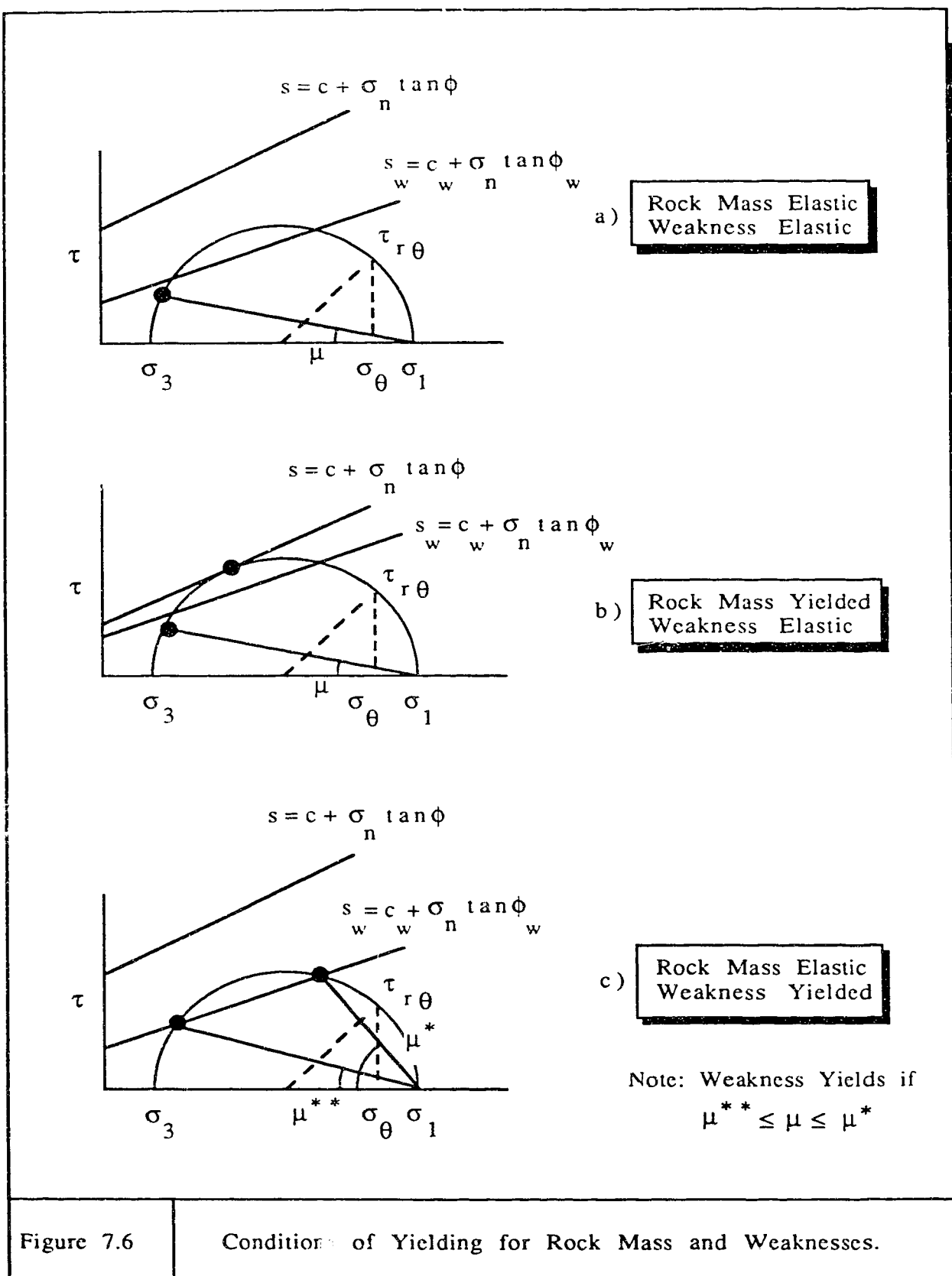
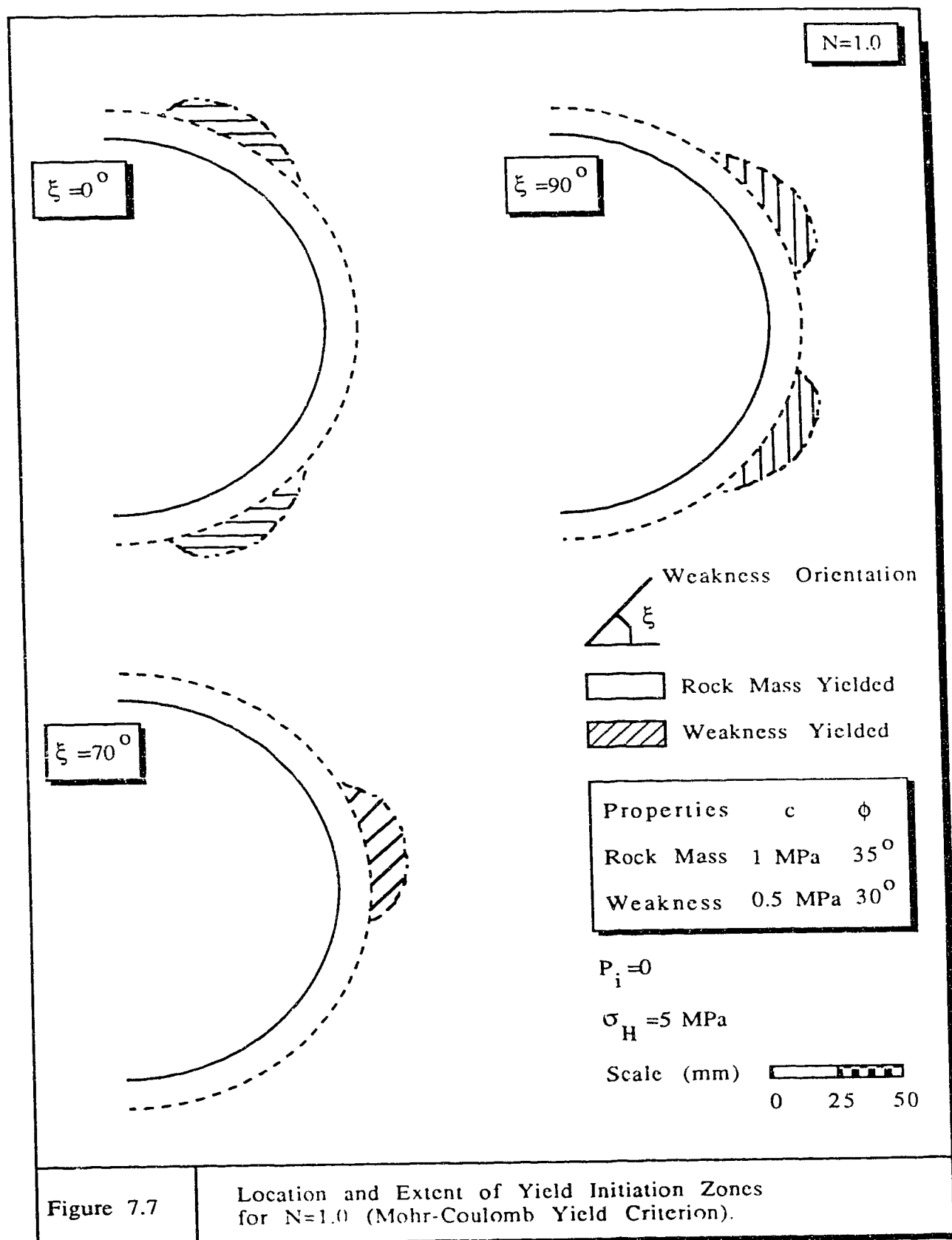
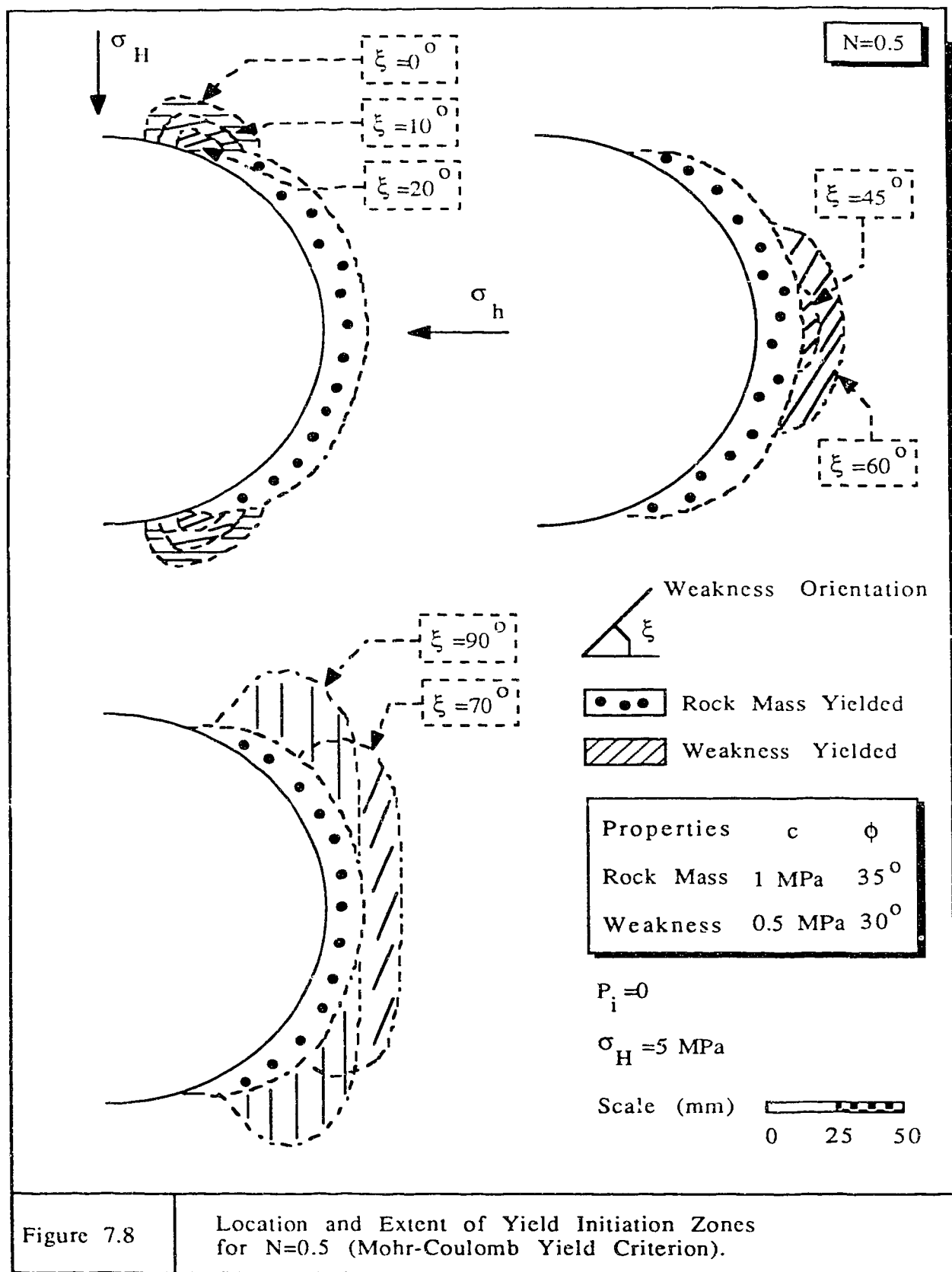
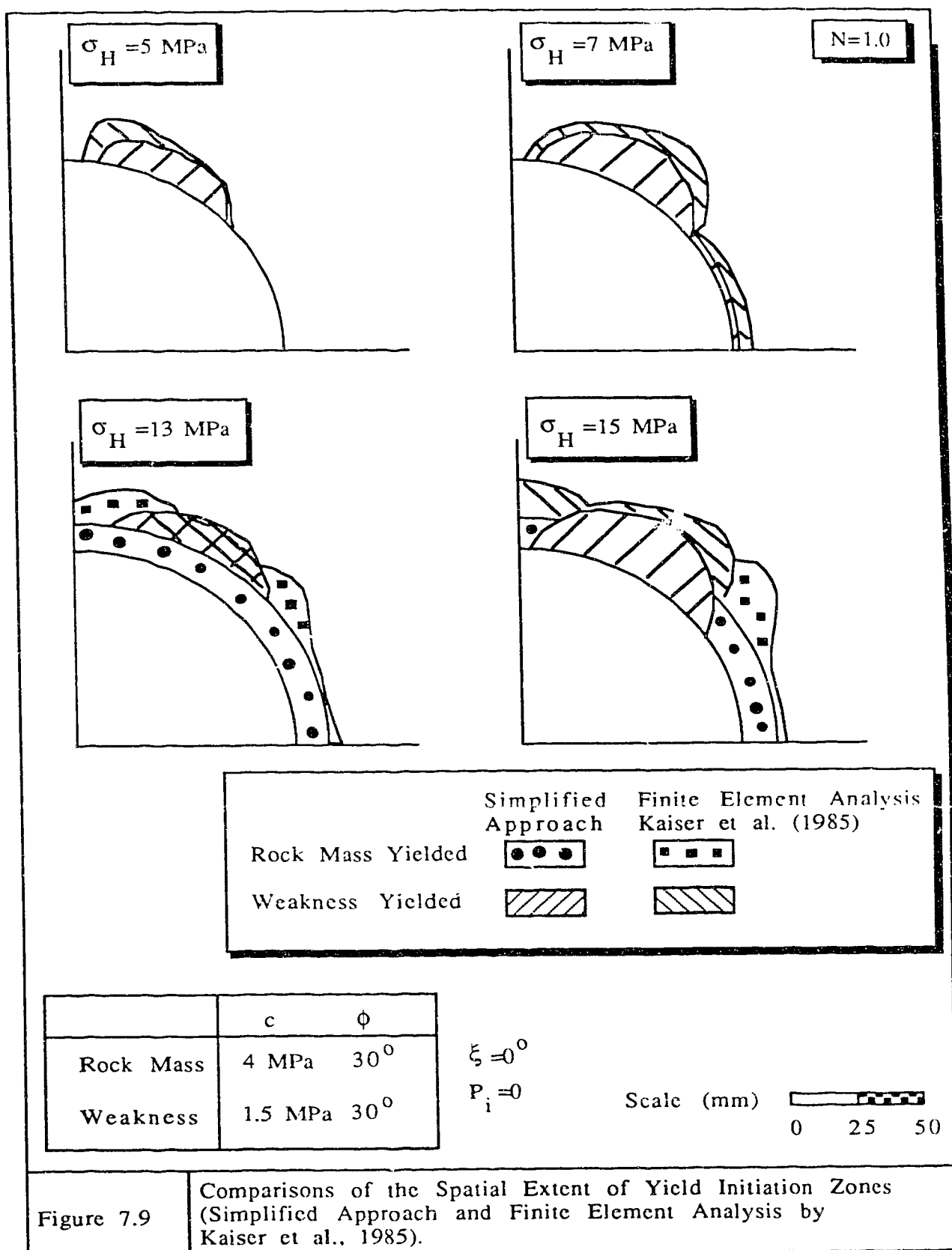


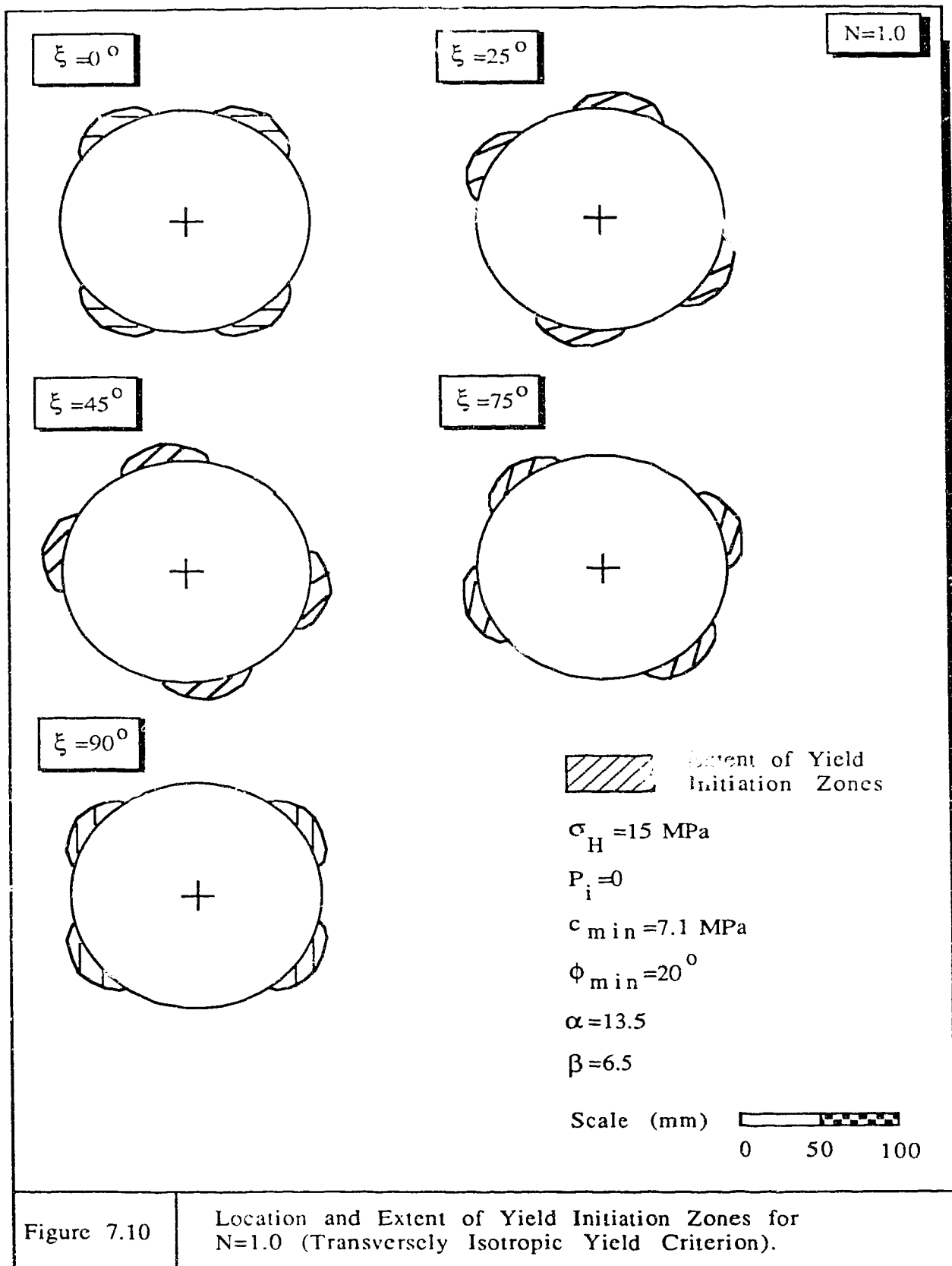
Figure 7.6

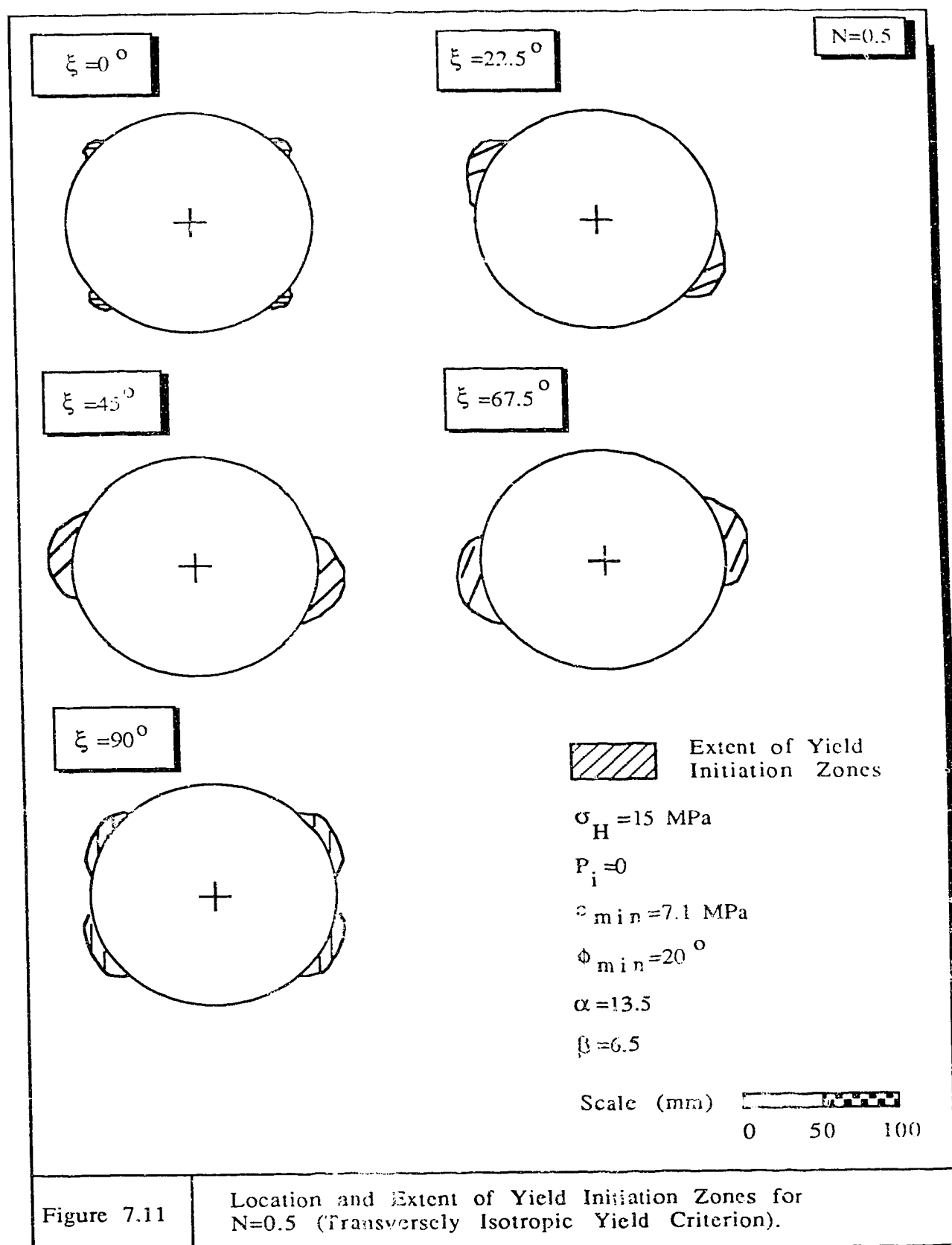
Conditions of Yielding for Rock Mass and Weaknesses.











8 SUMMARY, CONCLUSIONS AND PRACTICAL IMPLICATIONS

8.1 Summary

The effects of local weaknesses on the modes of deformation was first demonstrated with the numerical simulation of a confined compression test as outlined in Chapter 3. If local weaknesses are not present in the specimen, an extension/compression deformation mode was determined when the specimen was subjected to confined compression. However, a small local weakness within the specimen triggered a localization and formed two shear bands.

An evaluation of the eigenvalue of the global stiffness matrix in the finite element analysis can provide information on the stability of the structure. When the structure becomes unstable which is indicated by zero perturbation energy, the lowest eigenvalue will also equal to zero. This is the condition at which bifurcation occurs because there will be more than one set of displacement increment solution when the global stiffness matrix becomes singular. The eigenvectors belonging to the eigenvalues which are equal to zero represent different possible modes of deformation at bifurcation.

In order to evaluate different modes of deformation of a borehole when it approaches instability, an eigenvalue analysis was carried out for a borehole. The lowest eigenvalue obtained in this study is not exactly equal to zero, but it is small enough to be considered as zero because the structure has reached an unstable point and the corresponding eigenvectors show an uniform closure of

the borehole wall which is expected for a borehole situated in a homogeneous isotropic rock mass and subjected to a uniform stress field. The reasons of not getting zero eigenvalue may be due to numerical accuracy, both mesh refinement and calculation precision.

Three other groups of closely spaced eigenvalues were identified but they cannot be considered as zero energy mode because their eigenvalues do not converge to zero below the unstable point. The eigenvectors of these three groups served to identify a translation mode, an elliptical deformation mode and a warping mode. The warping mode of deformation of the borehole wall is similar to the surface wave mode described by Vardoulakis (1988).

Although the eigenvalues for the last three group are higher than the lowest eigenvalue, they are relatively close together. This may suggest that any of the these modes may be induced depending on the kind and amount of disturbance introduced in nature. There are many causes of disturbances that could govern the formation of these modes. Vardoulakis (1988) suggested that the warping mode may be induced by pre-existing, latent, surface parallel cracks leading to the buckling or peeling off of slabs. In other words, disturbances such as surface parallel cracks may govern the formation of the warping mode.

The effects of local weaknesses on the modes of failure around boreholes was then demonstrated by numerical simulations of failure mechanisms as outlined in Chapters 4 and 5. In Chapter 4, it was discovered that block-type failure mechanisms are possible if the borehole is subjected to non-uniform far-field stresses and if at least two local weaknesses are critically located. This will change the

stress distribution around the borehole and lead to a condition that is conducive to yielding at depth, away from the borehole wall. Chapter 5 demonstrates that block-type failure mechanisms similar to those introduced by local weaknesses are also possible if the weakness planes are parallel to the direction of the principal stress. This is because the locations of yield initiation, for this condition are very similar to those introduced selectively by local weaknesses. For weakness planes deviating from the direction of the principal stresses, only continuously yielded zones are formed around boreholes.

The findings presented in Chapter 4 and 5 provide the basis for simulating the failure mechanisms observed in laboratory tests and in the field during tunnel construction. In Chapter 6, the location and extent of yield zones determined by finite element simulations are compared with those observed in the laboratory and in the field. It is found that the location and extent of yield zones can be modelled reasonably well provided that weaknesses are present.

A generalized yield criterion developed by Nova and Sacchi (1979) for rock which exhibits transversely isotropic strength was implemented into the finite element code SAGE (Chan, 1986). The model is assumed to describe a linear elastic, brittle perfectly plastic rock. The yield criterion can be reduced to the Mohr-Coulomb and the Tresca yield criteria for isotropic material. This analytical tool was developed in order to study the effects of weakness properties and their orientation, and the far-field stress ratio on the extent of yield zones and the amount of deformations near an underground opening.

This study provides a deeper understanding of the various factors which control the formation of different types of failure mechanisms around borehole and other underground openings. These factors are:

- 1) The magnitude and directions of the in situ far-field stresses; and
- 2) The extent, orientation, location and number of weaknesses near an opening.

Figure 8.1 shows a chart which groups the modes of failure investigated in this research. It can be seen that block-type failure mechanisms (Modes IV, V and VI) are more likely to develop in the presence of weaknesses and if the far-field stresses are not uniform. It also indicates that the direction of breakout is not only controlled by the stress ratio and their direction, but also by the presence of weaknesses near an opening. The formation of a continuous uniform yield zone (Case I) is only a very special case of all the possible failure modes. This chart suggests that more research is needed to gain a better understanding of the other factors which control the problem of borehole instability and the formation of different types of failure mechanisms. In fact, this research constitutes only an incremental contribution toward the ultimate goal of developing tools to control borehole instability.

Chapter 7 introduced a simplified approach to approximately determine the location and extent of yield initiation zones around circular openings. It was found that the spatial distribution and extent of yield initiation zones determined by this simplified approach corresponds well with results from more complex methods as long as the yield zones are relatively small and confined.

However, the block-type failure modes cannot be identified by the simplified approach because the stress redistribution process is neglected. In other words, the simplified approach cannot be used if conditions are favourable for the development of block-type failure mechanisms. Nevertheless, the simplified approach provides a rational tool for the determination of the location and shape of the yield initiation zones around boreholes or underground openings before a detail finite element analysis is carried out.

8.2 Practical Implications to Oil Drilling

One of the methods of controlling borehole stability is by varying the support pressure. The support pressure can be adjusted by varying the density of the drilling fluid. The oil industry generally looks for simple measurements such as borehole breakout angle or borehole diameter ratio in the field in order to assess the magnitude and direction of stresses at the borehole wall, and then use this information to adjust the support pressure. In this study, it was found that the location and extent of yield zones were not uniquely related to the magnitude and direction of the in-situ stresses. Local weakness would change the shape and extent of a yield zone. This is demonstrated by the two examples (Cases A and D) in Chapter 4 where block-type failure mechanism was created by the presence of local weakness. The shape of the elastic block may also be different, depending on the location of the weaknesses. This is illustrated by Cases B and C in Figure 4.4B that even the support

pressures are about the same near unstable condition, the shape of the yield zones in Case C is very different from those of Case B.

Information regarding cuttings circulating in the drilling fluid can be seen from Figures 4.4A to 4.4C. Cases B to D in Figures 4.4B and 4.4C show the size of elastic block is relatively large compared to the size of the borehole. This may suggest that relatively large pieces of rocks (elastic blocks) found in the circulating fluid will indicate that it is more difficult to maintain a stable borehole.

Cases B and D, with an elastic block, reached unstable condition when the support pressure is reduced to about 50 %, whereas it is 30 % for Case A with general yielding. This suggests that much higher support pressure will be needed to reduce deformation for cases with elastic block than with general yielding. However, from the ground convergence curves in Figure 4.8, it can be seen that Case D with a weak plane shows that the borehole is likely to deform excessively even if a relatively high support pressure is provided.

Support pressure may drop temporarily when the drill rod is being removed from the borehole. Cases B to C in Figure 4.8 illustrate that slight reduction of support pressure (if P_i is at 50 % and 65 %, respectively) can be detrimental to borehole stability because a large amount of deformation will be induced.

If borehole instability is due to the presence of weaknesses, then one method to control stability is by reducing the size of the borehole. This is justified by Figure 4.5 which shows that reducing the size of the borehole essentially reduces the number of weaknesses intersecting the borehole, and hence, it is less likely to create elastic block-type failure.

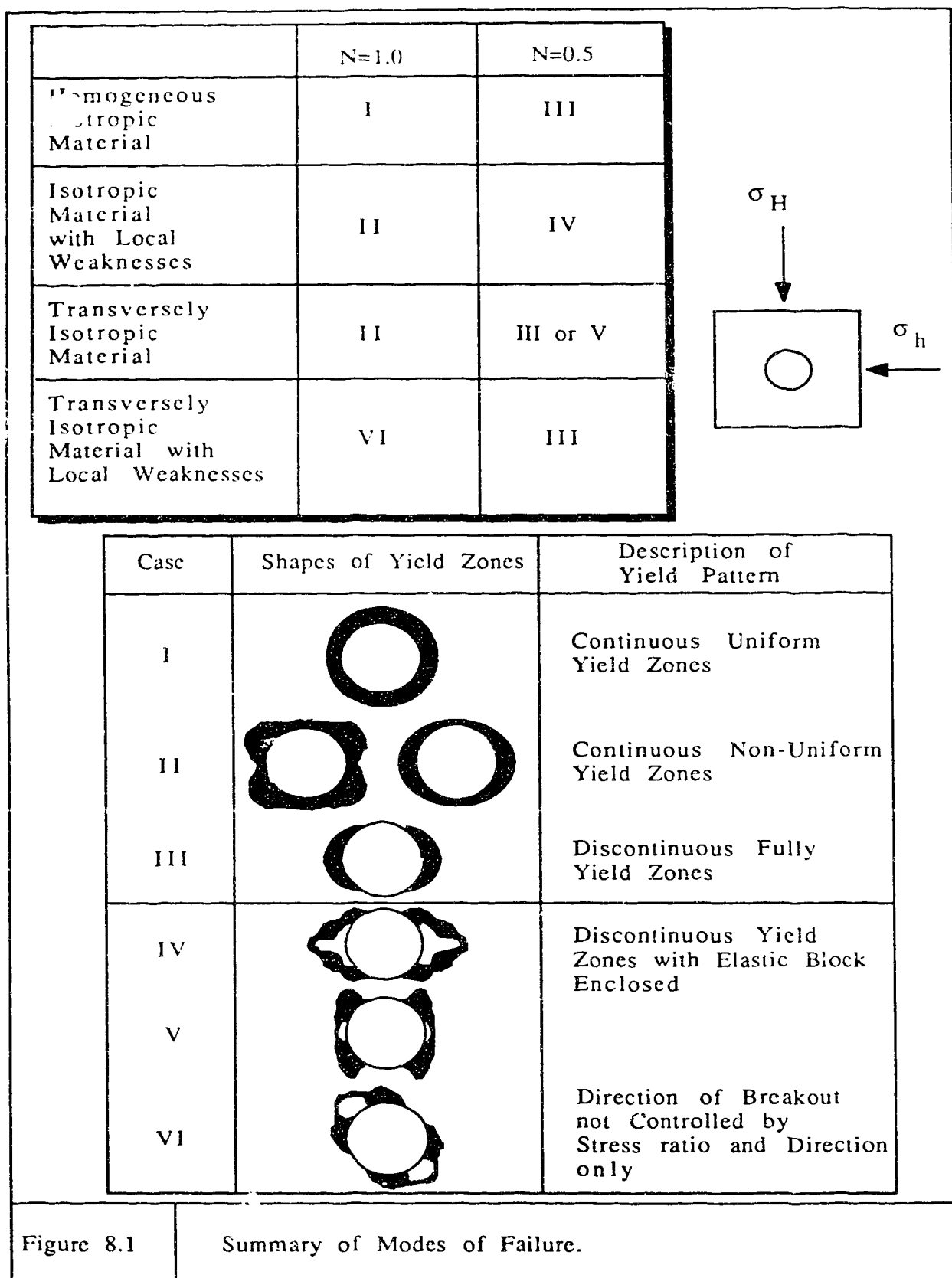
8.3 Practical Implications for Design and Monitoring of Underground Openings

The implications described above for borehole stability are generally true for the design and monitoring of underground openings such as a tunnel.

Practical implications for the monitoring of tunnels based on the ground convergence curves (Cases A to D in Figure 4.8 and Cases E to G in Figure 5.9) and the ground strain curves (Case D in Figure 4.9 and Case G in Figure 5.10) have been discussed in Sections 4.5 and 5.6. In general, it can be concluded that convergence measurements will give an indication of the stability of an opening, but it is insufficient to differentiate among the various modes of failure. Localized measurements of relative displacement at appropriate locations are needed to properly locate and identify the actual failure mode. Pattern monitoring will likely miss critical condition and only strategically well placed instruments, based on a clear vision of the potential failure mode, can provide useful information.

The presence of weaknesses will lead to a distribution of stress such that maximum deviatoric stress is away from the borehole wall. However, it does not much change the stress distribution of an elastic rock at a distance of 2 radii away from the opening. This is of practical importance for the design of frictional anchor because good frictional resistance can be mobilized at this distance for the

particular conditions illustrated by the block-type failure mechanism.



9 References

- Amadei, B., 1983. Rock Anisotropy and the Theory of Stress Measurements. Springer-Verlag Berlin Heidelberg, 477 p.
- Attewell, P. B. and Sandford, M. R., 1974. Intrinsic shear strength of a brittle anisotropic rock- experimental and mechanical interpretation. International Journal of Rock Mechanics and Mining Sciences and Geomechanics Abstracts, **11**, pp. 423-430.
- Babcock, E. A., 1978. Measurement of subsurface fractures from dipmeter logs. American Association of Petroleum Geologist Bulletin, **62**, pp. 1111-1126.
- Bandis, S. C. and Barton, N., 1986. Failure modes of deep boreholes. 27th. U. S. Symp. on Rock Mechanics, University of Alabama, pp. 599-605.
- Bardet, J. P., 1988. Numerical modeling of rockburst. 2nd. International Symposium of Rockbursts and Seismicity in Mines, pp. 83-92.
- Berest, P., Habib, P. and Nguyen, M. D., 1980. Tentative d'interpretation des deformations observees aux tunnels du Fréjus et du Gran Sasso. Révue Française de Geotechnique, **12**, pp. 44-55.
- Biot, M., 1965. Mechanics of Incremental Deformations. John Wiley and Sons, 504 p.

- Casagrande, A. and Carrillo, N., 1944. Shear failure of anisotropic materials. *Journal of the Boston Society of Civil Engineers*, **XXXI**, No. 4, pp. 122-135.
- Chan, D., 1986. Finite Element Analysis of Strain-Softening Materials. Ph. D. Thesis, Department of Civil Engineering, University of Alberta, Edmonton, Alberta, 355 p.
- Daemen, J. J. K., 1983. Slip zones for discontinuities parallel to circular tunnels or shafts. *International Journal of Rock Mechanics and Mining Sciences and Geomechanics Abstracts*, **20**, No. 3, pp. 135-148.
- Daemen, J. J. K. and Fairhurst, C., 1972. Rock failure and tunnel support loading. *International Symposium on Underground Openings*, Luzern, pp. 356-359.
- Davis, E. H. and Christian, J. T., 1971. Bearing capacity of anisotropic cohesive soil. *Journal of the Soil Mechanics and Foundations Division, Proc. of ASCE*, **1**, SM 5, pp. 753-769.
- Desai, C. S. and Reese, L. C., 1970. Stress-deformation and stability analyses of deep boreholes. 2nd. *International Congress of International Society of Rock Mechanics*, Belgrade, pp. 4-13.
- Detournay, E. and St. John, C. M., 1988. Design charts for a deep circular tunnel under non-uniform loading. *Rock Mechanics and Rock Engineering*, **21**, pp. 119-137.

- Donath, F. A., 1963. Strength variation and deformational behaviour in anisotropic rock. *State of Stress in the Earth's Crust*, pp. 281-297.
- de Borst, R., 1986. Numerical simulation of shear-band bifurcation in sand bodies. 2nd. International Symposium on Numerical Models in Geomechanics, pp. 91-98.
- Ewy, R. T., Cook, N. G. and Myer, L. R., 1988. Hollow cylinder tests for studying fracture around underground openings. 29th. U. S. Symposium on Rock Mechanics, pp. 67-74.
- Ewy, R. T., Kemeny, J. M., Zheng, Z. and Cook, N. G., 1987. Generation and analysis of stable excavation shapes under high rock stresses. 6th. International Rock Mechanics Congress of International Society of Rock Mechanics, Montreal, 2, pp. 875-881.
- Frank, R., Guenot, A. and Humbert, P., 1980. Etude par elements finis de quelques critères de plasticité orientés. Proceeding of 2nd. International Congress on Numerical Methods for Engineering (GAMNI), Paris, 2, pp. 765-775.
- Gnirk, P. F., 1972. The mechanical behaviour of uncased wellbores situated in elastic/plastic media under hydrostatic stress. *Journal of Society of Petroleum Engineering*, 253, pp. 49-59.
- Goodman, R. and Shi, G. H., 1985. Block Theory and its Application to Rock Engineering. Prentice-Hall Inc., 338 p.

- Gough, D. I. and Bell, J. S., 1982. Stress orientation from borehole wall fractures with examples from Colorado, east Texas and northern Canada. *Canadian Journal of Earth Sciences*, **19**, pp. 1358-1370.
- Guenot, A., 1979. Investigation of Tunnel Stability by Model Tests. M. Sc. Thesis, Department of Civil Engineering, University of Alberta, 217 p.
- Guenot, A., 1980. Simulation du comportement d'une roche schisteuse par la méthode des éléments finis. Department de Geotechnique, Laboratoire Central des ponts et chaussées, Rapport Preliminaire, 87 p.
- Guenot, A., 1987. Stress and rupture conditions around wellbores. 6th. International Rock Mechanics Congress of International Society of Rock Mechanics, Montreal, **1**, pp. 109-118.
- Guenot, A. and Santarelli, F. J., 1988. Borehole stability: A new challenge for an old problem. 29th. U. S. Symposium of Rock Mechanics, pp. 453-460.
- Haimson, B. C. and Herrick, C. G., 1986. Borehole breakouts- A new tool for estimating in situ stress. International Symposium on Rock Stress Measurements, Stockholm, pp. 271-280.
- Hill, R., 1950. The Mathematical Theory of Plasticity. Clarendon Press, 356 p.

- Hill, R., 1959. Some basic principles in the mechanics of solids without a natural time. *Journal of Mechanical Physics in Solids*, 7, pp. 209-225.
- Hoek, E. and Bray, J. W., 1977. *Rock Slope Engineering*. 2nd. Edition Institution of Mining and Metallurgy, 402 p.
- Hoek, E. and Brown, E. T., 1980. *Underground Excavations in Rock*. Institution of Mining and Metallurgy, London. 527 p.
- IMSL, 1987. *Mathematics Library- Fortran Subroutine for Mathematics Applications*. IMSL Problem-Solving Software System, IMSL, Incorporated, 1151 p.
- Jaeger, J. C., 1960. Shear failure of anisotropic rocks. *Geological Magazine*, 97, pp. 65-72.
- Jaeger, J. C. and Cook, N. G. W., 1979. *Fundamentals of Rock Mechanics*. 2nd. Edition., Chapman and Hall, London, 585 p.
- Kaiser, P. K., 1979. *Time-dependent Behaviour of Tunnels in Jointed Rock Masses*. Ph. D. Thesis, Department of Civil Engineering, University of Alberta, 395 p.
- Kaiser, P. K. and Maloney, S. M., 1987. Factors influencing the stability of deep boreholes. 6th. International Rock Mechanics Congress of International Society of Rock Mechanics, Montreal, 1, pp. 675-680.

- Kaiser, P. K. and Maloney, S. M., 1982. Deformation properties of a subbituminous coal mass. *International Journal of Rock Mechanics and Mining Sciences and Geomechanics Abstracts*, **19**, pp. 247-252.
- Kaiser, P. K. and Morgenstern, N. R., 1981. Time-dependent deformation of small tunnels- Part I: Test facility. *International Journal of Rock Mechanics and Mining Sciences and Geomechanics Abstracts*, **18**, pp. 129-140.
- Kaiser, P. K., Guenot, A. and Morgenstern, N. R., 1985. Deformation of small tunnels- Part IV: Behaviour during failure. *International Journal of Rock Mechanics and Mining Sciences and Geomechanics Abstracts*, **22**, pp. 141-152.
- Kastner, H., 1962. *Statik des Tunnel-und Stollenbaues*. 2nd. Edition.. Neubearbeitete Auflage Springer, Berlin, 313 p.
- Kirsch, G., 1898. Die Theorie der Elastizität und die Bedürfnisse der Festigkeitslehre. *Zeitschrift des Vereins Deutscher Ingenieure*, **42**, pp. 797-807.
- Lekhnitskii, S. G., 1963. *Theory of Elasticity of an Anisotropic Elastic Body*. Holden-Day, San Francisco, 404 p.
- Livneh, M. and Sharshy, E., 1965. Equations of failure stresses in material with anisotropic strength parameters. *Highway Research Record*, No. 74, pp. 44-54.

- Lunardi, P., 1980. Application de la mécanique des roches aux tunnels autoreutiers, exemple des tunnels du Fréjus (côté Italie) et du Gran Sasso. *Révue Française de Géotechnique*, No. 12, pp. 5-55.
- Maury, V., 1977. An example of underground storage in soft rock: the chalk. Rockstore, Stockholm.
- Maury, V., 1987. Observations, researches and recent results about failure mechanisms around single galleries. 6th. International Rock Mechanics Congress of International Society of Rock Mechanics, 3, pp. 1119-1128.
- McLamore, R. and Gray, K. E., 1967. A strength criterion for anisotropic rocks based upon experimental observations. 96th. AIME, Annual Meeting, paper SPE 1721.
- McLamore, R. and Gray, K. E., 1967. The mechanical behaviour of anisotropic sedimentary rocks. *Journal of Engineering Industry, Transactions of American Society of Mining Engineering*, 89, pp. 62-76.
- Miles, A. J. and Topping, A. D., 1949. Stress around a deep well. *Transaction of AIME*, 179, pp. 186-191.
- Mindlin, R. D., 1939. Stress distribution around a tunnel. *Transaction of American Society of Civil Engineer*, paper no. 2082, pp. 1117-1140.

- Morita, N. and Gray, K. E., 1980. A constitutive equation for non-linear stress-strain curves in rocks and its application to stress analysis around a borehole during drilling. 55th. Annual Fall Technical Conference of Society of Petroleum Engineer, AIME, Dallas, Texas, paper SPE 9328.
- Mühlhaus, H. B., 1988. Lamination phenomena in prestressed rock. 2nd. International Symposium of Rockbursts and Seismicity in Mines, pp. 117-127.
- Nova, R., 1980. The failure of transversely isotropic rock in triaxial compression. International Journal of Rock Mechanics and Mining Sciences and Geomechanics Abstracts, 17, pp. 325-332.
- Nova, R. and Sacchi, G., 1979. A generalized failure condition for orthotropic solids. EUROMECH 115- Mechanical Behaviour of Anisotropic Solids, Villand de Lans, pp. 623-641.
- Obert, L. and Duvall, W. I., 1967. Rock Mechanics and the Design of Structures in Rock. John Wiley & Sons, Inc., 650 p.
- Paker, W. H. and Krizek, R. J., 1970. Mohr-Coulomb strength theory for anisotropic soils. Journal of the Soil Mechanics and Foundation Division, Proceeding of American Society of Civil Engineer, 96, SM 1, pp. 269-292.
- Pariseau, W. G., 1968. Plasticity theory for anisotropic rocks and soils. 10th. Symposium on Rock Mechanics (AIME), pp. 267-295.

- Risnes, R., Bratli, R. K. and Horsrud, P., 1982. Sand stresses around a wellbore. *Journal of Society of Petroleum Engineer*, December, pp. 883-898.
- Santarelli, F. J. and Brown, E. T., 1987. Performance of deep wellbores in rock with a confining pressure-dependent elastic modulus. 6th. International Rock Mechanics Congress of International Society of Rock Mechanics, Montreal, 2, pp. 1217-1222.
- Santarelli, F. J., Brown, E. T. and Maury, V., 1986. Analysis of borehole stresses using pressure-dependent, linear elasticity. *International Journal of Rock Mechanics and Mining Sciences and Geomechanics Abstracts*, 23, pp. 445-449.
- Smith, M. B. and Cheatham, J. B., 1980. An anisotropic compacting yield condition applied to porous limestone. *International Journal of Rock Mechanics and Mining Sciences and Geomechanics Abstracts*, 17, pp. 159-165.
- Sulem, J. and Vardoulakis, I., 1988. A new approach to borehole stability based on bifurcation theory. *Numerical Methods in Geomechanics*, 3, pp. 1929-1935.
- Sulem, J., Panet, M. and Guenot, A., 1987. Closure analysis in deep tunnels. *International Journal of Rock Mechanics and Mining Sciences and Geomechanics Abstracts*, 24, No. 3, pp. 145-154.

- Szechy, K., 1966. The Art of Tunnelling. Akademiai Kiado, Budapest, 883 p.
- Vardoulakis, I., 1984. Rock bursting as a surface instability phenomenon. International Journal of Rock Mechanics and Mining Sciences and Geomechanics Abstracts, **21**, No. 3, pp. 137-144.
- Vardoulakis, I., Goldscheider, M. and Gudehus, G., 1978. Formation of shear bands in sand bodies as a bifurcation problem. International Journal of Numerical Analytical Method in Geomechanics, **2**, pp. 99-128.
- Vardoulakis, I., Sulem, J. and Guenot, A., 1988. Borehole instabilities as bifurcation phenomena. International Journal of Rock Mechanics and Mining Sciences and Geomechanics Abstracts, **25**, No. 3, pp. 159-170.
- Westergaard, H. M., 1940. Plastic state of stress around a deep well. Journal of Boston Society of Civil Engineer, **XXVII**, No. 1, January, pp. 387-391.
- Widerhofer, R., 1970. Die Theorie der Plastischen Zonen in der Geomechanik; Ihre Anwendung zu einer Wirtschaftlichen Bemessung einer Tunnelauskleidung. 2nd. International Society of Rock Mechanics Congress, Beograd, **2**, pp. 407-418.
- Wong, R. C. K. and Kaiser, P. K., 1986. Ground behaviour near soft ground tunnels. International Tunnelling Association-

Conference on Large Underground Openings, Florence, 1. pp. 942-951.

Zoback, M. D., Moos, D. and Mastin, L., 1985. Wellbore breakouts and in situ stress. *Journal of Geophysics Research*, **900**(B7), pp. 5523-5530.

APPENDIX A

Subroutine Program For Eigenvalue Computation

The global stiffness matrix, ABIF, in SAGE is stored as an one dimensional array. In order to call the IMSL library subroutine EIGRS for eigenvalues and eigenvectors computation, ABIF must be written in the format suitable for EIGRS.

After the element stiffness matrices are calculated and assembled into the global stiffness matrix, subroutine SETBIF is called to arrange the elements in ABIF suitable for EIGRS. Subroutine SETBIF is written as follows:

```

      SUBROUTINE SETBIF (ABIF, S, NVEL, LJ, NS, NNET, MAXABF,
      IOUT1, MMNNET)
      IMPLICIT REAL*8 (A-H, O-Z)
      ABIF = GLOBAL STIFFNESS MATRIX STORED AS A VECTOR
      S = ELEMENT STIFFNESS MATRIX
      NVEL = 16 FOR 2-D RECTANGULAR ELEMENT
      LJ = LISTING OF DEGREE OF FREEDOM FOR EACH ELEMENT
      NS = 16
      NNET = NET DEGREE OF FREEDOM
      MAXABF = ARRAY TO STORE THE DIAGONAL ADDRESSING IN
      THE SKYLINE AND EXTENDED SKYLINE METHOD
      IOUT1 = FILE CONTAINING OUTPUT INFORMATION
      MMNNET = (NNET*NNET+NNET)/2
      DIMENSION ABIF (MMNNET), S(NS,1), LJ(1), MAXABF(NNET)
      DO 12 I=1, NVEL
        LJR=LJ(I)
        IF (LJR.EQ.0) GO TO 12
        KK=1
        DO 11 J=KK, NVEL
          LJC=LJ(J)
          IF (LJC.EQ.0) GO TO 11
          IF (LJR-LJC) 5, 6, 7
        6 KLM=MAXABF(LJR)
          GOTO 10
        5 KLM=MAXABF(LJC)-(LJC-LJR)
          GOTO 10
        7 KLM=MAXABF(LJR)-(LJR-LJC)
      10 ABIF(KLM)=ABIF(KLM)+S(I,J)

```

```

11 CONTINUE
12 CONTINUE
   RETURN
   END

```

After obtaining ABIF, the program calls the subroutine EIGRS to carry out the eigenvalues and eigenvectors computation. Subroutine EIGRS is briefly described as follows:

IMSL ROUTINE NAME EIGRS

PURPOSE	To compute the eigenvalues and (optionally) the eigenvectors of a real symmetric matrix.						
USAGE	Call EIGRS (A, N, JOBN, D, Z, IZ, WK, IER)						
ARGUMENTS	<table border="0"> <tr> <td style="vertical-align: top; padding-right: 10px;">A</td> <td>Input real symmetric matrix of order N, whose eigenvalues and eigenvectors are to be computed. Input A is destroyed if IJOB is equal to 0 or 1.</td> </tr> <tr> <td style="vertical-align: top; padding-right: 10px;">N</td> <td>Input order of the matrix A.</td> </tr> <tr> <td style="vertical-align: top; padding-right: 10px;">JOBN</td> <td>Input option parameter. If JOBN.GE.10, A is assumed to be in full storage mode (in this case, A must be dimensioned exactly N by N in the calling program). If JOBN.LT.10 then A is assumed to be in symmetric storage mode. IJOB=0, compute eigenvalues only</td> </tr> </table>	A	Input real symmetric matrix of order N, whose eigenvalues and eigenvectors are to be computed. Input A is destroyed if IJOB is equal to 0 or 1.	N	Input order of the matrix A.	JOBN	Input option parameter. If JOBN.GE.10, A is assumed to be in full storage mode (in this case, A must be dimensioned exactly N by N in the calling program). If JOBN.LT.10 then A is assumed to be in symmetric storage mode. IJOB=0, compute eigenvalues only
A	Input real symmetric matrix of order N, whose eigenvalues and eigenvectors are to be computed. Input A is destroyed if IJOB is equal to 0 or 1.						
N	Input order of the matrix A.						
JOBN	Input option parameter. If JOBN.GE.10, A is assumed to be in full storage mode (in this case, A must be dimensioned exactly N by N in the calling program). If JOBN.LT.10 then A is assumed to be in symmetric storage mode. IJOB=0, compute eigenvalues only						

IJOB=1, compute eigenvalues and
eigenvectors.

IJOB=2, compute eigenvalues, eigenvectors
and performance index.

IJOB=3, compute performance index only.

If the performance index is computed, it is
returned in WK(1). The routines have
performed (well, satisfactorily, poorly) if
WK(1) is (less than 1, between 1 and 100,
greater than 100) respectively.

D Output vector of length N, containing the
eigenvalues of A.

Z Output N by N matrix containing the
eigenvectors of A. The eigenvector in column
J of Z corresponds to the eigenvalue D(J).
If IJOB=0, Z is not used.

IZ Input row dimension of matrix Z exactly as
specified in the dimension statement in the
calling program.

WK Work area, the length of WK depends on the
value of IJOB.

IJOB=0 or 1, the length of WK is at least N.

IJOB=2, the length of WK is at least

$$N(N+1)/(2+N).$$

IJOB=3, the length of WK is at least 1.

IER Output error parameter.

Terminal error:

IER=128+J, indicates that subroutine EQRT2S failed to converge on eigenvalue J.

Eigenvalues and eigenvectors 1 ... , J-1 have been computed correctly, but the eigenvalues are unordered. The performance index is set to 1000.0.

Warning error.

IER=66, indicates IJOB is less than 0 or IJOB is greater than 3. IJOB is set to 1.

IER=67, indicates IJOB is not equal to 0, and IZ is less than the order of matrix A. IJOB is set to 0.

PRECISION/

HARDWARE

Single and double/H32

Single/H36, H48, H60.

REQUIRED IMSL

ROUTINES

EHOBKS, EQRT2S, EQRT2S, UERTST, UGETIO.

NOTATION

Information on special notation and conventions is available in the manual introduction or through IMSL routine UHELP.

ALGORITHM

EIGRS calls IMSL routine EHOUSS and EQRT2S to compute eigenvalues and (optionally) eigenvectors. When eigenvectors are computed, EHOBKS is called to backtransform the eigenvectors.

When P (performance index) is less than 1, the performance of the routines is considered to be excellent. When P is between 1 and 100 the performance is good. When P is greater than 100 the performance is considered poor.

The performance index was first developed and used by the EISPACK project at Argonne National Laboratory. Details of the performance index can be found in the following two references:

1. Wilkinson, J. H., 1965. The Algebraic Eigenvalue Problem. Clarendon Press, Oxford.
2. Smith, B. T., Boyle, J. M., Garbow, B. S., Ikebe, Y., Klema, V. C. and Moler, C. B., 1974. Matrix Eigensystem Routines. Springer-Verlag.

PROGRAMMING NOTES

1. A is preserved when IJOB=2 or 3 (IJOB=MOD(JOBN,10)). In all other cases, A is destroyed.
2. The computed eigenvectors are normalized to each having Euclidean length of 1.

3. When IJOB=3 (i.e., to compute a performance index only) the eigenvalues, D, and eigenvectors, Z, are assumed to be the input.

EXAMPLE

In the following example, EIGRS is called with JOBN=2 so that eigenvalues, eigenvectors and a performance index are computed for matrix A, which is stored in symmetric storage mode.

INPUT:

```
INTEGER  N, JOBN, IZ, IER
REAL     D(10), D(4), Z(4,4), WK(14)
```

N=4

IZ=4

$$A = \begin{bmatrix} 5.0 & 4.0 & 1.0 & 1.0 \\ 4.0 & 5.0 & 1.0 & 1.0 \\ 1.0 & 1.0 & 4.0 & 2.0 \\ 1.0 & 1.0 & 2.0 & 4.0 \end{bmatrix}$$

In symmetric storage mode A(1)=5.0, A(2)=4.0,

A(3)=5.0, ..., A(10)=4.0

JOBN=2

Call EIGRS(A, N, JOBN, D, Z, IZ, WK, IER)

OUTPUT:

IER=0

D=(1.0, 2.0, 5.0, 10.0) (eigenvalue.)

$$Z = \begin{bmatrix} -0.70710 & 0.00000 & -0.31622 & 0.63245 \\ 0.70710 & 0.00000 & -0.31622 & 0.63245 \\ 0.00000 & 0.70710 & 0.63245 & 0.31622 \\ 0.00000 & -0.70710 & 0.63245 & 0.31622 \end{bmatrix}$$

(eigenvectors)

WK(1) < 1 (performance index)

Note: Z is unique to within a sign change for each column.

APPENDIX B

Elastic Deformation Properties of Transversely Isotropic Rock

B.1 Elastic Constitutive Matrix for Transverse Isotropic Rocks

Many sedimentary rocks (shales, sandstones, coal) or metamorphic rocks (schists, slates, gneisses) are anisotropic, meaning that their properties vary with directions. For a linear elastic homogeneous anisotropic rock, the strain and stress tensors are related as follows:

$$\epsilon_{ij} = A_{ijkl} \sigma_{kl} \quad (B.1a)$$

where, ϵ_{ij} = Strain tensor;
 σ_{kl} = Stress tensor;
 A_{ijkl} = Compliance tensor.

Equation B.1a in an arbitrary x, y, z coordinate system can be written in matrix form as follows:

$$\begin{bmatrix} \epsilon_x \\ \epsilon_y \\ \epsilon_z \\ \gamma_{xy} \\ \gamma_{yz} \\ \gamma_{zx} \\ \gamma_{xz} \\ \gamma_{zy} \\ \gamma_{yx} \end{bmatrix} = [A] \begin{bmatrix} \sigma_x \\ \sigma_y \\ \sigma_z \\ \tau_{xy} \\ \tau_{yz} \\ \tau_{zx} \\ \tau_{xz} \\ \tau_{zy} \\ \tau_{yx} \end{bmatrix} \quad (\text{B.1b})$$

In the most general three dimensional case, the compliance tensor A_{ijkl} has 81 independent components. However, due to the symmetry of both the strain tensors ($\gamma_{zx} = \gamma_{xz}$, $\gamma_{yz} = \gamma_{zy}$, $\gamma_{xy} = \gamma_{yx}$) and the stress tensors ($\tau_{zx} = \tau_{xz}$, $\tau_{yz} = \tau_{zy}$, $\tau_{xy} = \tau_{yx}$), the maximum number of independent elastic constants in the compliance tensor A_{ijkl} is reduced to 36 (i.e., $A_{ijkl} = A_{jikl}$ and $A_{ijkl} = A_{ijlk}$). Equation B.1b reduces to:

$$\begin{bmatrix} \epsilon_x \\ \epsilon_y \\ \epsilon_z \\ \gamma_{xy} \\ \gamma_{yz} \\ \gamma_{zx} \end{bmatrix} = [A] \begin{bmatrix} \sigma_x \\ \sigma_y \\ \sigma_z \\ \tau_{xy} \\ \tau_{yz} \\ \tau_{zx} \end{bmatrix} \quad (\text{B.2})$$

The number of independent constants in the compliance matrix can further be reduced to 21 if a strain energy function is assumed to exist such that $A_{ijkl} = A_{klij}$ (Lekhnitskii, 1963). Matrix A_{ijkl} in Equation B.2 now becomes symmetric. In some cases, the number of independent constants in the compliance matrix can be further reduced by modelling the anisotropic rock as an orthotropic or transversely isotropic material. Orthotropy implies that three

orthogonal planes of symmetry exist at each point in the rock and that these planes have the same orientation throughout the rock. Transverse isotropy implies that at each point in the rock, there is an axis of symmetry of rotation and that the rock has isotropic properties in the plane normal to this axis.

For a material with three orthogonal planes of symmetry in elastic properties normal to an x, y, z coordinate system, Equation B.2 reduces to the following:

$$\begin{bmatrix} \epsilon_x \\ \epsilon_y \\ \epsilon_z \\ \gamma_{xy} \\ \gamma_{yz} \\ \gamma_{zx} \end{bmatrix} = \begin{bmatrix} \frac{1}{E_x} & \frac{-\nu_{yx}}{E_y} & \frac{-\nu_{zx}}{E_z} & 0 & 0 & 0 \\ \frac{-\nu_{yx}}{E_y} & \frac{1}{E_y} & \frac{-\nu_{zy}}{E_z} & 0 & 0 & 0 \\ \frac{-\nu_{zx}}{E_z} & \frac{-\nu_{zy}}{E_z} & \frac{1}{E_z} & 0 & 0 & 0 \\ 0 & 0 & 0 & \frac{1}{G_{xy}} & 0 & 0 \\ 0 & 0 & 0 & 0 & \frac{1}{G_{yz}} & 0 \\ 0 & 0 & 0 & 0 & 0 & \frac{1}{G_{zx}} \end{bmatrix} \begin{bmatrix} \sigma_x \\ \sigma_y \\ \sigma_z \\ \tau_{xy} \\ \tau_{yz} \\ \tau_{zx} \end{bmatrix} \quad (\text{B.3})$$

where,

E_x, E_y, E_z = Modulus of elasticity in the x, y, z directions, respectively;

G_{xy}, G_{yz}, G_{zx} = Shear moduli in planes parallel to the xy, yz and zx coordinate planes, respectively;

ν_{yx} = Poisson's ratio characterizing the extensional strain in the x-direction due to a compressive stress acting in the y-direction (similarly for ν_{zx} and ν_{zy}).

The number of independent constants in the compliance matrix is now reduced to 9.

For a material with a plane of transverse isotropy parallel to the xz coordinate plane (see Figure B.1), Equation B.3 further reduces to:

$$\begin{bmatrix} \epsilon_x \\ \epsilon_y \\ \epsilon_z \\ \gamma_{xy} \\ \gamma_{yz} \\ \gamma_{zx} \end{bmatrix} = \begin{bmatrix} \frac{1}{E_1} & \frac{-\nu_2}{E_2} & \frac{-\nu_1}{E_1} & 0 & 0 & 0 \\ \frac{-\nu_2}{E_2} & \frac{1}{E_2} & \frac{-\nu_2}{E_2} & 0 & 0 & 0 \\ \frac{-\nu_1}{E_1} & \frac{-\nu_2}{E_2} & \frac{1}{E_1} & 0 & 0 & 0 \\ 0 & 0 & 0 & \frac{1}{G_2} & 0 & 0 \\ 0 & 0 & 0 & 0 & \frac{1}{G_2} & 0 \\ 0 & 0 & 0 & 0 & 0 & 2\frac{(1+\nu_1)}{E_1} \end{bmatrix} \begin{bmatrix} \sigma_x \\ \sigma_y \\ \sigma_z \\ \tau_{xy} \\ \tau_{yz} \\ \tau_{zx} \end{bmatrix} \quad (\text{B.4})$$

where,

$E_x = E_2 = E_1$ = Modulus of elasticity in the plane of transverse isotropy;

$E_y = E_2$ = Modulus of elasticity in plane normal to the plane of transverse isotropy;

G_2 = Shear modulus in plane normal to the plane of transverse isotropy;

ν_1 = Poisson's ratio characterizing the extensional strain in the plane of transverse isotropy due to a compressive stress acting parallel to the plane of transverse isotropy;

ν_2 = Poisson's ratio characterizing the extensional strain in the plane of transverse isotropy due to a compressive stress acting normal to the plane of transverse isotropy.

The number of independent constants needed to describe the elastic deformational response of a transversely isotropic material is five (E_1 , E_2 , G_2 , ν_1 and ν_2). Rocks such as shales, sandstones or coal are often treated as transversely isotropic materials by assuming the weakness planes, jointing, lamination or stratified layers are planes of transverse isotropy.

For a material with full symmetry, Equation B.4 reduces further to:

$$\begin{bmatrix} \epsilon_x \\ \epsilon_y \\ \epsilon_z \\ \gamma_{xy} \\ \gamma_{yz} \\ \gamma_{zx} \end{bmatrix} = \begin{bmatrix} \frac{1}{E} & \frac{-\nu}{E} & \frac{-\nu}{E} & 0 & 0 & 0 \\ \frac{-\nu}{E} & \frac{1}{E} & \frac{-\nu}{E} & 0 & 0 & 0 \\ \frac{-\nu}{E} & \frac{-\nu}{E} & \frac{1}{E} & 0 & 0 & 0 \\ 0 & 0 & 0 & \frac{1}{G} & 0 & 0 \\ 0 & 0 & 0 & 0 & \frac{1}{G} & 0 \\ 0 & 0 & 0 & 0 & 0 & \frac{1}{G_1} \end{bmatrix} \begin{bmatrix} \sigma_x \\ \sigma_y \\ \sigma_z \\ \tau_{xy} \\ \tau_{yz} \\ \tau_{zx} \end{bmatrix} \quad (B.5)$$

where, E = Modulus of elasticity for isotropic material;
 ν = Poisson's ratio for isotropic material.

The number of independent constants for isotropic material is finally reduced to two (E and ν).

The elastic constitutive matrix $[C^E]$ for a transversely isotropic rock is obtained by taking the inverse of the compliance matrix in Equation B.4, resulting in the following:

$$\begin{bmatrix} \sigma_x \\ \sigma_y \\ \sigma_z \\ \tau_{xy} \\ \tau_{yz} \\ \tau_{zx} \end{bmatrix} = [C^E] \begin{bmatrix} \epsilon_x \\ \epsilon_y \\ \epsilon_z \\ \gamma_{xy} \\ \gamma_{yz} \\ \gamma_{zx} \end{bmatrix} \quad (B.6)$$

where, $[C^E]$ = Elastic constitutive matrix;

$$[C^E] = \frac{1}{(2\nu_2^2 + \nu_1 - 1)} * \begin{bmatrix} \frac{E_1(\nu_2^2 - 1)}{(1 + \nu_1)} & -E_1\nu_2 & \frac{-E_1(\nu_2^2 + \nu_1)}{(1 + \nu_1)} & 0 & 0 & 0 \\ -E_1\nu_2 & E_2(\nu_1 - 1) & -E_1\nu_2 & 0 & 0 & 0 \\ \frac{-E_1(\nu_2^2 + \nu_1)}{(1 + \nu_1)} & -E_1\nu_2 & \frac{E_1(\nu_2^2 - 1)}{(1 + \nu_1)} & 0 & 0 & 0 \\ 0 & 0 & 0 & G_2(2\nu_2^2 + \nu_1 - 1) & 0 & 0 \\ 0 & 0 & 0 & 0 & G_2(2\nu_2^2 + \nu_1 - 1) & 0 \\ 0 & 0 & 0 & 0 & 0 & \frac{E_1(2\nu_2^2 + \nu_1 - 1)}{2(1 + \nu_1)} \end{bmatrix}$$

In this study, plane strain condition is assumed along the borehole axis (z-direction). The elastic constitutive matrix is obtained by setting $\epsilon_z = \gamma_{yz} = \gamma_{zx} = \tau_{yz} = \tau_{zx} = 0$ in Equation B.6:

$$\begin{bmatrix} \sigma_x \\ \sigma_y \\ \tau_{xy} \end{bmatrix} = \frac{1}{(\nu_1 + 1)(2\nu_2^2 + \nu_1 - 1)} *$$

$$\begin{bmatrix} E_1(v_2^2-1) & -E_1v_2(1+v_1) & 0 \\ -E_1v_2(1+v_1) & E_2(v_1^2-1) & 0 \\ 0 & 0 & G_2(1+v_1)(2v_2^2+v_1-1) \end{bmatrix} \begin{bmatrix} \varepsilon_x \\ \varepsilon_y \\ \gamma_{xy} \end{bmatrix} \quad (\text{B.7})$$

and,

$$\sigma_z = v_1 \sigma_x + \frac{v_2}{E_2} E_1 \sigma_y$$

B.2 Determination of Elastic Constants for Transversely Isotropic Rocks

The elastic constants of Equation B.7 refer to an arbitrary x, y, z coordinate system. Let x', y', z' be another coordinate system such that z' -direction coincides with and that the two coordinate systems are oriented to each other by a rotation angle χ (see Figure B.1). The transformation of elastic constants from the x, y, z coordinate system to the x', y', z' coordinate system is given by Amadei (1983) as follows:

$$\frac{1}{E'_1} = \frac{\cos^4\chi}{E_1} + \frac{\sin^4\chi}{E_2} + \frac{\sin^2 2\chi}{4} \left(\frac{1}{G_2} - \frac{2v_2}{E_1} \right) \quad (\text{B.8a})$$

$$\frac{1}{E'_2} = \frac{\cos^4\chi}{E_2} + \frac{\sin^4\chi}{E_1} + \frac{\sin^2 2\chi}{4} \left(\frac{1}{G_2} - \frac{2v_2}{E_1} \right) \quad (\text{B.8b})$$

$$\frac{1}{G'_2} = \frac{\cos^2 2\chi}{G_2} + \sin^2 2\chi \left(\frac{1}{E_2} + \frac{1}{E_1} + \frac{2v_2}{E_1} \right) \quad (\text{B.8c})$$

$$-\frac{v'_2}{E'_2} = -\frac{v_2 \cos^4\chi}{E_2} - \frac{v_2 \sin^4\chi}{E_1} + \frac{\sin^2 2\chi}{4} \left(\frac{1}{E_1} + \frac{1}{E_2} - \frac{1}{G_2} \right) \quad (\text{B.8d})$$

$$\frac{v'_1}{E'_1} = \frac{v_2 \sin^2\chi}{E_1} + \frac{v_1 \cos^2\chi}{E_1} \quad (\text{B.8e})$$

where, E_1' = Modulus of elasticity in x'-direction;
 E_2' = Modulus of elasticity in y'-direction;
 G_2' = Shear modulus in y'-direction;
 ν_1' = Poisson's ratio in x'z' coordinate plane;
 ν_2' = Poisson's ratio in x'y' coordinate plane.

The five elastic constants of transversely isotropic rocks can be determined by performing three uniaxial compression tests as shown in Figure B.2. If $\chi=0^\circ$ and 90° , four of the elastic constants (E_1 , E_2 , ν_1 , ν_2) can be determined as shown in Figure B.2. The last elastic constant G_2 can be determined by placing the planes of transverse isotropy at 45° to the applying stresses. For $\chi=45^\circ$, Equation B.8b becomes:

$$\frac{1}{E_2'} = \frac{1}{4 E_2} + \frac{1}{4 E_1} + \frac{1}{4} \left(\frac{1}{G_2} - \frac{2 \nu_2}{E_1} \right) = \frac{\epsilon_{45}}{\sigma_{y'}}$$

or,

$$\frac{1}{G_2} = \frac{4 \epsilon_{45}}{\sigma_{y'}} + \frac{2 \nu_2 - 1}{E_1} - \frac{1}{E_2} \quad (B.9)$$

where E_1 , E_2 and ν_2 are the parameter obtained from the previous two tests.

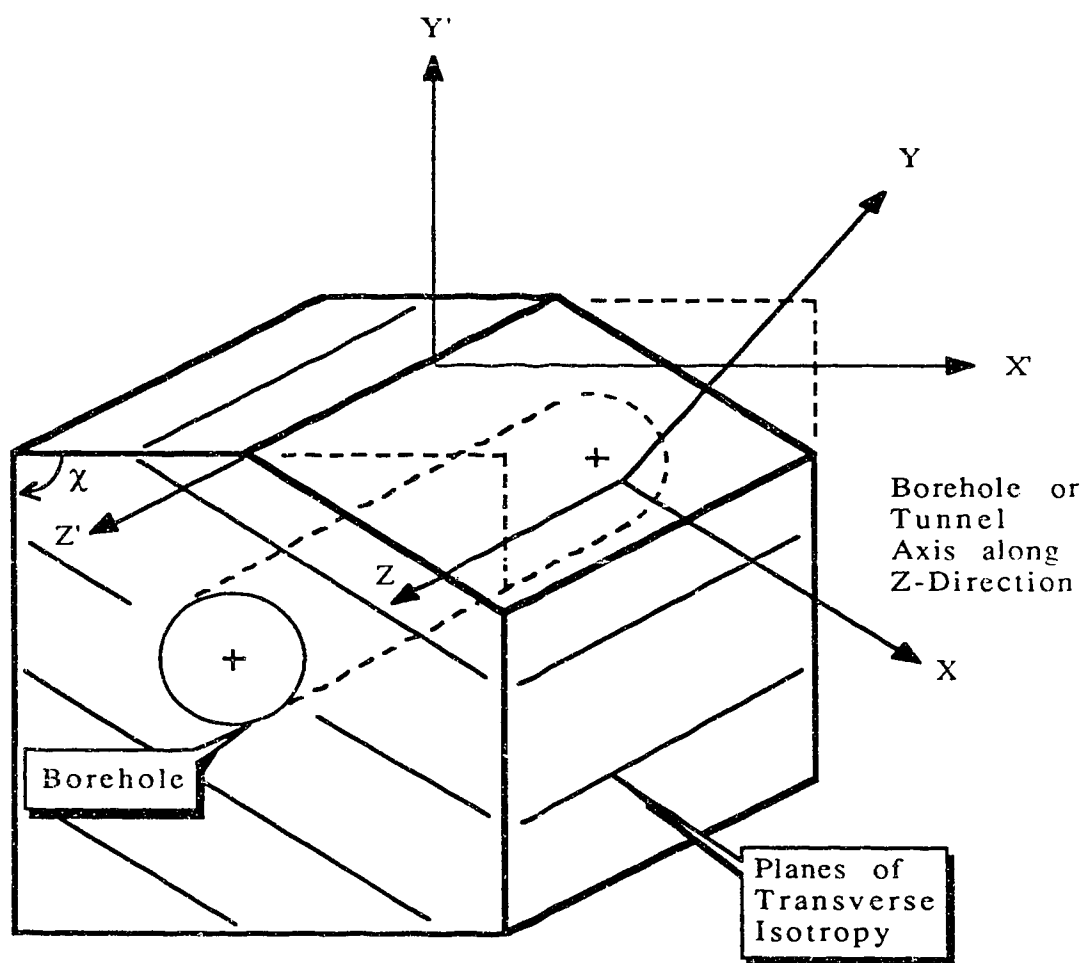
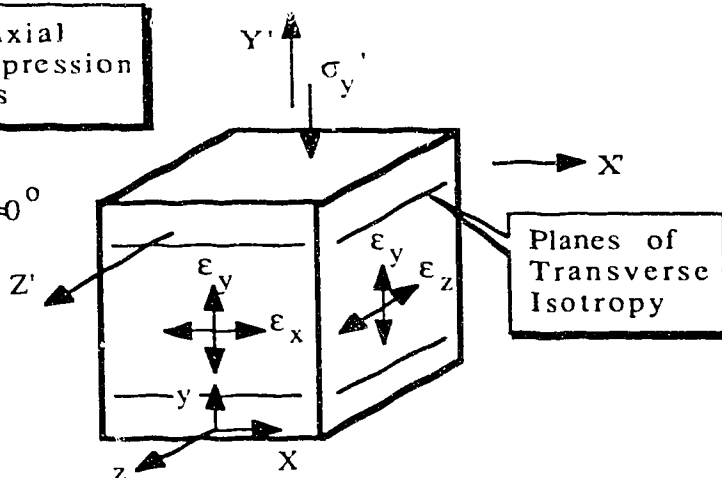


Figure B.1

Definitions for the Coordinate System.

Uniaxial Compression Tests

1) $\chi = 0^\circ$

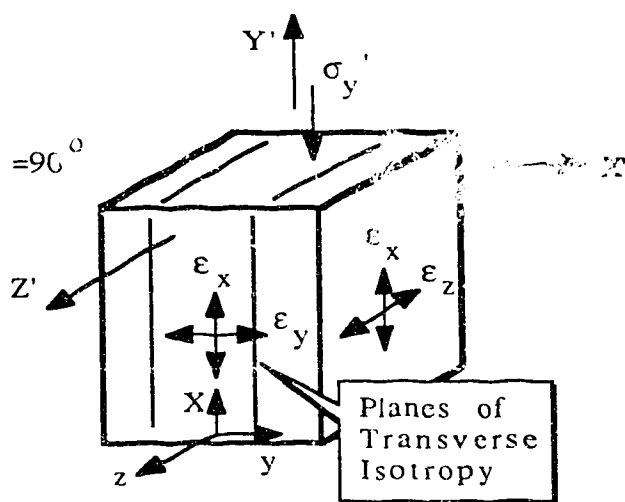


Determine

$$E_2 = \frac{\sigma_y'}{\epsilon_y}$$

$$\nu_2 = -\frac{\epsilon_x}{\epsilon_y} = -\frac{\epsilon_z}{\epsilon_y}$$

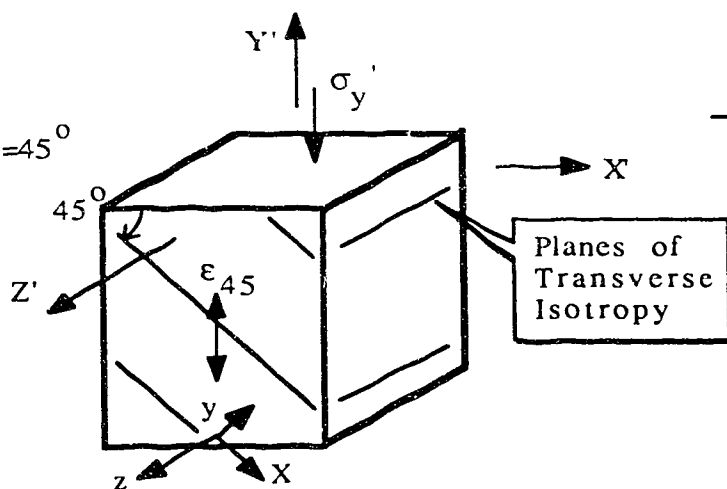
2) $\chi = 90^\circ$



$$E_1 = \frac{\sigma_y'}{\epsilon_x}$$

$$\nu_1 = -\frac{\epsilon_z}{\epsilon_x}$$

3) $\chi = 45^\circ$



$$\frac{1}{G_2} = \frac{4 \epsilon_{45}}{\sigma_y'} + \frac{(2 \nu_2 - 1)}{E_1}$$

$$- \frac{1}{E_2}$$

Figure B.2

Uniaxial Compression Tests for the Determination of Elastic Constants for Transversely Isotropic Rocks.

APPENDIX C

Properties of Transversely Isotropic Model

C.1 Summary of Transversely Isotropic Models

Year	Authors	Strength of material being a function of $c \neq 0, \phi = 0$ $c \neq 0, \phi \neq 0$	Parameters required in the model	Number of parameters
1944	Casagrande and Carillo	✓	S_{uh}, S_{uv}	2
1950	Hill	✓	F, L, N	3
1960	Jaeger	✓	S_1, S_2, T_1, T_2	4
1965	Livneh and Shklarsky	✓	$c_{max}, c_{min},$ ϕ_{max}, ϕ_{min}	4
1967	McLamore and Gray	✓	$S_1, S_2, T_1, T_2,$ n, m	6
1968	Pariseau	✓	F, G, M, U, V	5
1970	Baker and Krizek	✓	c_1, c_2, ϕ_1, ϕ_2	4
1971	Davis and Christian	✓	S_{uh}, S_{uv}, S_{u45}	3
1979	Nova and Sacchi	✓	c_r, c_t, μ_r, μ_t	4
1980	Smith and Cheatham	✓	a, b, c, d, e, f, g	7
Table C.1		List of References for Transversely Isotropic Models		

C.2 Reduction of Transversely Isotropic Yield Criterion to Isotropic Yield Criterion

The transversely isotropic yield criterion takes the following form:

$$\begin{aligned} \frac{(\sigma_1 - \sigma_3)}{2} = & \left\{ \left\{ [(\alpha \cos^2 \eta + \sin^2 \eta) c_{\min} \right. \right. \\ & + (\sigma_m \beta \cos^2 \eta + \sigma_n \sin^2 \eta + \tau_{mn} \sin 2\eta) \tan \phi_{\min}] \\ & * [(\cos^2 \eta + \alpha \sin^2 \eta) c_{\min} + (\sigma_m \beta \sin^2 \eta + \sigma_n \cos^2 \eta \\ & - \tau_{mn} \sin 2\eta) \tan \phi_{\min}] \Big\}^{1/2} \\ & - \sin 2\eta \left[\tan \phi_{\min} \sigma_m \frac{(\beta - 1)}{2} + c_{\min} \frac{(\alpha - 1)}{2} \right] \Big\} \quad (C.1) \end{aligned}$$

where,

$$\begin{aligned} \sigma_m &= \sigma_1 \cos^2 \eta + \sigma_3 \sin^2 \eta; \\ \sigma_n &= \sigma_1 \sin^2 \eta + \sigma_3 \cos^2 \eta; \\ \tau_{mn} &= \frac{(\sigma_1 - \sigma_3)}{2} \sin 2\eta. \end{aligned}$$

The following shows that for $\alpha=\beta=1$, Equation C.1 reduces to the yield criterion for isotropic rocks:

For $\alpha=\beta=1$, Equation C.1 becomes:

$$\frac{(\sigma_1 - \sigma_3)}{2} = \left\{ [c_{\min} + (\sigma_m \cos^2 \eta + \sigma_n \sin^2 \eta + \tau_{mn} \sin 2\eta) \tan \phi_{\min}] \right. \\ \left. * [c_{\min} + (\sigma_m \sin^2 \eta + \sigma_n \cos^2 \eta - \tau_{mn} \sin 2\eta) \tan \phi_{\min}] \right\}^{1/2} \quad (C.2)$$

The term $(\sigma_m \cos^2 \eta + \sigma_n \sin^2 \eta + \tau_{mn} \sin 2\eta)$ in Equation C.2 can be written as:

$$\begin{aligned} & \sigma_m \cos^2 \eta + \sigma_n \sin^2 \eta + \tau_{mn} \sin 2\eta \\ &= \sigma_m (1 - \sin^2 \eta) + \sigma_n (1 - \cos^2 \eta) + \tau_{mn} \sin 2\eta \\ &= (\sigma_m + \sigma_n) - (\sigma_m \sin^2 \eta + \sigma_n \cos^2 \eta - \tau_{mn} \sin 2\eta) \\ &= (\sigma_1 + \sigma_3) - (\sigma_m \sin^2 \eta + \sigma_n \cos^2 \eta - \tau_{mn} \sin 2\eta) \end{aligned} \quad (C.3)$$

The term $(\sigma_m \sin^2 \eta + \sigma_n \cos^2 \eta - \tau_{mn} \sin 2\eta)$ in Equation C.3 is reduced to σ_3 only, after substitution for σ_m , σ_n and τ_{mn} .

Therefore Equation C.2 is simplified to the following:

$$\frac{(\sigma_1 - \sigma_3)}{2} = [(c_{\min} + \sigma_1 \tan \phi_{\min})(c_{\min} + \sigma_3 \tan \phi_{\min})]^{1/2} \quad (C.4a)$$

or,

$$\frac{(\sigma_1 - \sigma_3)}{2} = [(c + \sigma_1 \tan \phi_{\min})(c + \sigma_3 \tan \phi_{\min})]^{1/2} \quad (C.4b)$$

where, $\phi_{\min} = \phi$ = Angle of friction for isotropic material;
 $c_{\min} = c$ = Cohesion intercept for isotropic material.

Equation C.4b is the yield criterion for isotropic material, although it is expressed in a form different from the well known Mohr-Coulomb yield criterion which is normally written as:

$$\frac{(\sigma_1 - \sigma_3)}{2} \cos\phi = c + \left(\frac{\sigma_1 + \sigma_3}{2} - \frac{\sigma_1 - \sigma_3}{2} \sin\phi \right) \tan\phi \quad (C.5)$$

Equation C.4b can be further reduced to the Tresca yield criterion if $\phi=0$, i.e.:

$$\frac{\sigma_1 - \sigma_3}{2} = c \quad (C.6)$$

C.3 Determination of Strength Parameters for Transversely Isotropic Yield Criterion

The procedure to determine the strength parameters for transversely isotropic yield criterion is best illustrated by an example. The experimental results on Martinsburg Slate from Donath (1963) are used for this purpose.

Section 5.2.2 and 5.2.3 show that failure will first occur on planes orientated at $45^\circ - \frac{\phi_{\min}}{2}$ from the direction of σ_1 . At this orientation, both α and β are equal to 1 which means that the transversely isotropic yield criterion reduces to the isotropic yield criterion as shown in Equation C.4b. Equation C.4b can be written in another form as shown in the following:

$$\sigma_1 = \frac{c_{\min}}{\tan \phi_{\min}} (N_\phi - 1) + N_\phi \sigma_3 \quad (C.7)$$

where, $N_\phi = \tan^2(45^\circ + \frac{\phi_{\min}}{2})$

Equation C.7 represents a straight line in a σ_1 versus σ_3 plot. The slope of the line is equal to N_ϕ and the intercept is equal to $\frac{c_{\min}}{\tan \phi_{\min}} (N_\phi - 1)$ at $\sigma_3 = 0$.

The experimental results on Martinsburg slate are given in Figure 5.3, and the procedures to determine the strength parameters are given in the following:

1. Choose the lowest strength values for each confining pressure. Plot these data in a diagram with axes σ_1 and σ_3 as shown in Figure C.1. The experimental results should approximately lie on a straight line. Determine the slope of the line and the intercept at σ_3 equal to zero. c_{\min} and ϕ_{\min} can now be calculated.
2. The determination of α and β is more involved. α and β are determined at each confining pressure level and the overall average is calculated. At $\eta = 0^\circ$, the transversely isotropic yield criterion in Equation 5.1 reduces:

At yielding,

$$\frac{(\sigma_1 - \sigma_3)}{2} = [(\alpha c_{\min} + \beta \sigma_1 \tan \phi_{\min})(c_{\min} + \sigma_3 \tan \phi_{\min})]^{1/2}$$

(C.8a)

Similarly, at $\eta=90^\circ$, Equation 5.1 reduces to:

$$\frac{(\sigma_1 - \sigma_3)}{2} = [(c_{\min} + \sigma_1 \tan \phi_{\min})(\alpha c_{\min} + \beta \sigma_3 \tan \phi_{\min})]^{1/2} \quad (C.8b)$$

In Equations C.8a and C.8b, the axial stress at failure at each confining pressure can be obtained from the experimental result. Therefore the only unknowns are α and β . Table C.2 shows the α and β values at each confining pressure, and the average of α and β were used for the transversely isotropic yield criterion.

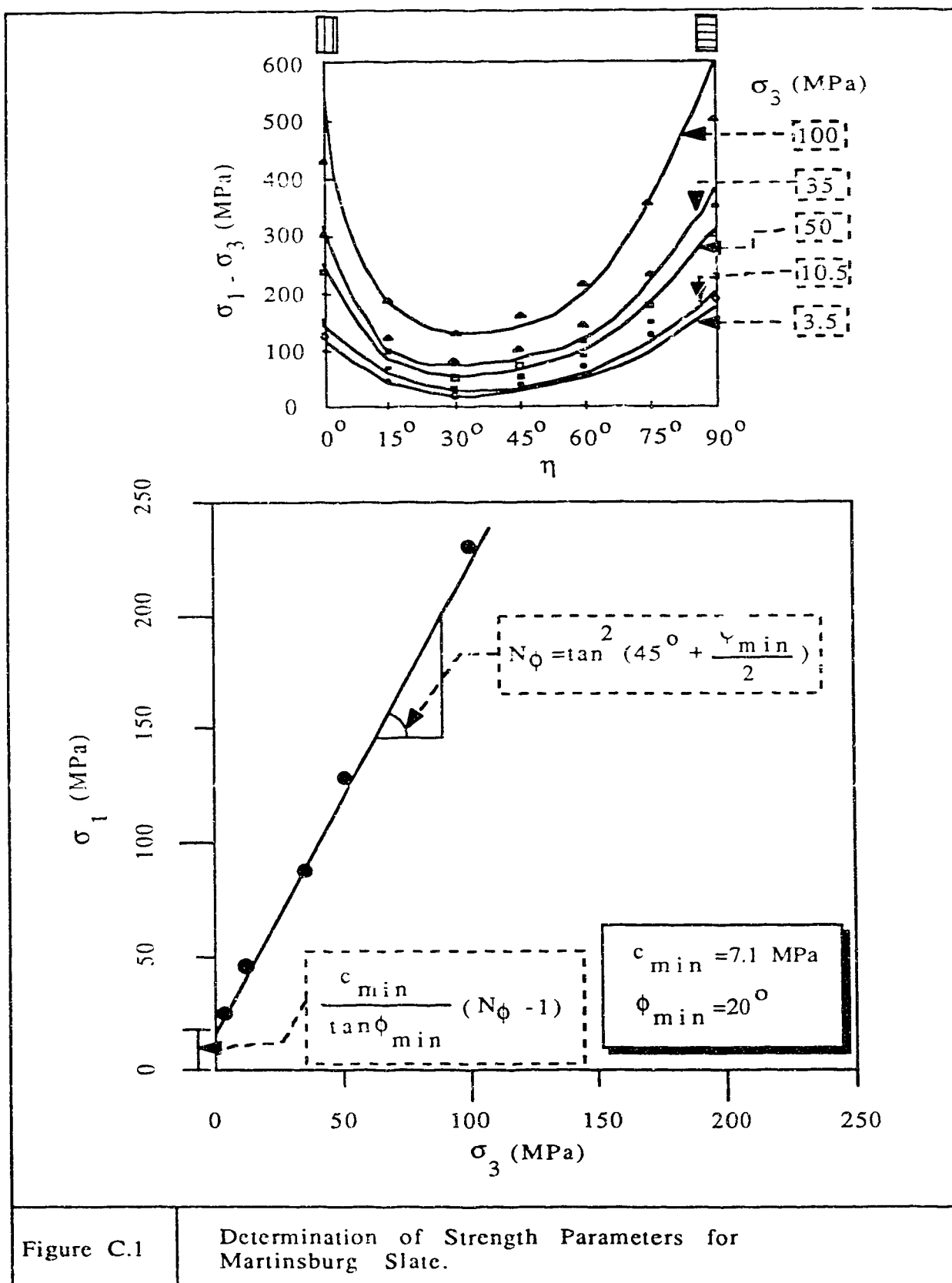


Figure C.1

Determination of Strength Parameters for Martinsburg Slate.

At $\eta = 0^\circ$,

$$\frac{\sigma_1 - \sigma_3}{2} = [(\alpha c_{\min} + \beta \sigma_1 \tan \phi_{\min})(c_{\min} + \sigma_3 \tan \phi_{\min})]^{\frac{1}{2}}$$

At $\eta = 90^\circ$,

$$\frac{\sigma_1 - \sigma_3}{2} = [(\alpha c_{\min} + \beta \sigma_3 \tan \phi_{\min})(c_{\min} + \sigma_1 \tan \phi_{\min})]^{\frac{1}{2}}$$

For Martinsburg Slate, $c_{\min} = 7.1$ MPa

$$\phi_{\min} = 20^\circ$$

Confining Pressure σ_3 (MPa)	Deviatoric Stress $\sigma_1 - \sigma_3$ (MPa) $\eta = 0^\circ$ $\eta = 90^\circ$		α	β
3.5	124	190	14.8	8.1
10.5	150	227	15.1	7.4
35	237	300	13.1	5.8
50	300	353	12.0	6.3
100	430	500	12.4	5.0
Average			13.5	6.5

Table C.2

Determination of α and β for the Transversely Isotropic Yield Criterion.

APPENDIX D

Elasto-plastic Finite Element Formulation

D.1 Elasto-plastic constitutive matrix formulation

To obtain an expression for the elasto-plastic constitutive matrix $[C^{EP}]$, the following assumptions were made:

1. The total strain increment is the sum of the elastic strain increment and the plastic strain increment, i.e.:

$$\{d\epsilon\} = \{d\epsilon^E\} + \{d\epsilon^P\}; \quad (D.1)$$

2. The change in stresses is due to the change in elastic strains only:

$$\{d\sigma\} = [C^E] \{d\epsilon^E\}; \quad (D.2)$$

where, $[C^E]$ = Elastic constitutive matrix;

3. A yield function exists such that:

$$\begin{aligned} \text{a)} \quad & F(\sigma_{ij}, \epsilon_{ij}^P) < 0, \quad F(\sigma_{ij} + \Delta\sigma_{ij}, \epsilon_{ij}^P + \Delta\epsilon_{ij}^P) < 0 \\ & \text{for elastic deformation;} \end{aligned} \quad (D.3a)$$

$$\text{b)} \quad F(\sigma_{ij}, \epsilon_{ij}^P) = 0, \quad F(\sigma_{ij} + \Delta\sigma_{ij}, \epsilon_{ij}^P + \Delta\epsilon_{ij}^P) < 0$$

$$\text{and } < \frac{\partial F}{\partial \sigma_{ij}} > \{d\sigma_{ij}\} < 0$$

for elastic unloading; (D.3b)

$$\text{c) } F(\sigma_{ij}, \epsilon_{ij}^P) = 0, \quad F(\sigma_{ij} + \Delta\sigma_{ij}, \epsilon_{ij}^P + \Delta\epsilon_{ij}^P) = 0$$

$$\text{and } < \frac{\partial F}{\partial \sigma_{ij}} > \{d\sigma_{ij}\} > 0$$

for plastic deformation and strain hardening; (D.3c)

$$\text{d) } F(\sigma_{ij}, \epsilon_{ij}^P) = 0, \quad F(\sigma_{ij} + \Delta\sigma_{ij}, \epsilon_{ij}^P + \Delta\epsilon_{ij}^P) = 0$$

$$\text{and } < \frac{\partial F}{\partial \sigma_{ij}} > \{d\sigma_{ij}\} < 0$$

for plastic deformation and strain softening; (D.3d)

4. A plastic potential exists such that:

$$\{d\epsilon^P\} = \tilde{\omega} \left\{ \frac{\partial Q}{\partial \sigma} \right\}; \quad (D.4)$$

5. The consistency condition is given as follows:

$$F(\sigma_{ij}, \epsilon_{ij}^P) > 0 \text{ is not permissible; and}$$

$$F(\sigma_{ij}, \epsilon_{ij}^P) = 0 \text{ for plastic deformation.} \quad (D.5)$$

The above five assumptions are commonly made for plasticity analyses. Substituting Equations D.1 and D.4 into D.2, one obtains:

$$\{d\sigma\} = [C^E] \left[\{d\varepsilon\} - \tilde{\omega} \left\{ \frac{\partial Q}{\partial \sigma} \right\} \right] \quad (D.6)$$

From Equation (D.5),

$$dF = \left\langle \frac{\partial F}{\partial \sigma} \right\rangle \{d\sigma\} + \left\langle \frac{\partial F}{\partial \varepsilon^P} \right\rangle \{d\varepsilon^P\} = 0 \quad (D.7)$$

Substituting Equations D.4 and D.6 into D.7, one obtains:

$$\left\langle \frac{\partial F}{\partial \sigma} \right\rangle [C^E] \{d\varepsilon\} - \tilde{\omega} \left\langle \frac{\partial F}{\partial \sigma} \right\rangle [C^E] \left\{ \frac{\partial Q}{\partial \sigma} \right\} + \tilde{\omega} \left\langle \frac{\partial F}{\partial \varepsilon^P} \right\rangle \left\{ \frac{\partial Q}{\partial \sigma} \right\} = 0 \quad (D.8)$$

therefore,

$$\tilde{\omega} = \frac{\left\langle \frac{\partial F}{\partial \sigma} \right\rangle [C^E]}{\left\langle \frac{\partial F}{\partial \sigma} \right\rangle [C^E] \left\{ \frac{\partial Q}{\partial \sigma} \right\} - \left\langle \frac{\partial F}{\partial \varepsilon^P} \right\rangle \left\{ \frac{\partial Q}{\partial \sigma} \right\}} \{d\varepsilon\} \quad (D.8)$$

Finally, substituting Equation D.8 into D.6, the following elasto-plastic constitutive matrix is provided:

$$\{d\sigma\} = [C^{EP}] \{d\varepsilon\} \quad (D.9a)$$

where,

$$[C^{EP}] = [C^E] - \frac{[C^E] \left\{ \frac{\partial Q}{\partial \sigma} \right\} < \frac{\partial F}{\partial \sigma} > [C^E]}{< \frac{\partial F}{\partial \sigma} > [C^E] \left\{ \frac{\partial Q}{\partial \sigma} \right\} - < \frac{\partial F}{\partial \epsilon^P} > \left\{ \frac{\partial Q}{\partial \sigma} \right\}} \quad (D.9b)$$

Note that the first term in the denominator of Equation D.9b represents perfectly plastic deformation and the second term represents strain hardening and softening deformation. The following three conditions may occur:

1. $< \frac{\partial F}{\partial \epsilon^P} > \left\{ \frac{\partial Q}{\partial \sigma} \right\} < 0$ for strain softening deformation;
2. $< \frac{\partial F}{\partial \epsilon^P} > \left\{ \frac{\partial Q}{\partial \sigma} \right\} = 0$ for perfectly plastic deformation;
3. $< \frac{\partial F}{\partial \epsilon^P} > \left\{ \frac{\partial Q}{\partial \sigma} \right\} > 0$ for strain hardening.

This study only deals with two dimensional perfectly plastic deformation and associated flow rule is assumed (i.e., $Q=F$), and therefore Equation (D.9b) is simplified to the following:

$$[C^{EP}] = [C^E] - \frac{[C^E] \left\{ \frac{\partial F}{\partial \sigma} \right\} < \frac{\partial F}{\partial \sigma} > [C^E]}{< \frac{\partial F}{\partial \sigma} > [C^E] \left\{ \frac{\partial F}{\partial \sigma} \right\}} \quad (D.9c)$$

The elastic constitutive matrix for the transversely isotropic material was already discussed in Appendix B. The following section evaluates the term $< \frac{\partial F}{\partial \sigma} >$ for the transversely isotropic yield criterion.

D.2 Evaluation of $\langle \frac{\partial F}{\partial \sigma} \rangle$ for Transversely Isotropic Yield Criterion

Recall that the transversely isotropic yield criterion takes the general form of Equation C.1. The plane of transverse isotropy is orientated at an angle η from the direction of σ_1 , and is defined in the finite element coordinate system as shown in Figure D.1.

The peak strength of the material is described by the transversely isotropic yield criterion, and it can be expressed in terms of σ_x , σ_y and τ_{xy} as follows:

$$\begin{aligned}
 F = D - \left\{ [(\alpha \cos^2 \eta + \sin^2 \eta) c_{\min} \right. \\
 + (\sigma_m \beta \cos^2 \eta + \sigma_n \sin^2 \eta + \tau_{mn} \sin 2\eta) \tan \phi_{\min}] \\
 * [(\cos^2 \eta + \alpha \sin^2 \eta) c_{\min} + (\sigma_m \beta \sin^2 \eta + \sigma_n \cos^2 \eta \\
 - \tau_{mn} \sin 2\eta) \tan \phi_{\min}] \Big\}^{1/2} \\
 + \sin 2\eta \left[\tan \phi_{\min} \sigma_m \frac{(\beta - 1)}{2} + c_{\min} \frac{(\alpha - 1)}{2} \right] \quad (D.10)
 \end{aligned}$$

$$\text{where, } \sigma_m = \frac{\sigma_x + \sigma_y}{2} + D (\cos^2 \eta - \sin^2 \eta)$$

$$\sigma_n = \frac{\sigma_x + \sigma_y}{2} + D (\sin^2 \eta - \cos^2 \eta)$$

$$\tau_{mn} = D (\sin 2\eta);$$

$$D = \left[\left(\frac{\sigma_x - \sigma_y}{2} \right)^2 + \tau_{xy}^2 \right]^{1/2};$$

$$\eta = 90^\circ - \xi + \omega \text{ for } \sigma_y \geq \sigma_x;$$

$$= 180^\circ - \xi + \omega \text{ for } \sigma_x > \sigma_y;$$

$$\omega = \frac{1}{2} \sin^{-1} \frac{\tau_{xy}}{D};$$

$$\xi = \text{Angle from planes of transverse isotropy}$$

to the direction of x-axis defined in Figure D.1

Since the model assumes that the transition from peak to residual strength corresponds to an abrupt reduction of c_{\max} to c_{res} and ϕ_{\max} to ϕ_{res} , the transversely isotropic yield criterion of Equation D.10 is reduced to the isotropic yield criterion of Equation C.4b as described in Appendix C.2. The residual strength of the material is described by Equation C.4b which can be expressed in terms of σ_x , σ_y , and τ_{xy} as follows:

$$F = D - \left\{ \left[c + \left(\frac{\sigma_x + \sigma_y}{2} + D \right) \tan \phi \right] \left[c + \left(\frac{\sigma_x + \sigma_y}{2} - D \right) \tan \phi \right] \right\}^{1/2} \quad (\text{D.11})$$

The derivatives of the yield criterion with respect to σ_x , σ_y , and τ_{xy} are:

$$\frac{\partial F}{\partial \sigma_x} = \frac{\sigma_x - \sigma_y}{4 D} - \frac{1}{2} \frac{1}{\sqrt{u} v} \left[u \frac{\partial v}{\partial \sigma_x} + v \frac{\partial u}{\partial \sigma_x} \right] \quad (\text{D.12a})$$

$$\frac{\partial F}{\partial \sigma_y} = \frac{\sigma_x - \sigma_y}{4 D} - \frac{1}{2} \frac{1}{\sqrt{u} v} \left[u \frac{\partial v}{\partial \sigma_y} + v \frac{\partial u}{\partial \sigma_y} \right] \quad (\text{D.12b})$$

$$\frac{\partial F}{\partial \tau_{xy}} = \frac{\tau_{xy}}{D} - \frac{1}{2} \frac{1}{\sqrt{u} v} \left[u \frac{\partial v}{\partial \tau_{xy}} + v \frac{\partial u}{\partial \tau_{xy}} \right] \quad (\text{D.12c})$$

where,

$$u = c + \left(\frac{\sigma_x + \sigma_y}{2} + D \right) \tan \phi$$

$$v = c + \left(\frac{\sigma_x + \sigma_y}{2} - D \right) \tan \phi$$

$$\frac{\partial u}{\partial \sigma_x} = \left[\frac{1}{2} + \frac{\sigma_x + \sigma_y}{4 D} \right] \tan \phi$$

$$\begin{aligned}
\frac{\partial u}{\partial \sigma_y} &= \frac{\partial u}{\partial \sigma_x} \\
\frac{\partial u}{\partial \tau_{xy}} &= \frac{\tau_{xy}}{D} \tan \phi \\
\frac{\partial v}{\partial \sigma_x} &= \left[\frac{1}{2} - \frac{\sigma_x - \sigma_y}{4 D} \right] \tan \phi \\
\frac{\partial v}{\partial \sigma_y} &= \frac{\partial v}{\partial \sigma_x} \\
\frac{\partial v}{\partial \tau_{xy}} &= - \frac{\partial u}{\partial \tau_{xy}}
\end{aligned}$$

The implementation of the transversely isotropic yield criterion, Equation D.10, and the derivatives of the yield criterion, Equations D.12a to D.12c, are provided in Appendix E.

For a General Coordinate System

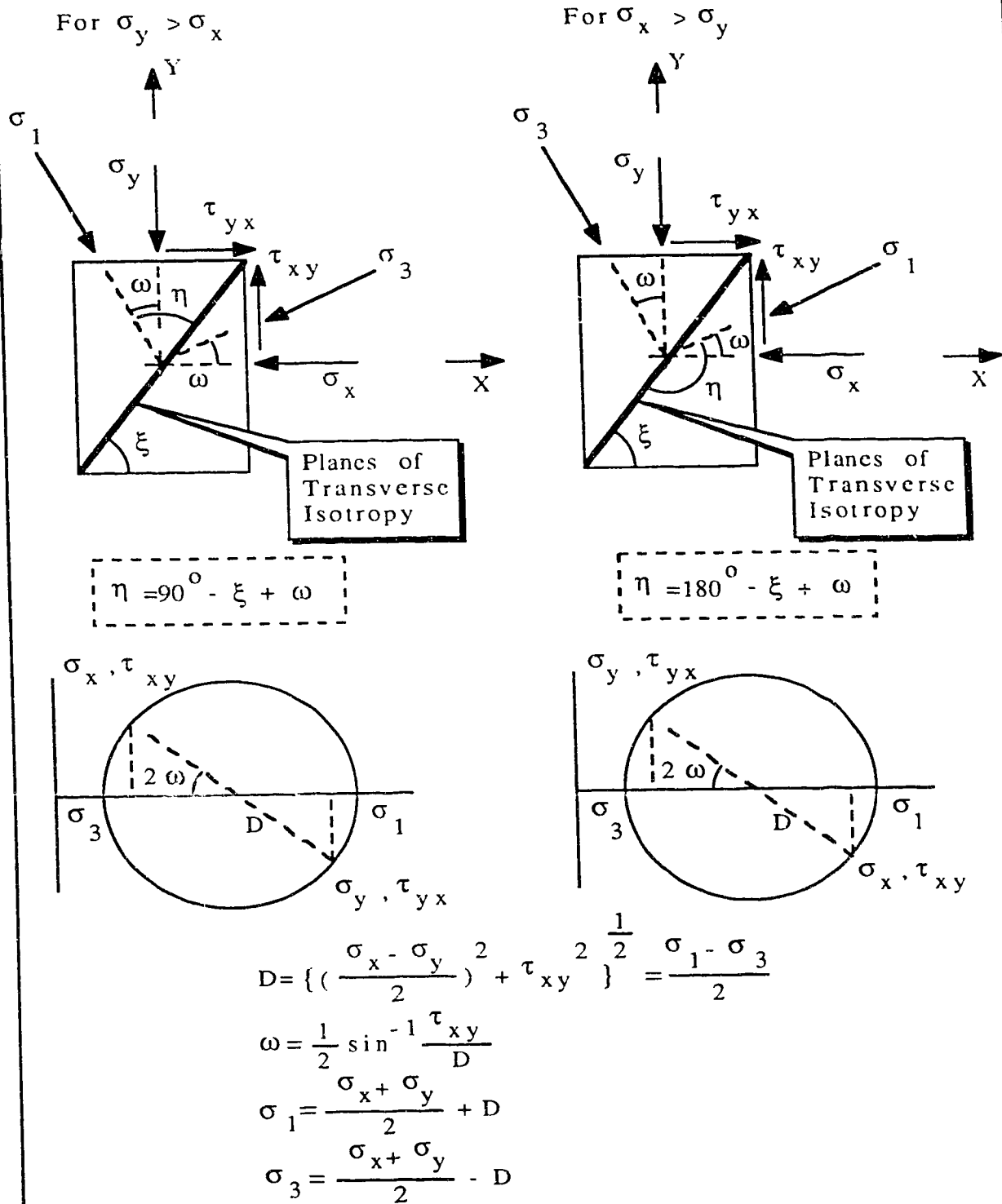


Figure D.1

Definitions for Planes of Transverse Isotropy
in the Finite Element Coordinate System.

APPENDIX E

IMPLEMENTATION OF MODEL AND INPUT DATA

INSTRUCTIONS FOR SAGE (Cyber 205 Version)

(Last Update - June 01, 1987)

E.1 General features of SAGE

SAGE is a computer program developed at the University of Alberta to analyze deformation of soil and rock structures. The program is written in FORTRAN and has been installed on different types of computer systems including the IBM system, the Amdahl MTS system, the CDC Cyber 205 vector computer system and the Apple Macintosh Microcomputer. The program has been applied in analyzing a wide variety of geotechnical problems such as excavation, dam, shaft and tunnel constructions.

The initial development of the program was to analyze the post peak deformation of strain softening soil. But the program has now been extended to include 2 and 3 dimensional analyses using total and effective stress formulation for fully undrained and drained conditions. A variety of non-linear elastic and plastic models with associated and non-associated flow rules are also available.

The following is a list of the main features of the program:

1. Basic Formulation.

Displacement finite element formulation assuming small strain and small deformation.

2. Element Types.

Two dimensional 3 to 6 nodes triangular, 4 to 8 nodes rectangular and three dimensional 8 to 20 nodes solid elements.

3. Types of Analyses.

3.1 Plane stress, plane strain, axisymmetric and three dimensional analyses;

3.2 Non-linear elastic hyperbolic model;

3.3 Elastic perfectly or brittle plastic model using Von-Mises, Tresca, Drucker-Prager, and Mohr-Coulomb yield criteria with associated and non-associated flow rule;

3.4 Elastic plastic strain hardening and softening (weakening) model;

3.5 Elastic hyperbolic softening model.

4. Drainage Condition.

4.1 Total stress analysis;

4.2 Fully undrained effective stress analysis;

4.3 Fully drained effective stress analysis.

5. Standard Features.

5.1 Prescribed concentrated point force or distributed pressure boundary condition;

5.2 Prescribed displacement boundary condition;

5.3 Changing material properties at any stage of the analysis,

5.4 Program restart at any stage of the analysis;

5.5 Newton Raphson and Modified Newton Raphson iterative scheme for non-linear analysis;

5.6 Choice of 2 x 2, 3 x 3, 2 x 2 x 2, 3 x 3 x 3 integration scheme;

5.7 Load increment subdivision for non-linear analysis.

6. Special Features.

6.1 Element birth and death option;

6.2 Automatic application of stress relieve due to excavation;

6.3 Skyline and extended skyline matrix equation solver;

6.4 Choice of stress calculation for non-linear analysis:

(i) Euler forward integration scheme;

(ii) Improved Euler scheme;

(iii) Runge-Kutta scheme.

7. Post Processing Programs.

7.1 Finite element mesh and deformed mesh plotting;

7.2 Stress and strain contour plotting;

7.3 Displacement arrow plotting.

E.2 Implementation of Transversely Isotropic Model into SAGE.

The structure of the program, SAGE, is written in a format which allows any additional models to be added into the program without changing the main routine. The model number used for the transversely isotropic material is 405. Subroutine, LAYOUT, in SAGE is used to read in the information for defining the problem such as x, y coordinates, element numbering and material properties. If the model number in LAYOUT is 405, the program will go into the subroutine, ELASTC, to obtain the elastic deformation properties for the transversely isotropic material. Subroutine, YIELD, is used to check whether the stresses have satisfied the yield criterion. If the model number in YIELD is 405, the program will pass the stresses into the subroutine, NOVA, to check whether yielding has been

reached (Equation D.10). NOVA also contains the derivatives of the transversely isotropic yield criterion (Equations D.12a to 12c). After the stresses have reached the peak strength, subroutine, MOBILE, is called to replace the peak strength parameters (ϕ_{max} , c_{max} , ϕ_{min} and c_{min}) by the residual strength parameters (ϕ_{res} , c_{res}).

Subroutines, ELASTC, NOVA AND MOBILE are provided in the following for references:

The definitions for the variables in the subroutines are given as follows:

ANS	DERIVATIVE OF SHAPE FUNCTION IN LOCAL S DIRECTION.
ANT	DERIVATIVE OF SHAPE FUNCTION IN LOCAL T DIRECTION.
AN	ELEMENT SHAPE FUNCTION.
CE	ELASTIC CONSTITUTIVE MATRIX.
LJ	LISTING OF DEGREE OF FREEDOM FOR EACH ELEMENT.
U	ELEMENT NODAL DISPLACEMENTS.
BL	ELEMENT STRAIN DISPLACEMENT MATRIX.
X	ELEMENT X COORDINATES.
Y	ELEMENT Y COORDINATES.
Z	ELEMENT Z COORDINATES.
FL	ELEMENT LOAD VECTOR.
DFDS	YIELD FUNCTION GRADIENTS WITH RESPECT TO STRESSES.
DQDS	PLASTIC POTENTIAL GRADIENTS WITH RESPECT TO STRESSES.
DFDE	YIELD FUNCTION GRADIENT WITH RESPECT TO PLASTIC STRAIN.
CEP	ELASTO-PLASTIC CONSTITUTIVE MATRIX.
ANR	DERIVATIVE OF SHAPE FUNCTION IN LOCAL R-DIRECTION.
IPRINT	PRINT-OUT CONTROL ARRAY.
XX	X COORDINATES IN GLOBAL NUMBERING.
YY	Y COORDINATES IN GLOBAL NUMBERING.
ZZ	Z COORDINATES IN GLOBAL NUMBERING.
IX	ARRAY STORING THE CODE FOR THE DEGREE OF FREEDOM. IX = 0, THAT DEGREE OF FREEDOM IS FIXED. IX = 1, THAT DEGREE OF FREEDOM IS FREE TO MOVE.
JX	ARRAY STORING THE DEGREE OF FREEDOM OF EACH NODE. JX = 0, THAT DEGREE OF FREEDOM IS FIXED. JX > 0, JX IS THE DEGREE OF FREEDOM OF THAT NODE. NOTE THAT BOTH IX AND JX STORE THE DEGREE OF FREEDOM IN ONE DIMENSIONAL FORM. THEREFORE IX(5) IS NOT THE CODE FOR NODE 5, BUT THE 1ST DEGREE OF FREEDOM OF NODE 3 IN 2-D ANALYSIS OR 2ND DEGREE OF FREEDOM OF NODE 2 IN 3-D ANALYSIS. SIMILIAR METHOD OF STORAGE IS USED FOR ARRAYS PP AND BB. ARRAYS P1 AND P2 ONLY STORE THE NON-ZERO DEGREE OF FREEDOM.
PP	TOTAL GLOBAL LOAD VECTOR FOR EACH NODE.

BB TOTAL NODAL DISPLACEMENT VECTOR.
 P1 UNBALANCED NODAL FORCES - ONLY NODES THAT ARE NOT
 FIXED ARE INCLUDED - DIMENSION OF P1 MUST BE AT LEAST
 THAT OF BB.
 P2 UNBALANCED NODAL FORCES - SIMILAR TO P1 BUT USED IN THE
 FEATURE OF SUB LOAD INCREMENT
 DIMENSION OF P2 MUST BE AT LEAST THAT OF BB.
 NNET NET DEGREE OF FREEDOM.
 NEL TOTAL NUMBER OF ELEMENTS
 A GLOBAL STIFFNESS MATRIX.
 MAXA ARRAY TO STORE THE DIAGONAL ADDRESSING IN THE SKYLINE
 AND EXTENDED SKYLINE METHOD.
 ELMP ELEMENT MATERIAL PROPERTIES ARRAY.
 THE FIRST SUBSCRIPT INDICATES THE MAXIMUM NUMBER OF
 PARAMETERS IN ANY ONE OF THE MATERIAL MODEL.
 THE SECOND SUBSCRIPT IS AT LEAST THE NUMBER OF MODEL
 USED IN THE ANALYSIS.
 ELMP (NELMP,NMT)
 ICO ELEMENT NUMBERING ARRAY
 STRESS ELEMENT STRESSES ARRAY (STRESS AT THE GAUSSIAN POINTS)
 STRAIN ELEMENT STRAIN ARRAY (STRAIN AT THE GAUSSIAN POINTS)
 STGTH ARRAY TO STORE THE YIELDING INFORMATION AT THE GAUSSIAN
 POINT OF EACH ELEMENT
 PORE ARRAY TO STORE THE PORE PRESSURE AT THE GAUSSIAN POINT
 THIS ARRAY IS USED ONLY IN EFFECTIVE ANALYSIS.
 NGP THE NUMBER OF INTEGRATION POINTS.
 =9 FOR 3X3 OR 2X2 INTEGRATION & NGP=4 FOR 2X2 INTEGRATION.
 =27 FOR 3X3 OR 2X2 INTEGRATION & NGP = 8 FOR 2X2X2 IN
 THREE DIMENSIONAL ANALYSIS.
 NICO =13 FOR 2-DIM. ANALYSIS AND 25 FOR 2 OR 3-D ANALYSIS.
 NELMP FIRST DIMENSION OF THE ELMP ARRAY.
 NSTGTH FIRST DIMENSION OF THE STGTH ARRAY.
 NSS FIRST DIMENSION OF THE STRESS AND STRAIN ARRAYS.
 FILE 1 =ITAP1 TEMPORARY FILE DURING PROGRAM EXECUTION.
 FILE 2 =ITAP2 INITIAL STRESS INPUT.
 FILE 3 =ITAP3 FILE FOR SPECIAL INTERMEDIATE RESTART.
 FILE 4 =ITAP4 TEMPORARY FILE DURING PROGRAM EXECUTION.
 FILE 5 =IN1 FILE CONTAINS INPUT INFORMATION.
 FILE 6 =IOUT1 FILE CONTAINS OUTPUT INFORMATION.
 FILE 7 =ITAP7 FILE CONTAINS OUTPUT INFORMATION IN BINARY CODE.
 IPRE =1 FOR SINGLE PRECISION ARITHMETICS.
 IPRE=2 FOR DOUBLE PRECISION ARITHMETICS.
 IBIN =0 FOR BINARY OUTPUT IN FILE 7 AND 8
 IBIN =1 FOR FORMATTED OUTPUT IN FILE 7 AND 8

SUBROUTINE ELASTIC

SUBROUTINE ELASTC(CE,ELMP,IEL,IM,NELMP,IPS,STRESS,STRAIN,NGP,
 1 IGP,MODEL,NSS,IPRE,IOUT1,STGTH,NSTGTH,TENERR,ITM,NITEQ)
 C IMPLICIT REAL*8(A-H,O-Z)

```

        DIMENSION CE(6,1),ELMP(NELMP,1),STRESS(NSS,NGP,1),
1 STRAIN(NSS,NGP,1),STGTH(NSTGTH,NGP,1)
C WRITE(6,1201) IEL,IM,NELMP,(ELMP(I,IM),I=1,NELMP)
C1201 FORMAT(/,5X,'IEL,IM,NELMP,ELMP',/,5X,3I5,/,5X,6E12.5).
        CALL PRESET(CE,6,6)
        IF(MODEL.LT.500) GO TO 5
        SIGM=STRESS(1,IGP,IEL)+STRESS(2,IGP,IEL)+STRESS(4,IGP,IEL)
        SIGM=-SIGM/3.D0
        VOID=STRAIN(1,IGP,IEL)+STRAIN(2,IGP,IEL)+STRAIN(4,IGP,IEL)
        VOID=ELMP(12,IM)+(1.D0+ELMP(12,IM))*VOID
        V=ELMP(7,IM)
        C1=3.D0*(1.D0-2.D0*V)
        IF(MODEL.EQ.9) C1=1.D0
        E=SIGM*(1.D0+VOID)*C1/ELMP(12,IM)
        IF(E.LE.0.D0) E=ELMP(6,IM)
        IF(MODEL.EQ.9) GO TO 1
        GO TO 6
5 IF((MODEL.LT.10).OR.(MODEL.GT.99)) GO TO 7
        CALL HYPER(STRESS,NSS,NGP,ELMP,NELMP,IEL,IM,
1 IGP,IPRE,E,V,IOUT1,IPS,MODEL,STGTH,NSTGTH,TENERR,ITM,NITEQ)
        GO TO 6
7 IF((MODEL.NE.3).AND.(MODEL.NE.405)) GO TO 9
        EX=ELMP(6,IM)
        VX=ELMP(7,IM)
        EY=ELMP(8,IM)
        VY=ELMP(9,IM)
        GY=ELMP(10,IM)
        SITA=ELMP(17,IM)
        DATA PI/3.14159265358979312D0/
        SITA=SITA*PI/180.D0
        COS=SITA
        SIN=SITA
        SITA=2.D0*SITA
        CSITA=SITA
        CALL FUNTN(COS,IPRE,2)
        COS=COS*COS
        CALL FUNTN(SIN,IPRE,4)
        SIN=SIN*SIN
        VXZ=(VY*SIN+VX*COS)/EX
        CALL FUNTN(SITA,IPRE,4)
        SITA=SITA*SITA
        COS=COS*COS
        SIN=SIN*SIN
        EYY=(COS/EY)+(SIN/EX)+0.25D0*SITA*(1.D0/GY-2.D0*VY/EX)
        EYY=1.D0/EYY
        CALL FUNTN(CSITA,IPRE,2)
        CSITA=CSITA*CSITA
        EXX=(COS/EX)+(SIN/EY)+0.25D0*SITA*(1.D0/GY-2.D0*VY/EX)
        EXX=1.D0/EXX
        VXY=0.25D0*SITA*(1.D0/EX+1.D0/EY-1.D0/GY)-
1 VY*COS/EY-VY*SIN/EX
        VY=-1.D0*VXY*EYY
        VX=VXZ*EXX
        GXY=CSITA/GY+SITA*(1.D0/EY+1.D0/EX+2.D0*VY/EX)

```

```

GY=1.D0/GXY
EX=EXX
EY=EYY
CE(3,3)=GY
IF(IPS.NE.1) GO TO 13
C=1.D0/(1.D0-VY*VY)
CE(1,1)=EX*C
CE(1,2)=VY*CE(1,1)
CE(2,2)=EY*C
CE(2,1)=CE(1,2)
GO TO 14
13 IF(IPS.NE.2) GO TO 15
C=(VX+1.D0)*(2.D0*VY*VY+VX-1.D0)
C=1.D0/C
CE(1,1)=EX*(VY*VY-1.D0)*C
CE(1,2)=-1.D0*(EX*VY*(1.D0+VX))*C
CE(2,1)=CE(1,2)
CE(2,2)=EY*(VX*VX-1.D0)*C
CE(4,1)=C*(VX*EX*(VY*VY-1.D0)-EX*EX*VY*VY*(1.D0+VX)/EY)
CE(4,2)=-1.D0*C*EX*VY*(1.D0+VX)
CE(4,4)=CE(1,1)
GO TO 14
15 C=1.D0/(EY*(1.D0-VX)-2.D0*EX*VY*VY)
CE(1,1)=C*EX*(EY-EX*VY*VY)/(1.D0+VX)
CE(4,4)=CE(1,1)
CE(1,2)=C*VY*EX*EY
CE(2,1)=CE(1,2)
CE(4,2)=CE(1,2)
CE(2,4)=CE(1,2)
CE(2,2)=C*EY*EY*(1.D0-VX)
CE(1,4)=C*EX*(EY*VX+EX*VY*VY)/(1.D0+VX)
CE(4,1)=CE(1,4)
9 E=ELMP(6,IM)
V=ELMP(7,IM)
6 IF(IPS.NE.1) GO TO 12
C1=E/(1.D0-V*V)
C2=V*C1
C3=(1.D0-V)*C1*0.5D0
GO TO 2
12 IF(MODEL.EQ.2) GO TO 1
C=E/((1.D0+V)*(1.D0-2.D0*V))
C1=(1.D0-V)*C
C2=V*C
C3=(1.D0-2.D0*V)*C*0.5D0
GO TO 2
1 C1=E+4.D0*V/3.D0
C2=E-2.D0*V/3.D0
C3=V
2 DO 4 I=1,2
DO 3 J=1,2
3 CE(I,J)=C2
CE(I,I)=C1
IF(IPS.LE.1) GO TO 4
CE(I,4)=C2

```

```

      CE(4,I)=C2
      CE(I+4,I+4)=C3
4     CONTINUE
      CE(3,3)=C3
      IF(IPS.GE.2) CE(4,4)=C1
14    RETURN
      END

```

SUBROUTINE NOVA

```

      SUBROUTINE NOVA(DFDS,IGP,IEL,IPRE,ELMP,NELMP,IM,NSTGTH,NGP,
1     STGTH,TAU,TOTSIG,F,ICONT)
C     IMPLICIT REAL*8(A-H,O-Z)
      DIMENSION TOTSIG(3),PTAU(3),DUDX(3),DVDX(3),DWDX(3),DSDX(3),
1     DSNDX(3),DFDS(6),TAU(3),STGTH(NSTGTH,NGP,1),ELMP(NELMP,1)
      IF(STGTH(2,IGP,IEL).EQ.0.D0) AUFA=1.D0
      IF(STGTH(2,IGP,IEL).EQ.0.D0) STGTH(4,IGP,IEL)=0.D0
      IF(STGTH(2,IGP,IEL).NE.0.D0) AUFA=
1     STGTH(2,IGP,IEL)/STGTH(4,IGP,IEL)
      IF(AUFA.LE.0.D0) WRITE(6,101) AUFA
      IF(STGTH(3,IGP,IEL).EQ.0.D0) BETA=1.D0
      IF(STGTH(3,IGP,IEL).EQ.0.D0) STGTH(5,IGP,IEL)=0.D0
      IF(STGTH(3,IGP,IEL).NE.0.D0) BETA=
1     STGTH(3,IGP,IEL)/STGTH(5,IGP,IEL)
      IF(BETA.LE.0.D0) WRITE(6,102) BETA
      DATA PI/3.14159265358979312D0/
      GO TO (1,2),ICONT
1     DO 3 I=1,3
      PTAU(I)=TAU(I)
3     CONTINUE
      GO TO 4
2     DO 5 I=1,3
      PTAU(I)=TOTSIG(I)
5     CONTINUE
4     PTAUX=PTAU(1)
      PTAUY=PTAU(2)
      SLIM=1.0D-10
      SIGM=(PTAU(1)-PTAU(2))*0.5D0
      SIGMM=SIGM
      IF(SIGMM.LT.0.D0) SIGMM=-1.D0*SIGMM
      TAUM=SIGM*SIGM+PTAU(3)*PTAU(3)
      CALL FUNTN(TAUM,IPRE,1)
      SIG3=(PTAU(1)+PTAU(2))*0.5D0
      PTAU(1)=SIG3+TAUM
      PTAU(2)=SIG3-TAUM
      TAU3=PTAU(3)
      IF(PTAU(3).LT.0.D0) TAU3=-1.D0*PTAU(3)
      IF(TAU3.LE.SLIM) PTAU(3)=0.D0
      IF((SIGMM.LE.SLIM).AND.(TAU3.LE.SLIM)) PTAU(3)=0.D0
      IF(TAUM.NE.0.D0) TAUM=PTAU(3)/TAUM
      CALL FUNTN(TAUM,IPRE,5)

```

```

PTAU(3)=0.5D0*TAUM
IF(PTAU(1).EQ.PTAU(2)) PTAU(3)=0.D0
TETA=(90.D0-ELMP(17,IM))*PI/180.D0+PTAU(3)
COTETA=TETA
SNTETA=TETA
TETA=2.D0*TETA
COTA=TETA
CALL FUNTN(COTETA,IPRE,2)
COTETA=COTETA*COTETA
CALL FUNTN(SNTETA,IPRE,4)
SNTETA=SNTETA*SNTETA
SIGT=-1.D0*(PTAU(1)*COTETA+PTAU(2)*SNTETA)
SIGR=-1.D0*(PTAU(1)*SNTETA+PTAU(2)*COTETA)
SIGTR=0.5D0*TETA*(PTAU(1)-PTAU(2))
UN=STGTH(4,IGP,IEL)*(AUFA*COTETA+SNTETA)+2.D0*
1 STGTH(5,IGP,IEL)*(SIGR*BETA*COTETA+SIGT*SNTETA+
2 SIGTR*TETA)
VN=STGTH(4,IGP,IEL)*(COTETA+AUFA*SNTETA)+2.D0*
1 STGTH(5,IGP,IEL)*(SIGR*BETA*SNTETA+SIGT*COTETA-
2 SIGTR*TETA)
WN=STGTH(5,IGP,IEL)*SIGR*(BETA-1.D0)+
1 0.5D0*STGTH(4,IGP,IEL)*(AUFA-1.D0)
WNT=WN*TETA
IF(WNT.LE.0.D0) WNT=-1.D0*WNT
QN=0.5D0*(PTAU(1)-PTAU(2))
IF(QN.LE.0.D0) QN=-1.D0*QN
SQUV=UN*VN
IF(SQUV.EQ.0.D0) GO TO 20
IF(SQUV.LT.0.D0) SQUV=-1.D0*SQUV
CALL FUNTN(SQUV,IPRE,1)
GO TO 21
20 SQUV=0.D0
21 SWN=SQUV-WNT
IF(SWN.LE.0.D0) SWN=-1.D0*SWN
GO TO (6,7), ICONT
7 F=QN-SWN
RETURN
6 SIGM=0.5D0*(TAU(1)-TAU(2))
R=SIGM*SIGM+TAU(3)*TAU(3)
CALL FUNTN(R,IPRE,1)
DSXY=TAU(1)-TAU(2)
IF(R.EQ.0.D0) GO TO 10
A=TAU(3)*(COTETA-SNTETA)/R
D=TETA*TAU(3)/R
E=-1.D0*(0.5D0+0.25D0*DSXY*(SNTETA-COTETA)/R)
F=-1.D0*(0.5D0+0.25D0*DSXY*(COTETA-SNTETA)/R)
H=0.25D0*TETA*DSXY/R
GO TO 11
10 A=0.D0
D=0.D0
E=-0.5D0
F=-0.5D0
H=0.D0
11 DUDX(1)=(BETA*COTETA*E+SNTETA*F+TETA*H)*2.D0*STGTH(5,IGP,IEL)

```



```

DUDX(2)=(BETA*COTETA*F+SNTETA*E-TETA*H)*2.D0*STGTH(5,IGP,IEL)
DUDX(3)=(BETA*COTETA*A-SNTETA*A+TETA*D)*2.D0*STGTH(5,IGP,IEL)
DVDX(1)=(BETA*SNTETA*E+COTETA*F-TETA*H)*2.D0*STGTH(5,IGP,IEL)
DVDX(2)=(BETA*SNTETA*F+COTETA*E+TETA*H)*2.D0*STGTH(5,IGP,IEL)
DVDX(3)=(BETA*SNTETA*A-COTETA*A-TETA*D)*2.D0*STGTH(5,IGP,IEL)
DWDX(1)=STGTH(5,IGP,IEL)*(BETA-1.D0)*E
DWDX(2)=STGTH(5,IGP,IEL)*(BETA-1.D0)*F
DWDX(3)=STGTH(5,IGP,IEL)*(BETA-1.D0)*A
IF(R.EQ.0.D0) GO TO 12
DSDX(1)=0.25D0*DSXY/R
DSDX(2)=-1.D0*DSDX(1)
DSDX(3)=1.D0*TAU(3)/R
GO TO 13
12 DSDX(1)=0.D0
   DSDX(2)=0.D0
   DSDX(3)=0.D0
13 DO 8 I=1,3
   DWDX(I)=DWDX(I)*TETA
   IF(SQUV.EQ.0.D0) GO TO 14
   DSNDX(I)=(0.5D0*(UN*DVDX(I)+VN*DUDX(I))/SQUV)-DWDX(I)
   GO TO 15
14 DSNDX(I)=-DWDX(I)
15 DFDS(I)=DSDX(I)-DSNDX(I)
8   CONTINUE
   DFDS(4)=0.D0
   DFDS(5)=0.D0
   DFDS(6)=0.D0
101 FORMAT(3X,'ERROR-AUFA SHOULD NOT BE NEGATIVE',1X,
1   'AUFA=',G13.5)
102 FORMAT(3X,'ERROR-BETA SHOULD NOT BE NEGATIVE',1X,
1   'BETA=',G13.5)
   RETURN
   END

```

SUBROUTINE MOBILE

```

SUBROUTINE MOBILE(TAU,STGTH,IPRE,NGP,IGP,IEL,MODEL,IM,ELMP,
1 NELMP,TAUP,IOUT1,DELEPS,STRAIN,IPS,DELSIG,NSTGTH,NSTRS,ICODE)
C   IMPLICIT REAL*8(A-H,O-Z)
   DIMENSION TAU(1),STGTH(NSTGTH,NGP,1),TAUP(1),ELMP(NELMP,1),
1   DELEPS(1),STRAIN(6,NGP,1),EPS(6),DELSIG(1)
   DATA PI,ROOT3/3.14159265358979312D0,1.7320508756887719D0/
   DATA EPS(5),EPS(6)/0.D0,0.D0/
   IF(MODEL.LE.99) RETURN
   IF((MODEL.EQ.100).OR.(MODEL.EQ.200)) GO TO 2
   IF((MODEL.GE.300).AND.(MODEL.LE.303)) GO TO 4
   IF((MODEL.EQ.400).OR.(MODEL.EQ.402)) GO TO 4
   IF(MODEL.EQ.405) GO TO 5
   IF(ICODE.NE.1) GO TO 1
   ICODE=0
   RETURN
2   IF(ELMP(9,IM).NE.0.D0) STGTH(2,IGP,IEL)=ELMP(9,IM)

```

```

RETURN
4 IF(ELMP(10,IM).NE.0.D0) STGTH(2,IGP,IEL)=ELMP(10,IM)
IF(ELMP(11,IM).NE.0.D0) STGTH(3,IGP,IEL)=ELMP(11,IM)*PI/180.D0
RETURN
5 IF(ELMP(15,IM).EQ.999.D0) STGTH(2,IGP,IEL)=STGTH(4,IGP,IEL)
IF(ELMP(15,IM).NE.999.D0) STGTH(2,IGP,IEL)=ELMP(15,IM)
IF(ELMP(15,IM).NE.999.D0) STGTH(4,IGP,IEL)=ELMP(15,IM)
IF(ELMP(16,IM).EQ.999.D0) STGTH(3,IGP,IEL)=STGTH(5,IGP,IEL)
IF(ELMP(16,IM).NE.999.D0) STGTH(3,IGP,IEL)=ELMP(16,IM)
IF(ELMP(16,IM).NE.999.D0) STGTH(5,IGP,IEL)=ELMP(16,IM)
RETURN
1 CALL SINVT(TAU,SIGM,XI2,XI3,XJ2,XJ3)
SIGM=SIGM/3.D0
RXJ2=XJ2
CALL FUNTN(RXJ2,IPRE,1)
CALL ELSTR(ELMP,NELMP,DELEPS,DELSIG,EPS,IPS,NGP,IGP,IEL,
1 MODEL,IM)
C WRITE(6,1202) (DELEPS(I),I=1,NSTRS),(EPS(I),I=1,NSTRS)
C1202 FORMAT(5X,'TOTAL STRAIN=',6E12.5/,5X,'ELASTIC STRAIN=',
C 1 6E12.5)
DO 14 I=1,NSTRS
EPS(I)=DELEPS(I)-EPS(I)
IF((I.EQ.3).OR.(I.GE.5)) EPS(I)=EPS(I)*0.5D0
14 CONTINUE
C WRITE(6,1203) (EPS(I),I=1,6)
C1203 FORMAT(5X,'PLASTIC STRAIN(TENSOR)=' ,6E12.5)
CALL SINVT(EPS,E1,E2,E3,EP2,EP3)
CALL FUNTN(EP2,IPRE,1)
EP2=2.D0*EP2*ELMP(11,IM)/ROOT3
IF(MODEL.LE.299) GO TO 6
STGTH(4,IGP,IEL)=STGTH(4,IGP,IEL)+EP2
PHI=ELMP(9,IM)*(ELMP(10,IM)*EP2*EP2+EP2)/
1 (1.D0+EP2*EP2)+ELMP(8,IM)
CALL FUNTN(PHI,IPRE,5)
STGTH(3,IGP,IEL)=PHI
RETURN
6 STGTH(3,IGP,IEL)=STGTH(3,IGP,IEL)+EP2
EP2=STGTH(3,IGP,IEL)
IF((MODEL.GT.99).AND.(MODEL.LE.109)) STGTH(2,IGP,IEL)=
1 ELMP(9,IM)*(ELMP(10,IM)*EP2*EP2+EP2)/(1.D0+EP2*EP2)+ELMP(8,IM)
IF((MODEL.GT.109).AND.(MODEL.LE.199)) STGTH(2,IGP,IEL)=
1 ELMP(8,IM)*(1.D0-(EP2/(ELMP(10,IM)+EP2/ELMP(9,IM))))
RETURN
8 VOL=-(DELEPS(1)+DELEPS(2)+DELEPS(4))
PO=ELMP(13,IM)
PRI=-(TAU(1)+TAU(2)+TAU(4))/3.D0
PRI1=-(TAUP(1)+TAUP(2)+TAUP(4))/3.D0
PIPI1=PRI/PRI1
PIPO=PRI/PO
PIIPO=PRI1/PO
CALL FUNTN(PIPI1,IPRE,9)
CALL FUNTN(PIPO,IPRE,9)
CALL FUNTN(PIIPO,IPRE,9)
VOL=VOL-ELMP(11,IM)*(1.D0+ELMP(12,IM))*PIPI1+ELMP(11,IM)*

```

```

1  ELMP(10,IM)*(PIPO*PIPO-PI1PO*PI1PO)*0.5D0
   IF(VOL.LE.0.D0) GO TO 999
   STGTH(2,IGP,IEL)=STGTH(2,IGP,IEL)+VOL
   SIDE=ELMP(10,IM)-ELMP(11,IM)
   IF(SIDE.LE.0.D0) CALL ERROR(IEL,IGP,IM,ELMP(10,IM),
1  ELMP(11,IM),3,'MOBI','LE ',IOUT1)
   SIDE=STGTH(2,IGP,IEL)*(1.D0+ELMP(12,IM))/SIDE
   CALL FUNTN(SIDE,IPRE,8)
   STGTH(3,IGP,IEL)=ELMP(13,IM)*SIDE
C   WRITE(6,1201) STGTH(2,IGP,IEL),STGTH(3,IGP,IEL)
C1201 FORMAT(5X,'P.VOL IN MOBILE = ',E15.5,5X,'PO IN MOBILE = ',
C   1 E15.5)
   999 RETURN
   END

```

E.3 Input Data Instructions

Instructions for setting up input files are provided below. Each card represents a single line with 80 columns in the input file. The cards must be arranged in the same order as indicated in the following:

CARD 1 Project Title Card

Input -	FORMAT
(TITLE(I),I=1,20)	(20A4)

note columns variable entry

1. 1-80 TITLE(20) Enter project title.

note/

1. Maximum 80 characters

CARD 2 General Information Card

Input -	FORMAT
IANALZ,IPS,INFORM,THICK,(IPRINT(I),I=1,5), ITAP8,IRES	(3I5,G10.0,7I5)

note columns variable entry

- | | | | |
|----|-------|-----------|---|
| 1. | 1-5 | IANALZ | Type of analysis.
=1, Linear elastic small deformation analysis.
=2, Linear elastic large deformation analysis.
=3, Non-linear elastic or plastic small deformation analysis.
=4, Non-linear elastic or plastic large deformation analysis. |
| | 6-10 | IPS | Mode of analysis.
=1, Two dimensional plane stress analysis.
=2, Two dimensional plane strain analysis.
=3, Two dimensional axisymmetric analysis.
=4, Three dimensional analysis. |
| 2. | 11-15 | INFORM | Information code for the size of the global stiffness matrix.
=0, Program execution proceed without interuption.
=1, Program execution will stop after determining the size of the global stiffness matrix. |
| 3. | 16-25 | THICK | Thickness of the 2-D elements. |
| 4. | 26-30 | IPRINT(1) | Displacements, stresses and strains print-out.
=0, No print-out is required during non-linear iteration process. Only final result is printed.
>0, Print-out is given at every IPRINT(1) iterations. |
| 5. | 31-35 | IPRINT(2) | Unbalanced load vector print-out
=0, No print-out is required.
>0, Print-out is given at every IPRINT(1) iterations. |

- | | | | |
|-----|-------|-----------|--|
| 6. | 36-40 | IPRINT(3) | Final nodal force vector print-out
=0, No print-out is required
=1, Final external nodal forces are printed. |
| 7. | 41-45 | IPRINT(4) | Element load vector due to external traction print-out.
=0, No print-out is required.
=1, Print-out is required. |
| 8. | 46-50 | IPRINT(5) | Listing of degrees of freedom print-out.
=0, No print-out is required.
=1, Print-out is required. |
| 9. | 51-55 | ITAP8 | Output in binary form during equilibrium iteration process.
=0, No output is required.
>0, Output is required and is stored in FORTRAN unit ITAP8. |
| 10. | 56-60 | IRES | Program restarting code.
=0, No intermediate restart.
=1, Analysis restart in between loading step. |

note/

1. The current version of the program can only perform small deformation analysis. Therefore IANALZ can only be 1 or 3.
2. The program will determine the degrees of freedom and the size of the global stiffness matrix if INFORM=1 so that the maximum size preset in the program will not be exceeded.
3. The thickness of the element in two dimensional analysis is assumed to be uniform. If THICK=0.0, a unit thickness is assigned. For axisymmetric analysis, THICK refers to the angle of rotation in radian. This entry is ignored in three dimensional analysis.
4. The nodal displacements, element stresses and strains will be printed at every IPRINT(1) iterations in non-linear analysis. If IPRINT(1)=0, only the final converged result is printed.

5. The unbalanced load during the equilibrium iteration process gives an indication on the rate of convergency of the problem and the region in the structure at which unbalanced nodal forces is the largest. When the problem has converged, the difference between the unbalanced nodal forces and the applied external forces at the nodes should be small.
6. For those elements subjected to external boundary traction, (i.e. pressure applied at the boundary), the program will calculate an equivalent nodal force vector based on the equivalent work principle so that the work done by the nodal forces at the nodes is equal to the work done by the traction over the surface boundary. This print-out gives the equivalent nodal forces at the nodes.
7. The listing of the degrees of freedom gives the sequential numbering of the degrees of freedom of each node. This information is useful when there is singularity in the stiffness matrix due to an input error. Also in modelling stage construction of a dam or excavation, the degrees of freedom at each node is changing throughout the analysis. If there is any input error on the numbering of the elements, this listing will give an indication of the location of the error.
8. In linear or non-linear analysis the final result of each loading step is stored in FORTRAN unit 7 in binary form. The information contains the nodal forces, nodal displacements and element stresses and strains. This enable the program to restart the analysis at any loading step desired. Moreover this information can be used in post processing programs to interpret results such as plotting stress contours. However, if program execution is terminated during the equilibrium iteration process in between loading steps due to insufficient computer time or other reasons, the analysis can be restarted from the point where the program execution was terminated if the intermediate information is stored in FORTRAN unit ITAP8. Otherwise the analysis can only be restarted from the last loading step. The information in unit ITAP8 is essentially the same as that in unit 7 except that unit ITAP8 stores the current displacements and state of stress of the problem while unit ITAP7 store the converged result of each loading step. When the solution of a given loading step has converged, the information in unit ITAP8 is transferred and accumulated on unit 7. However in order to save storage space

and avoid storing duplicated information, the information for the last loading step is not transfer from unit ITAP8 to 7 unless ITAP8=0 in which case only the converged results are stored in unit 7 including the final loading step. ITAP8 can be any positive integer number from 8 to 99.

9. If the program execution is terminated in between loading steps, the analysis can be restarted provided FORTRAN unit ITAP8 is available and set IRES=1. Otherwise set IRES=0. To restart at the beginning of any loading step, IRES should be zero.

CARD 3 General Information Card

Input -	FORMAT
NSTEP,ISTEP1,NEL,NNOD,NIP,NMT,IDGR,ISITE, IEFF,ITAP7	(1015)

note	columns	variable	entry
1.	1-5	NSTEP	Total number of loading steps.
2.	5-10	ISTEP1	Analysis starts at step number ISTEP1.
3.	10-15	NEL	Total number of elements.
4.	16-20	NNOD	Total number of nodes.
5.	21-25	NIP	Number of integration points. =2, For 2x2 integration. =3, For 3x3 integration.
6.	26-30	NMT	Total number of material types.
7.	31-35	IDGR	Displacements and strains reset code. =-1, Both strains and displacements will be reset zero after the first step. =0, Only displacement will be reset zero after the first step. =1, Displacements and strains will not be reset zero.
8.	36-40	ISITE	Initial stress code.

=0, No initial stresses are specified.
 >0, Initial stresses are specified.

9. 41-45 IEFF Effective stress analysis code.
 =0, Total stress analysis.
 =1, Undrained effective analysis with B effect only.
 =2, Undrained effective analysis with A effect only.
 =3, Undrained effective analysis with both A and B effects.
10. 46-50 ITAP7 Number of steps of binary information stored in FORTRAN unit 7.

note/

1. The total number of steps refers to the number of steps in this run. It can be less than or equal to the total number of steps of the analysis. By specifying a number less than the total number of steps of the analysis enable the intermediate results to be seen before proceed any further.
2. If ISTEP1 is greater than 1, FORTRAN unit 7 must be available with the information of the last loading step (i.e. step ISTEP1 -1) in order to resume the analysis.
3. The total number of elements includes those elements which may be absent at the beginning of the analysis. It is the total number of elements in the entire finite element mesh.
4. The total number of nodes is similar to the total number of element above. It includes those nodes which may not be active at the beginning of the analysis and all boundary nodes whether they are fixed or free to move.
5. NIP refers to the number of integration points in evaluating the stiffness matrix and in calculating the element stresses and strains for two dimensional rectangular elements and three dimensional solid elements. The number of integration points for the two dimensional triangular elements is always 4. For two dimensional elements, NIP=2 indicates 2x2 integration and NIP=3

indicates 3x3 integration. For three dimensional elements, NIP=2 indicates 2x2x2 integration and NIP=3 indicates 3x3x3 integration.

6. NMT is the maximum number of material types in the whole analysis. It is not necessary to use all the material model in any one step of the analysis. Therefore you can have material type which is not being used in step 1, for example, but will be used in step 3.
7. To incorporate in-situ stresses into the soil, the switch-on-gravity technique is often used. The material properties used in the switch on gravity analysis can be different from the actual properties of the material. Therefore different K_0 condition can be incorporated. In fact the Poisson's ratio can be any value between 0.0 and 0.5 but cannot be equal to 0.5 in the switch on gravity analysis to simulate different K_0 condition. Since displacements and strains are relative to an arbitrary datum, the displacements and strains due to the switch-on-gravity analysis are usually neglected. However in non-linear analysis where the material is depended on the amount of straining, then the reference state of the strain can be important and the strain is often referenced to the state of zero stress. Therefore in this case only the displacement may be reset to zero.
8. Rather than using the switch-on-gravity technique, the in-situ stress field can be specified. This can be done by specifying the number of stress quantities to be entered.
 - ISITE=0, no initial stress is specified.
 - ISITE=1, Stress x-x and Press are specified.
 - ISITE=2, Stress x-x, Stress y-y and Press are specified.
 - ISITE=3, Stress x-x, Stress y-y, Stress x-y and Press are specified.
 - ISITE=4, Stress x-x, Stress y-y, Stress x-y, Stress z-z and Press are specified.
 - ISITE=5, Stress x-x, Stress y-y, Stress x-y, Stress z-z, Stress y-z and Press are specified.
 - ISITE=6, Stress x-x, Stress y-y, Stress x-y, Stress z-z, Stress y-z, Stress x-z and Press are specified.

If ISITE is not zero, the stresses must be contained in FORTRAN unit 2 with maximum of 6 stresses in any one line and FORMAT (6G10.0). For the case of 6 stress components the

pore pressure, Press, will be entered in the second line. The pore pressure must be specified at all time even in total stress analysis but it may not be used. Therefore in total stress analysis with 6 stress components are specified, a blank line must be introduced between each line before other stress components are entered. The pore pressure entered will act as the initial pore pressure in effective stress analysis which may be hydrostatic pore pressure or any departure from hydrostatic under steady state flow condition. In either case the total pore pressure should be entered. The initial stress components should be in terms of effective stresses in effective stress analysis.

The first line will contain the stresses at the first integration point of the first element and the second line contains the stresses at the second integration point of the first element etc. The number of lines is equal to $NR \times NIP \times NIP + 4 \times NT$ where NR is the number of two dimensional rectangular elements and NT is the number of triangular elements or $NS \times NIP \times NIP \times NIP$ for three dimensional analysis where NS is the number of solid elements. The input must be in order starting with the first element and ended with the last integration point of the last element.

It is important to input a stress field which in itself is in equilibrium and satisfy the equation of equilibrium at the nodes. Unbalanced stress field will lead to instability in non-linear analysis. The program will automatically calculate the unbalanced load whenever an initial stress field is specified and applied on the structure as an external load. The magnitude of this artificial load will depend on the degree of unbalance forces the initial stress field introduced. A stress field which satisfies the equation of equilibrium will have zero unbalanced load. In the case of effective stress analysis, the stress components entered are effective stresses but equilibrium must be satisfied using total stresses.

9. When IEFF is not zero, either the pore pressure B effect or the A effect or both may be considered. The B effect considers the generation of the pore pressure due to changes in the hydrostatic component of the stress tensor only while A effect considered the generation of the pore pressure due to shearing. When IEFF is not equal to zero, the stiffness matrix may not be symmetric.

10. ITAP7 indicates the number of steps of binary information stored in FORTRAN unit 7 in restarting the analysis at the beginning of the loading step. To restart the analysis other than step 1, the information on the current state of the problem must be given in FORTRAN unit 7. To minimize computer storage space, only the information of the latest step is actually required to restart the analysis. Therefore if ITAP7=1, only the latest step is supplied; if ITAP7 =2, the last 2 steps are supplied etc.

CARD 4	Equilibrium Iteration Control Card
--------	------------------------------------

Input -	FORMAT
IEQM,MITEQ,EQTOL	(2I5,G10.0)

note	columns	variable	entry
------	---------	----------	-------

- | | | | |
|----|-------|-------|---|
| 1. | 1-5 | IEQM | Frequency of updating the stiffness matrix.
=1, Stiffness matrix updated at every iteration.
=2, Stiffness matrix updated at every other iterations.
=3, Stiffness matrix updated at every third iterations etc. |
| | 5-10 | MITEQ | Maximum number of equilibrium iterations allowed. |
| 2. | 10-20 | EQTOL | Tolerance in displacement error. |

note/

1. In non-linear analysis, an elastic analysis is first performed at the beginning of every loading step. The stiffness is then updated at the second iteration and will be updated according to that specified by IEQM.
2. The displacement error is calculated by the norm of the incremental displacements to the norm of the total displacements. The tolerance should be expressed in decimal and not in percentage. A typical tolerance is 0.0001.

CARD 5	Methods of Stress Calculation Control Card
--------	--

Input - FORMAT
 ISM, MITS, STOL (2I5, G10.0)

	note	columns	variable	entry
1.	1-5	ISM	Select stress calculation method. =1, Euler Forward Integration Scheme. =2, Improved Euler Scheme. =3, Runge-Kutter Scheme.	
2.	5-10	MTS	Number of subinterval during the integration process.	
3.	10-20	STOL	Tolerance in stress calculation.	

note/

1. The Improved Euler scheme requires approximately double the computational effort than the Euler Forward scheme and the Runge-Kutter requires four time that of the Euler Forward scheme. However, the Improved scheme gives better result than the Forward scheme even though the number of subinterval is reduced. This scheme is recommended in non-linear analysis. To gain higher accuracy in sensitive problem, the Runge-Kutter scheme should be used
2. MITS specifies the number of subintervals the strain increment is subdivided into in calculating stresses. More subinterval will result in higher accuracy but also higher cost. A typical value will be 10.
3. The stresses in elasto-plastic analysis may not satisfy the yield criterion exactly. The value STOL limit the error in satisfying the yield criterion which is expressed in decimal and not in percentage. A typical value will be 0.0001.

CARD 6	No Tension Analysis Control Card
--------	----------------------------------

Input - FORMAT
 INTM, MITNT, TNTOL (2I5, G10.0)

note	columns	variable	entry
	1-5	INTM	=0, All material is capable of taking tension. =1, Some material is not capable of taking tension.
1.	5-10	MITNT	Maximum number of iterations allowed in determining the principal stresses in three dimensional analysis.
2.	10-20	STOL	Tolerance in principal stresses.

note/

1. The no tension analysis is performed using the stress transfer method by applying equivalent nodal forces due to the excess tension in the major principal stress direction (Since compression is considered as positive quantities, tension will first occur in the major principal stress direction). Presently the stiffness of the element which is in tension is not reduced during the no tension analysis. This procedure in the current version of the program results in very slow convergence characteristics and sometimes give unexpected results. The no-tension feature should be used with caution. In three dimensional analysis the principal stresses are calculated using an iterative procedure therefore a limit on the number of iterations is required. Also if the Hyperbolic Elastic model is used in three dimensional analysis, the principal stresses are required in evaluating the stiffness matrix. This input will also be used in calculating the principal stresses. This input will also be used in calculating the principal stresses. This input is ignored in two dimensional analysis. Whenever INTM=1, the analysis should be considered as material nonlinear analysis and IANALZ in card 1 should be 3 or 4.
2. The principal stresses in three dimensional analysis are determined by an iterative method which may contain error. The tolerance in stresses must be expressed in decimal. A typical tolerance in stresses is 0.0001.

CARD ENTRIES 7 A Series of Cards for Entering the Nodal Coordinates

The number of cards must be equal to the total number of nodes (NNOD) specified in card 2.

Each card must contain the x and y coordinates and two displacement codes for two dimensional analysis, or x, y and z coordinates and three displacement codes for three dimensional analysis.

The cards must be in sequence starting with node 1 and ended with node NNOD.

Input - FORMAT
 X(I),Y(I),IX1,IX2 for two dimensional analysis. (2G10.0,2I3)
 X(I),Y(I),Z(I),IX1,IX2,IX3 for three dimensional analysis.
(2G10.0,2I3)

For two dimensional analysis.

note	columns	variable	entry
	1-10	X(I)	x coordinate of node I.
	11-20	Y(I)	y coordinate of node I.
	21-23	IX1	x displacement code. =0, Node is fixed in the x-direction. =1, Node is free to move in the x-direction.
	24-26	IX2	y displacement code. =0, Node is fixed in the y-direction. =1, Node is free to move in the y-direction.

For three dimensional analysis.

note	columns	variable	entry
	1-10	X(I)	x coordinate of node I.

11-20	Y(I)	y coordinate of node I.
21-30	Z(I)	z coordinate of node I.
31-33	IX1	x displacement code. =0, Node is fixed in the x-direction. =1, Node is free to move in the x-direction.
34-36	IX2	y displacement code. =0, Node is fixed in the y-direction. =1, Node is free to move in the y-direction.
37-40	IX3	z displacement code. =0, Node is fixed in the z-direction. =1, Node is free to move in the z-direction.

CARD ENTRIES 8 A Series of Cards for Element Numbering
--

The number of inputs (each may contain 2 or 3 cards) must be equal to the total number of elements (NEL) specified in card 2.

Each input must contain 13 entries for two dimensional analysis or 25 entries for three dimensional analysis.

The cards must be in sequence starting with element 1 and ended with element NEL.

Input - FORMAT
 (ICO(I),I=1,8),IE,IS,IG,IB,IM for 2 dimensional analysis. (1215)
 (ICO(I),I=1,25),IE,IS,IG,IB,IM for 3 dimensional analysis. (1215)

For two dimensional analysis.

note	columns	variable	entry
1.	1-5	ICO(1)	Global node number of node 1 of the element.
	6-10	ICO(2)	Global node number of node 2 of the element.

	11-15	ICO(3)	Global node number of node 3 of the element.
	16-20	ICO(4)	Global node number of node 4 of the element.
	21-25	ICO(5)	Global node number of node 5 of the element.
	26-30	ICO(6)	Global node number of node 6 of the element.
2.	31-35	ICO(7)	Global node number of node 7 of the element.
	36-40	ICO(8)	Global node number of node 8 of the element.
3.	41-45	ICO(9)	Element type code (IE). =1, Two dimensional triangular element. =2, Two dimensional rectangular element. =3, Two dimensional rectangular Lagrangian element.
4.	46-50	ICO(10)	Element present or absent code (IS). =0, Element is absent in step 1 of the analysis. =1, Element is present in step 1 of the analysis.
5.	51-55	ICO(11)	Body forces code (IG). =0, No body forces for this element in step 1 of the analysis. =1, Body forces are applied in step 1 of the analysis.
6.	56-60	ICO(12)	Boundary traction code (IB). =0, No boundary traction is applied on this element in step 1. =1, Boundary traction is applied on one side of the element. =2, Boundary traction is applied on two side of the element. =3, Boundary traction is applied on three side of the element. =4, Boundary traction is applied on four side of the element.
7.	1-5	ICO(13)	Element material properties number (IM). (Note new line)

For three dimensional analysis.

note	columns	variable	entry
8.	1-5	ICO(1)	Global node number of node 1 of the element.
	6-10	ICO(2)	Global node number of node 2 of the element.
	11-15	ICO(3)	Global node number of node 3 of the element.
	16-20	ICO(4)	Global node number of node 4 of the element.
	21-25	ICO(5)	Global node number of node 5 of the element.
	26-30	ICO(6)	Global node number of node 6 of the element.
	31-35	ICO(7)	Global node number of node 7 of the element.
	36-40	ICO(8)	Global node number of node 8 of the element.
	41-45	ICO(9)	Global node number of node 9 of the element.
	46-50	ICO(10)	Global node number of node 10 of the element.
	51-55	ICO(11)	Global node number of node 11 of the element.
	56-60	ICO(12)	Global node number of node 12 of the element.
	1-5	ICO(13)	Global node number of node 13 of the element.
			(note new line)
	6-10	ICO(14)	Global node number of node 14 of the element.
	11-15	ICO(15)	Global node number of node 15 of the element.
	16-20	ICO(16)	Global node number of node 16 of the element.
	21-25	ICO(17)	Global node number of node 17 of the element.
	26-30	ICO(18)	Global node number of node 18 of the element.
	31-35	ICO(19)	Global node number of node 19 of the element.

	36-40	ICO(20)	Global node number of node 20 of the element.
	41-45	ICO(21)	Element type code (IE). =4, Three dimensional solid element.
	46-50	ICO(22)	Element present or absent code (IS). =0, Element is absent in step 1 of the analysis. =1, Element is present in step 1 of the analysis.
	51-55	ICO(23)	Body force code (IG). =0, No body forces for this element in step 1 of the analysis. =1, Body forces for applied in step 1 of the analysis.
9	56-60	ICO(24)	Boundary traction code (IB). =0, No boundary traction is applied on this element in step 1. =1, Boundary traction is applied on one side of the element. =2, Boundary traction is applied on two side of the element. =3, Boundary traction is applied on three side of the element. =4, Boundary traction is applied on four side of the element.
	1-5	ICO(25)	Element material properties number (IM). (Note new line)

note/

1. The first 8 entries are the node numbers of each element. The first 4 entries must be positive integers and any of the remain 4 can be zero if the intermediate nodes in the rectangular element are absent. For the triangular elements the first 3 entries must be positive integers and the following entries can be zero if the intermediate nodes are absent. It is not recommended to degenerate the quadrilateral element into triangular element by collapsing the corner nodes unless some element singular is desired. The element must be numbered in the counter clockwise direction and all corner nodes must be numbered first and followed the intermediate nodes, see Figure E.1.

2. The 7 and 8 entries should be zero for triangular elements.
3. The Lagrangian element has a node in the center of the element and the stiffness matrix is formed using static condensation technique.
4. By using this code which can be changed at any step during the analysis, any element in the finite element domain can be added or deleted. This enables the modelling of dam construction of foundation excavation.
5. Body forces include that due to gravity and the horizontal forces due to earthquakes. The unit weight of the material is entered through the material properties card but note that if the y-axis is in the vertical upward direction, the y-body force should be negative. similarly in the x and z direction, the sign of the body force should coincide with the direction of the axes. If only gravity is acting on the element, enter zero for the body forces in the other idrections. The body forces are applied only once at the beginning of the analysis. The body forces can also be applied to any element after the first step which is done through the control cards of each loading step.
6. The program calculate an equivalent nodal force due to the surface traction applied on the element. The number IB refers to the number of sides at which the element is subjected to surface traction.
7. This is the material number defined by the user and not the model number for different types of model such as linear elastic models or elasto-plastic models.
8. The three dimensional elements must have at least 8 corner nodes with varying number of side nodes yp to a total of 20 nodes. The corner nodes must be numbered first with the first four nodes on one face and the other four nodes at the opposite face. The mid-side nodes on the first face are then numbered followed by the mid-sides of the other face. finally the mid-side nodes in between these two faces are numbered, see Figure E.1.
9. The value of IB in three dimensional analysis refers to the number of faces at which the element is subjected to surface traction.

CARD ENTRIES 9 Element Material Properties Cards
--

The following cards contain the properties of each type of material. The number of material must be the same as is specified by NMT in card 2. There will be 17 entries for each type of material with 6 entries per line. The first entry is a code in real number to identify the type of model to be used. Refer to Table E.1 for detail.

Input -	FORMAT
(ELMP(I),I=1,17)	(6G10.0)

note/

Some general comments for all types of material.

1. The first entry is the model number and it must be a real number, preferably with a decimal.
2. Second entry is the tensile strength of the material. This entry is ignored if the material is capable of taking tension as specified in card 6. In this case, simply enter zero. If some of the materials is not capable of taking tension, enter the tensile strength of these material and enter a very large number (larger than the maximum stress the material will likely experience) for the rest of the materials.
3. The thirds, fourth and fifth entries are the body forces in the x, y and z directions respectively. The body forces is in force/unit volume, i.e. the unit weight of the material. The signs of the body forces must coincide with the direction of the corresponding axes. Enter zero if the body force in that direction is absent. The body forces should be in terms of total stresses even in effective stress analysis.
4. The sixteenth entry is the pore pressure A parameter which will be used only in effective stress analysis and the other material parameters should be in terms of effective stress except the body forces. Whenever the A effect is being considered, the analysis becomes non-linear even the material is linear elastic and IANALYZ in card 1 should be 3 or 4. Also the A effect will result

in a non-symmetric stiffness matrix. This input is ignored if IEFF is not 2 or 3 in card 2.

5. The seventeenth entry is the pore pressure B parameter when only the pore pressure B effect is being considered, the stiffness matrix is symmetrical for linear elastic material and frictionless material. for frictional material the stiffness matrix will not be symmetrical. No iterative process is required for B effect only unless the material is non-linear. In effective stress analysis, the material parameters should be in terms of effective stresses except the body forces. This input is ignored if IEFF is not 1 or 3 in card 2.
6. The Poisson's ratio is required for most of the material. If the material is incompressible, such as saturated clay, the Poisson's ratio is equal to 0.5. In this case a Poisson's ratio of 0.499 should be used because Poisson's ratio of 0.5 will result in a numerically ill-condition stiffness matrix and lead to inaccurate results.

CARD ENTRIES 9 Linear Elastic Model (1)

Input -		FORMAT
First line	MODEL,SIGMAT,GAMMAX,GAMMAY,GAMMAZ,E,	(6G10.0)
Second line	NU, (enter 5 zeros)	(6G10.0)
Third line	(enter 3 zeros) A, B	(6G10.0)

note	columns	variable	entry
1-10		MODEL	Material model number. =1.0, Linear elastic material (1).
11-20		SIGMAT	Tensile strength of the material.
21-30		GAMMAX	Body force in the x-direction.
31-40		GAMMAY	Body force in the y-direction.
41-50		GAMMAZ	Body force in the z-direction.
51-60		E	Elastic modulus.

1-10	NU	Poisson's Ratio. (note new line)
31-40	A	Pore pressure A parameter. (note new line and column position)
41-50	B	Pore pressure B parameter.

CARD ENTRIES 9 Linear Elastic Model (2)

Input -	FORMAT
First line	MODEL,SIGMAT,GAMMAX,GAMMAY,GAMMAZ,K, (6G10.0)
Second line	G, (enter 5 zeros) (6G10.0)
Third line	(enter 3 zeros) A, B (6G10.0)

note	columns	variable	entry
------	---------	----------	-------

1-10	MODEL	Material model number. =2.0, Linear elastic material (2).
11-20	SIGMAT	Tensile strength of the material.
21-30	GAMMAX	Body force in the x-direction.
31-40	GAMMAY	Body force in the y-direction.
41-50	GAMMAZ	Body force in the z-direction.
51-60	K	Bulk modulus.
1-10	G	Shear modulus. (note new line)
31-40	A	Pore pressure A parameter. (note new line and column position)
41-50	B	Pore pressure B parameter.

CARD ENTRIES 9 Hyperbolic Elastic Model

Input -		FORMAT
First line	MODEL,SIGMAT,GAMMAX,GAMMAY,GAMMAZ,K,	(6G10.0)
Second line	KU,N,RF,C,PHI,PA	(6G10.0)
Third line	G,F,D,A,B	(6G10.0)

note	columns	variable	entry
	1-10	MODEL	Material model number. =10.0, Hyperbolic elastic material.
	11-20	SIGMAT	Tensile strength of the material.
	21-30	GAMMAX	Body force in the x-direction.
	31-40	GAMMAY	Body force in the y-direction.
	41-50	GAMMAZ	Body force in the z-direction.
1.	51-60	K	Initial modulus in the hyperbolic model.
	1-10	KU	Unloading modulus in the hyperbolic model. (note new line)
	10-20	N	Exponent in the hyperbolic model.
	21-30	RF	Ultimate strength factor.
	31-40	C	Cohesion.
	41-50	PHI	Soil friction.
	51-60	PA	Atmospheric pressure.
	1-10	G	Initial Poisson's ratio. (note new line)
	11-20	F	Factor to determine the variation of Poisson's ratio.

21-30	D	Factor to determine the variation of Poisson's ratio.
31-40	A	Pore pressure A parameter.
41-50	B	Pore pressure B parameter.

note/

1. An explanation of the material parameters in the hyperbolic model can be found in the following publications:

Duncan, J. M. and Chang, C. Y., 1970. Non-linear analysis of stress and strain in soils. Journal of the Soil Mechanics and Foundation Division, A.S.C.E. vol. 96, SM5, pp. 1629-1653.

Duncan, J. M., Byrne, P., Wong, K. S. and Mabry, P., 1980. Strength, stress-strain and bulk modulus parameters for finite element analysis of stresses and movements in soil masses. Report No. UCB/GT/80-01, University of California.

CARD ENTRIES 9 Elastic Brittle Perfectly Plastic Von-Mises Model
--

Input -		FORMAT
First line	MODEL,SIGMAT,GAMMAX,GAMMAY,GAMMAZ,E,	(6G10.0)
Second line	NU,SIGYP,SIGYR (enter 3 zeros)	(6G10.0)
Third line	(enter 3 zeros) A, B	(6G10.0)

note columns variable entry

1-10	MODEL	Material model number. =100.0, Associated Von-Mises material.
11-20	SIGMAT	Tensile strength of the material.
21-30	GAMMAX	Body force in the x-direction.
31-40	GAMMAY	Body force in the y-direction.
41-50	GAMMAZ	Body force in the z-direction.

	51-60	E	Elastic modulus.
	1-10	NU	Poisson's Ratio. (note new line)
1.	11-20	SIGYP	Peak uniaxial yield strength.
2.	21-30	SIGYR	Residual uniaxial yield strength.
	31-40	A	Pore pressure A parameter. (note new line and column position)
	41-50	B	Pore pressure B parameter.

note/

1. The material is assumed to be linear elastic until the peak yield strength is reached. Residual strength is mobilized immediately after peak and subsequently unloading and reloading will only mobilize residual strength.
2. If SIGYR=0.0 or SIGYR=SIGYP, the residual is assumed to be equal to the peak strength. If SIGYR=0.0 is desired, enter a small non-zero value such as 0.000001.

CARD ENTRIES 9 Elastic Brittle Perfectly Plastic Tresca Model

Input - FORMAT

First line	MODEL,SIGMAT,GAMMAX,GAMMAX,GAMMAX,E,	(6G10.0)
Second line	NU,SIGYP,SIGYR (enter 3 zeros)	(6G10.0)
Third line	(enter 3 zeros) A, B	(6G10.0)

note columns variable entry

1-10	MODEL	Material model number. =200.0, Associated Tresca material.
11-20	SIGMAT	Tensile strength of the material.
21-30	GAMMAX	Body force in the x-direction.

	31-40	GAMMAY	Body force in the y-direction.
	41-50	GAMMAZ	Body force in the z-direction.
	51-60	E	Elastic modulus.
	1-10	NU	Poisson's Ratio. (note new line)
1.	11-20	SIGYP	Peak uniaxial yield strength.
2.	21-30	SIGYR	Residual uniaxial yield strength.
	31-40	A	Pore pressure A parameter. (note new line and column position)
	41-50	B	Pore pressure B parameter.

note/

1. The material is assumed to be linear elastic until the peak yield strength is reached. Residual strength is mobilized immediately after peak and subsequently unloading and reloading will only mobilize residual strength.
2. If SIGYR=0.0 or SIGYR=SIGYP the residual is assumed to be equal to the peak strength. If SIGYR=0.0 is desired, enter a small non-zero value such as 0.000001.

<p>CARD ENTRIES 9 Elastic Brittle Perfectly Plastic Drucker-Prager Model</p>
--

Input -	FORMAT
First line	MODEL,SIGMAT,GAMMAX,GAMMAY,GAMMAZ,E, (6G10.0)
Second line	NU,ALPHAP,KAPPAP,ALPHAR,KAPPAR (enter 1 zero) (6G10.0)
Third line	(enter 3 zeros) A, B (6G10.0)

note columns variable entry

	1-10	MODEL	Material model number. =300.0, Associated Drucker-Prager material.
	11-20	SIGMAT	Tensile strength of the material.
	21-30	GAMMAX	Body force in the x-direction.
	31-40	GAMMAY	Body force in the y-direction.
	41-50	GAMMAZ	Body force in the z-direction.
	51-60	E	Elastic modulus.
	1-10	NU	Poisson's Ratio. (note new line)
1.	11-20	ALPHAP	Modified peak cohesion.
1.	21-30	KAPPAP	Modified peak friction.
2.	31-40	ALPHAR	Modified residual cohesion.
3.	41-50	KAPPAR	Modified residual friction.
	31-40	A	Pore pressure A parameter. (note new line and column position)
	41-50	B	Pore pressure B parameter.

note/

1. The material is assumed to be linear elastic until the peak yield strength is reached. Residual strength is mobilized immediately after peak and subsequently unloading and reloading will only mobilize residual strength.
2. If ALPHAR=0.0 or ALPHAR=ALPHAP, the residual is assumed to be equal to the peak strength. If ALPHAR=0.0 is desired, enter a small non-zero value such as 0.000001.

3. If KAPPAR=0.0 or KAPPAR=KAPPAP, the residual is assumed to be equal to the peak strength. If KAPPAR=0.0 is desired, enter a small non-zero value such as 0.000001.

CARDENTRIES 9 Elastic Brittle Perfectly Plastic Mohr-Coulomb Model
--

Input -		FORMAT
First line	MODEL,SIGMAT,GAMMAX,GAMMAY,GAMMAZ,E,	(6G10.0)
Second line	NU,COHP,PHIP,COHR,PHIR (enter 1 zero)	(6G10.0)
Third line	(enter 3 zeros) A, B	(6G10.0)

note	columns	variable	entry
	1-10	MODEL	Material model number. =400.0, Associated Mohr-Coulomb material.
	11-20	SIGMAT	Tensile strength of the material.
	21-30	GAMMAX	Body force in the x-direction.
	31-40	GAMMAY	Body force in the y-direction.
	41-50	GAMMAZ	Body force in the z-direction.
	51-60	E	Elastic modulus.
	1-10	NU	Poisson's Ratio. (note new line)
1.	11-20	COHP	Peak cohesion.
1.	21-30	PHIP	Peak friction.
2.	31-40	COHR	Residual cohesion.
3.	41-50	PHIR	Residual friction.
	31-40	A	Pore pressure A parameter. (note new line and column position)

41-50 B Pore pressure B parameter.

note/

1. The material is assumed to be linear elastic until the peak yield strength is reached. Residual strength is mobilized immediately after peak and subsequently unloading and reloading will only mobilize residual strength.
2. If COHR=0.0 or COHR=COHP, the residual is assumed to be equal to the peak strength. If COHR=0.0 is desired, enter a small non-zero value such as 0.000001.
3. If PHIR=0.0 or PHIR=PHIP, the residual is assumed to be equal to the peak strength. If PHIR=0.0 is desired, enter a small non-zero value such as 0.000001.

CARD ENTRIES 9 Elastic Brittle Perfectly Plastic Transversely
Isotropic Model

Input -	FORMAT
First line MODEL,SIGMAT,GAMMAX,GAMMAY,GAMMAZ,E1,	(6G10.0)
Second line v1,E2,v2,G2,cmax,cmin	(6G10.0)
Third line $\mu_{\max}, \mu_{\min}, c_{\text{res}}, \mu_{\text{res}}, \chi, (\text{enter } 1 \text{ zero})$	(6G10.0)

note	columns	variable	entry
	1-10	MODEL	Material model number. =405.0, Associated transversely isotropic material.
	11-20	SIGMAT	Tensile strength of the material.
	21-30	GAMMAX	Body force in the x-direction.
	31-40	GAMMAY	Body force in the y-direction.
	41-50	GAMMAZ	Body force in the z-direction.

	51-60	E_1	Modulus of elasticity in the plane of transverse isotropy.
	1-10	ν_1	Poisson's ratio characterizing the extensional strain response in the plane of transverse isotropy due to a compressive stress acting parallel to the plane of transverse isotropy. (note new line)
	11-20	E_2	Modulus of elasticity normal to the plane of transverse isotropy.
	21-30	ν_2	Poisson's ratio characterizing the extensional strain response in the plane of transverse isotropy due to a compressive stress acting normal to the plane of transverse isotropy.
	31-40	G_2	Shear modulus in plane normal to the plane of transverse isotropy.
	41-50	c_{\max}	Maximum cohesion intercept for transversely isotropic material.
	51-60	c_{\min}	Minimum cohesion intercept for transversely isotropic material.
1	1-10	μ_{\max}	Maximum coefficient of friction for transversely isotropic material. (note new line).
1	11-20	μ_{\min}	Minimum coefficient of friction for transversely isotropic material.
2	21-30	c_{res}	Cohesion intercept at residual strength for transversely isotropic material.
2	31-40	μ_{res}	Coefficient of friction at residual strength for transversely isotropic material.

3 41-50 χ Angle of rotation between the plane of transverse isotropy and the coordinate systems x, y, z.

51-60 (enter 1 zero).

note/

1. $2\mu_{\max} = \tan\phi_{\max}$, and $2\mu_{\min} = \tan\phi_{\min}$. ϕ_{\max} and ϕ_{\min} are the maximum and minimum angle of friction for the transversely isotropic material respectively.
2. The material is assumed to be linear elastic until the peak yield strength is reached. Residual strength is mobilized immediately after peak and subsequently unloading and reloading will only mobilize residual strength.
3. See Figure B.1 for definition of symbols.

GROUP CARD ENTRIES 10 Control Cards For Each Loading Step
--

The following input is composed of a title card and other cards to indicate any changes in information up to the current loading step. This sequence of input is to be repeated NSTEP number of times where NSTEP is the total number of steps specified in card 2. The first set of input should correspond to the first loading step and the last set corresponds loading step NSTEP.

CARD ENTRIES 10.1 Title Card For This Step

Input -	FORMAT
(TITLE(I), I=1,20)	(20A4)

note columns variable entry

1. 1-80 TITLE(20) Enter title for this step.

note/

1. Maximum 80 characters.

CARD ENTRIES 10.2 Loading Step Control Card
--

Input -	FORMAT
NCEL,NCNO,NCSLOP,NCPL,NCPD,NLOAD,KLOAD	(715)

note	columns	variable	entry
1.	1-5	NCEL	The number of cards to be entered to change the element information.
2.	5-10	NCNO	The number of cards to be entered to change the nodal information.
3.	11-15	NCSLOP	The number of cards to be entered for elements on an inclined boundary.
4.	16-20	NCPL	The number of cards to be entered for point load at the nodes.
5.	21-25	NCPD	The number of cards to be entered for prescribed displacements
6.	26-30	NLOAD	The number of subincrement the load vector is being subdivided into within one loading step.
7.	31-35	KLOAD	The subincrement number during intermediate restarting.

note/

1. This indicates the number of entries in below to change the element information such as the element material properties, boundary load, etc. This is not the number of elements to be changed.
2. This indicates the number of entries below to change the nodeal information and not the number of nodes to be changed. Any change in point load, boundary traction or prescribed displacement should not use this variable. Only changes in the degrees of freedom of the nodes should be used.

3. This feature is presently not available.
4. This indicates the number of entries below in applying concentrated point loads at the nodes.
5. This indicates the number of entries below to prescribed the nodal displacements a certain value. For prescribing zero displacement it is more efficient to use the feature on varying the degree of freedom of the nodes.
6. The load vector of each loading step can be subdivided into NLOAD subincrements. An iterative process is used in each subincrement until the solution has converged. The maximum number of iterations specified in card 3 refers to the total number of iterations allowed in each loading step and not in each subincrement. It is expected that the number of subincrement increases. For situation of excavation or constructing an embankment, the loadings due to adding or deleting elements are determined by the size of the elements. This loading can sometimes be too large if the structure is marginally stable or the material is very sensitive to the change in loading. Therefore the applied load can be subdivided into subincrement in order to obtain stable solution. If NLOAD=0, NLOAD is set equal to 1.
7. If program execution terminated in between loading step, the analysis can be restarted using the restarting feature described in card 2. To restart the analysis with NLOAD>0, the number of subincrement already applied must be known which can be determined from the computer output. KLOAD represents the number of subincrements at which the analysis should be restarted. For example if the load vector of a loading step is subdivided into 10 subincrements, i.e. NLOAD=10, and KLOAD=1 initially and let say the analysis is terminated after applying 6 subincrements with a total of 30 equilibrium iterations already completed but the solution has not yet converged to the seventh subincrement. The analysis can be restarted at the 31-st iteration of the sixth subincrement provided FORTRAN unit ITAP8 and FORTRAN unit 4 are available. Only in this case where the information in FORTRAN unit 4 is useful and must be stored in permanent disk space after program execution has been terminated. When restarting the analysis in between loading step and subincrement, FORTRAN unit 4 from previous step now

becomes FORTAN unit 3 and a new unit name should be used for unit 4. A permanent file space is recommended for unit 4 whenever the subincrement feature is used. For this example, IRES=1 in card 2 and KLOAD=7 for restarting. Without unit 4 being available restarting can only be done at the beginning of a loading step, i.e. IRES=0 and KLOAD=1. If KLOAD=0, KLOAD is set equal to 1.

CARD ENTRIES 10.3 Change of Element Information Card

Skip the following entries if NCEL=0.

Supply NCEL number of cards with the following format.

Input -		FORMAT
	IEL1,IS,IG,IB,IM,IEL2	(615)

note	columns	variable	entry
	1-5	IEL1	Beginning element number.
1.	6-10	IS	Element present or absent code. =0, Element is absent in this step. =1, Element is present in this step.
2.	11-15	IG	Gravity load code. =0, Gravity load is not applied. =1, Gravity load is applied on this element in this step.
3.	16-20	IB	Boundary traction code. =0, No boundary traction is applied on this element in this step. =1, Boundary traction is applied on one side of the element. =2, Boundary traction is applied on two side of the element. =3, Boundary traction is applied on three side of the element. =4, Boundary traction is applied on four side of the element.
4.	21-25	IM	Element material number.

=0, No change in element material number.
 >0, Element material is changed to type IM.

26-30 IEL2 Ending element number.
 =0, The above changes only applied to element IEL1.
 >0, The above changes applied from element IEL1 to IEL2 for IEL2 > IEL1.

note/

1. The following cases may apply.

- a. IS=1 in previous step and IS=1 in this step.
 In this case there will be no changes in the degrees of freedom of the element. This will be the case if the element material type is changed or some external boundary traction is applied on the element.
- b. IS=0 in previous step and IS=1 in this step.
 The element is added in this step. The degrees of freedom for all the nodes in this element are set free in all directions even though some of the nodes in this element may be fixed in the previous step. Note that in the process of setting the nodes free to move, the degrees of freedom of the nodes which are attached to other elements with IS=1 will be set free even though some of these degrees of freedom were fixed before. For example if the element being deleted is on a vertical boundary which allows movement of the boundary nodes in the vertical direction only, the deletion of this element will set both degrees of freedom free of the node which is attached to the element adjacent to it. Therefore it is necessary to reset the degrees of freedom of this node or similar nodes using the change of nodal information card. Note that the element stresses, strains and the displacements of the nodes not attached to other elements are zero at the beginning of this step.
- c. IS=1 in the previous step and IS=0 in this step.

The element is being deleted in this step and the degrees of freedom of all the nodes which are not attached to other elements with $IS=1$ will be eliminated. Note that in the process of fixing some of the degree of freedom for this element, the degrees of freedom of the nodes which are attached to other elements with $IS=1$ will be set free even though some of these degrees of freedom were fixed before. This is similar to the case above, therefore it is necessary to reset the degree of freedom on this node using the change of nodal information cards. Moreover in this case the element stresses and strains and the nodes not attached to other elements are all being set equal to zero.

- d. $IS=0$ in the previous step and $IS=0$ in this step. The element is absent in previous step and absent in present step. This is an unusual case and produce no changes in the information of this element except IM .

2. The gravity load is only applied on the elements specified for this step only. IG is set zero after every step.
3. The value of IB in three dimensional analysis refers to the number of faces at which the element is subjected to surface traction.
4. If $IM>0$, the material number will be changed to type IM and the degree of freedom of this element will be unchanged for the case when the element is removed, $IS=0$, or the element is being added, $IS=1$.

CARDENTRIES 10.4 Change of Nodal Information Card
--

Skip this entry if $NCNO=0$.

Supply $NCNO$ number of cards if $NCNO>0$.

Input -		FORMAT
	NODE1,IX1,IX2,NODE2 for 2 dimensional analysis.	(4I5)
	NODE1,IX1,IX2,IX3,NODE2 for 3 dimensional analysis.	(5I5)

For Two Dimensional Analysis

note columns	variable	entry
1-5	NODE1	Beginning node number.
6-10	IX1	Nodal degree of freedom code. =0, First (x-direction) degree of freedom is fixed. =1, First (x-direction) degree of freedom is free to move.
11-15	IX2	Nodal degree of freedom code. =0, Second (y-direction) degree of freedom is fixed. =1, Second (y-direction) degree of freedom is free to move.
16-20	NODE2	Ending node number. =0, The above changes only applied to node NODE1. >0, The above changes applied from nodes NODE1 to NODE2 (NODE2>NODE1).

For Three Dimensional Analysis

note columns	variable	entry
1-5	NODE1	Node number.
6-10	IX1	Nodal degree of freedom code. =0, First (x-direction) degree of freedom is fixed. =1, First (x-direction) degree of freedom is free to move.
11-15	IX2	Nodal degree of freedom code. =0, Second (y-direction) degree of freedom is fixed. =1, Second (y-direction) degree of freedom is free to move.
16-20	IX3	Nodal degree of freedom code.

=0, Third (z-direction) degree of freedom is fixed.

=1, Third (z-direction) degree of freedom is free to move.

21-25 NODE2 Node number 2.
 =0, The above changes only applied to node NODE1.
 >0, The above changes applied from nodes NODE1 to NODE2 (NODE2>NODE1).

CARD ENTRIES 10.5 Boundary Traction Input Card

The following set of cards are used to specify the element surface traction.

Skip these cards if IB for all elements are zero.

It is important to keep track of the value of IB and the number of times IB are being specified with non zero values in card entries 8 and 10.3. There will be $2 \times IB$ number of cards for each element. Therefore there will be $2 \times IB \times NE$ number of cards where NE is the number of element subjected to surface traction. The first two cards contains information on the first side of the element with non zero IB value. If IB is greater than one for any element, then there will be $2 \times IB$ number of cards for that element. After the surface traction has been read in for that element, the value of IB will be assigned zero. Therefore the value of the surface traction only applies to the current step..

CARD ENTRIES 10.5.1 Boundary Nodes Card
--

Skip these cards if IB for all elements are zero for this step which include step number 1.

Enter the boundary nodes subject to boundary traction.

Input -

FORMAT

NODE1,NODE2,NODE3 for 2 dimensional analysis. (315)

IAXIS,NODE1,NODE2,NODE3,NODE4,NODE5,NODE6,NODE7,NODE8
For 3 dimensional analysis (915)

For Two Dimensional Analysis

note	columns	variable	entry
1.	1-5	NODE1	Node number 1 (corner node).
2.	6-10	NODE2	Node number 2 (mid-side node).
	11-15	NODE3	Node number 3 (corner node).

For Three Dimensional Analysis

note	columns	variable	entry
1.	1-5	IAXIS	Code to identify the face of the element.
	6-10	NODE1	Node number 1 (corner node).
	11-15	NODE2	Node number 2 (mid-side node).
	16-20	NODE3	Node number 3 (corner node).
	21-25	NODE4	Node number 4 (mid-side node).
2.	26-30	NODE5	Node number 5 (corner node).
	31-35	NODE6	Node number 6 (mid-side node).
	36-40	NODE7	Node number 7 (corner node).
	41-45	NODE8	Node number 8 (mid-side node).

note/

1. The corner node number must be positive.
The axis code for the 3-D analysis, IAXIA=1, 2 and 3 for the faces on the positive r, s and t direction and IAXIS=-1, -2 and -3 for the faces on the negative r, s and t directions respectively.

The positive r axis will contain local corner node number 1, 4, 5 and 8. The positive s axis will contain local corner node number 1, 5 6 and 2. The positive t axis will contain local corner node number 1, 2, 3 and 4.

2. If the mid-side node is absent, enter zero.
For the 3-D case, the node numbers must be always be in the counter-clockwise direction.

CARD ENTRIES 10.5.2 Boundary Traction Card

Enter the boundary value of the boundary traction at the nodes.

Skip these cards if IB for all elements are zero.

Input -		FORMAT
	XF1,YF1,XF2,YF2,XF3,YF3 for 2 dimensional analysis	(6G10.0)
	XF1,YF1,XF2,YF2,XF3,YF3,XF4,YF4,XF5,YF5,XF6,YF6,,XF7,YF7,XF8,YF8 for 3 dimensional analysis	(6G10.0)

For Two Dimensional Analysis

note	columns	variable	entry
1.	1-10	XF1	Traction in x-direction at node 1.
	11-20	YF1	Traction in y-direction at node 1.
2.	21-30	XF2	Traction in x-direction at node 2.
	31-40	YF2	Traction in y-direction at node 2.
1.	41-50	XF3	Traction in x-direction at node 3.
	51-60	YF3	Traction in y-direction at node 3.

For Three Dimensional Analysis

note	columns	variable	entry
------	---------	----------	-------

1.	1-10	XF1	Traction in x-direction at node 1.
	11-20	YF1	Traction in y-direction at node 1.
	21-30	ZF1	Traction in z-direction at node 1.
	31-40	XF2	Traction in x-direction at node 2.
	41-50	YF2	Traction in y-direction at node 2.
	51-60	ZF2	Traction in z-direction at node 2.
	1-10	XF3	Traction in x-direction at node 3. (note new line)
	11-20	YF3	Traction in y-direction at node 3.
	21-30	ZF3	Traction in z-direction at node 3.
	31-40	XF4	Traction in x-direction at node 4.
	41-50	YF4	Traction in y-direction at node 4.
	51-60	ZF4	Traction in z-direction at node 4.
2.	1-10	XF5	Traction in x-direction at node 5. (note new line)
	11-20	YF5	Traction in y-direction at node 5.
	21-30	ZF5	Traction in z-direction at node 5.
	31-40	XF6	Traction in x-direction at node 6. (note new line)
	41-50	YF6	Traction in y-direction at node 6.
	51-60	ZF6	Traction in z-direction at node 6.
	1-10	XF7	Traction in x-direction at node 7. (note new line)
	11-20	YF7	Traction in y-direction at node 7.

21-30	ZF7	Traction in z-direction at node 7.
31-40	XF8	Traction in x-direction at node 8. (note new line)
41-50	YF8	Traction in y-direction at node 8.
51-60	ZF8	Traction in z-direction at node 8.

note/

1. The values of XF1, XF2 etc. are the tractions at the nodes in pressure units and they are not the nodal forces. The program will approximate the pressure distribution with a parabola using the values of the pressure given at the nodes. If the mid-side nodes is absent, only a linear distribution can be made. The signs are determined according to the direction of the axes. For example if XF1 is positive, the pressure is acting in the positive x direction etc. To resolve the traction in the x, y and z direction, just multiply the pressure by the sine or cosine of the angle with respect to the axes.
2. If the mid-side node is absent, enter zero pressure.

CARD ENTRIES 10.6 Point Load Card
--

Skip this entry if NCPL=0.

Supply NCPL number of cards if NCPL>0.

Input - FORMAT
 NODE1,XLOAD,YLOAD,NODE2 for 2 dimensional analysis
(I5,2G10.0,I5)
 NODE1,XLOAD,YLOAD,ZLOAD,NODE2 for 3 dimensional analysis
(I5,3G10.0,I5)

For Two Dimensional Analysis

note columns variable entry

	1 - 5	NODE1	Beginning node number.
1.	6 - 15	XLOAD	Point load in x-direction.
	16 - 25	YLOAD	Point load in y-direction.
	26 - 30	NODE2	Ending node number. =0, The above changes only applied to node NODE1. >0, The above changes applied from nodes NODE1 to NODE2 (NODE2>NODE1).

For Three Dimensional Analysis

note	columns	variable	entry
	1 - 5	NODE1	Beginning node number.
1.	6 - 15	XLOAD	Point load in x-direction.
	16 - 25	YLOAD	Point load in y-direction.
	26 - 35	ZLOAD	Point load in z-direction.
	36 - 40	NODE2	Ending node number. =0, The above changes only applied to node NODE1. >0, The above changes applied from nodes NODE1 to NODE2 (NODE2>NODE1).

notes/

1. The signs of the point loads should coincide with the directions of the corresponding axes.

CARD ENTRIES 10.7 Prescribed Displacement Card

Skip this entry if NCDL=0.

Supply NCDL number of cards if NCDL>0.

Input - FORMAT
 NODE1,ID1,DISPL,NODE2 for 2 and 3 dimensional analysis
(2I5,G10.0,I5)

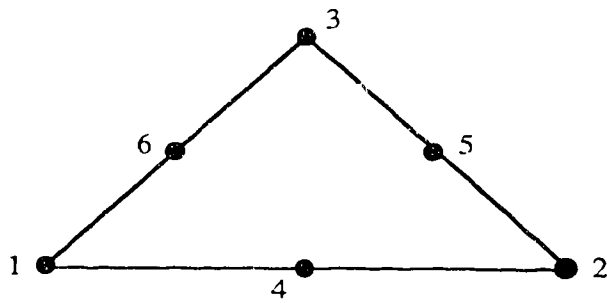
note	columns	variable	entry
	1-5	NODE1	Beginning node number.
	6-10	ID1	Degree of freedom code. =1, Displacement applied in x-direction. =2, Displacement applied in y-direction. =3, Displacement applied in z-direction for three dimensional analysis.
1.	11-20	DISPL	Prescribed displacement.
	21-25	NODE2	Ending node number. =0, The above changes only applied to node NODE1. >0, The above changes applied from nodes NODE1 to NODE2 (NODE2>NODE1).

notes/

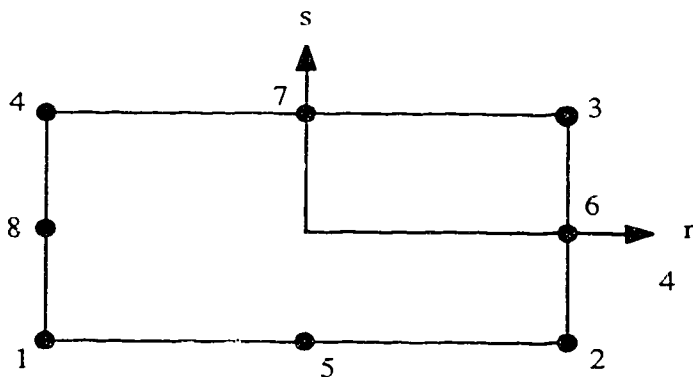
1. The sign of the displacement should coincide with the directions of the corresponding axes.

Table E.1: Material Properties Input for SAGE.

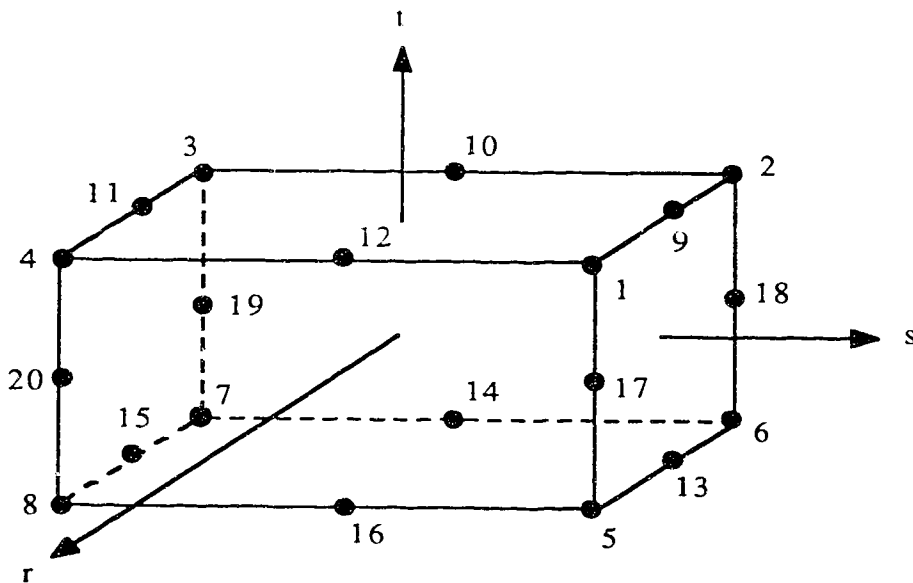
ENTRIES																
MODELS	1	2	3	4	5	6	7	8	9	10	11	12	13	14	15	16 17
Linear Elastic	1.	σ_t	γ_x	γ_y	γ_z	E	ν	-	-	-	-	-	-	-	-	A B
Linear Elastic	2.	σ_t	γ_x	γ_y	γ_z	K	G	-	-	-	-	-	-	-	-	A B
Hyperbolic Elastic	10.	σ_t	γ_x	γ_y	γ_z	κ	κ_u	n	R_f	C	ϕ	P_a	G	F	D	A B
Von Mises	100.	σ_t	γ_x	γ_y	γ_z	E	ν	σ_p^y	σ_R^y	-	-	-	-	-	-	A B
Tresca	200.	σ_t	γ_x	γ_y	γ_z	E	ν	σ_p^y	σ_R^y	-	-	-	-	-	-	A B
Drucker-Prager-1	300.	σ_t	γ_x	γ_y	γ_z	E	ν	κ_p	α_p	κ_R	α_R	-	-	-	-	A B
Mohr-Coulomb-1	400.	σ_t	γ_x	γ_y	γ_z	E	ν	C_p	ϕ_p	C_R	ϕ_R	-	-	-	-	A B
Transversely Isotropic	405.	σ_t	γ_x	γ_y	γ_z	E1	ν_1	E2	ν_2	G2	c_{max}	c_{min}	μ_{max}	μ_{min}	c_{res}	μ_{res} χ



3 - 6 Nodes Triangular Element



4 - 8 Nodes Rectangular Element



8 - 20 Nodes Solid Three Dimensional Element

Figure E.1

Types of Elements Available in SAGE.

APPENDIX F

INPUT FILE EXAMPLE

A simple confined compression test under plain strain conditions was selected, as an example to demonstrate how to set up an input file. The finite element mesh is shown in Figure F.1. Four elements with 21 nodes were used for the finite element mesh and it was loaded by prescribing vertical displacements in small increments under a constant confining pressure of 35 MPa. The analysis was carried out with weakness planes orientated at $\eta=35^\circ$.

The parameters selected for this example are summarized in the following table:

Elastic Deformation	Strength Parameters	
Properties	Peak	Residual
$E_1 = 91.5 \text{ GPa}$	$c_{\max} = 95.1 \text{ MPa}$	$c_{\text{res}} = 0$
$E_2 = 59.1 \text{ GPa}$	$c_{\min} = 7.05 \text{ MPa}$	$\phi_{\text{res}} = 20.0^\circ$
$\nu_1 = 0.204$	$\phi_{\max} = 67.1^\circ$	
$\nu_2 = 0.331$	$\phi_{\min} = 20.0^\circ$	
$G_2 = 24 \text{ GPa}$		

The analyses were carried out in 5 steps, summarized as follows:

1. Step 1 is to apply uniform stress of 35 MPa to all the elements.

2. Step 2 is to apply vertical pressure to elements 1 and 3 until the peak strength is reached.
3. After the peak strength is reached, steps 3 to 5 are to apply uniform vertical displacements to nodes 5, 8, 13, 16 and 21 to calculate the stresses at residual strength.

The program is stored in CDC Cyber 175, at the University of Calgary. Cyber 175 is the front end of the computer system which performs the editing function and the storing of the input and output files. The name of the source code is called SAFEANI205, and the object code is called SAFELO. The actual execution of the program is carried out in CDC Cyber 205 which is called the back end of the computer system. In order to submit a run, a batch file is created to transfer the input file and the object code from Cyber 175 to Cyber 205. When the execution is completed, the batch file will then transfer the output from Cyber 205 back to Cyber 175 for editing and storing. The batch file is listed as the following:

```

/JOB
/NOSEQ
UOFA620,STDEX.
USER,U=300620,AC=UOFA2,PA=PASS.
RESOURCE,JCAT=STANDBY,WS=1500,TL=1500.
REQUEST,BHFIL6/1000.
REQUEST,T1/1000,RT=W.
REQUEST,T4/1000,RT=W.
REQUEST,BHFIL7/1000.
REQUEST,BHFIL8/1000.
MFLINK,BHFIL5,DD=C6,ST=MD2,JCS="USER,620,CECI.,"GET,ANITEST.".
MFLINK,MAPROG,DD=UU,ST=MD2,JCS="USER,620,CECI.,"ATTACH,SAFEANI205.".
LOAD,MAPROG,CN=GO/1000,LIB=F200LIB,L=O.
GO,BHFIL5,BHFIL6,BHFIL7,BHFIL8,TAPE5=BHFIL5,TAPE6=BHFIL6,TAPE7=BHFIL7,TAPE8=BHFIL8.
MFLINK,BHFIL6,DD=C6,ST=MD2,JCS="USER,620,CECI.,"DEFINE,RESULT.".
MFLINK,BHFIL7,DD=C6,ST=MD2,JCS="USER,620,CECI.,"DEFINE,RESTART7.".
MFLINK,BHFIL8,DD=C6,ST=MD2,JCS="USER,620,CECI.,"DEFINE,RESTART8.".

```


SUMMARY.
END OF FILE.

The input file is called ANITEST, and the output file is called RESULT. RESTART7 and RESTART8 are files which store the necessary information to restart the program in case the execution is terminated due to insufficient computer time assigned, or to restart the program at any intermediate steps.

ANITEST is listed below:

PLANE STRAIN COMPRESSION TEST (TRANSVERSELY ISOTROPIC MATERIAL)

3	2	0	1.0	0	0	0	0	0	8	0
5	1	4	21	2	2	1	0	0	1	
2	20	0.0001								
2	20	0.0001								
1	20	0.0001								
-0.00635	-0.015875	0	0							
-0.00635	-0.0079375	0	1							
-0.00635	0.00	0	1							
-0.00635	0.0079375	0	1							
-0.00635	0.015875	0	1							
-0.003175	-0.015875	1	0							
-0.003175	0.000000	1	1							
-0.003175	0.015875	1	1							
0.00	-0.015875	1	0							
0.00	-0.0079375	1	1							
0.00	0.00	1	1							
0.00	0.0079375	1	1							
0.00	0.015875	1	1							
0.003175	-0.015875	1	0							
0.003175	0.00	1	1							
0.003175	0.015875	1	1							
0.00635	-0.015875	1	0							
0.00635	-0.0079375	1	1							
0.00635	0.00	1	1							
0.00635	0.0079375	1	1							
0.00635	0.015875	1	1							
3	11	13	5	7	12	8	4	2	1	0
1										
1	9	11	3	6	10	7	2	2	1	0
1										
11	19	21	13	15	20	16	12	2	1	0
1										
9	17	19	11	14	18	15	10	2	1	0
1										
	405.0	0.000		0.0		0.0		0.0		91500.0

0.204	59100.0	0.331	24000.00	95.10	7.05
1.21	0.185	0.0	0.185	55.0	0.0
1.0	0.000	0.0	0.0	0.0	91500.0
0.204	0.0	0.0	0.0	0.0	0.0
0.0	0.0	0.0	0.0	0.0	

STEP 1 ALL ROUND CONFINING PRESSURE=35 MPa ,ORIET=55DEG.TO HORIZ.

3	0	0	0	0	1	1
1	1	0	1	0	0	
3	1	0	2	0	0	
4	1	0	1	0	0	
3	7	4				
	0.0	-35.0		0.0	-35.0	0.0
2	6	3				
	-35.0	0.0		-35.0	0.0	-35.0
3	7	4				
	0.0	-35.0		0.0	-35.0	0.0
2	6	3				
	-35.0	0.0		-35.0	0.0	-35.0

STEP 2 APPLY VERTICAL PRESSURE=-57.20 MPa TOTAL SIGMA1=-92.20 MPa

2	0	0	0	0	1	1
1	1	0	1	0	0	
3	1	0	1	0	0	
3	7	4				
	0.0	-57.2		0.0	-57	20.0
3	7	4				
	0.0	-57.2		0.0	-57.2	0.0

STEP 3 PRESCRIBE DISPL.=-0.0000001 TOTAL PRESC. DISPL.=-0.0000001

0	0	0	0	5	1	1
5	2	-0.0000001	0			
8	2	-0.0000001	0			
13	2	-0.0000001	0			
16	2	-0.0000001	0			
21	2	-0.0000001	0			

STEP 4 PRESCRIBE DISPLACEMENT=-0.00005 TOTAL DISPL.=-0.0000501

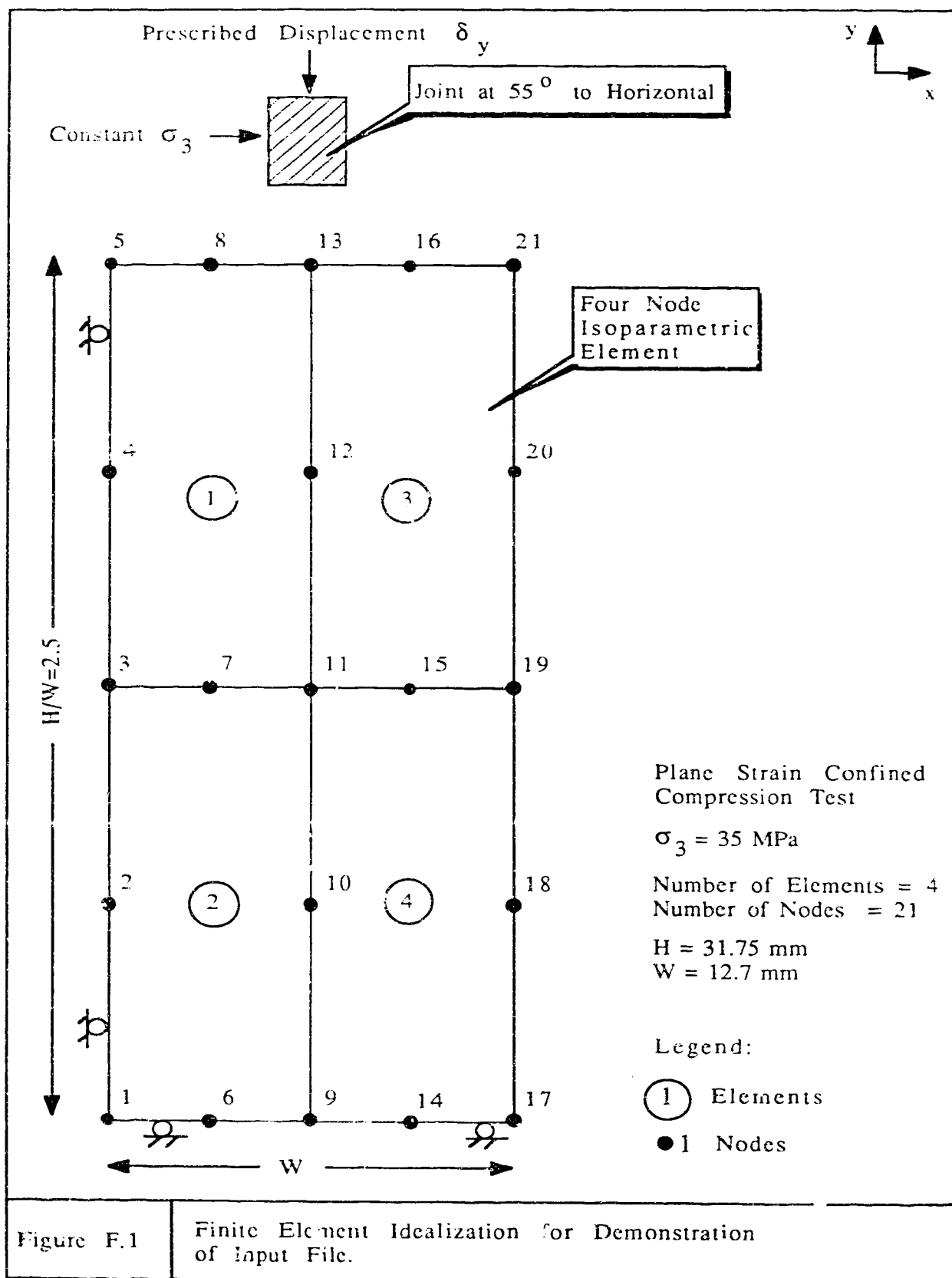
0	0	0	0	5	1	1
5	2	-0.0000001	0			
8	2	-0.0000001	0			
13	2	-0.0000001	0			
16	2	-0.0000001	0			
21	2	-0.0000001	0			

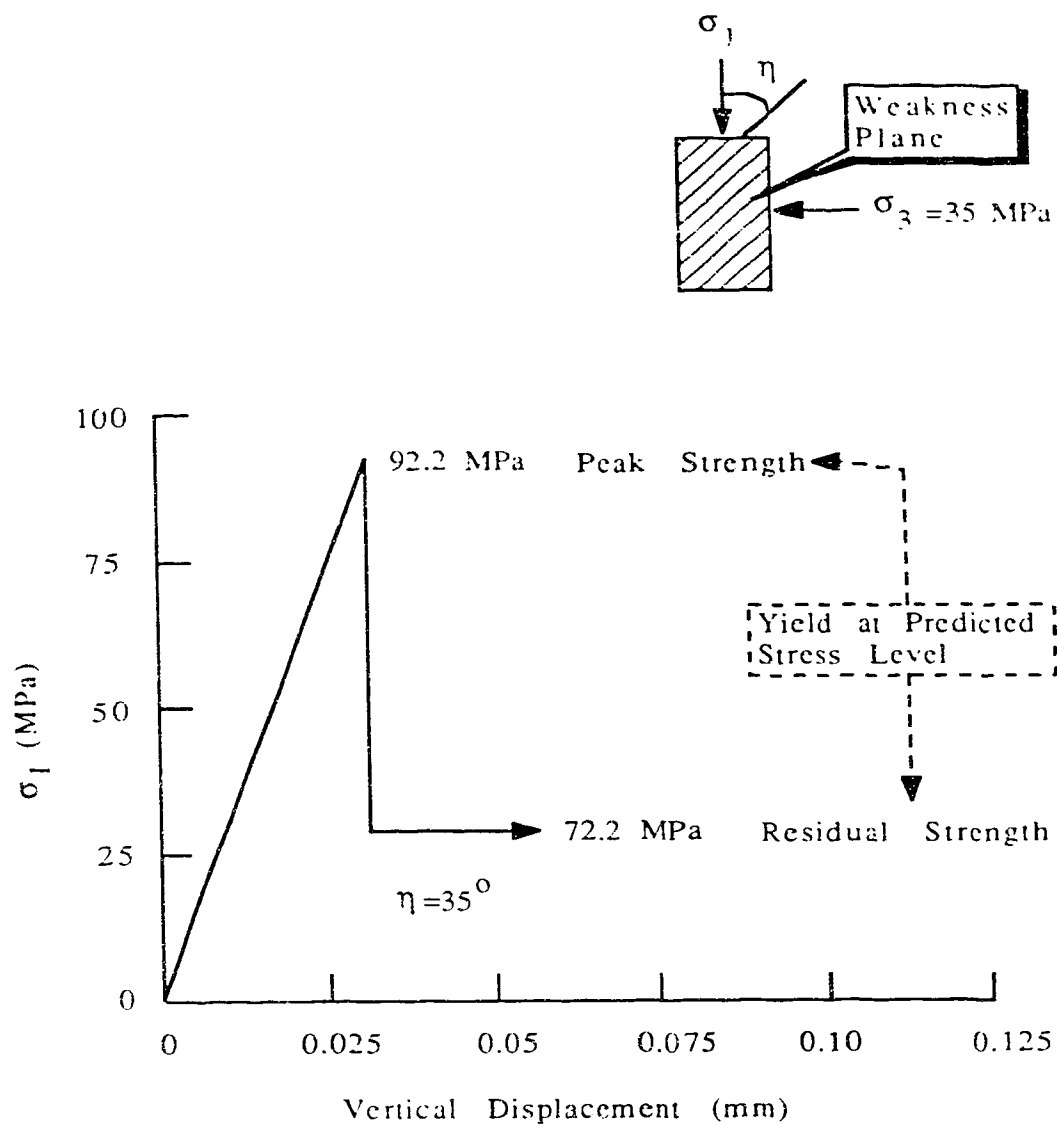
STEP 5 PRESCRIBE DISPLACEMENT=-0.00010 TOTAL DISPL.=-0.0001501

0	0	0	0	5	1	1
5	2	-0.0000001	0			
8	2	-0.0000001	0			
13	2	-0.0000001	0			
16	2	-0.0000001	0			
21	2	-0.0000001	0			

To begin the execution of the program, enter "submit, batch, e".
The results of this analysis is shown in Figure F.2. This figure shows

that the material behaves as a linear elastic, brittle, perfectly plastic material with yielding reached at the predicted stress level. The output file, RESULT, is attached at the end of this appendix for reference.





	Peak		Residual
c_{min} (MPa)	7.1	c_{res} (MPa)	0.0
ϕ_{min}	20°	ϕ_{res}	20°
α	13.5		
β	6.5		

Figure F.2

Confined Compression Test for Demonstration of Input File.

```

.....
..
..
..      1. COMPUTER PROGRAM FOR
..      SOIL ANALYSIS BY FINITE ELEMENT
..
..
..      SSSSSSSSSSSS  LLLLLLLLLL  FFFFFFFF  FFFFFFFF  TTTTTTTTTT
..      SSSSSSSSSSSS  LLLLLLLLLL  FFFFFFFF  FFFFFFFF  TTTTTTTTTT
..      SS          AA          AA          FF          EE
..      SS          AA          AA          FF          EE
..      SSSSSSSSSSSS  LLLLLLLLLL  FFFFFFFF  FFFFFFFF  TTTTTTTTTT
..      SSSSSSSSSSSS  LLLLLLLLLL  FFFFFFFF  FFFFFFFF  TTTTTTTTTT
..      SS          AA          AA          FF          EE
..      SS          AA          AA          FF          EE
..      SSSSSSSSSSSS  LLLLLLLLLL  FFFFFFFF  FFFFFFFF  TTTTTTTTTT
..      SSSSSSSSSSSS  LLLLLLLLLL  FFFFFFFF  FFFFFFFF  TTTTTTTTTT
..
..      THIS PROGRAM IS DEVELOPED BY DAVE M. CHAN
..      DEPARTMENT OF CIVIL ENGINEERING
..      UNIVERSITY OF ALBERTA, EDMONTON, ALBERTA
..
..      ALL RIGHTS RESERVED
..
..
.....

```

WARNING THE DEVELOPER OF THIS PROGRAM AND/OR THE UNIVERSITY OF ALBERTA MAKES NO WARRANTY WHATSOEVER, EXPRESSED OR IMPLIED, THAT THE PROGRAM AND ANY MODIFICATIONS, INCLUDING UPDATES, AND THE DOCUMENTATION ARE FREE FROM ERRORS AND/OR DEFECTS

GENERAL INFORMATION

PROJECT TITLE ANISOTROPIC PLANE STRAIN COMPRESSION TEST (NOVA BRITTLE MODEL)

DATE APR 1, 1987 TIME (HRS:MIN:SEC) : 13:59:49

THIS IS A SMALL DEFORMATION NON-LINEAR ELASTIC-PLASTIC
TWO DIMENSIONAL PLANE STRAIN ANALYSIS

DOUBLE PRECISION ARITHMETICS

TOTAL STRESS ANALYSIS IEFF = 0

GOOD LUCK

TOTAL NUMBER OF STEPS IN THE ANALYSIS = 1 ANALYSIS STARTS AT STEP NUMBER = 1

TOTAL NUMBER OF ELEMENTS (NEL) = 4 TOTAL NUMBER OF NODES (NNOD) = 21

NUMBER OF INTEGRATION POINTS (NIP) = 2

NO. OF MATERIAL TYPE = 2 THICKNESS = 1.00000

IN-SITE DISPLACEMENT CODE (IDGR) = 1
IDGR = 0, DISPLACEMENTS WILL BE SET TO ZERO AFTER THE FIRST ANALYSIS
IDGR = 1, DISPLACEMENTS AND STRAINS WILL BE SET ZERO AFTER THE FIRST ANALYSIS

IN-SITE STRESS AND STRAIN CODE (ISITE) = 0
ISITE = 0, NO INITIAL STRESS IS GIVEN
ISITE = 1, ONLY SIGMA-XX WILL BE GIVEN
ISITE = 2, SIGMA-XX AND SIGMA-YY WILL BE GIVEN
ISITE = 3, SIGMA-XX, SIGMA-YY AND SIGMA-XY WILL BE GIVEN

INFORMATION CODE (INFORM) = 0
INFORM = 1, EXECUTION WILL STOP AFTER DETERMINING THE SIZE OF THE GLOBAL MATRIX
INFORM = 0, PROGRAM PROCEED WITHOUT INTERRUPTION

PRINT-OUT CONTROL (IPRINT)

```

IPRINT(1) = 0 DISPLACEMENTS, STRESSES AND STRAINS PRINT-OUT
IF IPRINT(1) = 0, NO PRINT-OUT IS REQUIRED DURING EQUILB. ITERATION, ONLY FINAL VALUES ARE PRINTED
IF IPRINT(1) > 0, INTERMEDIATE RESULTS WILL BE GIVEN FOR EVERY IPRINT(1) ITERATION
IPRINT(2) = 0 UNBALANCED LOAD VECTOR DURING EQUILB. ITERATION
IF IPRINT(2) = 0, NO PRINT-OUT IS REQUIRED
IF IPRINT(2) > 0, UNBALANCED LOAD VECTOR WILL BE GIVEN FOR EVERY IPRINT(1) ITERATION ABOVE
IPRINT(3) = 0 FINAL UNBALANCED LOAD VECTOR
IF IPRINT(3) = 0, NO FINAL UNBALANCED LOAD VECTOR WILL BE PRINTED
IF IPRINT(3) > 0, FINAL UNBALANCED VECTOR WILL BE GIVEN
IPRINT(4) = 0 ELEMENT LOAD VECTOR
IF IPRINT(4) = 0, NO ELEMENT LOAD VECTOR WILL BE PRINTED
IF IPRINT > 0, ELEMENT LOAD VECTOR FOR SURFACE TRACTION WILL BE PRINTED
IPRINT(5) = 0 LISTING OF DEGREES OF FREEDOM

```


ANALYSIS STEP NUMBER *****

261

TITLE FOR THIS STEP STEP 1 ALL ROUND CONFINING PRESSURE=35MPA ORIENT=55DEG TO HORIZ

NUMBER OF LINE INPUT FOR NEW ELEMENT 1 3
NUMBER OF LINE INPUT FOR NEW NODES 1 0
NUMBER OF LINE INPUT FOR SLOPE BOUNDARY 1 0
NUMBER OF LINE INPUT FOR NEW POINT LOAD 1 0
NUMBER OF LINE INPUT FOR NEW DISPLACEMENT 1 0
NUMBER OF LOAD INCREMENTS 1
LOAD INCREMENT BEGIN AT INCREMENT NUMBER 1

***NEW ELEMENT ADDED OR DELETED**

FROM EL	TO EL	S	IC	IB	IM
1	3	1	0	1	0
3	4	1	0	2	0
4	1	1	0	1	0

TOTAL DEGREE OF FREEDOM = 22 MAX HALF BANDWIDTH = 16 EL = 19 STIFFNESS MATRIX SIZE = 376

STEP NUMBER = 1 APPLIED LOAD INCREMENT = 1 ITERATION = 0

NODAL DISPLACEMENTS

NODE	U-DISPL	V-DISPL	W-DISPL	U-DISPL	V-DISPL	W-DISPL	U-DISPL	V-DISPL	W-DISPL	U-DISPL	V-DISPL	W-DISPL
1	0.0	0.0	0.0	2.0	0.0	0.0	3.0	0.0	0.0	4.0	0.0	0.0
3	0.0	0.0	0.0	5.0	0.0	0.0	7.0	0.0	0.0	8.0	0.0	0.0
4	0.0	0.0	0.0	10.0	0.0	0.0	11.0	0.0	0.0	12.0	0.0	0.0
13	0.0	0.0	0.0	14.0	0.0	0.0	15.0	0.0	0.0	16.0	0.0	0.0
17	0.0	0.0	0.0	18.0	0.0	0.0	19.0	0.0	0.0	20.0	0.0	0.0
21	0.0	0.0	0.0	22.0	0.0	0.0	23.0	0.0	0.0	24.0	0.0	0.0

ELEMENT STRESSES AND STRAINS

EL	X-COORD	Y-COORD	SIGMA-XX	SIGMA-YY	SIGMA-ZZ	SIGMA-XY	SIGMA-XZ	SIGMA-YZ	ANGLE	YIELD	STGTH-2
11	0.000E+00	0.335E+02	0.350E+02	0.350E+02	0.350E+02	0.000E+00	0.000E+00	0.000E+00	0.0	0.0	0.0
12	0.1210E+01	0.7050E+01	0.350E+02	0.350E+02	0.350E+02	0.000E+00	0.000E+00	0.000E+00	0.0	0.0	0.0
21	0.1342E+02	0.335E+02	0.350E+02	0.350E+02	0.350E+02	0.000E+00	0.000E+00	0.000E+00	0.0	0.0	0.0
22	0.1210E+01	0.7050E+01	0.350E+02	0.350E+02	0.350E+02	0.000E+00	0.000E+00	0.000E+00	0.0	0.0	0.0

EL	X-COORD	Y-COORD	SIGMA-XX	SIGMA-YY	SIGMA-ZZ	SIGMA-XY	SIGMA-XZ	SIGMA-YZ	ANGLE	YIELD	STGTH-2
11	0.000E+00	0.335E+02	0.350E+02	0.350E+02	0.350E+02	0.000E+00	0.000E+00	0.000E+00	0.0	0.0	0.0
12	0.1210E+01	0.7050E+01	0.350E+02	0.350E+02	0.350E+02	0.000E+00	0.000E+00	0.000E+00	0.0	0.0	0.0
21	0.1342E+02	0.335E+02	0.350E+02	0.350E+02	0.350E+02	0.000E+00	0.000E+00	0.000E+00	0.0	0.0	0.0
22	0.1210E+01	0.7050E+01	0.350E+02	0.350E+02	0.350E+02	0.000E+00	0.000E+00	0.000E+00	0.0	0.0	0.0

SUMMARY OF COMPUTER TIME

ITERATION	STIFF REFORM (MILLI SEC.)	SOLUTION TIME (MILLI SEC.)	STRESS CALCUL. (MILLI SEC.)
1	97	6	33
TOTAL	97	6	33

TIME IN FOR THIS STEP = 141 MILLI SEC
TIME OUT FOR THIS STEP = 387 MILLI SEC
TIME ELAPSED FOR THIS STEP = 255 MILLI SEC

END OF STEP NUMBER 1

A COMPUTER PROGRAM FOR
SOIL ANALYSIS BY FINITE ELEMENT

```

SSSSSSSSSSSS  AAAAAAAAAA  FFFFFFFFFFFFFF  EEEEEEEEEEE
SSSSSSSSSSSS  AAAAAAAAAA  FFFFFFFFFFFFFF  EEEEEEEEEEE
SS          SS  AA          AA  FF          FF  EE
SS          SS  AA          AA  FF          FF  EE
SSSSSSSSSSSS  AAAAAAAAAA  FFFFFFFFFFFFFF  EEEEEEEEEEE
SSSSSSSSSSSS  AAAAAAAAAA  FFFFFFFFFFFFFF  EEEEEEEEEEE
          SS  AA          AA  FF          FF  EE
          SS  AA          AA  FF          FF  EE
SSSSSSSSSSSS  AA          AA  FF          FF  EEEEEEEEEEE
SSSSSSSSSSSS  AA          AA  FF          FF  EEEEEEEEEEE

```

THIS PROGRAM IS DEVELOPED BY DAVE H. CHAN
DEPARTMENT OF CIVIL ENGINEERING
UNIVERSITY OF ALBERTA, EDMONTON, ALBERTA

ALL RIGHTS RESERVED

WARNING THE DEVELOPER OF THIS PROGRAM AND/OR THE UNIVERSITY OF ALBERTA MAKES NO
WARRANTY WHATSOEVER EXPRESSED OR IMPLIED THAT THE PROGRAM AND ANY MODIFICATIONS
INCLUDING UPDATES, AND THE DOCUMENTATION ARE FREE FROM ERRORS AND/OR DEFECTS

GENERAL INFORMATION

PROJECT TITLE ANISOTROPIC PLANE STRAIN COMPRESSION TEST (NOVA BRITTLE MODEL)

DATE APR 1, 1987 TIME (HRS:MIN:SEC) 14:08:50

THIS IS A SMALL DEFORMATION NON-LINEAR ELASTIC-PLASTIC
TWO DIMENSIONAL PLANE STRAIN ANALYSIS

DOUBLE PRECISION ARITHMETICS

TOTAL STRESS ANALYSIS LEFF = 0

GOOD LUCK

TOTAL NUMBER OF STEPS IN THE ANALYSIS = 2 ANALYSIS STARTS AT STEP NUMBER = 2

TOTAL NUMBER OF ELEMENTS (NEL) = 4 TOTAL NUMBER OF NODES (NNOD) = 21

NUMBER OF INTEGRATION POINTS (NIP) = 2

NO. OF MATERIAL TYPE = 2 THICKNESS = 1.00000

IN-SITE DISPLACEMENT CODE (IDGR) = 1
IDGR = 0, DISPLACEMENTS WILL BE SET TO ZERO AFTER THE FIRST ANALYSIS
IDGR < 0, DISPLACEMENTS AND STRAINS WILL BE SET ZERO AFTER THE FIRST ANALYSIS

IN-SITE STRESS AND STRAIN CODE (ISITE) = 0
ISITE = 0, NO INITIAL STRESS IS GIVEN
ISITE = 1, ONLY SIGMA-XX WILL BE GIVEN
ISITE = 2, SIGMA-XX AND SIGMA-YY WILL BE GIVEN
ISITE = 3, SIGMA-XX, SIGMA-YY AND SIGMA-XY WILL BE GIVEN

INFORMATION CODE (INFORM) = 0
INFORM = 1, EXECUTION WILL STOP AFTER DETERMINING THE SIZE OF THE GLOBAL MATRIX
INFORM = 0, PROGRAM PROCEED WITHOUT INTERRUPTION

PRINT-OUT CONTROL (IPRINT)

```

IPRINT(1) = 0 DISPLACEMENTS, STRESSES AND STRAINS PRINT-OUT
IF IPRINT(1) = 0, NO PRINT-OUT IS REQUIRED DURING EQUILB. ITERATION, ONLY FINAL VALUES ARE PRINTED
IF IPRINT(1) > 0, INTERMEDIATE RESULTS WILL BE GIVEN FOR EVERY IPRINT(1) ITERATION
IPRINT(2) = 0 UNBALANCED LOAD VECTOR DURING EQUILB. ITERATION
IF IPRINT(2) = 0, NO PRINT-OUT IS REQUIRED
IF IPRINT(2) > 0, UNBALANCED LOAD VECTOR WILL BE GIVEN FOR EVERY IPRINT(1) ITERATION ABOVE
IPRINT(3) = 0 FINAL UNBALANCED LOAD VECTOR
IF IPRINT(3) = 0, NO FINAL UNBALANCED LOAD VECTOR WILL BE PRINTED
IF IPRINT(3) > 0, FINAL UNBALANCED VECTOR WILL BE GIVEN
IPRINT(4) = 0 ELEMENT LOAD VECTOR
IF IPRINT(4) = 0, NO ELEMENT LOAD VECTOR WILL BE PRINTED
IF IPRINT(4) > 0, ELEMENT LOAD VECTOR FOR SURFACE TRACTION WILL BE PRINTED
IPRINT(5) = 0 LISTING OF DEGREES OF FREEDOM

```


ANALYSIS STEP NUMBER 2

264

TITLE FOR THIS STEP STEP 2 APPLY VERTICAL PRESSURE=57 ZONPA TOTAL SIGMA=92 ZONPA

NUMBER OF LINE INPUT FOR NEW ELEMENT 1 2
 NUMBER OF LINE INPUT FOR NEW NODES 1 C
 NUMBER OF LINE INPUT FOR SLOPE BOUNDARY 1 C
 NUMBER OF LINE INPUT FOR NEW POINT LOAD 1 0
 NUMBER OF LINE INPUT FOR NEW DISPLACEMENT 1 0
 NUMBER OF LOAD INCREMENTS 1 1
 LOAD INCREMENT BEGIN AT INCREMENT NUMBER 1 1

NEW ELEMENT ADDED OR DELETED

FROM EL TO EL IS IC IE IM
 1 3 1 C 1 C
 3 3 1 C 1 C

TOTAL DEGREE OF FREEDOM = 32 MAX HALF BANDWIDTH NO DIA EL = 19 STIFFNESS MATRIX SIZE = 376

STEP NUMBER = 2 APPLIED LOAD INCREMENT = 1 ITERATION = 0

NODAL DISPLACEMENTS

NODE	U-DISPL	V-DISPL	NODE	U-DISPL	V-DISPL	NODE	U-DISPL	V-DISPL	NODE	U-DISPL	V-DISPL
1	0.0	0.0	2	0.0	-0.708252E-05	3	0.0	-0.141250E-04	4	0.0	-0.211878E-04
5	0.0	-0.282501E-04	6	0.870071E-07	0.0	7	0.870071E-07	-0.141250E-04	8	0.870071E-07	-0.282501E-04
9	0.174014E-08	0.0	10	0.174014E-08	-0.708252E-05	11	0.174014E-08	-0.141250E-04	12	0.174014E-08	-0.211878E-04
13	0.174014E-08	-0.282501E-04	14	0.281021E-08	0.0	15	0.281021E-08	-0.141250E-04	16	0.281021E-08	-0.282501E-04
17	0.348028E-08	0.0	18	0.348028E-08	-0.708252E-05	19	0.348028E-08	-0.141250E-04	20	0.348028E-08	-0.211878E-04
21	0.348028E-08	-0.282501E-04									

ELEMENT STRESSES AND STRAINS

EL	X-COORD	Y-COORD	SIGMA-XX	SIGMA-YY	SIGMA-XY	SIGMA-ZZ	SIGMA-1	SIGMA-2	SIGMA-3	ANGLE	YIELD
	STGTH-3	STGTH-4	STRAIN-XX	STRAIN-YY	GAMMA-XY	STRAIN-ZZ	STRAIN-1	STRAIN-2	STRAIN-3	ANGLE	STGTH-3
***** STRESSES AND STRAINS IN ELEMENT NUMBER 1 *****											
11	0.5008E-02	0.3355E-02	-0.3500E-02	-0.8220E-02	0.1334E-13	-0.3645E-02	-0.3500E-02	-0.8220E-02	0.1334E-13	-0.8308E-01	0.8510E-02
12	0.1210E+01	0.7050E+01	-0.2740E-04	-0.8898E-03	0.487	0.0	-0.2740E-04	-0.8898E-03	0.487	-0.8308E-01	0.8510E-02
21	0.1342E-02	0.1252E-01	-0.3500E-02	-0.8220E-02	0.8332E-13	-0.3645E-02	-0.2740E-04	-0.8898E-03	0.1067E-12	-0.8308E-01	0.8510E-02
22	0.1210E+01	0.7050E+01	-0.2740E-04	-0.8898E-03	0.3415E-17	0.0	-0.2740E-04	-0.8898E-03	0.3415E-17	-0.8308E-01	0.8510E-02
21	0.1342E-02	0.1252E-01	-0.3500E-02	-0.8220E-02	0.8332E-13	-0.3645E-02	-0.2740E-04	-0.8898E-03	0.1067E-12	-0.8308E-01	0.8510E-02
22	0.1210E+01	0.7050E+01	-0.2740E-04	-0.8898E-03	0.3415E-17	0.0	-0.2740E-04	-0.8898E-03	0.3415E-17	-0.8308E-01	0.8510E-02
21	0.1342E-02	0.1252E-01	-0.3500E-02	-0.8220E-02	0.8332E-13	-0.3645E-02	-0.2740E-04	-0.8898E-03	0.1067E-12	-0.8308E-01	0.8510E-02
22	0.1210E+01	0.7050E+01	-0.2740E-04	-0.8898E-03	0.3415E-17	0.0	-0.2740E-04	-0.8898E-03	0.3415E-17	-0.8308E-01	0.8510E-02
21	0.1342E-02	0.1252E-01	-0.3500E-02	-0.8220E-02	0.8332E-13	-0.3645E-02	-0.2740E-04	-0.8898E-03	0.1067E-12	-0.8308E-01	0.8510E-02
22	0.1210E+01	0.7050E+01	-0.2740E-04	-0.8898E-03	0.3415E-17	0.0	-0.2740E-04	-0.8898E-03	0.3415E-17	-0.8308E-01	0.8510E-02

EL	X-COORD	Y-COORD	SIGMA-XX	SIGMA-YY	SIGMA-XY	SIGMA-ZZ	SIGMA-1	SIGMA-2	SIGMA-3	ANGLE	YIELD
	STGTH-3	STGTH-4	STRAIN-XX	STRAIN-YY	GAMMA-XY	STRAIN-ZZ	STRAIN-1	STRAIN-2	STRAIN-3	ANGLE	STGTH-3
***** STRESSES AND STRAINS IN ELEMENT NUMBER 2 *****											
11	0.5008E-02	0.3355E-02	-0.3500E-02	-0.8220E-02	0.1334E-13	-0.3645E-02	-0.3500E-02	-0.8220E-02	0.1334E-13	-0.8308E-01	0.8510E-02
12	0.1210E+01	0.7050E+01	-0.2740E-04	-0.8898E-03	0.487	0.0	-0.2740E-04	-0.8898E-03	0.487	-0.8308E-01	0.8510E-02
21	0.1342E-02	0.1252E-01	-0.3500E-02	-0.8220E-02	0.8332E-13	-0.3645E-02	-0.2740E-04	-0.8898E-03	0.1067E-12	-0.8308E-01	0.8510E-02
22	0.1210E+01	0.7050E+01	-0.2740E-04	-0.8898E-03	0.3415E-17	0.0	-0.2740E-04	-0.8898E-03	0.3415E-17	-0.8308E-01	0.8510E-02
21	0.1342E-02	0.1252E-01	-0.3500E-02	-0.8220E-02	0.8332E-13	-0.3645E-02	-0.2740E-04	-0.8898E-03	0.1067E-12	-0.8308E-01	0.8510E-02
22	0.1210E+01	0.7050E+01	-0.2740E-04	-0.8898E-03	0.3415E-17	0.0	-0.2740E-04	-0.8898E-03	0.3415E-17	-0.8308E-01	0.8510E-02
21	0.1342E-02	0.1252E-01	-0.3500E-02	-0.8220E-02	0.8332E-13	-0.3645E-02	-0.2740E-04	-0.8898E-03	0.1067E-12	-0.8308E-01	0.8510E-02
22	0.1210E+01	0.7050E+01	-0.2740E-04	-0.8898E-03	0.3415E-17	0.0	-0.2740E-04	-0.8898E-03	0.3415E-17	-0.8308E-01	0.8510E-02
***** STRESSES AND STRAINS IN ELEMENT NUMBER 3 *****											
11	0.5008E-02	0.3355E-02	-0.3500E-02	-0.8220E-02	0.1334E-13	-0.3645E-02	-0.3500E-02	-0.8220E-02	0.1334E-13	-0.8308E-01	0.8510E-02
12	0.1210E+01	0.7050E+01	-0.2740E-04	-0.8898E-03	0.487	0.0	-0.2740E-04	-0.8898E-03	0.487	-0.8308E-01	0.8510E-02
21	0.1342E-02	0.1252E-01	-0.3500E-02	-0.8220E-02	0.8332E-13	-0.3645E-02	-0.2740E-04	-0.8898E-03	0.1067E-12	-0.8308E-01	0.8510E-02
22	0.1210E+01	0.7050E+01	-0.2740E-04	-0.8898E-03	0.3415E-17	0.0	-0.2740E-04	-0.8898E-03	0.3415E-17	-0.8308E-01	0.8510E-02
21	0.1342E-02	0.1252E-01	-0.3500E-02	-0.8220E-02	0.8332E-13	-0.3645E-02	-0.2740E-04	-0.8898E-03	0.1067E-12	-0.8308E-01	0.8510E-02
22	0.1210E+01	0.7050E+01	-0.2740E-04	-0.8898E-03	0.3415E-17	0.0	-0.2740E-04	-0.8898E-03	0.3415E-17	-0.8308E-01	0.8510E-02
21	0.1342E-02	0.1252E-01	-0.3500E-02	-0.8220E-02	0.8332E-13	-0.3645E-02	-0.2740E-04	-0.8898E-03	0.1067E-12	-0.8308E-01	0.8510E-02
22	0.1210E+01	0.7050E+01	-0.2740E-04	-0.8898E-03	0.3415E-17	0.0	-0.2740E-04	-0.8898E-03	0.3415E-17	-0.8308E-01	0.8510E-02
***** STRESSES AND STRAINS IN ELEMENT NUMBER 4 *****											
11	0.5008E-02	0.3355E-02	-0.3500E-02	-0.8220E-02	0.1334E-13	-0.3645E-02	-0.3500E-02	-0.8220E-02	0.1334E-13	-0.8308E-01	0.8510E-02
12	0.1210E+01	0.7050E+01	-0.2740E-04	-0.8898E-03	0.487	0.0	-0.2740E-04	-0.8898E-03	0.487	-0.8308E-01	0.8510E-02
21	0.1342E-02	0.1252E-01	-0.3500E-02	-0.8220E-02	0.8332E-13	-0.3645E-02	-0.2740E-04	-0.8898E-03	0.1067E-12	-0.8308E-01	0.8510E-02
22	0.1210E+01	0.7050E+01	-0.2740E-04	-0.8898E-03	0.3415E-17	0.0	-0.2740E-04	-0.8898E-03	0.3415E-17	-0.8308E-01	0.8510E-02
21	0.1342E-02	0.1252E-01	-0.3500E-02	-0.8220E-02	0.8332E-13	-0.3645E-02	-0.2740E-04	-0.8898E-03	0.1067E-12	-0.8308E-01	0.8510E-02
22	0.1210E+01	0.7050E+01	-0.2740E-04	-0.8898E-03	0.3415E-17	0.0	-0.2740E-04	-0.8898E-03	0.3415E-17	-0.8308E-01	0.8510E-02
21	0.1342E-02	0.1252E-01	-0.3500E-02	-0.8220E-02	0.8332E-13	-0.3645E-02	-0.2740E-04	-0.8898E-03	0.1067E-12	-0.8308E-01	0.8510E-02
22	0.1210E+01	0.7050E+01	-0.2740E-04	-0.8898E-03	0.3415E-17	0.0	-0.2740E-04	-0.8898E-03	0.3415E-17	-0.8308E-01	0.8510E-02

SUMMARY OF COMPUTER TIME

ITERATION	STIFF REFORM. (MILLI SEC.)	SOLUT (MILLI SEC.)	STRESS CALCUL. (MILLI SEC.)
1	95	6	31
TOTAL	95	6	31
TIME IN FOR THIS STEP = 138 MILLI SEC.			
TIME OUT FOR THIS STEP = 381 MILLI SEC.			
TIME ELAPSED FOR THIS STEP = 243 MILLI SEC.			

END OF STEP NUMBER 2

A COMPUTER PROGRAM FOR
SOIL ANALYSIS BY FINITE ELEMENT

```

S S S S S S S S S S      L A A A A A A A L      F F F F F F F F F F      E E E E E E E E E E
S S S S S S S S S S      L A A A A A A A A A      F F F F F F F F F F      E E E E E E E E E E
S S      A L      F F
S S      A A      F F
S S S S S S S S S S      A A A A A A A A A A      F F F F F F F      E E E E E E E E E E
S S S S S S S S S S      A A A A A A A A A A      F F F F F F F      E E E E E E E E E E
S S      A A      A A      F F      E E
S S      A A      A A      F F      E E
S S S S S S S S S S      A A      A A      F F      E E E E E E E E E E
S S S S S S S S S S      A A      A A      F F      E E E E E E E E E E

```

THIS PROGRAM IS DEVELOPED BY DAVE M CHAN
DEPARTMENT OF CIVIL ENGINEERING
UNIVERSITY OF ALBERTA, EDMONTON, ALBERTA

ALL RIGHTS RESERVED

WARNING: THE DEVELOPER OF THIS PROGRAM AND/OR THE UNIVERSITY OF ALBERTA MAKES NO WARRANTY WHATSOEVER, EXPRESSED OR IMPLIED, THAT THE PROGRAM AND ANY MODIFICATIONS, INCLUDING UPDATES, AND THE DOCUMENTATION ARE FREE FROM ERRORS AND/OR DEFECTS

GENERAL INFORMATION

PROJECT TITLE ANISOTROPIC PLANE STRAIN COMPRESSION TEST (NOVA BRITTLE MODEL)

DATE APR 1, 1987 TIME (HRS:MIN:SEC) 14:10:37

THIS IS A SMALL DEFORMATION NON-LINEAR ELASTIC-PLASTIC
TWO DIMENSIONAL PLANE STRAIN ANALYSIS

DOUBLE PRECISION ARITHMETICS

TOTAL STRESS ANALYSIS IEPP = 0

G O O D L U C K

TOTAL NUMBER OF STEPS IN THE ANALYSIS = 3 ANALYSIS STARTS AT STEP NUMBER = 3

TOTAL NUMBER OF ELEMENTS (NEL) = 4 TOTAL NUMBER OF NODES (NNOD) = 21

NUMBER OF INTEGRATION POINTS (NIP) = 2

NO. OF MATERIAL TYPE = 2 THICKNESS = 1.00000

```
IN-SITE DISPLACEMENT CODE (IDGR) = 1
IDGR = 0. DISPLACEMENTS WILL BE SET TO ZERO AFTER THE FIRST ANALYSIS
IDGR = 0. DISPLACEMENTS AND STRAINS WILL BE SET ZERO AFTER THE FIRST ANALYSIS
```

```
IN-SITE STRESS AND STRAIN CODE: (ISITE) = 0
ISITE = 0, NO INITIAL STRESS IS GIVEN
ISITE = 1, ONLY SIGMA-XX WILL BE GIVEN
ISITE = 2, SIGMA-XX AND SIGMA-YY WILL BE GIVEN
ISITE = 3, SIGMA-XX, SIGMA-YY AND SIGMA-XY WILL BE GIVEN
```

```

INFORMATION CODE (INFORM) =      0
INFORM = 1. EXECUTION WILL STOP AFTER DETERMINING THE SIZE OF THE GLOBAL MATRIX
INFORM = 0. PROGRAM PROCEED WITHOUT INTERRUPTION

```

```

PRINT-OUT CONTROL (IPRINT)
IPRINT(1) = 0 DISPLACEMENTS, STRESSES AND STRAINS PRINT-OUT
IF IPRINT(1) = 0, NO PRINT-OUT IS REQUIRED DURING EQUILIBRATION. ONLY FINAL VALUES ARE PRINTED
IF IPRINT(1) > 0, INTERMEDIATE RESULTS WILL BE GIVEN FOR EVERY IPRINT(1) ITERATION
IPRINT(2) = 0 UNBALANCED LOAD VECTOR DURING EQUILIBRATION
IF IPRINT(2) = 0, NO PRINT-OUT IS REQUIRED
IF IPRINT(2) > 0, UNBALANCED LOAD VECTOR WILL BE GIVEN FOR EVERY IPRINT(1) ITERATION ABOVE
IPRINT(3) = 0 FINAL UNBALANCED LOAD VECTOR
IF IPRINT(3) = 0, NO FINAL UNBALANCED LOAD VECTOR WILL BE PRINTED
IF IPRINT(3) > 0, FINAL UNBALANCED VECTOR WILL BE GIVEN
IPRINT(4) = 0 ELEMENT LOAD VECTOR
IF IPRINT(4) = 0, NO ELEMENT LOAD VECTOR WILL BE PRINTED
IF IPRINT(4) > 0, ELEMENT LOAD VECTOR FOR SURFACE TRACTION WILL BE PRINTED
IPRINT(5) = 0 LISTING OF DEGREES OF FREEDOM

```

266

```

BINARY OUTPUT CODE (ITAPB) = 0
IF ITAPB < OR = 0 ONLY CONVERGED RESULTS WILL BE STORED IN TAPE # 7
IF ITAPB > 0 RESULTS OF THE LATEST EQUILIBRIUM ITERATION, OR FINAL RESULTS OF THE LAST STEP,
WILL BE STORED IN ITAPB
PROGRAM RESTARTING CODE (IRES) = 0
IF IRES < OR = 0 PROGRAM RESTART AT THE BEGINNING OF THE LOADING STEP
IF IRES = 1 PROGRAM RESTART IN BETWEEN LOADING STEPS
ADDITIONAL OUTPUT CODE (ITAPB) = 0
IF ITAPB < = 0 NO ADDITIONAL OUTPUT IS REQUIRED
IF ITAPB > 0 ADDITIONAL OUTPUT INDICATING THE CONVERGING CHARACTERISTIC OF THE PROBLEM IS PROVIDED IN FILE ITAPB
NUMBER OF FILE PROVIDE IN RESTARTING FILE = 1

```

```

EQUILIBRIUM ITERATION
METHOD OF EQUILIBRIUM ITERATION: IEOM = 2
IEOM = 1 FULL NEWTON-RAPHSON ITERATION
IEOM = 2 FULL NEWTON EVERY OTHER ITERATION
IEOM = 3 FULL NEWTON EVERY SECOND ITERATION ETC
MAXIMUM NUMBER FOR EVERY LOAD INCREMENT: IMITEO = 15
CONVERGENCE TOLERANCE: IEOTOL = 1.0000E-03
IF IEOTOL IS LESS THAN OR EQUAL TO ZERO, DEFAULT IS 0.001
AITKEN ACCELERATOR DURING MODIFY NEWTON-RAPHSON ITERATION: IEIOT = 0

```

```

STRESS CALCULATION ITERATION
METHOD OF STRESS CALCULATION ITERATION (ISM) = 2
ISM = 1. EULER FORWARD SCHEME
ISM = 2. IMPROVED EULER SCHEME
ISM = 3. RUNGE-KUTTER METHOD
NUMBER OF SUBINTERVALS DURING STRESS CALCULATION (MITS) = 10
CONVERGENCE TOLERANCE (STOL) = 0.10000E-03
IF STOL IS LESS THAN OR EQUAL TO ZERO, DEFAULT IS 0.001

```

```

NO-TENSION ANALYSIS
CODE OF NO TENSION ANALYSIS (INTM) = 1
IF INTM=0 ALL MATERIALS ARE CAPABLE TO SUSTAIN TENSION
INTM = 0 SOME MATERIALS CANNOT SUSTAIN TENSION
MAXIMUM NUMBER OF ITERATION ALLOWED TO DETERMINE PRINCIPAL STRESSES IN 3- DIMENSIONAL ANALYSIS (MITNT) = 0
CONVERGENCE TOLERANCE IN 3-DIMENSIONAL ANALYSIS (TNTOL) = 0.10000E-14
IF TNTOL IS LESS THAN OR EQUAL TO ZERO, DEFAULT IS E-15

```

N O D D A L C O O R D I N A T E S														
NODE	X-COORD.	Y-COORD.	U	V	NODE	X-COORD.	Y-COORD.	U	V	NODE	X-COORD.	Y-COORD.	U	V
1	-0.635000E-02	-0.158750E-01	0	0	2	-0.635000E-02	-0.783750E-02	0	1	3	-0.635000E-02	0	0	0
4	-0.635000E-02	0.783750E-02	0	1	5	-0.635000E-02	0.158750E-01	0	1	6	-0.317500E-02	-0.158750E-01	1	0
7	-0.317500E-02	0	0	1	8	-0.317500E-02	0.158750E-01	1	1	9	0	-0.158750E-01	1	0
10	0	0.783750E-02	1	1	11	0	0	1	1	12	0	0.783750E-02	1	1
13	0	0.158750E-01	1	1	14	0.317500E-02	-0.158750E-01	1	0	15	0.317500E-02	0	0	0
16	0.317500E-02	-0.158750E-01	1	1	17	0.635000E-02	-0.158750E-01	1	0	18	0.635000E-02	-0.783750E-02	1	0
19	0.635000E-02	0	1	1	20	0.635000E-02	0.783750E-02	1	1	21	0.635000E-02	0.158750E-01	1	1

ELEMENT NUMBERING										ELEMENT NUMBERING																			
ELEM.					NODE NUMBERS					TP IS IC IB IM					ELEM.					NODE NUMBERS					TP IS IC IB IM				
1	3	11	13	5	8	4	2	1	0	1	1	2	1	9	11	3	6	10	7	2	2	1	0	0	1				
3	11	19	21	13	16	12	2	1	0	2	1	4	9	17	19	11	14	18	15	10	2	1	0	1	1				

MATERIAL PROPERTIES FOR MOD				LINEAR ELASTIC ISOTROPIC MODEL							
MAT. TYPE	MODEL	TEN. STGTH EMPTY	X BODY FORCE EMPTY	Y BODY FORCE EMPTY	Z BODY FORCE EMPTY	E-MODULUS EMPTY	POI. RATIO EMPTY	EMPTY	EMPTY		
2	1	0.0 0.0	0.0 0.0	0.0 0.0	0.0 0.0	0.1600 0.0	0.30400 0.0	0.0 0.0	0.0 0.0		

MATERIAL PROPERTIES FOR MODEL NUMBER 408				ELASTIC PLASTICS TRANSVERSELY ISOTROPIC MODEL					
MAT. TYPE	MODEL	TEN. STG. (H)	X-BODY FORCE	Y-BODY FORCE	Z-BODY FORCE	E (H) MOD.	POI. RATIO (H)	RED. ANGLE	
		COH(P)	COH(P)	FRIC(P)	FRIC(P)	COH(R)	FRIC(R)	E (V) MOD.	
		(MAXI)	(MINI)	(MAXI)	(MINI)			POI. RATIO (V)	
								SNEAR (V) MOD.	
1	408	0.0	0.0	0.0	0.0	91800	0.20400	88.000	
		88.100	7.0800	1.2100	1.18500	0	0.33100	24000	

TITLE FOR THIS STEP STEP 3 PRESCRIBE DISPL * 0 0000001 TOTAL PRESC DISPL * 0 0000001

NUMBER OF LINE INPUT FOR NEW ELEMENT 1 0
 NUMBER OF LINE INPUT FOR NEW NODES 1 0
 NUMBER OF LINE INPUT FOR SLOPE BOUNDARY 1 0
 NUMBER OF LINE INPUT FOR NEW POINT LOAD 1 0
 NUMBER OF LINE INPUT FOR NEW DISPLACEMENT 1 5
 NUMBER OF LOAD INCREMENTS 1 1
 LOAD INCREMENT BEGIN AT INCREMENT NUMBER 1 1

TOTAL DEGREE OF FREEDOM = 32 MAX HALF BANDWIDTH NO FL = 19 STIFFNESS MATRIX SIZE = 376

STEP NUMBER = 3 APPLIED LOAD INCREMENT = 1 ITERATION = 0

**PRESCRIBED DISPLACEMENT
FROM NODE TO NODE

DISPLACEMENT

5	5	2	-0.10000E-08
8	8	2	-0.10000E-08
13	13	2	-0.10000E-08
16	16	2	-0.10000E-08
21	21	2	-0.10000E-08

EQUILIBRIUM ITERATION 1 UNBALANCED LOAD = 0.40170E-14 DISPLACEMENT ERROR = 0.28891E-02
 EQUILIBRIUM ITERATION 2 UNBALANCED LOAD = 0.15902E+00 DISPLACEMENT ERROR = 0.14446E+00
 EQUILIBRIUM ITERATION 3 UNBALANCED LOAD = 0.16733E+00 DISPLACEMENT ERROR = 0.23248E-04

MODAL DISPLACEMENTS

MODE	U-DISPL	V-DISPL	MODE	U-DISPL	V-DISPL	MODE	U-DISPL	V-DISPL	MODE	U-DISPL	V-DISPL
1	0.0	0.0	2	0.0	-0.70875E-05	3	0.0	-0.141750E-04	4	0.0	-0.21262E-04
5	0.0	-0.283501E-04	10	0.0	1.12894E-05	11	0.0	1.12894E-05	12	0.0	2.25788E-05
8	0.0	2.25788E-05	14	0.0	3.38631E-05	15	0.0	3.38631E-05	16	0.0	3.38631E-05
13	0.0	2.25788E-05	18	0.0	4.61677E-05	19	0.0	4.61677E-05	20	0.0	4.61677E-05
17	0.0	5.1577E-05									
21	0.0	4.61677E-05									

ELEMENT STRESSES AND STRAINS

1J	X-COORD	Y-COORD	SIGMA-XX	SIGMA-YY	SIGMA-XY	SIGMA-ZZ	SIGMA-1	SIGMA-3	ANGLE	YIELD	STGTH-2
	STGTH-3	STGTH-4	STRAIN-XX	STRAIN-YY	GAMMA-XY	STRAIN-ZZ	STRAIN-1	STRAIN-3	ANGLE	STGTH-3	STGTH-6

***** STRESSES AND STRAINS IN ELEMENT NUMBER 1 *****

11	0.0008E-02	0.3558E-02	-0.3500E-02	-0.7220E-02	-0.5018E-13	-0.2872E+02	-0.3500E-02	-0.7220E+02	-0.7728E-13	0.0	0.0
12	0.0008E-02	0.1262E-01	-0.3500E-02	-0.7220E-02	-0.1080E-12	-0.2872E+02	-0.3500E-02	-0.7220E+02	-0.8047E-13	0.0	0.0
21	0.1342E-02	0.3558E-02	-0.3500E-02	-0.7220E-02	-0.8311E-13	-0.2872E+02	-0.3500E-02	-0.7220E+02	-0.1430E-12	0.0	0.0
22	0.1342E-02	0.1262E-01	-0.3500E-02	-0.7220E-02	-0.1875E-12	-0.2872E+02	-0.3500E-02	-0.7220E+02	-0.3039E-12	0.0	0.0
11	0.0008E-02	0.1262E-01	-0.3500E-02	-0.7220E-02	-0.1412E-12	-0.2872E+02	-0.3500E-02	-0.7220E+02	-0.2178E-12	0.0	0.0
12	0.0008E-02	0.3248E-02	-0.3500E-02	-0.7220E-02	-0.4834E-13	-0.2872E+02	-0.3500E-02	-0.7220E+02	-0.3853E-13	0.0	0.0
21	0.1342E-02	0.1262E-01	-0.3500E-02	-0.7220E-02	-0.2078E-12	-0.2872E+02	-0.3500E-02	-0.7220E+02	-0.4202E-13	0.0	0.0
22	0.1342E-02	0.3558E-02	-0.3500E-02	-0.7220E-02	-0.1003E-13	-0.2872E+02	-0.3500E-02	-0.7220E+02	-0.2302E-12	0.0	0.0
11	0.0008E-02	0.3558E-02	-0.3500E-02	-0.7220E-02	-0.8274E-13	-0.2872E+02	-0.3500E-02	-0.7220E+02	-0.8124E-13	0.0	0.0
12	0.0008E-02	0.1262E-01	-0.3500E-02	-0.7220E-02	-0.7115E-17	-0.2872E+02	-0.3500E-02	-0.7220E+02	-0.4884E-13	0.0	0.0
21	0.1342E-02	0.3558E-02	-0.3500E-02	-0.7220E-02	-0.8228E-13	-0.2872E+02	-0.3500E-02	-0.7220E+02	-0.8877E-14	0.0	0.0
22	0.1342E-02	0.1262E-01	-0.3500E-02	-0.7220E-02	-0.1885E-13	-0.2872E+02	-0.3500E-02	-0.7220E+02	-0.5446E-14	0.0	0.0
11	0.0008E-02	0.3558E-02	-0.3500E-02	-0.7220E-02	-0.8083E-13	-0.2872E+02	-0.3500E-02	-0.7220E+02	-0.1388E-13	0.0	0.0
12	0.0008E-02	0.1262E-01	-0.3500E-02	-0.7220E-02	-0.6157E-13	-0.2872E+02	-0.3500E-02	-0.7220E+02	-0.5528E-13	0.0	0.0
21	0.1342E-02	0.3558E-02	-0.3500E-02	-0.7220E-02	-0.1393E-13	-0.2872E+02	-0.3500E-02	-0.7220E+02	-0.3187E-13	0.0	0.0
22	0.1342E-02	0.1262E-01	-0.3500E-02	-0.7220E-02	-0.7438E-13	-0.2872E+02	-0.3500E-02	-0.7220E+02	-0.1148E-12	0.0	0.0
11	0.0008E-02	0.3558E-02	-0.3500E-02	-0.7220E-02	-0.8084E-13	-0.2872E+02	-0.3500E-02	-0.7220E+02	-0.1388E-13	0.0	0.0
12	0.0008E-02	0.1262E-01	-0.3500E-02	-0.7220E-02	-0.1479E-13	-0.2872E+02	-0.3500E-02	-0.7220E+02	-0.4840E-13	0.0	0.0
21	0.1342E-02	0.3558E-02	-0.3500E-02	-0.7220E-02	-0.1175E-17	-0.2872E+02	-0.3500E-02	-0.7220E+02	-0.2584E-13	0.0	0.0
22	0.1342E-02	0.1262E-01	-0.3500E-02	-0.7220E-02	-0.9767E-14	-0.2872E+02	-0.3500E-02	-0.7220E+02	-0.1607E-13	0.0	0.0
11	0.0008E-02	0.3558E-02	-0.3500E-02	-0.7220E-02	-0.3822E-13	-0.2872E+02	-0.3500E-02	-0.7220E+02	-0.8732E-14	0.0	0.0
12	0.0008E-02	0.1262E-01	-0.3500E-02	-0.7220E-02	-0.1280E-13	-0.2872E+02	-0.3500E-02	-0.7220E+02	-0.1971E-13	0.0	0.0
21	0.1342E-02	0.3558E-02	-0.3500E-02	-0.7220E-02	-0.6093E-18	-0.2872E+02	-0.3500E-02	-0.7220E+02	-0.1388E-13	0.0	0.0

SUMMARY OF COMPUTER TIME

ITERATION	STIFF REFORM (MILLI SEC.)	SOLUTION TIME (MILLI SEC.)	STRESS CALCUL (MILLI SEC.)
1	88	8	305
2	102	8	374
3	MC	1	325
TOTAL	3	200	13

TIME IN FOR THIS STEP = 148 MILLI SEC.
 TIME OUT FOR THIS STEP = 1478 MILLI SEC.
 TIME ELAPSED FOR THIS STEP = 1323 MILLI SEC.

END OF STEP NUMBER 3

269

```

BINARY OUTPUT CODE (ITAPB) = 0
IF ITAPB (OR = 0 ONLY CONVERGED RESULTS WILL BE STORED IN TAPE # 7
IF ITAPB > 0, RESULTS OF THE LATEST EQUILIBRIUM ITERATION, OR FINAL RESULTS OF THE LAST STEP
WILL BE STORED IN ITAPB
PROGRAM RESTARTING CODE (IRES) = 0
IF IRES (OR = 0, PROGRAM RESTART IN THE BEGINNING OF THE LOADING STEP
IF IRES = 1, PROGRAM RESTART IN BETWEEN LOADING STEPS
ADDITIONAL OUTPUT CODE (ITAPS) = 0
IF ITAPS = 0 NO ADDITIONAL OUTPUT IS REQUIRED
IF ITAPS > 0, ADDITIONAL OUTPUT INDICATING THE CONVERGING CHARACTERISTIC OF THE PROBLEM IS PROVIDED IN FILE ITAPS
NUMBER OF FILE PROVIDED IN RESTARTING FILE = 1

```

```

EQUILIBRIUM ITERATION
METHOD OF EQUILIBRIUM ITERATION (IEOM) = 2
IEOM = 1 FULL NEWTON-RAPHSON ITERATION
IEOM = 2 FULL NEWTON EVER OTHER ITERATION
IEOM = 3 FULL NEWTON EVER SECOND ITERATION ETC
MAXIMUM NUMBER FOR EVER INCR INCREMENT (MITEO) = 15
CONVERGENCE TOLERANCE (CTO) = 0.0000E-03
IF CTO IS LESS THAN OR EQUAL TO ZERO DEFAULT IS 0.001
ATTEN ACCELERATOR DURING MODIFY NEWTON-RAPHSON ITERATION (ICDT) = 0

```

```

      STRESS CALCULATION ITERATION
METHOD OF STRESS CALCULATION ITERATION (ISM) =      2
  ISM = 1. EULER FORWARD SCHEME
  ISM = 2. IMPROVED EULER SCHEME
  ISM = 3. RUNGE-KUTTER METHOD
NUMBER OF SUBINTERVALS DURING STRESS CALCULATION (MITS) =      10
CONVERGENCE TOLERANCE (STOL) =      0.1000E-03
IF STOL IS LESS THAN OR EQUAL TO ZERO, DEFAULT IS 0.001

```

```

      NO-TENSION ANALYSIS
CODE OF NO TENSION ANALYSIS (INTMI) = 1
  IF INTMI ALL MATERIALS ARE CAPABLE TO SUSTAIN TENSION
  INTM > 0 SOME MATERIALS CANNOT SUSTAIN TENSION
MAXIMUM NUMBER OF ITERATION ALLOWED TO DETERMINE PRINCIPAL STRESSES IN 3- DIMENSIONAL ANALYSIS (MITNT) = 0
CONVERGENCE TOLERANCE IN 3-DIMENSIONAL ANALYSIS (TNYOL) = 0.0000E-14
  IF INTOL IS LESS THAN OR EQUAL TO ZERO, DEFAULT IS E-15

```

N O D E C O O R D I N A T E S					N O D E C O O R D I N A T E S				
NODE	X-COORD	Y-COORD	U	V	NODE	X-COORD	Y-COORD	U	V
1	-0.635000E-02	-0.158750E-01	0	0	2	-0.635000E-02	-0.753750E-02	0	1
4	-0.635000E-02	-0.753750E-02	0	1	5	-0.635000E-02	-0.158750E-01	0	1
10	-0.317500E-02	-0.158750E-01	1	1	8	-0.317500E-02	-0.753750E-02	1	1
7	0.0	-0.753750E-02	1	1	11	0.0	0.0	1	1
10	0.0	-0.158750E-01	1	1	14	-0.317500E-02	-0.158750E-01	1	0
12	0.0	-0.158750E-01	1	1	16	-0.635000E-02	-0.158750E-01	1	0
18	-0.317500E-02	-0.158750E-01	1	1	17	-0.635000E-02	-0.753750E-02	1	1
19	-0.635000E-02	0.0	1	1	20	-0.635000E-02	-0.753750E-02	1	1

ELEMENT NUMBERING										NODE NUMBERS										TP IS IG IS IM																																																											
ELE										ELE										ELE																																																											
1	3	11	13	5	7	12	8	4	2	1	0	1	1	2	1	9	11	3	5	10	7	2	2	1	0	0	1																																																				
3	11	18	21	13	13	20	18	12	2	1	0	2	1	4	9	17	19	11	14	18	18	10	2	1	0	1	1																																																				
MATERIAL PROPERTIES FOR MODEL NUMBER 1										LINEAR ELASTIC ISOTROPIC MODEL																																																																					
MAT. TYPE										MODEL										TEN. STGTH X BODY FORCE Y BODY FORCE Z BODY FORCE										E-MODULUS										POI. RATIO										EMPTY																													
										EMPTY										EMPTY										EMPTY										EMPTY										EMPTY																													
2										1										0.0										0.0										0.0										0.0										0.0																			
										0.0										0.0										0.0										0.0										0.0										0.0																			
MATERIAL PROPERTIES FOR MODEL NUMBER 408										ELASTIC PLASTIC TRANSVERSELY ISOTROPIC MODEL																																																																					
MAT. TYPE										MODEL										TEN. STGTH X-BODY FORCE Y-BODY FORCE Z-BODY FORCE										E(M) MOD.										POI. RATIO(M)										SEC. ANGLE																													
																				CON(P) CON(P) PRCT(P) PRCT(P) CON(R) PRCT(R)										E(V) MOD.										POI. RATIO(V)										SHEAR(V) MOD.																													
										(MAXI) (MINI) (MAXI) (MINI)																																																																					
1										408										0.0										0.0										0.0										0.0																													
										88.100										7.0800										1.2100										18600										18600										58100										24000.									

TITLE FOR THIS STEP

STEP 4 PRESCRIBE DISPLACEMENTS=0.00005 TOTAL DISPL. INC. OCCURED

NUMBER OF LINE INPUT FOR NEW ELEMENT 1 0
NUMBER OF LINE INPUT FOR NEW NODES 2 0
NUMBER OF LINE INPUT FOR SLOPE BOUNDARY 3 0
NUMBER OF LINE INPUT FOR NEW POINT LOAD 4 0
NUMBER OF LINE INPUT FOR NEW DISPLACEMENT 5 0
NUMBER OF LOAD INCREMENTS 6 1
LOCAL INCREMENT BEGIN AT INCREMENT NUMBER 7 1

TOTAL DEGREE OF FREEDOM = 32 MAX HALF BANDWIDTH NS DIA EL = 19 STIFFNESS MATRIX SIZE = 376

STEP NUMBER = 4 APPLIED LOAD INCREMENT = 1 ITERATION = 0

APPROXIMATED DISPLACEMENT FROM NODE TO NODE C D V DISPLACEMENT

S	S	2	-0.00000E-04
8	8	2	-0.00000E-04
12	12	2	-0.00000E-04
16	16	2	-0.00000E-04
20	20	2	-0.00000E-04

EQUILIBRIUM ITERATION	1	UNBALANCED LOAD =	0.18738E+00	DISPLACEMENT ERROR =	0.14007E+00
EQUILIBRIUM ITERATION	2	UNBALANCED LOAD =	0.14265E+01	DISPLACEMENT ERROR =	0.34288E+00
EQUILIBRIUM ITERATION	3	UNBALANCED LOAD =	0.18738E+00	DISPLACEMENT ERROR =	0.14155E-12

NODAL DISPLACEMENTS

NODE	U-DISPL	V-DISPL	NODE	U-DISPL	V-DISPL	NODE	U-DISPL	V-DISPL	NODE	U-DISPL	V-DISPL
1	0.0	0.0	2	0.0	-0.18587E-04	3	0.0	-0.38175E-04	4	0.0	-0.58782E-04
5	0.0	-0.78350E-04	6	0.0	1.14432E-04	7	0.0	1.14432E-04	8	0.0	1.14432E-04
9	0.22868E-04	0.0	10	0.22868E-04	-0.18587E-04	11	0.22868E-04	-0.38175E-04	12	0.22868E-04	-0.58782E-04
13	0.22868E-04	-0.78350E-04	14	0.34325E-04	0.0	15	0.34325E-04	-0.38175E-04	16	0.34325E-04	-0.58782E-04
17	0.45772E-04	0.0	18	0.45772E-04	-0.18587E-04	19	0.45772E-04	-0.38175E-04	20	0.45772E-04	-0.58782E-04
21	0.45772E-04	-0.78350E-04									

ELEMENT STRESSES AND STRAINS

EL	X-COORD	Y-COORD	SIGMA-XX	SIGMA-YY	SIGMA-XY	SIGMA-XX	SIGMA-YY	SIGMA-XY	ANGLE	YIELD	STGTH-2
	STGTH-3	STGTH-4	STRAIN-XX	STRAIN-YY	GAMMA-XY	STRAIN-XX	STRAIN-YY	STRAIN-XY	STRAIN-3	STGTH-5	STGTH-6

***** STRESSES AND STRAINS IN ELEMENT NUMBER 1 *****

11	0.0000E+00	0.0000E+00	-0.3500E+02	-0.7220E+02	-0.2400E-13	-0.2872E+02	-0.3500E+02	-0.7220E+02	-0.2400E-13	0.0	0.0
12	0.0000E+00	0.0000E+00	-0.3500E+02	-0.7220E+02	-0.2400E-13	-0.2872E+02	-0.3500E+02	-0.7220E+02	-0.2400E-13	0.0	0.0
21	0.0000E+00	0.0000E+00	-0.3500E+02	-0.7220E+02	-0.2400E-13	-0.2872E+02	-0.3500E+02	-0.7220E+02	-0.2400E-13	0.0	0.0
22	0.0000E+00	0.0000E+00	-0.3500E+02	-0.7220E+02	-0.2400E-13	-0.2872E+02	-0.3500E+02	-0.7220E+02	-0.2400E-13	0.0	0.0
11	0.0000E+00	0.0000E+00	-0.3500E+02	-0.7220E+02	-0.2400E-13	-0.2872E+02	-0.3500E+02	-0.7220E+02	-0.2400E-13	0.0	0.0
12	0.0000E+00	0.0000E+00	-0.3500E+02	-0.7220E+02	-0.2400E-13	-0.2872E+02	-0.3500E+02	-0.7220E+02	-0.2400E-13	0.0	0.0
21	0.0000E+00	0.0000E+00	-0.3500E+02	-0.7220E+02	-0.2400E-13	-0.2872E+02	-0.3500E+02	-0.7220E+02	-0.2400E-13	0.0	0.0
22	0.0000E+00	0.0000E+00	-0.3500E+02	-0.7220E+02	-0.2400E-13	-0.2872E+02	-0.3500E+02	-0.7220E+02	-0.2400E-13	0.0	0.0
11	0.0000E+00	0.0000E+00	-0.3500E+02	-0.7220E+02	-0.2400E-13	-0.2872E+02	-0.3500E+02	-0.7220E+02	-0.2400E-13	0.0	0.0
12	0.0000E+00	0.0000E+00	-0.3500E+02	-0.7220E+02	-0.2400E-13	-0.2872E+02	-0.3500E+02	-0.7220E+02	-0.2400E-13	0.0	0.0
21	0.0000E+00	0.0000E+00	-0.3500E+02	-0.7220E+02	-0.2400E-13	-0.2872E+02	-0.3500E+02	-0.7220E+02	-0.2400E-13	0.0	0.0
22	0.0000E+00	0.0000E+00	-0.3500E+02	-0.7220E+02	-0.2400E-13	-0.2872E+02	-0.3500E+02	-0.7220E+02	-0.2400E-13	0.0	0.0
11	0.0000E+00	0.0000E+00	-0.3500E+02	-0.7220E+02	-0.2400E-13	-0.2872E+02	-0.3500E+02	-0.7220E+02	-0.2400E-13	0.0	0.0
12	0.0000E+00	0.0000E+00	-0.3500E+02	-0.7220E+02	-0.2400E-13	-0.2872E+02	-0.3500E+02	-0.7220E+02	-0.2400E-13	0.0	0.0
21	0.0000E+00	0.0000E+00	-0.3500E+02	-0.7220E+02	-0.2400E-13	-0.2872E+02	-0.3500E+02	-0.7220E+02	-0.2400E-13	0.0	0.0
22	0.0000E+00	0.0000E+00	-0.3500E+02	-0.7220E+02	-0.2400E-13	-0.2872E+02	-0.3500E+02	-0.7220E+02	-0.2400E-13	0.0	0.0

SUMMARY OF COMPUTER TIME

ITERATION	STEP REFORM (MILLI SEC)	SOLUTION TIME (MILLI SEC)	STRESS CALCUL (MILLI SEC)
1	94	5	253
2	98	5	261
3	NO		261
TOTAL	190	11	775

TIME IN FOR THIS STEP = 144 MILLI SEC.
TIME OUT FOR THIS STEP = 1270 MILLI SEC.
TIME ELAPSED FOR THIS STEP = 1128 MILLI SEC.

END OF STEP NUMBER 4

```

.....
..
..          A COMPUTER PROGRAM FOR
..        SOIL ANALYSIS BY FINITE ELEMENT
..
..
..        SSSSSSSSSSSS  AAAAAAAAAA  FFFFFFFFFFFFF  EEEEEEEEEEEF
..        SSSSSSSSSSSS  AAAAAAAAAA  FFFFFFFFFFFFF  EEEEEEEEEEEF
..        SS           AA          LL          FF          EE
..        SS           AA          AA          FF          EE
..        SSSSSSSSSSSS  AAAAAAAAAA  FFFFFFFFFFFFF  EEEEEEEEEEEF
..        SSSSSSSSSSSS  AAAAAAAAAA  FFFFFFFFFFFFF  EEEEEEEEEEEF
..        SS           AA          AA          FF          EE
..        SS           AA          AA          FF          EE
..        SSSSSSSSSSSS  AA          AA          FF          EEEEEEEEEEEF
..        SSSSSSSSSSSS  AA          AA          FF          EEEEEEEEEEEF
..
..        THIS PROGRAM IS DEVELOPED BY DAVE N. CHAN
..        DEPARTMENT OF CIVIL ENGINEERING
..        UNIVERSITY OF ALBERTA, EDMONTON, ALBERTA
..
..        ALL RIGHTS RESERVED
..
..
.....

```

WARNING : THE DEVELOPER OF THIS PROGRAM AND/OR THE UNIVERSITY OF ALBERTA MAKES NO WARRANTY WHATSOEVER, EXPRESSED OR IMPLIED, THAT THE PROGRAM AND ANY MODIFICATIONS, INCLUDING UPDATES, AND THE DOCUMENTATION ARE FREE FROM ERRORS AND/OR DEFECTS

GENERAL INFORMATION

PROJECT TITLE : ANISOTROPIC PLANE STRAIN COMPRESSION TEST (NOVA BRITTLE MODEL)

DATE : APR 1, 1987 TIME (HRS:MIN:SEC) : 14:19:48

THIS IS A SMALL DEFORMATION NON-LINEAR ELASTIC-PLASTIC
TWO DIMENSIONAL PLANE STRAIN ANALYSIS

DOUBLE PRECISION ARITHMETICS

TOTAL STRESS ANALYSIS IEFF = 0

GOOD LUCK

TOTAL NUMBER OF STEPS IN THE ANALYSIS = 5 ANALYSIS STARTS AT STEP NUMBER = 5

TOTAL NUMBER OF ELEMENTS (NEL) = 4 TOTAL NUMBER OF NODES (NNOD) = 21

NUMBER OF INTEGRATION POINTS (NIP) = 2

NO. OF MATERIAL TYPE = 2 THICKNESS = 1.00000

IN-SITE DISPLACEMENT CODE: (IDGR) = 1
IDGR = 0, DISPLACEMENTS WILL BE SET TO ZERO AFTER THE FIRST ANALYSIS
IDGR < 0, DISPLACEMENTS AND STRAINS WILL BE SET ZERO AFTER THE FIRST ANALYSIS

IN-SITE STRESS AND STRAIN CODE: (ISITE) = 0
ISITE = 0, NO INITIAL STRESS IS GIVEN
ISITE = 1, ONLY SIGMA-XX WILL BE GIVEN
ISITE = 2, SIGMA-XX AND SIGMA-VY WILL BE GIVEN
ISITE = 3, SIGMA-XX, SIGMA-VY AND SIGMA-XY WILL BE GIVEN

INFORMATION CODE (INFORM) = 0
INFORM = 1, EXECUTION WILL STOP AFTER DETERMINING THE SIZE OF THE GLOBAL MATRIX
INFORM = 0, PROGRAM PROCEED WITHOUT INTERRUPTION

PRINT-OUT CONTROL (IPRINT)

```

IPRINT(1) = 0    DISPLACEMENTS, STRESSES AND STRAINS PRINT-OUT
IF IPRINT(1) = 0, NO PRINT-OUT IS REQUIRED DURING EQUILB. ITERATION. ONLY FINAL VALUES ARE PRINTED
IF IPRINT(1) > 0, INTERMEDIATE RESULTS WILL BE GIVEN FOR EVERY IPRINT(1) ITERATION
IPRINT(2) = 0    UNBALANCED LOAD VECTOR DURING EQUILB. ITERATION
IF IPRINT(2) = 0, NO PRINT-OUT IS REQUIRED
IF IPRINT(2) > 0, UNBALANCED LOAD VECTOR WILL BE GIVEN FOR EVERY IPRINT(1) ITERATION ABOVE
IPRINT(3) = 0    FINAL UNBALANCED LOAD VECTOR
IF IPRINT(3) = 0, NO FINAL UNBALANCED LOAD VECTOR WILL BE PRINTED
IF IPRINT(3) > 0, FINAL UNBALANCED LOAD VECTOR WILL BE GIVEN
IPRINT(4) = 0    ELEMENT LOAD VECTOR
IF IPRINT(4) = 0, NO ELEMENT LOAD VECTOR WILL BE PRINTED
IF IPRINT(4) > 0, ELEMENT LOAD VECTOR FOR SURFACE TRACTION WILL BE PRINTED
IPRINT(5) = 0    LISTING OF DEGREES OF FREEDOM

```

IF IPRINTS = 0, NO LISTING OF DEGREES OF FREEDOM WILL BE PRINTED
 IF IPRINTS > 0, LISTING OF DEGREES OF FREEDOM WILL BE PRINTED

BINARY OUTPUT CODE (ITAPB) = 1
 IF ITAPB < 0, ONLY CONVERGED RESULTS WILL BE STORED IN TAPE # 7
 IF ITAPB > 0, RESULTS OF THE LATEST EQUILIBRIUM ITERATION, OR FINAL RESULTS OF THE LAST STEP,
 WILL BE STORED IN ITAPB
 PROGRAM RESTARTING CODE (IRES) = 0
 IF IRES < 0, PROGRAM RESTART AT THE BEGINNING OF THE LOADING STEP
 IF IRES = 1, PROGRAM RESTART IN BETWEEN LOADING STEPS
 ADDITIONAL OUTPUT CODE (ITAPB) = 0
 IF ITAPB < 0, NO ADDITIONAL OUTPUT IS REQUIRED
 IF ITAPB > 0, ADDITIONAL OUTPUT INDICATING THE CONVERGING CHARACTERISTIC OF THE PROBLEM IS PROVIDED IN FILE ITAPB

NUMBER OF FILE PROVIDED IN RESTARTING FILE = 1

EQUILIBRIUM ITERATION
 METHOD OF EQUILIBRIUM ITERATION (IEOM) = 2
 IEOM = 1, FULL NEWTON-RAPHSON ITERATION
 IEOM = 2, FULL NEWTON EVERY OTHER ITERATION
 IEOM = 3, FULL NEWTON EVERY SECOND ITERATION ETC
 MAXIMUM NUMBER FOR EVERY LOAD INCREMENT (IMITEO) = 15
 CONVERGENCE TOLERANCE (ECTOL) = 0.10000E-03
 IF ECTOL IS LESS THAN OR EQUAL TO ZERO, DEFAULT IS 0.001
 AITKEN ACCELERATOR DURING MODIFY NEWTON-RAPHSON ITERATION (IEQIT) = 0

STRESS CALCULATION ITERATION
 METHOD OF STRESS CALCULATION ITERATION (ISM) = 2
 ISM = 1, EULER FORWARD SCHEME
 ISM = 2, IMPROVED EULER SCHEME
 ISM = 3, RUNGE-KUTTER METHOD
 NUMBER OF SUBINTERVALS DURING STRESS CALCULATION (IMITS) = 10
 CONVERGENCE TOLERANCE (STOL) = 0.10000E-03
 IF STOL IS LESS THAN OR EQUAL TO ZERO, DEFAULT IS 0.001

NO-TENSION ANALYSIS
 CODE OF NO-TENSION ANALYSIS (INTMI) = 1
 IF INTMI ALL MATERIALS ARE CAPABLE TO SUSTAIN TENSION
 INTMI = 0, SOME MATERIALS CANNOT SUSTAIN TENSION
 MAXIMUM NUMBER OF ITERATION ALLOWED TO DETERMINE PRINCIPAL STRESSES IN 3-DIMENSIONAL ANALYSIS (MITNTI) = 0
 CONVERGENCE TOLERANCE IN 3-DIMENSIONAL ANALYSIS (INTOLI) = 0.10000E-14
 IF INTOLI IS LESS THAN OR EQUAL TO ZERO, DEFAULT IS 2E-16

MODAL COORDINATES

NODE	X-COORD	Y-COORD	U	V	NODE	X-COORD	Y-COORD	U	V	NODE	X-COORD	Y-COORD	U	V
1	-0.836000E-02	-0.158750E-01	0	0	2	-0.836000E-02	-0.793750E-02	0	1	3	-0.836000E-02	0.0	0	1
4	-0.836000E-02	0.793750E-02	0	1	5	-0.836000E-02	0.158750E-01	0	1	6	-0.836000E-02	-0.158750E-01	1	0
7	-0.317500E-02	0.0	1	1	8	-0.317500E-02	0.158750E-01	1	1	9	0.0	-0.158750E-01	1	0
10	0.0	-0.793750E-02	1	1	11	0.0	0.0	1	1	12	0.0	0.793750E-02	1	1
13	0.0	0.158750E-01	1	1	14	0.317500E-02	-0.158750E-01	1	0	15	0.317500E-02	0.0	1	1
16	0.317500E-02	0.158750E-01	1	1	17	0.836000E-02	-0.158750E-01	1	0	18	0.836000E-02	-0.793750E-02	1	1
19	0.836000E-02	0.0	1	1	20	0.836000E-02	0.793750E-02	1	1	21	0.836000E-02	0.158750E-01	1	1

ELEMENT NUMBERING

ELS	NODE NUMBERS								TP	IS	IC	IB	IM	ELS	NODE NUMBERS								TP	IS	IC	IB	IM
1	3	11	13	5	7	12	8	4	2	1	0	1	1	2	1	9	11	3	6	10	7	2	2	1	0	0	1
3	11	19	21	13	15	20	18	12	2	1	0	2	1	4	9	17	19	11	14	16	15	10	2	1	0	1	1

MATERIAL PROPERTIES FOR MODEL NUMBER 1

LINEAR ELASTIC ISOTROPIC MODEL

MAT	TYPE	MODEL	TEN	STGYH	X BODY	FORCE	Y BODY	FORCE	Z BODY	FORCE	E-MODULUS	POI. RATIO	EMPTY	EMPTY
2	1	0.0	0.0	0.0	0.0	0.0	0.0	0.0	0.0	0.0	91500	0.20400	0.0	0.0
		0.0	0.0	0.0	0.0	0.0	0.0	0.0	0.0	0.0	0.0	0.0	0.0	0.0

MATERIAL PROPERTIES FOR MODEL NUMBER 405

ELASTICS PLASTICS TRANSVERSELY ISOTROPIC MODEL

MAT	TYPE	MODEL	TEN	STGYH	Y-BODY	FORCE	Y-BODY	FORCE	Z-BODY	FORCE	E(H) MOD.	POI. RATIO(H)	2RD. ANGLE
			CON(P)	CON(P)	FRIC(P)	CON(R)	FRIC(R)	CON(R)	FRIC(R)	CON(R)	FRIC(R)	POI. RATIO(V)	SHEAR(V) MOD.
			(MAXI)	(MINI)	(MAXI)	(MINI)	(MAXI)	(MINI)	(MAXI)	(MINI)	(MAXI)	(MINI)	(MAXI)
1	405	0.0	0.0	0.0	0.0	0.0	0.0	0.0	0.0	0.0	91500	0.20400	55.000
		55.100	7.0500	1.2100	16800	0.0	16800	55100	0.33100	24000			

ANALYSIS STEP NUMBER 5 *****

273

TITLE FOR THIS STEP STEP 5 PRESCRIBE DISPLACEMENTS=0.00010 TOTAL DISPL =0.0001001

NUMBER OF LINE INPUT FOR NEW ELEMENT = 0
NUMBER OF LINE INPUT FOR NEW NODES = 0
NUMBER OF LINE INPUT FOR SLOPE BOUNDARY = 0
NUMBER OF LINE INPUT FOR NEW POINT LOAD = 5
NUMBER OF LINE INPUT FOR NEW DISPLACEMENT = 1
NUMBER OF LOAD INCREMENTS = 1
LOAD INCREMENT BEGIN AT INCREMENT NUMBER = 1

TOTAL DEGREE OF FREEDOM = 32 MAX HALF BANDWIDTH NO DIA EL = 15 STIFFNESS MATRIX SIZE = 376

STEP NUMBER = 5 APPLIED LOAD INCREMENT = 1 ITERATION = 0

***PRESCRIBED DISPLACEMENT
FROM NODE TO NODE D.O.F DISPLACEMENT
5 5 2 -0.10000E-03
8 8 2 -0.10000E-03
13 13 2 -0.10000E-03
16 16 2 -0.10000E-03
21 21 2 -0.10000E-03

EQUILIBRIUM ITERATION 1 UNBALANCED LOAD = 0.15735E+00 DISPLACEMENT ERROR = 0.53560E+00
EQUILIBRIUM ITERATION 2 UNBALANCED LOAD = 0.28452E+01 DISPLACEMENT ERROR = 0.25308E+00
EQUILIBRIUM ITERATION 3 UNBALANCED LOAD = 0.15735E+00 DISPLACEMENT ERROR = 0.31180E-12

NODAL DISPLACEMENTS

NODE	U-DISPL	V-DISPL	NODE	U-DISPL	V-DISPL	NODE	U-DISPL	V-DISPL	NODE	U-DISPL	V-DISPL
1 0 0	0 0	2 0 0	-0.445875E-04	3 0 0	-0.891750E-04	4 0 0	-0.133763E-03				
5 0 0	-0.178350E-03	6 0 0	0.320718E-04	7 0 0	0.320718E-04	8 0 0	0.320718E-04				
8 0.841432E-04	0 0	10 0.841432E-04	-0.445875E-04	11 0.841432E-04	-0.891750E-04	12 0.841432E-04	-0.133763E-03				
13 0.841432E-04	-0.178350E-03	14 0.841432E-04	-0.445875E-04	15 0.841432E-04	-0.891750E-04	16 0.841432E-04	-0.133763E-03				
17 0.128288E-03	0 0	18 0.128288E-03	-0.445875E-04	19 0.128288E-03	-0.891750E-04	20 0.128288E-03	-0.133763E-03				
21 0.128288E-03	-0.178350E-03										

ELEMENT STRESSES AND STRAINS

EL	X-COORD	Y-COORD	SIGMA-XX	SIGMA-YY	SIGMA-XY	SIGMA-ZZ	SIGMA-1	SIGMA-3	ANGLE	YIELD	STGTH-2	STGTH-6
	STGTH-3	STGTH-4	STRAIN-XX	STRAIN-YY	GAMMA-XY	STRAIN-22	STRAIN-1	STRAIN-3		STGTH-8	STGTH-9	

***** STRESSES AND STRAINS IN ELEMENT NUMBER *****

11-0.5008E-02	0.3355E-02	-0.3500E-02	-0.7220E-02	-0.2831E-13	-0.2872E-02	-0.3500E-02	-0.7220E-02	-0.4380E-13	0 0	0.1850E+00	0.1722E-05
0.8880E+00	0 0	0.1010E-01	-0.5517E-02	-0.2321E-15	0 0	0.1010E-01	-0.5517E-02	-0.4229E-13	0 0	0.1850E+00	0.1722E-05
12-0.5008E-02	0.1252E-01	-0.3500E-02	-0.7220E-02	0.1032E-12	-0.2872E-02	-0.3500E-02	-0.7220E-02	0.1889E-12	0 0	0.1850E+00	0.1722E-05
0.8880E+00	0 0	0.1010E-01	-0.5517E-02	0.5537E-15	0 0	0.1010E-01	-0.5517E-02	0.1027E-12	0 0	0.1850E+00	0.1722E-05
21-0.1342E-02	0.3355E-02	-0.3500E-02	-0.7220E-02	0.1799E-12	-0.2872E-02	-0.3500E-02	-0.7220E-02	0.2771E-12	0 0	0.1850E+00	0.1722E-05
0.8880E+00	0 0	0.1010E-01	-0.5517E-02	0.1224E-15	0 0	0.1010E-01	-0.5517E-02	0.2231E-12	0 0	0.1850E+00	0.1722E-05
22-0.1342E-02	0.1252E-01	-0.3500E-02	-0.7220E-02	0.2842E-15	-0.2872E-02	-0.3500E-02	-0.7220E-02	0.4390E-12	0 0	0.1850E+00	0.1722E-05
0.8880E+00	0 0	0.1010E-01	-0.5517E-02	0.1740E-15	0 0	0.1010E-01	-0.5517E-02	-0.3170E-12	0 0	0.1850E+00	0.1722E-05
***** STRESSES AND STRAINS IN ELEMENT NUMBER *****											
11-0.5008E-02	0.1252E-01	-0.3500E-02	-0.7220E-02	0.1025E-12	-0.2872E-02	-0.3500E-02	-0.7220E-02	0.1576E-12	0 0	0.1850E+00	0.1722E-05
0.8880E+00	0 0	0.1010E-01	-0.5517E-02	0.5448E-15	0 0	0.1010E-01	-0.5517E-02	0.1175E-12	0 0	0.1850E+00	0.1722E-05
12-0.5008E-02	0.3355E-02	-0.3500E-02	-0.7220E-02	-0.4637E-13	-0.2872E-02	-0.3500E-02	-0.7220E-02	0.7142E-13	0 0	0.1850E+00	0.1722E-05
0.8880E+00	0 0	0.1010E-01	-0.5517E-02	-0.3098E-15	0 0	0.1010E-01	-0.5517E-02	-0.5442E-13	0 0	0.1850E+00	0.1722E-05
21-0.1342E-02	0.1252E-01	-0.3500E-02	-0.7220E-02	-0.2842E-12	-0.2872E-02	-0.3500E-02	-0.7220E-02	-0.4531E-12	0 0	0.1850E+00	0.1722E-05
0.8880E+00	0 0	0.1010E-01	-0.5517E-02	-0.1853E-15	0 0	0.1010E-01	-0.5517E-02	-0.3377E-12	0 0	0.1850E+00	0.1722E-05
22-0.1342E-02	0.3355E-02	-0.3500E-02	-0.7220E-02	0.5898E-13	-0.2872E-02	-0.3500E-02	-0.7220E-02	0.1524E-12	0 0	0.1850E+00	0.1722E-05
0.8880E+00	0 0	0.1010E-01	-0.5517E-02	0.5537E-15	0 0	0.1010E-01	-0.5517E-02	0.1084E-12	0 0	0.1850E+00	0.1722E-05
***** STRESSES AND STRAINS IN ELEMENT NUMBER *****											
11-0.1342E-02	0.3355E-02	-0.3500E-02	-0.7220E-02	0.5185E-13	-0.2872E-02	-0.3500E-02	-0.7220E-02	0.9527E-13	0 0	0.1850E+00	0.1722E-05
0.8880E+00	0 0	0.1010E-01	-0.5517E-02	0.5005E-15	0 0	0.1010E-01	-0.5517E-02	0.7305E-13	0 0	0.1850E+00	0.1722E-05
12-0.1342E-02	0.1252E-01	-0.3500E-02	-0.7220E-02	-0.3274E-13	-0.2872E-02	-0.3500E-02	-0.7220E-02	-0.5042E-13	0 0	0.1850E+00	0.1722E-05
0.8880E+00	0 0	0.1010E-01	-0.5517E-02	-0.2258E-15	0 0	0.1010E-01	-0.5517E-02	-0.4133E-13	0 0	0.1850E+00	0.1722E-05
21-0.5008E-02	0.3355E-02	-0.3500E-02	-0.7220E-02	-0.5558E-13	-0.2872E-02	-0.3500E-02	-0.7220E-02	-0.1011E-12	0 0	0.1850E+00	0.1722E-05
0.8880E+00	0 0	0.1010E-01	-0.5517E-02	-0.3635E-15	0 0	0.1010E-01	-0.5517E-02	-0.8989E-13	0 0	0.1850E+00	0.1722E-05
22-0.5008E-02	0.1252E-01	-0.3500E-02	-0.7220E-02	0.1378E-12	-0.2872E-02	-0.3500E-02	-0.7220E-02	0.2124E-12	0 0	0.1850E+00	0.1722E-05
0.8880E+00	0 0	0.1010E-01	-0.5517E-02	0.5111E-15	0 0	0.1010E-01	-0.5517E-02	0.1551E-12	0 0	0.1850E+00	0.1722E-05
***** STRESSES AND STRAINS IN ELEMENT NUMBER *****											
11-0.1342E-02	0.1252E-01	-0.3500E-02	-0.7220E-02	-0.4283E-13	-0.2872E-02	-0.3500E-02	-0.7220E-02	-0.5951E-13	0 0	0.1850E+00	0.1722E-05
0.8880E+00	0 0	0.1010E-01	-0.5517E-02	-0.3290E-15	0 0	0.1010E-01	-0.5517E-02	-0.5995E-13	0 0	0.1850E+00	0.1722E-05
12-0.1342E-02	0.3355E-02	-0.3500E-02	-0.7220E-02	-0.5458E-14	-0.2872E-02	-0.3500E-02	-0.7220E-02	-0.5372E-14	0 0	0.1850E+00	0.1722E-05
0.8880E+00	0 0	0.1010E-01	-0.5517E-02	-0.5135E-17	0 0	0.1010E-01	-0.5517E-02	-0.1483E-13	0 0	0.1850E+00	0.1722E-05
21-0.5008E-02	0.1252E-01	-0.3500E-02	-0.7220E-02	0.1458E-12	-0.2872E-02	-0.3500E-02	-0.7220E-02	0.2281E-12	0 0	0.1850E+00	0.1722E-05
0.8880E+00	0 0	0.1010E-01	-0.5517E-02	0.5410E-15	0 0	0.1010E-01	-0.5517E-02	0.1715E-12	0 0	0.1850E+00	0.1722E-05
22-0.5008E-02	0.3355E-02	-0.3500E-02	-0.7220E-02	-0.7807E-13	-0.2872E-02	-0.3500E-02	-0.7220E-02	-0.1172E-13	0 0	0.1850E+00	0.1722E-05
0.8880E+00	0 0	0.1010E-01	-0.5517E-02	-0.3922E-15	0 0	0.1010E-01	-0.5517E-02	-0.7168E-13	0 0	0.1850E+00	0.1722E-05

SUMMARY OF COMPUTER TIME

ITERATION	STIFF REFORM (MILLI SEC.)	SOLUTION TIME (MILLI SEC.)	STRESS CALCUL. (MILLI SEC.)
1	82	5	254
2	100	5	250
3	NO	1	255
TOTAL	182	13	759

TIME IN FOR THIS STEP = 135 MILLI SEC.
TIME OUT FOR THIS STEP = 1241 MILLI SEC.
TIME ELAPSED FOR THIS STEP = 1106 MILLI SEC.

END OF STEP NUMBER 5
